U.S. Department
of Transportation
Federal Railroad
Administration

Office of Research,
Development and Technology
Washington, DC 20590

Monitoring and Modeling of Differential Movement at Railway Transitions

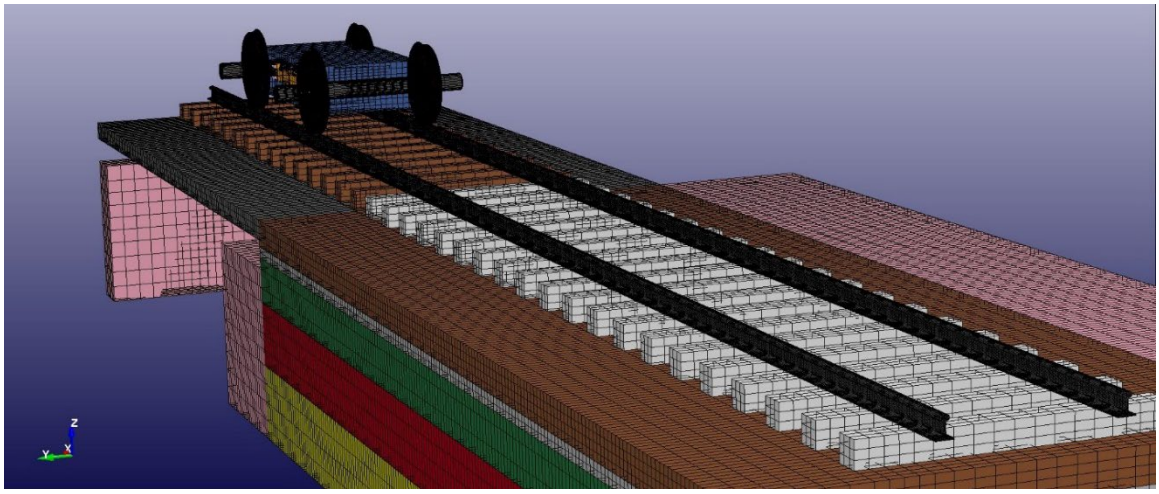

DOT/FRA/ORD-24/30

Final Report | August 2024

REPORT DOCUMENTATION PAGE

Form Approved

OMB No. 0704-0188

1. AGENCY USE ONLY (Leave blank)	2. REPORT DATE	3. REPORT TYPE AND DATES COVERED
	April 2020	Technical Report 09-27-2011 to 12-31-2015

4. TITLE AND SUBTITLE

Monitoring and Modeling of Differential Movement at Railway Transitions

5. FUNDING NUMBERS

DTFR53-11-C-00028

6. AUTHOR(S)

Timothy D. Stark ORCID 0000-0003-2384-1868

Stephen T. Wilk ORCID 0000-0001-5347-569X

7. PERFORMING ORGANIZATION NAME(S) AND ADDRESS(ES)

University of Illinois
Office of Sponsored Programs & Research Administration (OSPRA)
1901 South First Street, Suite A
Champaign, IL 61820

8. PERFORMING ORGANIZATION REPORT NUMBER

Final Report 1

9. SPONSORING/MONITORING AGENCY NAME(S) AND ADDRESS(ES)

U.S. Department of Transportation
Federal Railroad Administration
Office of Railroad Policy and Development
Office of Research, Development, and Technology
Washington, DC 20590

10. SPONSORING/MONITORING AGENCY REPORT NUMBER

DOT/FRA/ORD-24/30

11. SUPPLEMENTARY NOTES

COTR: Cameron Stuart

12a. DISTRIBUTION/AVAILABILITY STATEMENT

This document is available to the public through the FRA eLibrary.

12b. DISTRIBUTION CODE

13. ABSTRACT (Maximum 200 words)

The Federal Railroad Administration sponsored a research team from the University of Illinois at Urbana-Champaign to conduct laboratory and field research of railroad bridge transitions between September 2011 and December 2015. In this report, researchers present an interpretation of Amtrak and Norfolk Southern (NS) railway transitions and 3-dimensional numerical analyses of the instrumented transitions using available software packages to develop recommendations for future designs. The team used data from previous studies, including field measurements along the Amtrak Northeast Corridor near Chester, Pennsylvania, and two NS N-Line bridges in southern West Virginia, and the results of the numerical modeling that were calibrated using field data from the monitored railway transitions.

14. SUBJECT TERMS

Transition zones, differential movement, bridge approach, unsupported, track geometry, track modulus, modulus

15. NUMBER OF PAGES

196

16. PRICE CODE

17. SECURITY CLASSIFICATION OF REPORT	18. SECURITY CLASSIFICATION OF THIS PAGE	19. SECURITY CLASSIFICATION OF ABSTRACT	20. LIMITATION OF ABSTRACT
Unclassified	Unclassified	Unclassified	

Standard Form 298 (Rev. 8/98)
Prescribed by ANSI Std. Z39.18

METRIC/ENGLISH CONVERSION FACTORS

ENGLISH TO METRIC	METRIC TO ENGLISH
LENGTH (APPROXIMATE)	**LENGTH (APPROXIMATE)**
1 inch (in) = 2.5 centimeters (cm)	1 millimeter (mm) = 0.04 inch (in)
1 foot (ft) = 30 centimeters (cm)	1 centimeter (cm) = 0.4 inch (in)
1 yard (yd) = 0.9 meter (m)	1 meter (m) = 3.3 feet (ft)
1 mile (mi) = 1.6 kilometers (km)	1 meter (m) = 1.1 yards (yd)
	1 kilometer (km) = 0.6 mile (mi)
AREA (APPROXIMATE)	**AREA (APPROXIMATE)**
1 square inch (sq in, in^2) = 6.5 square centimeters (cm^2)	1 square centimeter (cm^2) = 0.16 square inch (sq in, in^2)
1 square foot (sq ft, ft^2) = 0.09 square meter (m^2)	1 square meter (m^2) = 1.2 square yards (sq yd, yd^2)
1 square yard (sq yd, yd^2) = 0.8 square meter (m^2)	1 square kilometer (km^2) = 0.4 square mile (sq mi, mi^2)
1 square mile (sq mi, mi^2) = 2.6 square kilometers (km^2)	10,000 square meters (m^2) = 1 hectare (ha) = 2.5 acres
1 acre = 0.4 hectare (he) = 4,000 square meters (m^2)	
MASS - WEIGHT (APPROXIMATE)	**MASS - WEIGHT (APPROXIMATE)**
1 ounce (oz) = 28 grams (gm)	1 gram (gm) = 0.036 ounce (oz)
1 pound (lb) = 0.45 kilogram (kg)	1 kilogram (kg) = 2.2 pounds (lb)
1 short ton = 2,000 pounds (lb) = 0.9 tonne (t)	1 tonne (t) = 1,000 kilograms (kg) = 1.1 short tons
VOLUME (APPROXIMATE)	**VOLUME (APPROXIMATE)**
1 teaspoon (tsp) = 5 milliliters (ml)	1 milliliter (ml) = 0.03 fluid ounce (fl oz)
1 Tablespoon (tbsp) = 15 milliliters (ml)	1 liter (l) = 2.1 pints (pt)
1 fluid ounce (fl oz) = 30 milliliters (ml)	1 liter (l) = 1.06 quarts (qt)
1 cup (c) = 0.24 liter (l)	1 liter (l) = 0.26 gallon (gal)
1 pint (pt) = 0.47 liter (l)	
1 quart (qt) = 0.96 liter (l)	
1 gallon (gal) = 3.8 liters (l)	
1 cubic foot (cu ft, ft^3) = 0.03 cubic meter (m^3)	1 cubic meter (m^3) = 36 cubic feet (cu ft, ft^3)
1 cubic yard (cu yd, yd^3) = 0.76 cubic meter (m^3)	1 cubic meter (m^3) = 1.3 cubic yards (cu yd, yd^3)
TEMPERATURE (EXACT)	**TEMPERATURE (EXACT)**
[(x-32)(5/9)] °F = y °C	[(9/5) y + 32] °C = x °F

QUICK INCH - CENTIMETER LENGTH CONVERSION

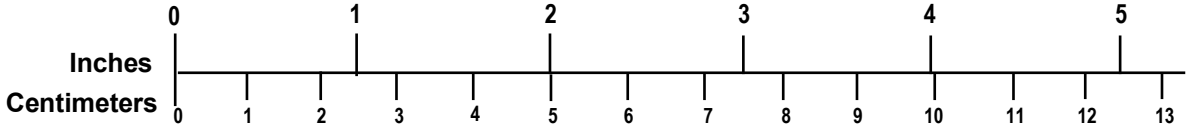

QUICK FAHRENHEIT - CELSIUS TEMPERATURE CONVERSIO

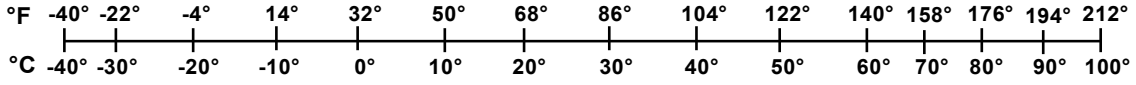

For more exact and or other conversion factors, see NIST Miscellaneous Publication 286, Units of Weights and Measures. Price $2.50 SD Catalog No. C13 10286 **Updated 6/17/98**

Acknowledgements

The research team acknowledges the assistance of Mike Tomas, Marty Perkins, and Carl Walker of Amtrak for their assistance with installation of the field railroad track instrumentation, monitoring the instrumentation, and interpretation of the Amtrak results. The research team acknowledges the assistance of Brad Kerchof of Norfolk Southern (NS) Railway for his assistance with installation of the field railroad track instrumentation, monitoring the instrumentation, and interpretation of the NS results. Full-time Post-doctoral Research Assistant Debakanta Mishra and Graduate Research Assistants Huseyin Boler, Wenting Hou, and Maziar Moaveni, working with Co-Project Manager Erol Tutumluer, are also acknowledged for their work on this project. James P. Hyslip of Hyground Engineering served as a Research Engineer for the University of Illinois at Urbana-Champaign during this project, and his assistance is also acknowledged.

Contents

Illustrations

Tables

Executive Summary

The Federal Railroad Administration (FRA) sponsored a research team from the University of Illinois at Urbana-Champaign (UIUC) to conduct laboratory and field research of railroad bridge transitions between September 2011 and December 2015. In this report, researchers present an interpretation of Amtrak and Norfolk Southern (NS) railway transitions and 3-dimensional numerical analyses of the instrumented transitions using available software packages to develop recommendations for future designs. The team used data from previous studies, including field measurements along the Amtrak Northeast Corridor (NEC) near Chester, Pennsylvania, and two NS N-Line bridges in southern West Virginia, and the results of the numerical modeling that were calibrated using field data from the monitored railway transitions.

The team analyzed the Amtrak NEC instrumentation sites and determined the root causes of permanent vertical displacements at the instrumented bridge approaches were (1) track stiffness variation between the bridge structure and the adjacent track, (2) increased dynamic loads in the transition zone, and (3) undesirable ballast conditions. Researchers developed four transition zone design recommendations to prevent permanent vertical displacements in the bridge approach: (1) reduce the bridge stiffness with a ballasted bridge decks and a combination of pad or mat systems, (2) install compacted ballast, ensure adequate drainage systems, (3) reduce ballast and subgrade settlement by confining the approach areas, and (4) reduce ballast settlement by increasing the tie-ballast contact area.

The Amtrak field data suggested the main factor contributing to the increased loads was the existence of a gap between the ties and ballast (i.e., poor tie support). The research team used five indicators to determine whether poor tie support existed at an instrumentation site: (1) observing large vertical tie displacements and rebounding during train passage, (2) measured transient vertical displacements using video cameras, (3) measured acceleration time histories data for selected ties, (4) measured tie reactions, and (5) measured permanent vertical displacements. The team used accelerometers installed on crossties at two of the Amtrak instrumentation sites in Chester, Pennsylvania, to identify and quantify poor tie support.

The instrumented NS site research enhanced the relationships found in the Amtrak sites. The combination of light empty cars and heavy loaded cars on NS provided additional data to characterize the non-linear force-displacement relationship below the tie seating load.

Researchers used LS-DYNA numerical modeling software to replicate the train and track system, including the train wheels, rails, ties, tie fasteners, ballast, sub-ballast, and various subgrade layers. The team simulated the mechanisms that increased the applied loads on the ballast due to a tie-ballast gap. In the model, the tie-ballast gap allowed bending of the rail, which redistributed some of the wheel load to nearby ties. This load redistribution can lead to a progressive increase of the tie-ballast gap under adjacent ties and unsupported tie conditions developing among a group of ties instead of just one. The terms “progressive loss of tie support” and “progressive tie failure” are used in this report to describe this load redistribution behavior. The modeling also showed an increase in downward tie velocity due to a greater tie-ballast gap can cause significant impact loads to the ballast that can exceed the actual wheel loads. These impact loads can cause damage to the ballast and/or tie.

The team also conducted bridge approach simulations using LS-DYNA to investigate increased loading from a freight car truck entering the bridge and wheel load redistribution due to ties not

being fully supported. Ties that are not fully supported transfer some of the applied wheel load to adjacent ties. Differential settlement between the bridge and the transition zone and within the transition zone itself can increase and concentrate dynamic loads in the transition zone.

Another important aspect of the numerical modeling is the estimation of modulus values for the various layers at each field instrumentation site, e.g., ballast, sub-ballast, and subgrade layers, using numerical models. Researchers used both LS-DYNA and FLAC3D to perform an inverse analysis using the measured transient and permanent displacements with depth to estimate layer moduli for the various layers. FLAC3D implements a quick and programmable static analysis while LS-DYNA incorporates the full wheel-rail-tie-ballast-subgrade interaction to calibrate the behavior of the entire track system. The team found that FLAC3D is more efficient and yields similar values to LS-DYNA and recommended its use for future inverse moduli analyses. The modulus values for the various layers at each instrumentation site are presented in this report.

1. Introduction

The Federal Railroad Administration (FRA) sponsored a research team from the University of Illinois at Urbana-Champaign (UIUC) to conduct laboratory and field research of railroad bridge transitions between September 2011 and December 2015. In this report, researchers present an interpretation of Amtrak and Norfolk Southern (NS) railway transitions and 3-dimensional numerical analyses of the instrumented transitions using available software packages to develop recommendations for future designs. The team used data from previous studies, including field measurements along the Amtrak Northeast Corridor (NEC) near Chester, Pennsylvania, and two NS N-Line bridges in southern West Virginia, and the results of the numerical modeling that were calibrated using field data from the monitored railway transitions.

1.1 Background

As with most highway bridges, railway transitions experience differential movement due to differences in track system stiffness and damping, foundation type, ballast settlement, fouling, and/or degradation, or subgrade settlement. This differential movement is especially problematic for high-speed rail infrastructure because the abrupt "bump" at the transition is accentuated at high speeds. This bump is a major safety concern for high-speed rail because of possible uncoupling of cars, derailment, bridge damage, or passenger injury. Improving the differential movement at railway transitions for high-speed rail is also beneficial for freight lines operating in joint corridors. These variables must be considered when designing or remediating railway transitions.

1.2 Objectives

The objective of this research project was to determine the causes of differential settlements at joint high-speed passenger and freight track transitions and to develop effective designs for new railway transitions and for rehabilitating existing transitions. UIUC researchers employed state-of-the-art field monitoring, field investigation, and numerical modeling of new and problematic railway transitions during this project. The team anticipates the proposed design and rehabilitation methodologies will result in safer railways, faster operating speeds, lower life-cycle costs, lengthened maintenance intervals, increased capacity to operate trains, less frequent and shorter track outages, and reduced annual operating costs for high-speed and intercity passenger rail systems.

1.3 Overall Approach

Researchers achieved the project's interconnected objectives by monitoring several existing and rehabilitated railway transitions identified by Amtrak and NS Railway to better understand the location, cause, and magnitude of the differential movement at railway transitions and predict field performances through numerical modeling.

1.4 Scope

The scope of the research project involved extensive field instrumentation and numerical analyses. The main tasks of the literature review, field instrumentation, monitoring, and data analysis, portion of the project were:

- Identify the location(s) of the observed differential movement using field monitoring data from selected Amtrak and NS sites and available literature
- Determine the cause(s) of the movement (e.g., ballast, fill, subgrade, ties, and/or a combination of these sources)
- Compare the location(s) and cause(s) of the observed differential movement to similar cases found in highway bridge transitions to identify possible remedial measures

The main tasks of the numerical modeling portion of the project were:

- Develop numerical models and material properties of monitored railway transitions
- Calibrate the numerical models using field vertical displacement and wheel load measurements
- Investigate increased loads in open-track and transition-zone environments caused by differential ballast settlement and tie-ballast gaps
- Assess the effectiveness of various design and remedial measures on the performance of joint high-speed passenger and freight track transitions

1.5 Organization of the Report

Report Section 1 through Section 9 document the field instrumentation, monitoring and data analysis efforts and the root cause analysis of the differential movement presented in Section 10. Section 11 through Section 15 present the numeric modeling work. The findings from field measurements and numerical simulations are summarized in the Conclusion (Section 16).

Additional results are included in four Appendices:

Appendix A – Tie Reaction Plots

Appendix B – Transient Vertical Displacement Plots

Appendix C – FLAC3D Results

Appendix D – Ballast Settlement Information from Literature Review

2. Instrumented Bridge Transitions

Amtrak's NEC supports high-speed intercity passenger and some freight trains while NS Railway's N-Line carries slower freight trains. Researchers analyzed both sites to determine the cause of differential movements at transition zones and to compare the behavior of bridge transitions with high-speed passenger and slow-moving freight traffic.

2.1 Amtrak Field Sites

A portion of Amtrak's NEC located south of Philadelphia in Chester, Pennsylvania, includes closely spaced bridges. Some of these bridges experience differential movement at the bridge/approach fill interfaces that cause ride quality and safety concerns. The NEC is primarily a high-speed railway with occasional freight traffic. High-speed passenger trains operate up to a maximum speed of 150 mph (241 km/h). This segment of the NEC is comprised of four tracks, with Tracks 2 and 3 being used for high-speed passenger trains (e.g., Acela Express) that operate at 110 mph (177 km/h). The predominant direction of traffic along Track 2 is northbound, whereas Track 3 predominantly carries southbound traffic, although the directions can vary.

UIUC researchers selected the following Amtrak bridge approaches for field instrumentation based on a review of existing track geometry data:

- Madison Avenue bridge – Track 2 (see Figure 1)
    - West rail, 12 ft south of Madison Avenue bridge (Madison (12 ft)), entrance transition
    - West rail, 60 ft south of Madison Avenue bridge (Madison (60 ft)), entrance open track
- Upland Avenue bridge – Track 2
    - West rail, 15 ft north of Upland Avenue bridge (Upland (15 ft)), entrance transition
    - West rail, 60 ft north of Upland Avenue bridge (Upland (60 ft)), entrance open track
- Caldwell Avenue bridge – Track 3
    - East rail, 80 ft south of Caldwell Avenue bridge (Caldwell (East)), exit open track
    - West rail, 80 ft south of Caldwell Avenue bridge (Caldwell (West)), exit open track

Figure 1 is a plan view showing the location of the Madison, Upland, and Caldwell Avenue instrumentation locations relative to the bridge that spans these streets. The diagrams in Figure 1 also show the condition of the ties surrounding the instrumented tie because of its relevance to load redistribution. The track conditions changed during the study due to wear and track maintenance. Field instrument installation was completed on 6 August 2012.

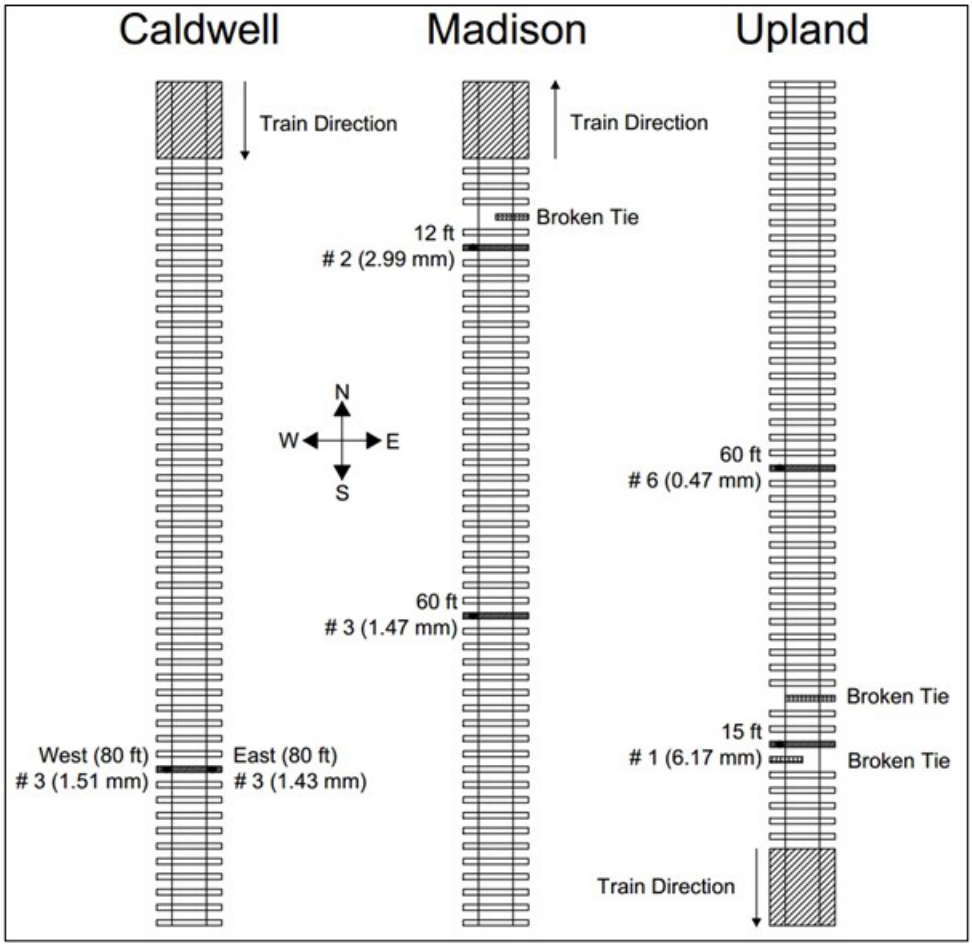

Figure 1. Plan view of Amtrak instrumentation locations in Chester, PA

2.2 Norfolk Southern Field Sites

Researchers instrumented two under-grade bridge approaches on the NS N-Line at mileposts (MP) 352.2 and 352.8 between Roanoke, Virginia, and Bluefield, West Virginia. The bridge at MP 352.2 is located on a 10 degree curve and on a 1.1 percent grade, and the bridge at MP 352.8 is located on a 9.7 degree compound curve on a 0.9 percent grade. Track speed in the region is commonly 25 mph (40 km/h). Loaded trains frequently move down this grade from west to east with full dynamic brakes applied, often coupled with air brakes, to remain within the speed limit. This track section is subjected to heavy-axle-load train operation with an annual tonnage of approximately 55 million gross tons (MGT). However, the track also carries empty or lightweight cars, providing a range of wheel loads and track response. Installation at NS was completed on 2 November 2013.

The team instrumented the following locations:

- MP 352.8 – Track 1
    - Near Site; 11 ft east of MP 352.8 bridge (MP 352.8 (11 ft))
    - Far Site; 29 ft east of MP 352.8 bridge (MP 352.8 (29 ft))

- MP 352.2 – Track 1
    - Near Site; 13 ft north of MP 352.2 bridge (MP 352.2 (13 ft))
    - Far Site; 31 ft north of MP 352.2 bridge (MP 352.2 (31 ft))

Figure 2 shows an aerial view of the two NS bridges. Both bridges are in curves.

Figure 2. Aerial view of NS instrumentation locations near Bluefield, WV

2.3 Instrumentation

Researchers selected a multi-depth deflectometer (MDD) to measure subsurface vertical displacements. An MDD consists of linear variable differential transformers (LVDTs) installed at various depths to measure displacements with depth. Strain gages were applied to the rail at each MDD location to measure the vertical wheel loads.

The subsurface movements at the Caldwell, Madison, and Upland Avenue bridges along the NEC were expected to be vertical because the track in this area is essentially straight, and the elevated railways are confined by large masonry walls (see Figure 3). This is important because MDDs can only measure vertical displacements.

Figure 3. Photograph of masonry walls at Upland Avenue below the Upland (15 ft) MDD location

The NS sites were in curves, so the track displacement at these locations would likely involve both vertical and lateral displacements. One limitation of using only MDDs at these locations was that only the vertical displacements were measured. It was unknown how much effect lateral forces had on the track behavior at these locations, so the team focused the numerical modeling on the Amtrak bridges in Chester, PA.

MDDs consist of multiple LVDTs located at five or six different depths at each instrumentation location. MDDs can measure both transient and permanent vertical displacements at each LVDT depth (DeBeer et al., 1989). Sussmann and Selig (1998) and Billow and Li (2005) also used MDDs to measure vertical displacements in railroad track.

The clamping nut at the top of an LVDT (see Figure 4) is tightened to displace the washer and steel balls of the loading washer out radially and secure the LVDT to the inside wall of the borehole casing or tubing at the desired depth. As the layer deforms under train loading, the LVDT registers the vertical displacement with respect to the bottom of the MDD string. The bottom of the MDD string is frequently referred to as the anchor point, but this point can undergo vertical displacement if not founded in rock or another unyielding material. MDDs are installed using hand-operated drill equipment, so the depth of the anchor is usually limited to less than 15 ft (4.57 m). There is potential for the anchor point to move due to settlement of the underlying layers.

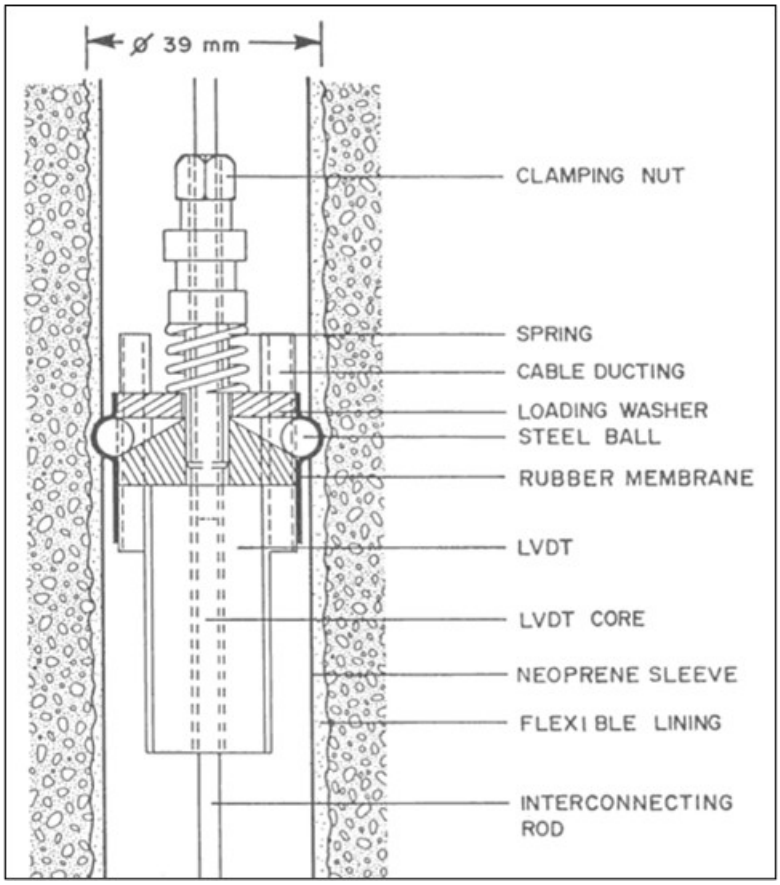

Figure 4. Schematic of a MDD module from DeBeer et al. (1989)

The five LVDTs in each MDD string installed at the Amtrak transitions were placed at depths that roughly corresponded to the following track features: (1) top of crosstie, (2) bottom of ballast layer, (3) bottom of sub-ballast layer, (4) within upper approach fill layer, and (5) within the lower approach fill layer. The transition points from one layer to another layer were determined during the hand-drilling process, and roughly correspond to changes in the materials or properties within the track substructure system.

The approach fill below the fifth LVDT in the elevated track sections in Chester, PA (see Figure 3), can settle, so the total measured vertical displacement could be greater than the measured values. In this system, each LVDT served as the anchor for the LVDT immediately above it. This concept is schematically shown in Figure 5. The inner core for LVDT 5 (attached to MDD module 5) was mounted on the bottom anchor, or Core 5. The core for LVDT 4 (attached to MDD 4) was then mounted on module 5. This configuration was repeated for LVDTs 3, 2, and 1. Researchers assumed that LVDTs 1 through 4 had movable anchors, while the anchor for LVDT 5 (i.e., Core 5) was assumed to be stationary. As a result, the deflection value measured by each LVDT represents the deflection in that layer. For example, the deflection of LVDT 2 corresponds to the deformation of the second layer (d_2, or distance between LVDTs 2 and 3), or Core 2 (shown in Figure 5). The vertical movement of each LVDT was measured and used to describe the vertical displacement of the corresponding layer. If the bottom of the MDD string is assumed to be stationary, the total vertical displacement of the MDD string can be calculated by adding all the LVDT readings together. The MDD strings installed along the NEC terminated at a depth of 118 in (3.0 m) below the top of the concrete crosstie, which placed the anchor within the approach fill. The vertical walls confining the elevated track in Chester, PA, are approximately 12.5 ft (3.8 m) high (see vertical clearance sign in Figure 3). Therefore, the anchor point was well above the bottom of the wall in the approach fill material.

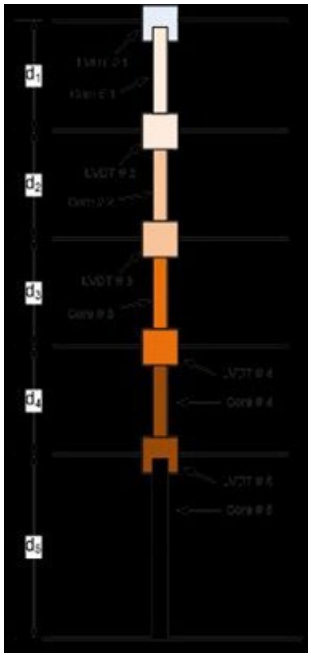

Figure 5. Schematic showing five LVDTs in an MDD string with the bottom founded on an unyielding layer (Tutumluer et al., 2012)

2.4 Amtrak Test Site Soil Profiles

To separate the effect of various soil materials in the track substructure, the team divided each site into five or six different layers with an LVDT measuring the displacement of each layer. Figure 6 through Figure 11 show the soil profiles of Caldwell (East), Caldwell (West), Madison (12 ft), Madison (60 ft), Upland (15 ft), and Upland (60 ft), respectively, along Amtrak's NEC. While the depths of the ballast and sub-ballast are similar at each location, the subgrade profiles vary significantly at each site. This variation exists between Caldwell (East) and (West) where instrumentation was installed on opposite ends of the same tie (Figure 6 and Figure 7).

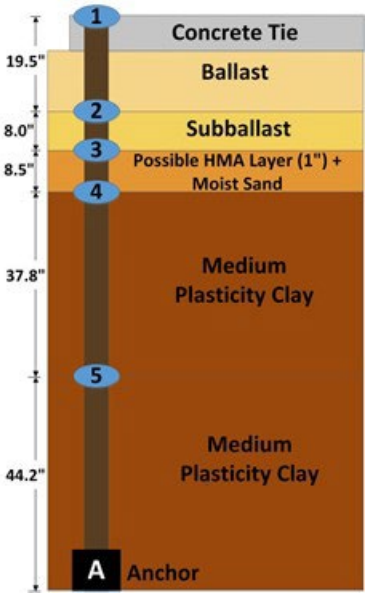

Figure 6. Subsurface profile for MDD at Caldwell (East)

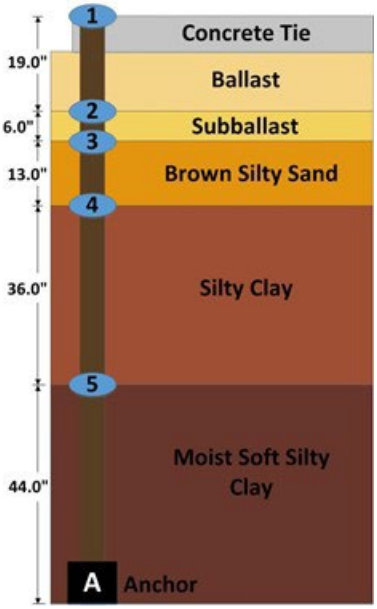

Figure 7. Subsurface profile for MDD location Caldwell (West)

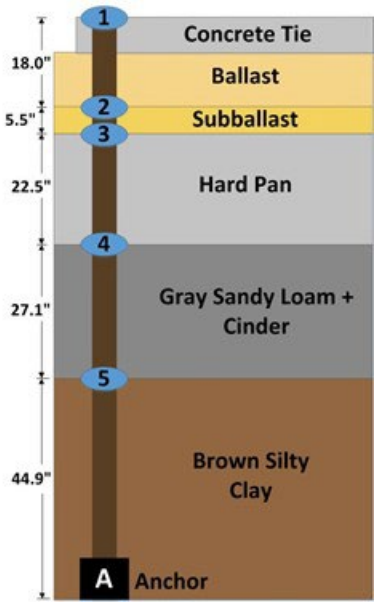

Figure 8. Subsurface profile for MDD location at Madison (12)

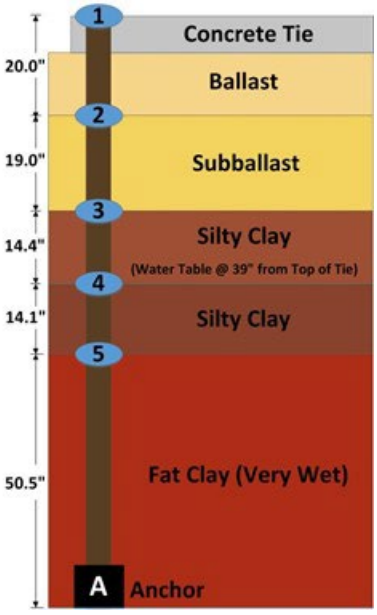

Figure 9. Subsurface profile for MDD location at Madison (60)

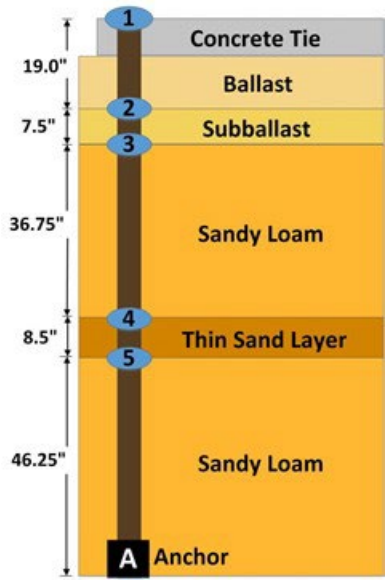

Figure 10. Subsurface profile for MDD location at Upland (15)

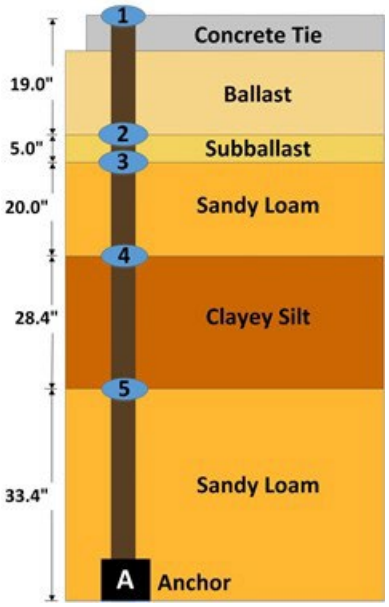

Figure 11. Subsurface profile for MDD location at Upland (60)

2.5 NS Test Site Soil Profiles

Figure 12 through Figure 14 show the boring logs for MP 352.8 and MP 352.2, respectively, at the NS sites. As with the NEC sites, the soil profiles at MP 352.8 and 352.2 are similar, but different LVDT lengths were installed at each site.

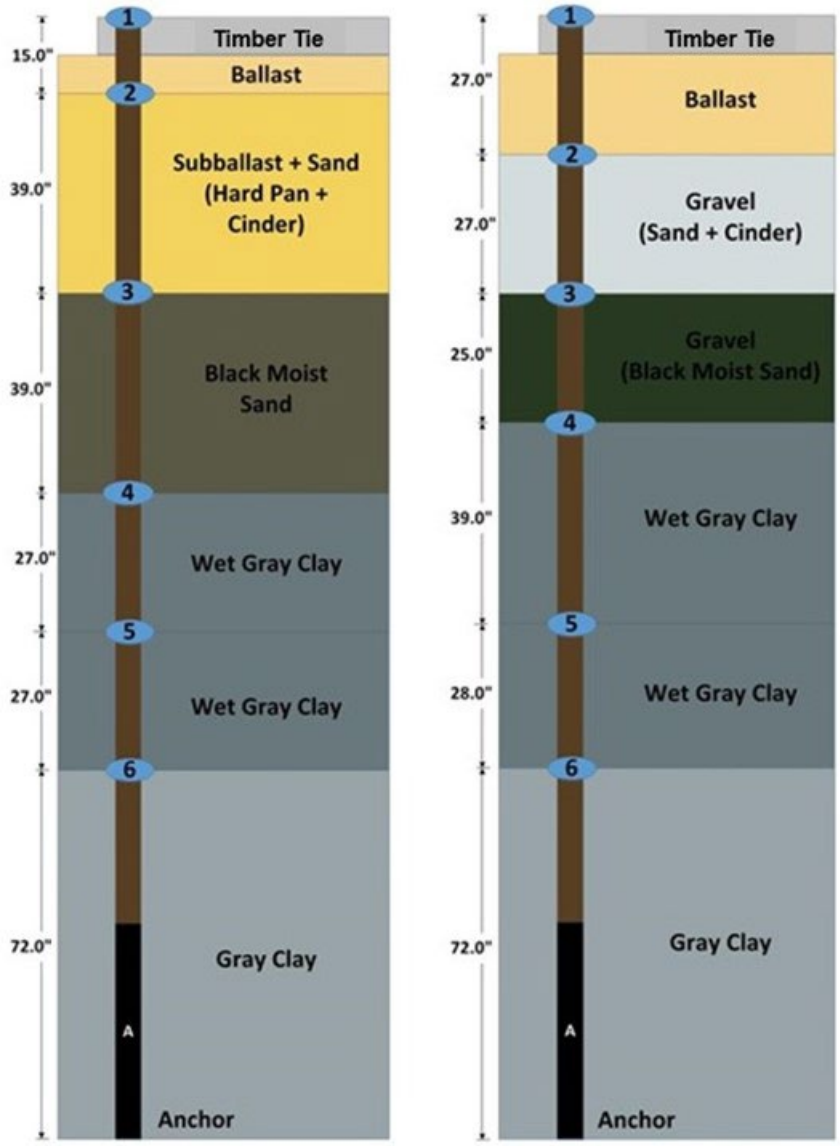

(a) **(b)**

Figure 12. Subsurface profile for MDD location (a) MP 352.8 (11 ft) and (b) MP 352.8 (29 ft)

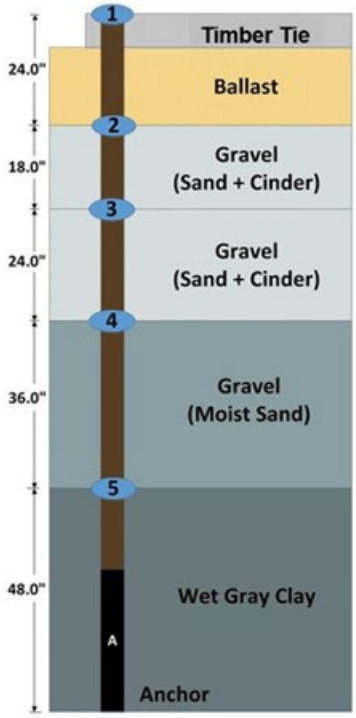

Figure 13. Subsurface profile for MDD location MP 352.2 (13 ft)

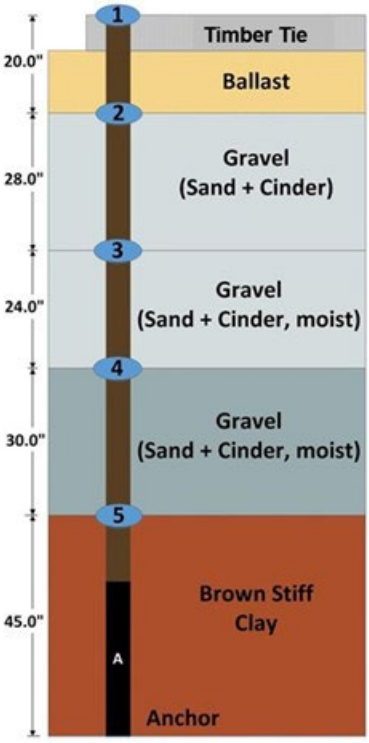

Figure 14. Subsurface profile for MDD location MP 352.2 (31 ft)

2.6 Measurement of Vertical Wheel Loads and Tie Reactions Using Strain Gages

Amtrak installed strain gages to record wheel load and tie reactions in the vicinity of the MDD strings, with a total of eight strain gages (four on each side of the rail) installed next to each MDD string. Figure 15 shows the instrumented rail with four strain gages at Upland (15 ft). The two leftmost strain gages in Figure 15 are in the crib area and were used to estimate the applied wheel loads. The two rightmost strain gages are located above the tie and were used to estimate the "tie reaction" (i.e., the tie-ballast behavior) based on a comparison with the crib area.

Figure 15. Two strain gages in crib area for vertical wheel load and two strain gages above the tie for tie reaction

2.7 Data Collection

The team recorded forty-two train passes at the 10 instrumented sites on Amtrak NEC and NS, thirty-four high-speed passenger trains at the Amtrak site, and eight freight trains at the NS site. A breakdown of the number of trains recorded on each day at each site is displayed in Table 1 (Amtrak) and Table 2 (NS).

Table 1. Number of data measurements at the NEC sites

AMTRAK Site	6,7 August 2012	5 November 2012	29 January 2013	25 June 2013	4 September 2013	Total
Caldwell	2	2	5	3	0	12
Madison	2	3	3	2	2	12
Upland	2	2	2	2	2	10

Table 2. Number of data measurements at the NS sites

NS Site	1 November 2013	19 March 2014
352.8 (11 ft)	1	1
352.8 (29 ft)	0	2
352.2 (13 ft)	1	1
352.2 (31 ft)	1	1

3. Measured Permanent Vertical Displacements

This section presents the analysis of the permanent vertical displacements measured at the various MDD locations along Amtrak NEC and NS lines. The two main objectives of instrumenting these sites were: (1) locate the depth(s) at which most of the transient and permanent vertical displacements occur and (2) determine which instrumented sites exhibited the largest permanent vertical displacement. To accomplish these objectives, the team measured the permanent vertical displacements of each Amtrak LVDT periodically between 2 August 2012 and 25 June 2013 before some remedial maintenance measures were implemented. Data from two NS sites from 1 November 2013 to 19 March 2014 were also available.

3.1 Permanent Vertical Displacements – Amtrak Data

Researchers determined the permanent change in vertical displacement over an extended time by interpreting the MDD data. The team compared relative vertical displacements of all five LVDTs over time to determine the depth of maximum permanent vertical displacement. The first 57 days of data were omitted from the dataset because some LVDTs may have displaced after installation, as the tube and foam around the tubing compressed due to the weight of the MDD string and/or the tubing became fully engaged in the ballast and underlying materials. This settling phenomenon helps explain the high initial rate of permanent vertical displacements of all six sites after instrumentation. For example, Caldwell (East) and Madison (12 ft) (Figure 16 and Figure 17) illustrated the net permanent vertical displacement for 503 days, from 2 August 2012 to 18 December 2013. The term "net" is used in this report to refer to the vertical displacement of a single layer, and "total" is used when the vertical displacements of the underlying or deeper layers were also included in the value of vertical displacement. The sign convention used is positive vertical displacements (numbered downward) to indicate settlement, or downward movement, and negative vertical displacements (numbered upward) to indicate expansion or heave.

At Caldwell (East), the rate of permanent vertical displacement changed after the first 1 or 2 months (Figure 16). Researchers felt this indicated the initial settlement of the instrument. At Madison (12 ft), tamping of the MDD site occurred sometime between 18 and 26 days after MDD installation, which raised and loosened the ballast (Figure 17). This resulted in higher permanent vertical displacements for a short period of time. The team recorded 0.22 in (5.7 mm) of permanent vertical displacement over the 18 days preceding the tamping.

To ensure a proper comparison of all six instrumented Amtrak sites, the temporary increase in permanent vertical displacements from tamping at Madison (12 ft) and (60 ft) was omitted from the analysis.

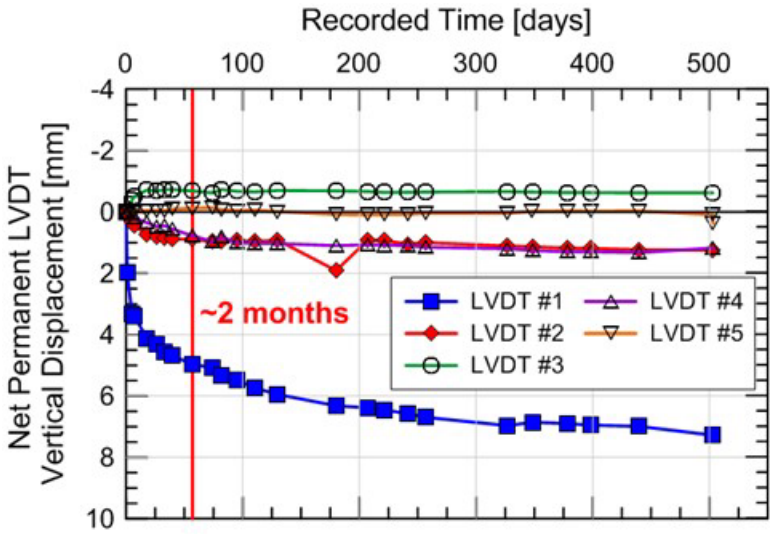

Figure 16. Net permanent vertical displacement at Caldwell (East)

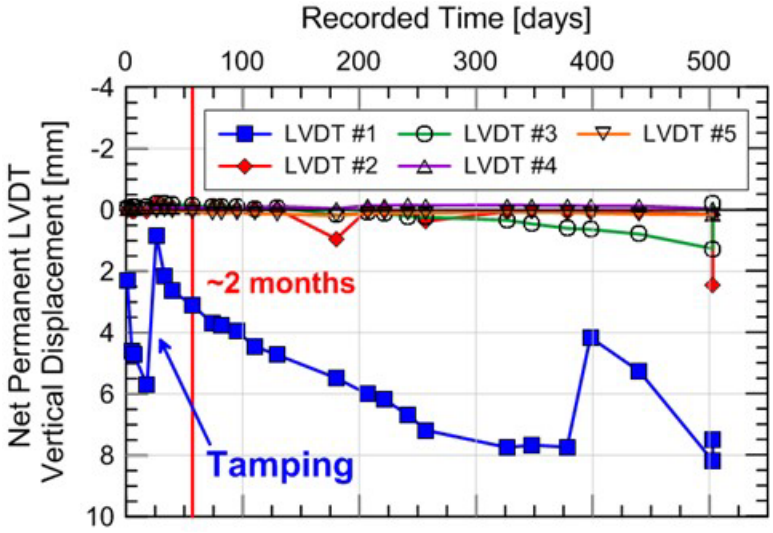

Figure 17. Net permanent vertical displacement at Madison (12 ft)

Figure 16 and Figure 17 show that most of the permanent vertical displacement occurred in LVDT 1, which spanned from the top of the concrete tie to the bottom of the ballast layer. Figure 17 also illustrates the expansion of LVDT 1 due to tamping and the subsequent compression of the ballast after tamping.

Figure 18 through Figure 23 show the permanent vertical displacements of each LVDT with time for all six MDD instrumentation sites for 446 days, from 27 September 2012 to 18 December 2013. The removal of the first two months of permanent vertical displacement resulted in a significant decrease in the permanent vertical displacement at LVDT 1 (i.e., ballast). However, LVDT 1 still exhibited the largest permanent vertical displacements, which matched with previous observations (Selig and Waters, 1994). Figure 18 through Figure 23 also show little permanent vertical displacement occurred in LVDTs 2 through 5. This result reflects the dissipation of load with depth.

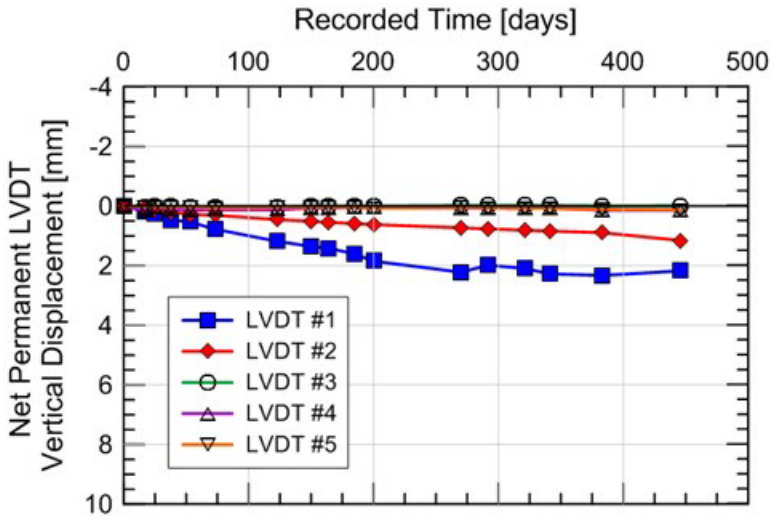

Figure 18. Net permanent vertical displacement at Caldwell (East) with first two months of data removed

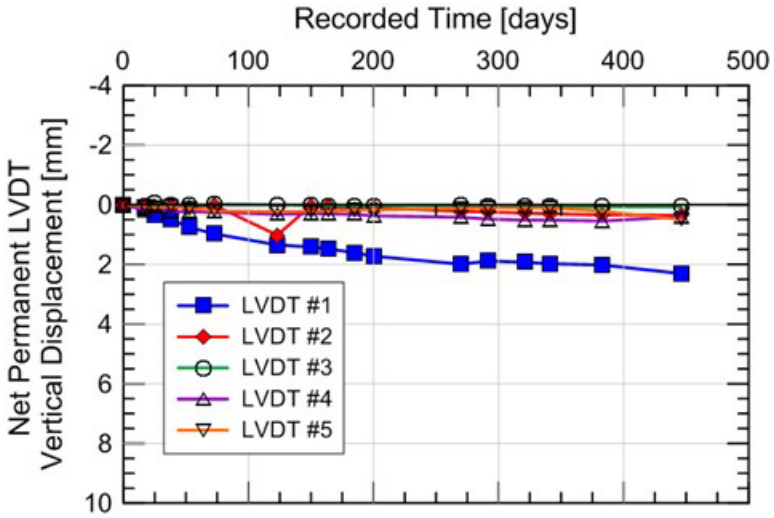

Figure 19. Net permanent vertical displacement at Caldwell (West) with first two months of data removed

The noticeable increase in permanent vertical displacement of LVDT 2 in January, 2013 (i.e., 123 days), at Caldwell (West) (Figure 19), Madison (12 ft) (Figure 20), and Upland (15 ft) (Figure 21) was likely caused by high precipitation at or before the measurement time, equipment error, and/or the LVDT undergoing more vertical displacement due to muddy conditions but rebounding after loading. This increase was temporary, and the LVDT returned to about its original position shortly thereafter.

Tamping at Madison (12 ft) occurred sometime between 15 August 2013 (i.e., 321 days) and 4 September 2013 (i.e., 341 days) (see Figure 20). Afterward, the rate of permanent vertical displacements increased significantly because of the loosened state of the ballast. This may have been due to inadequate compaction during tamping or increased fouling from ballast breakdown during the tamping process.

Tamping at Upland (15 ft) is evident between 1 April 2013 (i.e., 185 days) and 16 April 2013 (i.e., 200 days) (see Figure 21). The negative reading on 16 April 2013 (i.e., 200 days) was likely due to the "zero" reading not corresponding to the rail elevation immediately after tamping.

The Madison (60 ft) and Upland (60 ft) locations were not tamped (see Figure 21, Figure 23).

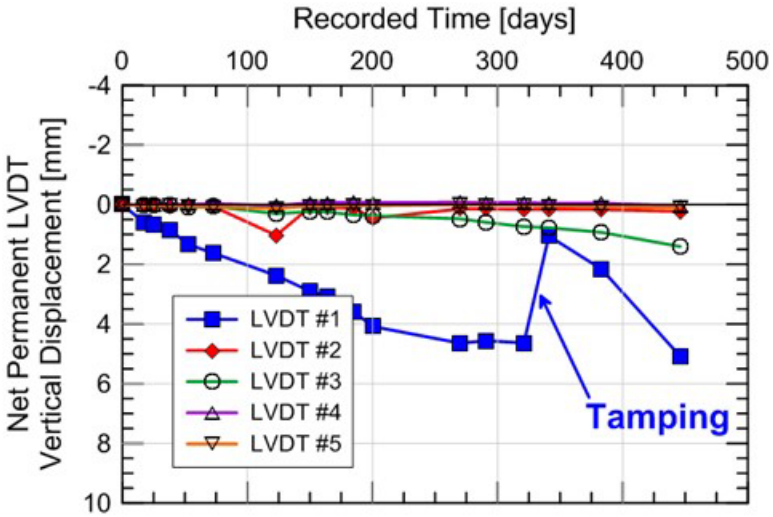

Figure 20. Net permanent vertical displacement at Madison (12 ft) with first two months of data omitted

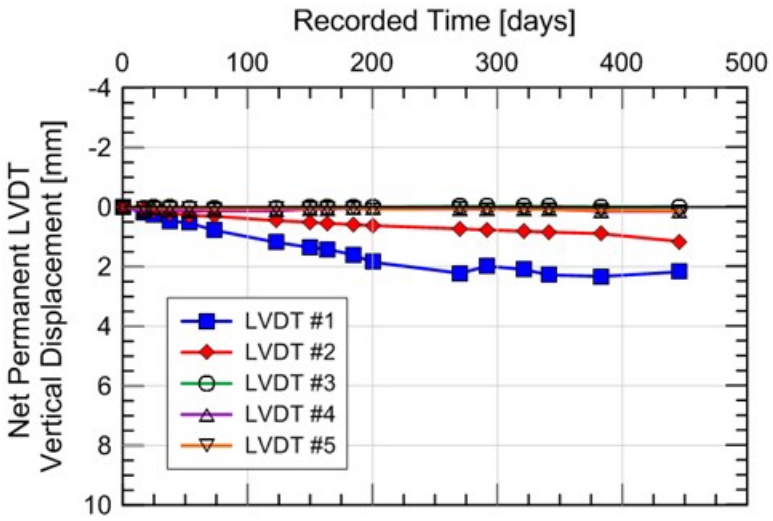

Figure 21. Net permanent vertical displacement at Madison (60 ft) with first two months of data removed

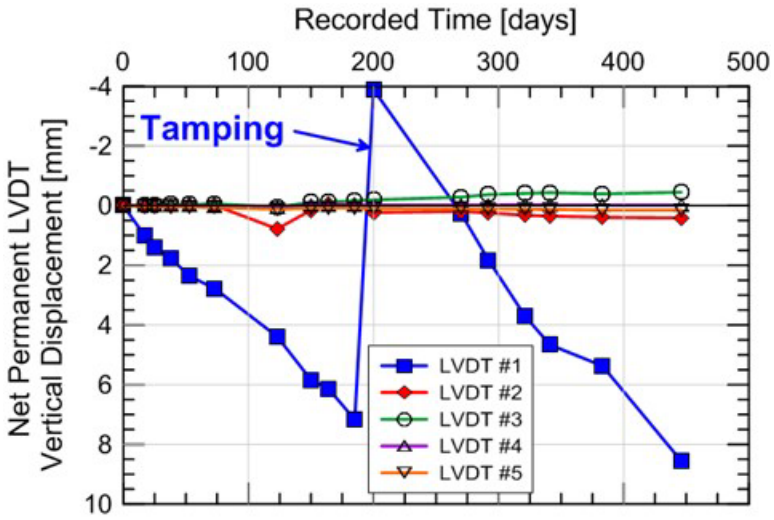

Figure 22. Net permanent vertical displacement at Upland (15 ft) with first two months of data removed

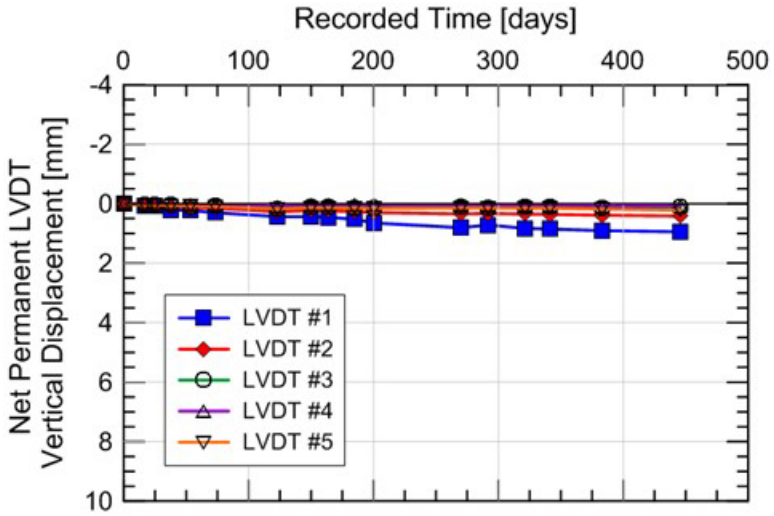

Figure 23. Net permanent vertical displacement at Upland (60 ft) with first two months of data removed

The magnitudes of the permanent vertical displacements for the five LVDTs at each instrumented site are compared in Table 3. The permanent vertical displacements spanned 185 days, from 27 September 2012 to 1 April 2013. During this period, no tamping or LVDT drift occurred. Prior to the 5 June 2013 data collection, the Upland (15 ft) and (60 ft) sites were tamped.

The largest magnitude and variation in permanent vertical displacement occurred in LVDT 1 (i.e., from the top of the tie to the bottom of the ballast) at all locations. Permanent vertical displacement, both expansion and compression, occurred in LVDTs 2 through 5, but to a lesser extent.

Some possible reasons for permanent vertical displacements in LVDT 1 include: (1) increased applied loads (e.g., damaged or hanging ties), (2) unequal wheel loads, (3) increased distance between the tie and ballast, (4) degradation of ballast, (5) ballast fouling, (6) poor drainage, (7)

uneven rails (i.e., potential crosslevel issues), and (8) ballast loosening from tamping, etc. The soils at the LVDT 3 through 5 level did not undergo as much permanent vertical displacement because they were confined by the elevated structure and may have been fully compacted. As a result, additional permanent vertical displacement was likely to be small unless there was a reduction in confinement, an increase in applied load, or a loss of drainage in the future.

Table 3. Permanent vertical displacements of each LVDT at the six MDD locations from 27 September 2012 until 1 April 2013 (Note: negative values indicate heave and positive values indicate settlement)

	Caldwell		Madison		Upland	
	East	West	12 ft.	60 ft.	15 ft.	60 ft.
LVDT	[mm]	[mm]	[mm]	[mm]	[mm]	[mm]
1	1.61	1.61	3.58	2.02	7.17	0.52
2	0.15	0.59	0.12	-0.09	-0.03	0.27
3	0.04	-0.01	0.35	-0.11	-0.16	0.13
4	0.32	0.04	-0.08	0.02	-0.02	0.03
5	0.17	0.04	0.04	0.23	0.08	0.15

3.1.1 Comparison of Ballast Transient Vertical Displacements

A comparison of the LVDT 1 permanent vertical displacements for all six MDD sites is shown in Figure 24, and the rates of permanent vertical displacement are displayed in Table 4. Again, the first two months of data were omitted to ensure the LVDTs were fully engaged with the ballast and other materials.

The largest permanent vertical displacement in LVDT 1 occurred at Upland (15 ft), followed by Madison (12 ft). These are located within the transition zone at each bridge and were expected to exhibit the greatest permanent vertical settlement. Caldwell (East), Caldwell (West), and Madison (60 ft) represent an open-track condition and exhibited similar permanent vertical displacement rates but less permanent vertical displacement than Upland (15 ft) and Madison (12 ft). The Upland (60 ft) location is also an open-track condition and exhibited the smallest permanent vertical displacement, about 0.02 in (0.52 mm) over 185 days, from 27 September 2012 until 1 April 2013.

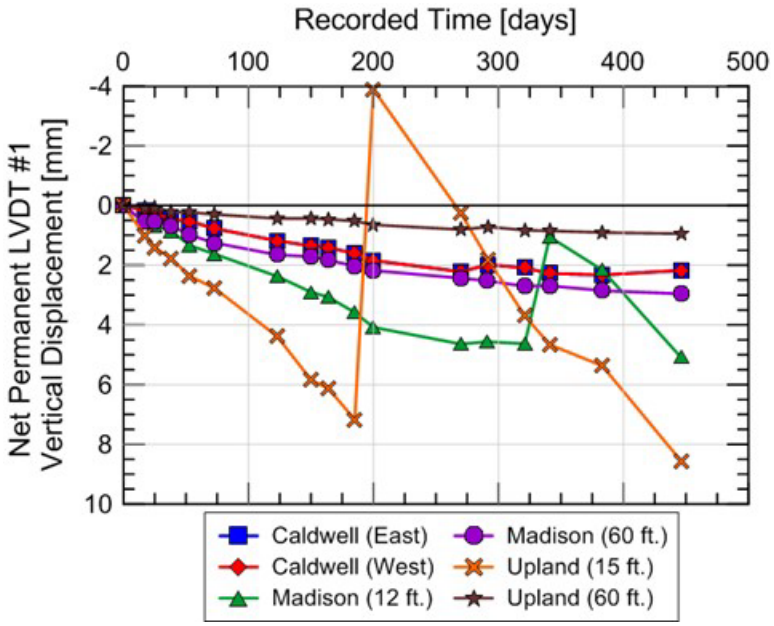

Figure 24. Comparison of net permanent vertical displacements for LVDT 1 at all six MDD instrumentation sites with first two months of data omitted (Note: positive values indicate settlement/downward movement)

Table 4 displays the rates of permanent vertical displacements for the initial 185 days and the entire 446 days of monitoring. The rates before and after tamping for Madison (12 ft) and Upland (60 ft) are also included.

The data shows that the rates of permanent vertical displacements decreased over time. This agreed with previous monitoring (Selig and Waters, 1994) and was likely caused by increasing ballast density over time. Increases in the rate of permanent vertical displacement were observed for both Madison (12 ft) and Upland (15 ft) after tamping. This may have been due to inadequate ballast compaction after tamping, or an increase in ballast degradation and fouling from ballast damage during the tamping process.

Table 4. Permanent vertical displacement rate of LVDT 1 at the six MDD locations

Time Frame	Caldwell		Madison		Upland	
	East	West	12 ft.	60 ft.	15 ft.	60 ft.
	[mm/yr]	[mm/yr]	[mm/yr]	[mm/yr]	[mm/yr]	[mm/yr]
10/27/12 – 4/1/13	3.18	3.18	7.07	3.99	14.1	1.03
10/27/12 – 12/18/13	1.89	1.78	-	2.42	-	0.77
Pre-tamping	-	-	5.30	-	14.1	-
Post-tamping	-	-	14.0	-	18.5	-

3.2 Permanent Vertical Displacements – Norfolk Southern Data

Researchers had limited permanent displacement data from the NS site. Only two data points at MP 352.2 (13 ft) were collected. The permanent displacements displayed in Figure 25 and Figure 26 show similar behavior to the Amtrak sites in that the permanent LVDT 1 displacement is greater at the transition zone site than the open track (Figure 27). The rate of LVDT 1 permanent displacement at MP 352.2 (13 ft) was about equal to Upland (15 ft) with a value of 0.63 in/yr (15.9 mm/yr). The results at MP 352.2 (31 ft) show the greatest permanent displacement occurring in LVDT 3. This suggests that the subgrade may have experienced greater settlement at some track locations than others. Comparisons of permanent LVDT 1 displacement between the two sites in Figure 27 show significantly greater permanent displacement in the transition zone than the open track. This also agrees with the conclusions from the Amtrak sites.

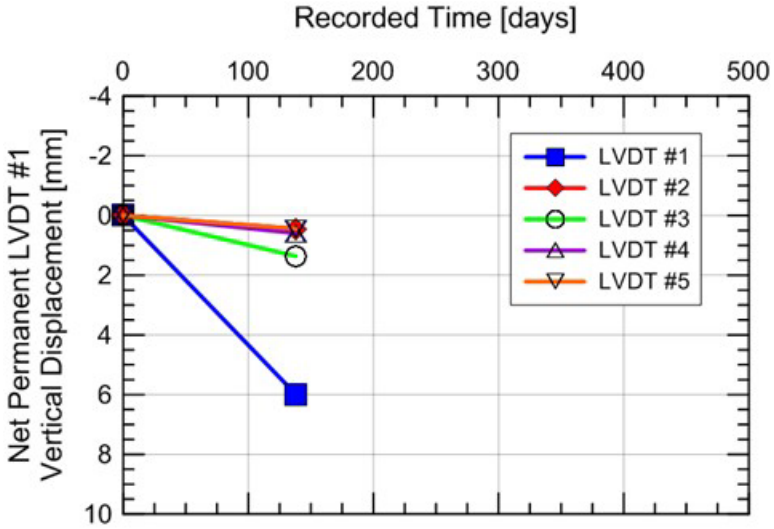

Figure 25. Net permanent vertical displacement at MP 352.2 (13 ft)

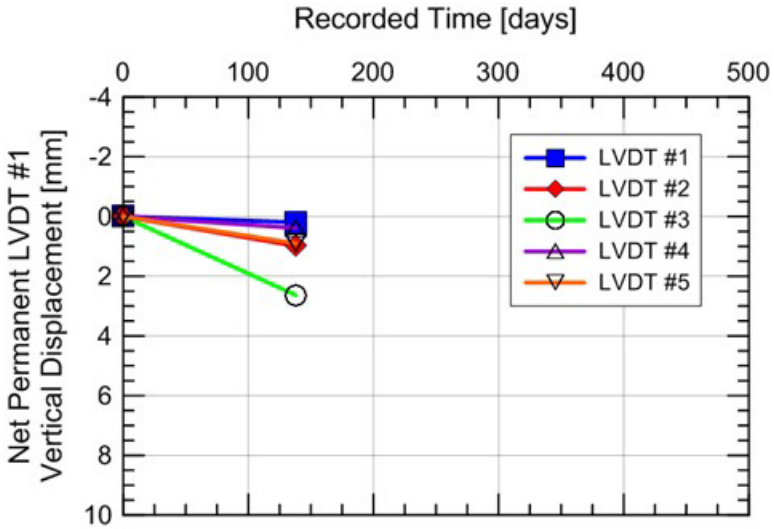

Figure 26. Net permanent vertical displacement at MP 352.2 (31 ft)

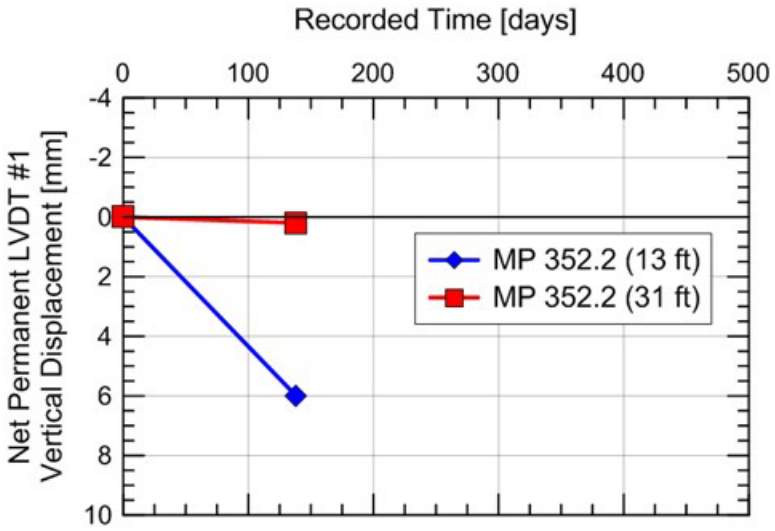

Figure 27. Comparison of Net Permanent Vertical Displacements for LVDT 1 at MP 352.2 (13 ft) and MP 352.2 (31 ft)

4. Dynamic Train Loads

The team considered how the passing train applied load to the tie and substructure related to the measured vertical displacements. Strain gages installed on the rail over the crib area measured wheel load while strain gages on the rail above the instrumented tie measure the tie reaction force, which provided insight to the amount of load being transmitted to the tie.

4.1 Amtrak Wheel Loads

Wheel loads are distributed between the rail, tie, ballast, and subgrade, and a full understanding of the wheel loads is necessary to understand the transient vertical displacements. Also, wheel loads may give insight into performance differences between approach and open-track sites as well as between passenger and freight traffic.

Strain gages (see Figure 15) measured the bending of the rail above the crib area. Researchers used a load frame to calibrate these gages (Figure 28). A load cell at the base of the load-frame recorded the applied load, which was correlated with the rail bending measured using the two strain gages. When a train passed, the stain gages measured the strain of the rail due to bending, and the result was converted to applied load using the conversion factor shown below. The calculated load from the strain gages was directly proportional to the amount of rail bending. The strain gages installed above the tie (see Figure 15) used the same principles.

$$Measured\ Load\ (kN) = 0.0818 * Voltage\ from\ Strain\ Gage$$

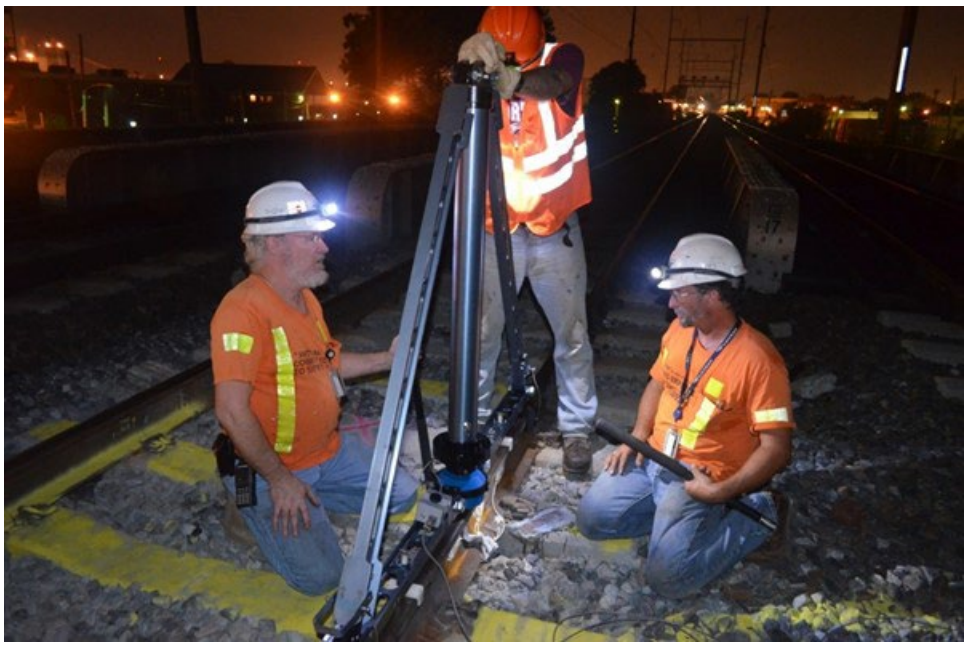

Figure 28. Photo of load frame used to calibrate strain gages on Amtrak NEC

Figure 29 shows a set of measured wheel load data for a passing Acela high-speed passenger train at Upland (60 ft) (7 August 2012, 11:18 AM EDT). The train consisted of two heavy power cars and six lighter passenger cars with four axles per car. The first and last set of four measured wheel loads clearly showed the heavier power cars.

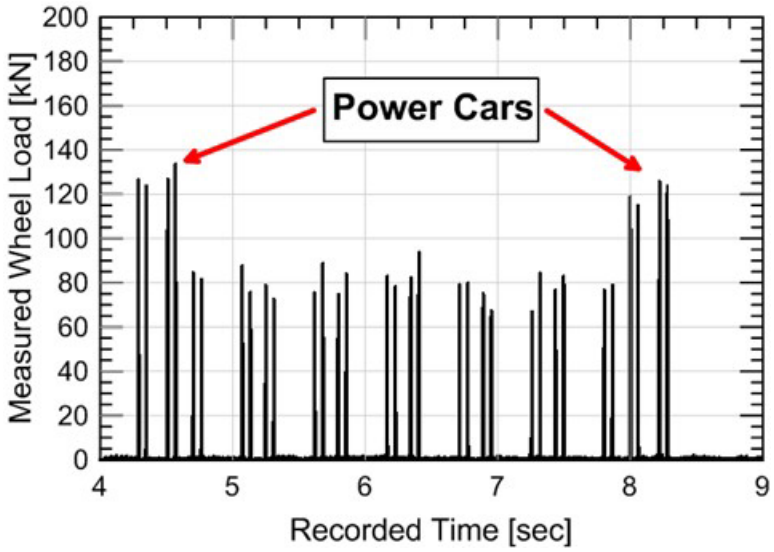

Figure 29. Measured passing wheel load at Upland (60 ft) on 7 August 2013 at 11:18 AM EDT

Figure 30 shows a set of measured wheel load data for a passing freight train at NS MP 352.2 (13 ft) (2 November 2013, 8:43 AM EST). The train consisted of locomotives and both loaded and unloaded freight cars, resulting in significant variations of applied load within a single train. This variation in load was helpful in analyzing the behavior of ballast and subgrade.

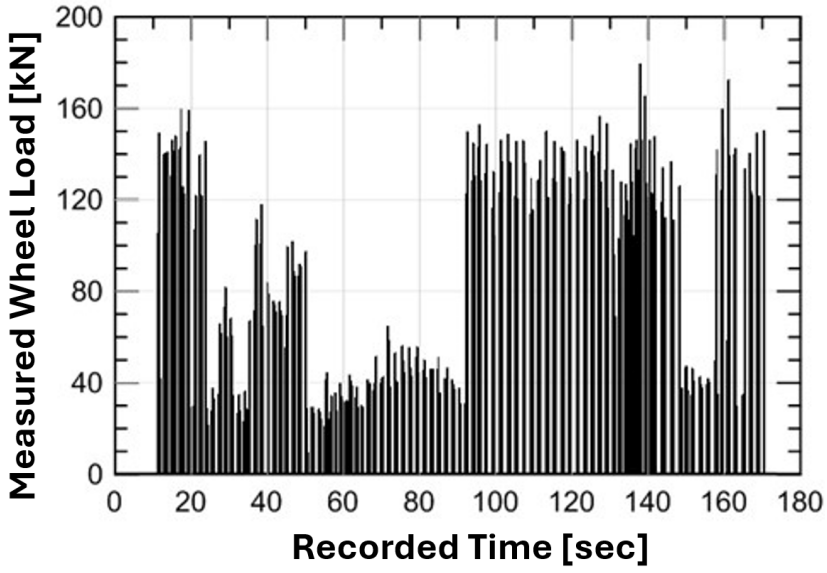

Figure 30. Measured passing wheel load at MP 352.2 (13 ft) on 2 November 2013 at 8:43 AM EST

To emphasize the differences between passenger and freight trains, Figure 31 compares the measured wheel load time histories. Figure 31 shows the freight trains were much longer and moved at a much slower speed than the passenger trains. The nine-car Acela train passed in less than five seconds, while the freight trains passed over the instrumented tie for several minutes. Figure 31 also shows similar maximum wheel loads for freight and passenger cars, which

implies the underlying components experienced similar loads for both freight and passenger trains but with different durations.

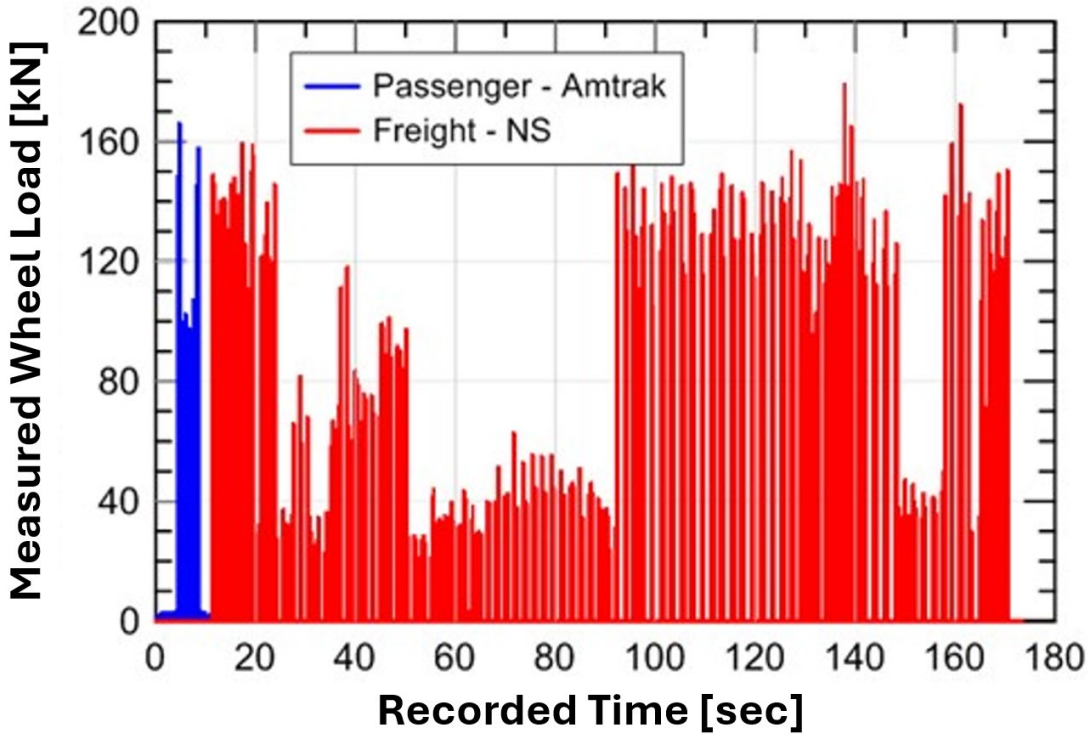

Figure 31. Comparison of passenger vs. freight wheel load measurements (Passenger train is Upland (15 ft) on 7 August 2013 and freight train is at 352.2 (13 ft) on 2 November 2013)

The average peak wheel loads for all six instrumented NEC sites are listed in Table 5, which shows the highest wheel loads corresponded to the transition zones at Upland (15 ft) and Madison (12 ft). These tests sites also had the largest permanent vertical displacement in Figure 24.

Table 5. Average peak wheel loads at NEC instrumented sites

Caldwell Avenue		Madison Avenue		Upland Avenue		All Sites
East	West	12 ft.	60 ft.	15 ft.	60 ft.	
[kN]	[kN]	[kN]	[kN]	[kN]	[kN]	[kN]
75.6	85.7	93.2	89.5	96.3	83.3	86.7

Figure 32 and Figure 33 compare the peak wheel loads at the transition zone with open-track conditions at the Madison and Upland Avenue bridges, respectively. The data for Madison Avenue (Figure 32) showed slightly more scatter than for Upland Avenue (Figure 33). Figure 33 shows that Upland (15 ft) exhibited slightly higher peak wheel loads than Upland (60 ft), which may have been due to dynamic loads being applied in the transition zone. This effect was increased in the 4 September 2013 data.

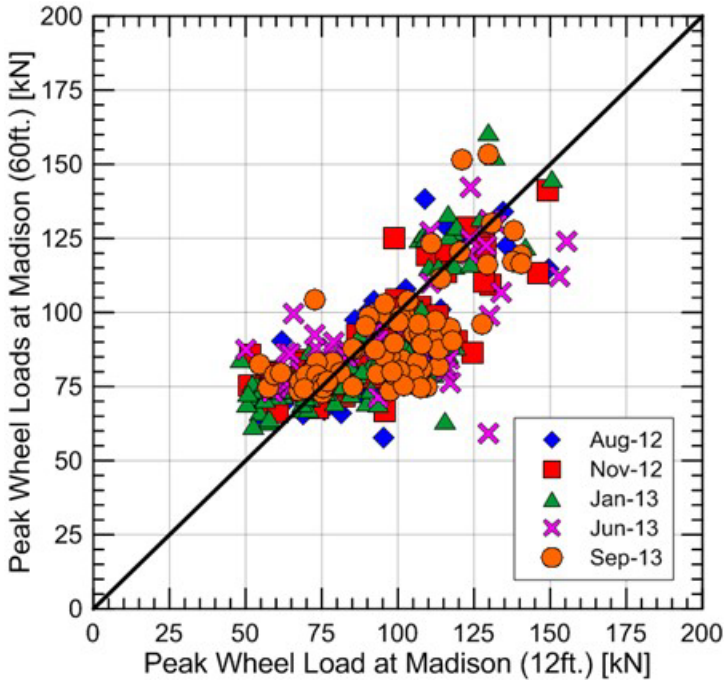

Figure 32. Comparison of wheel loads between Madison (12 ft) and Madison (60 ft) with 1:1 trend line

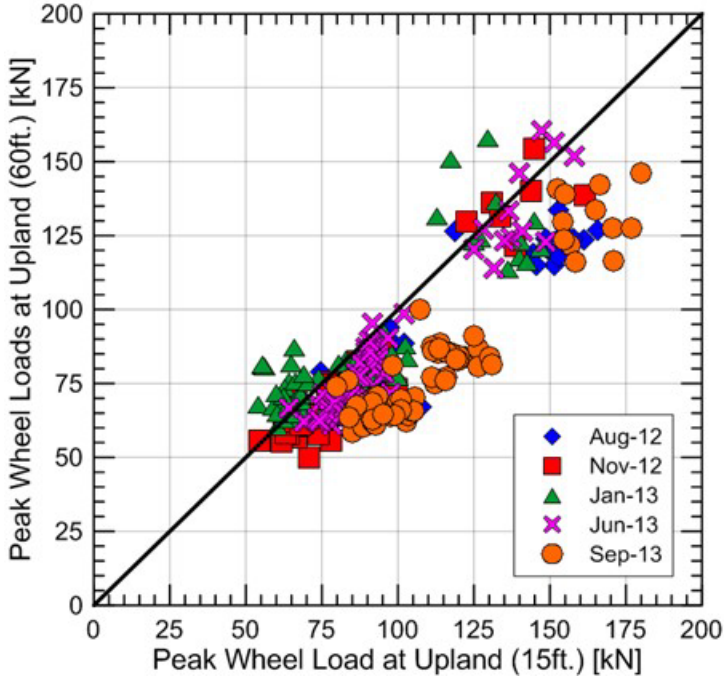

Figure 33. Comparison of wheel loads at Upland (15 ft) and Upland (60 ft) with 1:1 trend line

Figure 34 compares the peak wheel loads at the Caldwell (80 ft) where both MDD strings were located on the same tie. The peak wheel loads at Caldwell (West) were higher than Caldwell (East) even though the instrumentation was located on the same tie. The increase in wheel load

on the west side of the tie was likely due to the west rail being 1/8 in lower than the east rail; the lower tie carried more of the load.

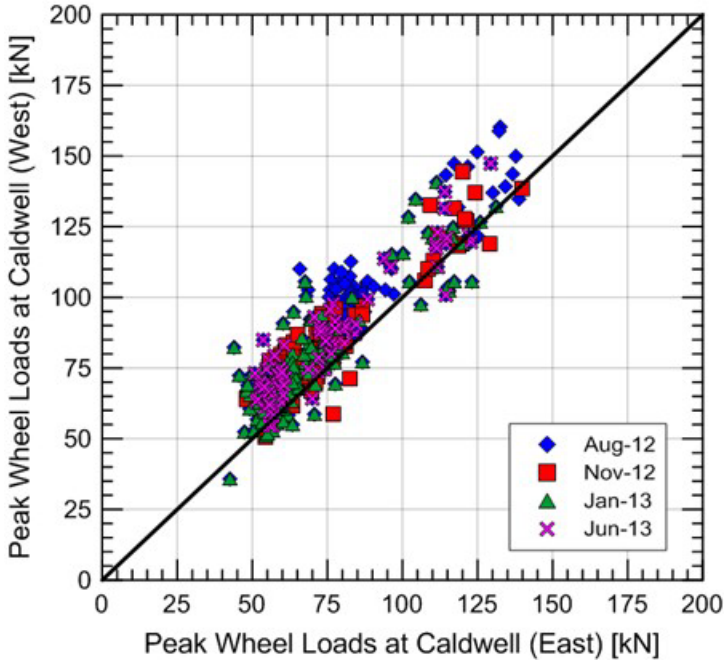

Figure 34. Comparison of wheel loads at Caldwell Avenue East and West (80 ft) with 1:1 trend line

Figure 35 compares the peak wheel load distribution of all Amtrak NEC sites by displaying the percentage of measured peak wheel loads lower than the given value. The figure shows that Upland (15 ft) and Madison (12 ft) experienced the largest peak wheel loads and Caldwell (East) experienced the smallest peak wheel load. However, the peak wheel load distributions were very similar at all sites.

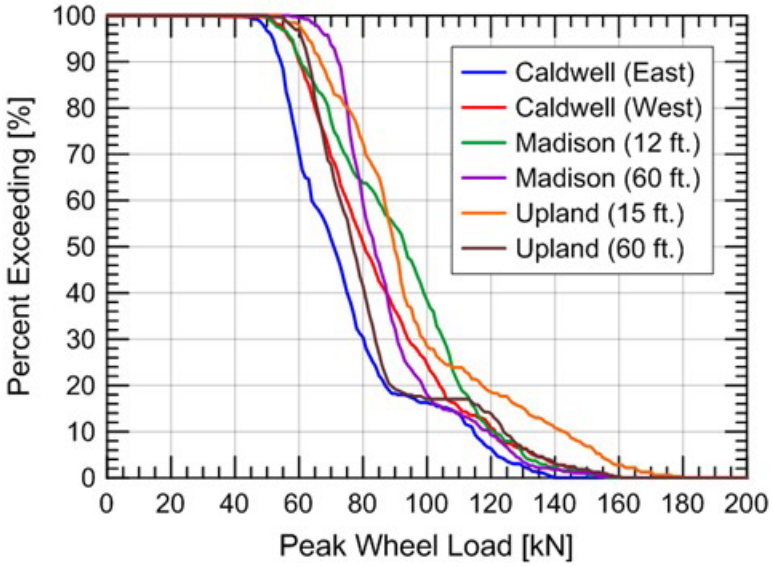

Figure 35. Comparison of load distributions for all six Amtrak NEC sites

4.2 NS Wheel Loads

The average peak wheel load of the eight measured freight trains along the NS track is displayed in Table 6. The table shows a wide range of peak wheel loads, which should be expected as some of the freight cars may have been unloaded or partially loaded. The load distribution of all four recorded NS freight trains is displayed in Figure 36.

Table 6. Average peak wheel loads at NS N-Line sites

MP 352.2 (31 ft) [kN]	MP 352.2 (13 ft) [kN]	MP 352.8 (11 ft) [kN]	MP 352.8 (29 ft) [kN]	All Sites [kN]
141.5	53.5	66.9	50.7	79.0

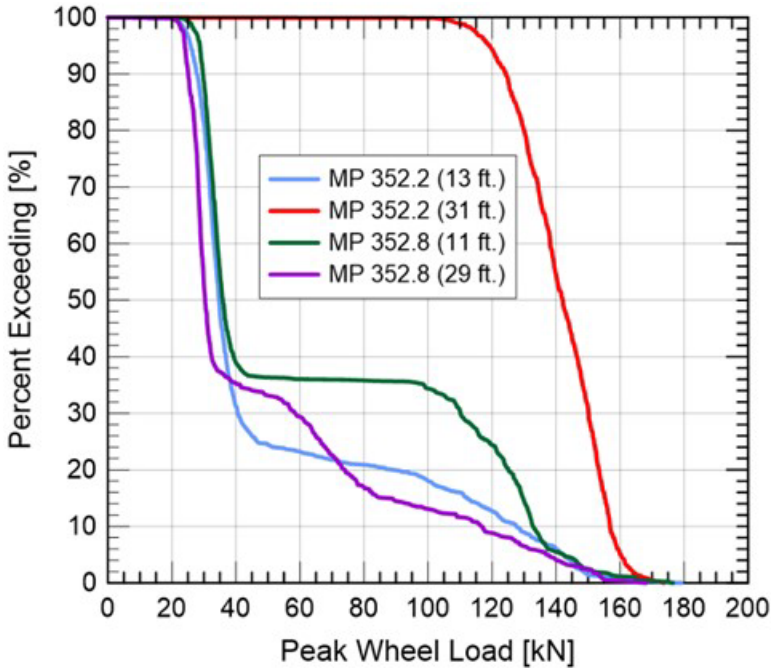

Figure 36. Comparison of load distributions for four measured trains on the NS N-Line

The distribution of peak wheel load was compared between passenger and freight trains. Figure 37 compares the peak wheel load distribution for all measured passenger trains along Amtrak's NEC and freight trains on NS. The left-hand axis corresponds to the solid lines and shows the distribution of measured peak wheel loads in the form of a percentage. For example, most peak wheels loads for all measured NEC passenger trains, about 2.7 percent of all wheel loads, have a value of 17085 lbf (76 kN). The right hand axis corresponds to the dotted lines and represents the percent exceedance metric of wheel loads.

Most wheel loads for the Acela passenger cars ranged from 11240 to 22480 lbf (50 to 100 kN), with the power cars representing loads above 22480 lbf (100 kN). A consistent wheel load distribution was expected because the high-speed passenger cars were of similar weights. The freight load distribution was split, with most of the peak wheel loads either ranging from 44961 to 11240 lbf (20 to 50 kN) for unloaded or partially loaded cars, or 247289 to 382175 lbf (110 to 170 kN) for loaded cars.

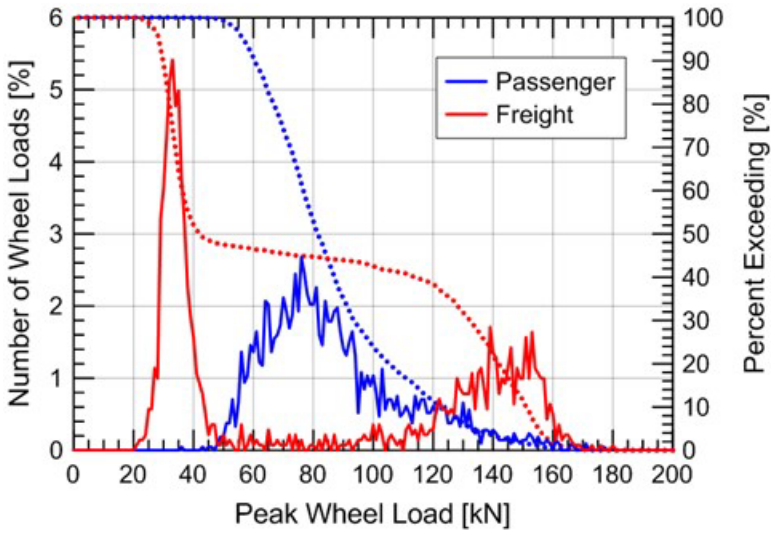

Figure 37. Comparison of peak wheel load distributions for passenger and freight wheel loads

While the static loads of the loaded freight cars were larger than the passenger trains, the fast-moving passenger trains (110 mph) produced a dynamic load like that of the slow-moving freight trains (25 mph).

4.3 Summary of Wheel Loads

In summary, recorded wheel loads can change at different locations along a section of track for the same train. For example, at both bridge approach sites along the NEC (i.e., Upland (15 ft) and Madison (12 ft)), the recorded peak wheel load of a specific wheel was consistently greater than its open-track counterparts (i.e., Upland (60 ft) and Madison (60 ft)). Uneven rail heights also can cause differences in recorded wheel loads, such as Caldwell (West) having consistently higher wheel loads than Caldwell (East).

Both passenger and freight wheel loads had similar peak magnitudes, while freight trains had a wider variation of wheel loads compared to passenger trains. The similar peak wheel load between passenger and freight traffic occurred because the lighter high-speed passenger trains produce dynamic loads that are comparable to those generated by the heavier slower-speed freight trains.

4.4 Tie Reaction

Tie reaction is the amount of load carried by the tie and is indicative of the quality of tie support. Tie reaction is calculated by subtracting the wheel load measured by the strain gages above the tie from the wheel load measured by the strain gages above the crib, as shown below. It was assumed that the load measured above the crib was the actual wheel load, which was usually greater than the tie load because the tie was not rigidly supported. The tie reaction is calculated using the following expression:

$$Tie\ Reaction = Load\ above\ crib - Load\ above\ tie$$

The ratio of tie reaction and wheel load gives insight into how well the tie is supported along with an estimate of the load being passed from the rail to the tie, ballast, and subgrade.

This section provides an explanation of tie reaction for the Amtrak and NS measurements. If a perfectly rigid tie lies on a perfectly rigid foundation, 100 percent of the train load will be transferred from the rail to the tie directly below the wheel. Conversely, if the tie is not in contact with an underlying layer, 0 percent of the train load will be transferred from the rail to the tie because the tie is unsupported. AREMA (2013) and Chang et al. (1980) suggest that good tie support will distribute around 40 percent of the wheel load to the tie when the train is directly above it. A similar percentage of wheel load was calculated using the numerical modeling discussed in subsequent sections. The load distribution will not equal 100 percent because the actual tie and ballast foundation do not form a perfectly rigid system.

Figure 38 and Figure 39 compare the measured wheel load above the crib and tie for Upland (60 ft) and Upland (15 ft), respectively, on 7 August 2012. Because the peak measured loads above the crib and tie were different at Upland (60 ft) but similar at Upland (15 ft), the team postulated that Upland (60 ft) was experiencing good tie support while Upland (15 ft) was experiencing poor tie support.

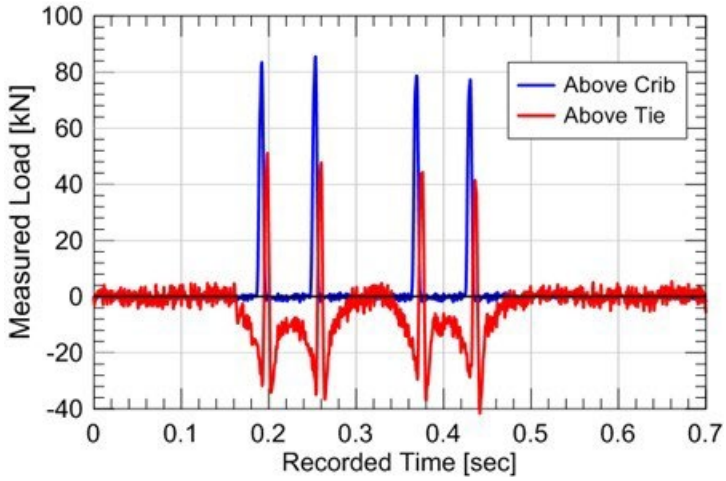

Figure 38. Measured wheel load at Upland (60 ft) on 7 August 2012 showing good tie support

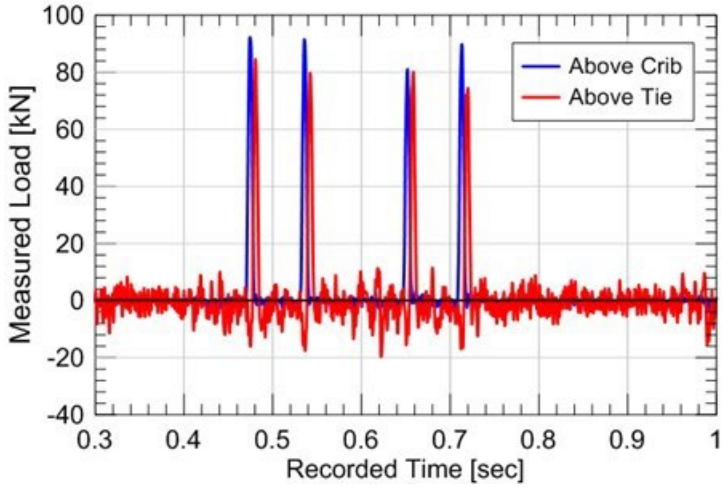

Figure 39. Measured wheel load at Upland (15 ft) on 7 August 2012 showing poor tie support

To facilitate interpretation of Figure 38 and Figure 39, the wheel load recorded above the crib and tie were obtained by measuring the amount of rail bending at each location under the applied loading and converting the rail bending to applied load using the calibration factor developed using the calibration load frame shown in Figure 28.

Therefore, if the tie is perfectly supported (i.e., a rigid tie on a rigid foundation), no rail bending will occur and, therefore, no load is measured above the tie. This leads to a tie reaction equal to the crib bending and wheel load (i.e., 100 percent). If the tie is completely unsupported, the rail should experience identical bending over the tie as it experiences over the crib, leading to equal wheel load values. As a result, the calculated tie reaction is zero because there is no difference between the crib and tie wheel loads. However, it is possible that an initially unsupported tie eventually contacts the ballast and transfers load during train passage. This implies that forces (e.g., momentum of the unsupported tie) can exist but will not be measured by the strain gages on the rail. This led researchers to believe tie reaction may not be representative of tie loading for unsupported ties because impact and momentum forces are not measured at the bottom of the tie.

To illustrate the difference between good and poor tie support, the tie reaction is plotted with time at Upland (60 ft) and Upland (15 ft) on 7 August 2012 in Figure 40 and Figure 41, respectively. The figures show significantly different tie reaction behavior. For example, at Upland (60 ft), four tie reaction load peaks were present, each of which equaling about 40 percent of the peak wheel load measured in the crib. This indicates good tie support and agrees with data presented by Chang et al. (1980) and numerical modeling discussed below. At Upland (15 ft), the four tie reaction load peaks are not easily distinguished from the surrounding data and all the tie reactions values were less than 30 percent, indicating poor tie support. The low-to-negative tie reaction values indicate poor tie support because the rail bending above the tie was equal to or greater than the rail bending measured above the crib.

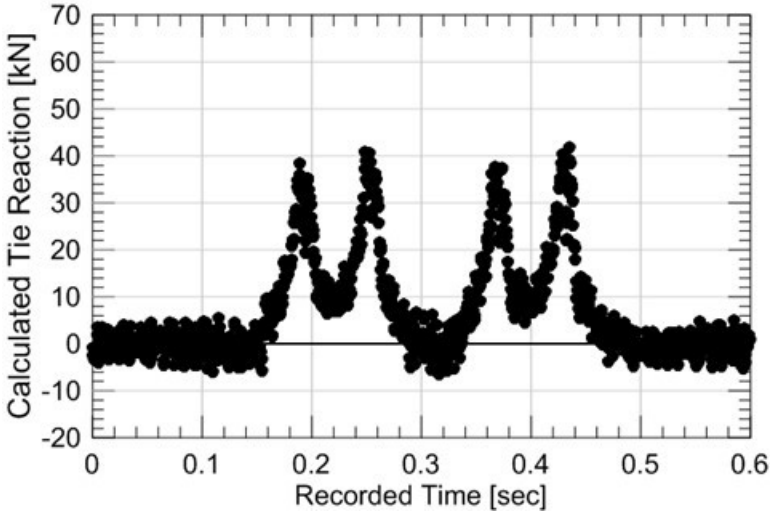

Figure 40. Tie reaction loading at Upland (60 ft) on 7 August 2012 showing good tie support

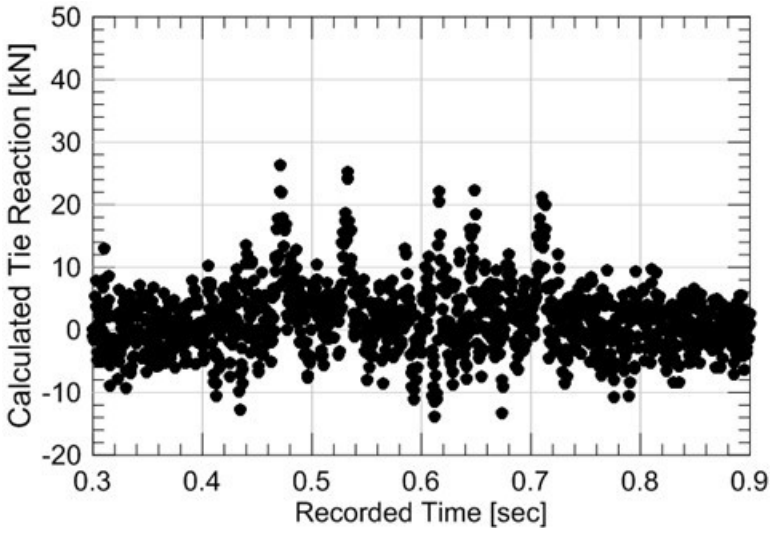

Figure 41. Tie reaction loading at Upland (15 ft) on 7 August 2012 showing poor tie support

4.4.1 Tie Load Ratio

Researchers developed the term "tie load ratio" to quantify the quality of tie support. This is the ratio between the peak measured tie reaction and peak measured wheel load in the crib. A value of 100 percent indicates full and rigid tie support while 0 percent indicates no support.

$$Tie\ Load\ Ratio = \frac{Tie\ Reaction}{Wheel\ Load} = \frac{Load\ above\ crib - Load\ above\ tie}{Load\ above\ crib}$$

Figure 42 through Figure 47 show the tie load ratio at the six Amtrak NEC instrumented locations for each measured passing wheel. Each plot has a green line at 40 percent to indicate the value corresponding to good tie support. Table 7 displays the average tie load ratio at each NEC site. The average tie load ratio was calculated from all passing wheels at a particular site. From the data in Figure 42 through Figure 47 and Table 7, the team made the following observations of track behavior:

- The tie load ratios correspond with permanent vertical displacement levels. For example, Upland (60 ft), which experienced the least amount of permanent vertical displacement, showed the best tie support, and had an average tie load ratio of 44 percent. Conversely, Upland (15 ft), which experienced the greatest amount of permanent vertical displacement, showed the worst tie support, and had an average tie load ratio of only 3 percent. The other sites had average tie load ratios between these two extremes.
- The average tie load ratios presented in Figure 42 through Figure 47 show tie support can be inconsistent during the passing of a single train. While the data show a lack of support at low values, the high tie load ratio (60 percent) at large wheel loads can result in higher average tie load ratios (see Table 7) even though the tie was not experiencing good support. As a result, the average tie load ratio may not be a suitable parameter to assess tie support.

- A wide range of tie load ratios were observed in the data from 0 to greater than 60 percent. This range and variation of tie load ratio from one wheel to another in the same train implies that wheel loads were being distributed in an inconsistent manner between adjacent ties. These erratic tie load ratios within the same train pass can be attributed to poor tie support at the instrumented and surrounding ties, as well as damaged ties. If adjacent ties have poor tie support or are damaged, a redistribution of load occurs, and the surrounding ties will experience higher loads. If support conditions change during the passing of a train (e.g., development of pore-water pressures in wet fouled ballast), this load redistribution also will change.

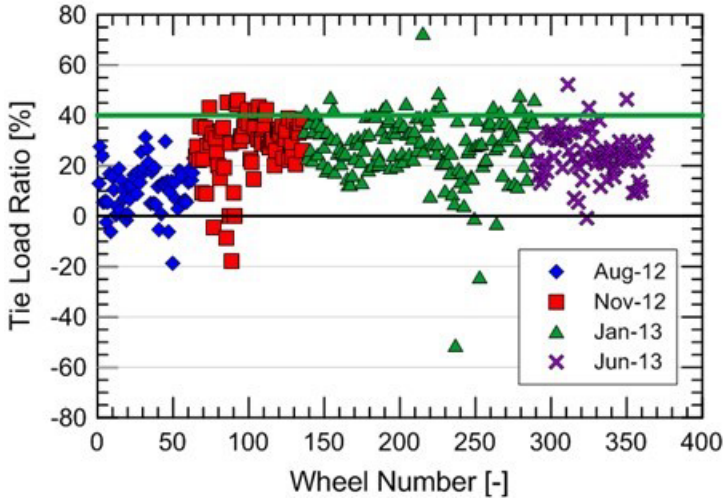

Figure 42. Tie load ratio at Caldwell (East) for each passing wheel

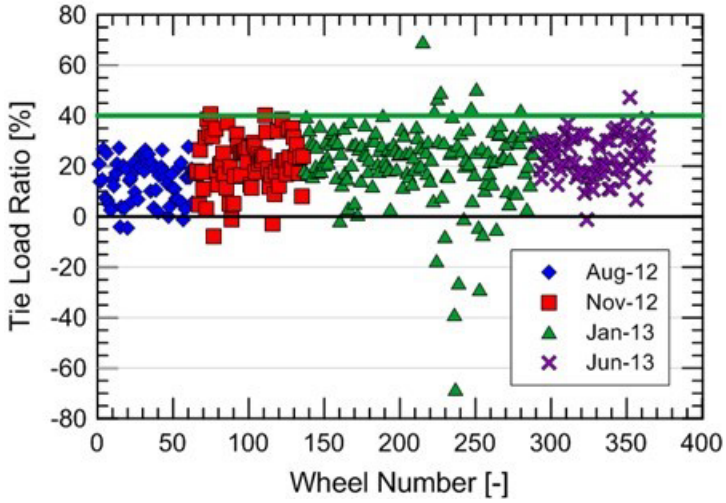

Figure 43. Tie load ratio at Caldwell (West) for each passing wheel

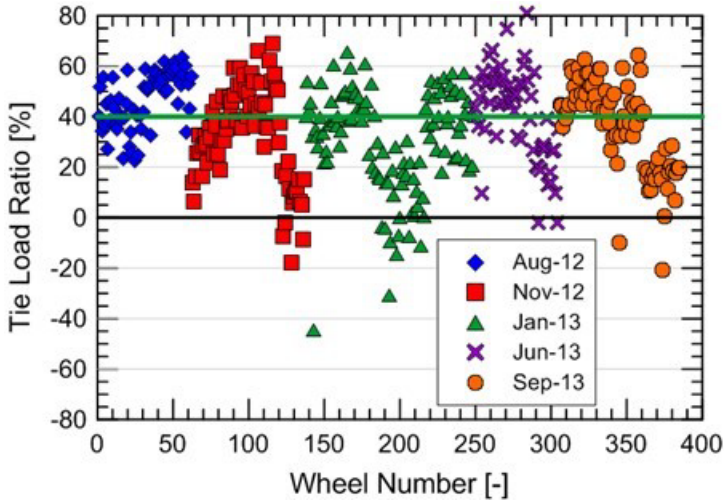

Figure 44. Tie load ratio at Madison (12 ft) for each passing wheel

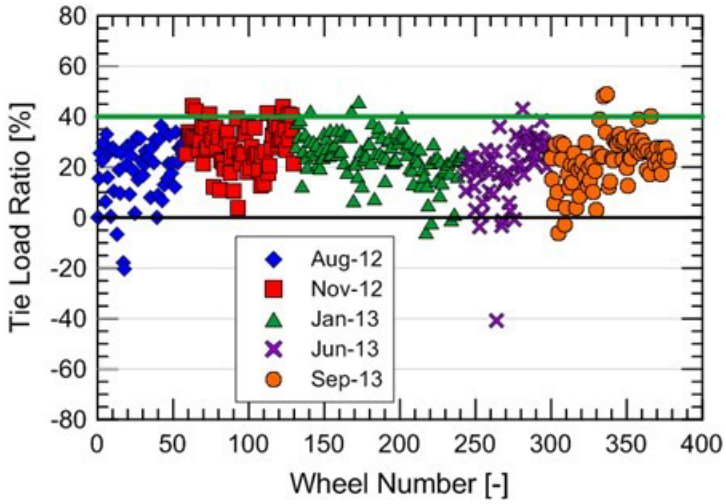

Figure 45. Tie load ratio at Madison (60 ft) for each passing wheel

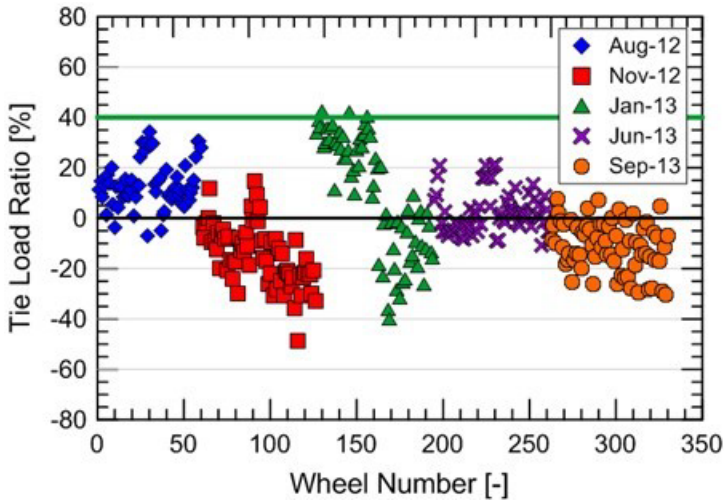

Figure 46. Tie load ratio at Upland (15 ft) for each passing wheel

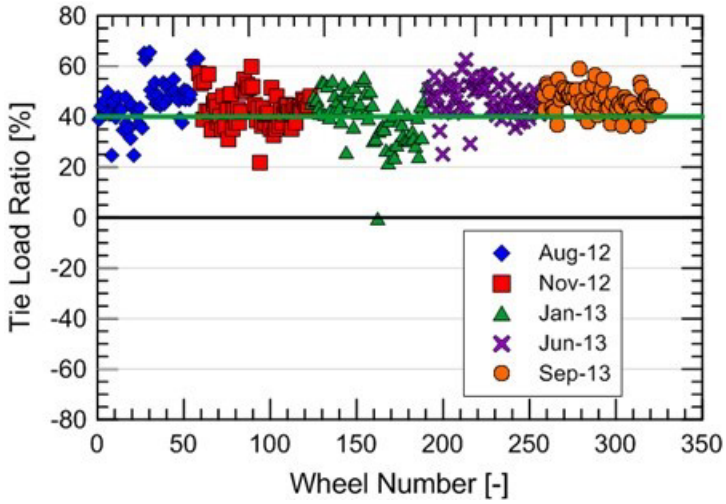

Figure 47. Tie load ratio at Upland (60 ft) for each passing wheel

Table 7. Average tie load ratio at the six Amtrak NEC sites

Caldwell		Madison		Upland	
East	West	12 ft.	60 ft.	15 ft.	60 ft.
24%	21%	36%	23%	3%	44%

Negative tie load ratios are explained by defects in wheels, damage to rails, or wheel bouncing. These conditions resulted in higher wheel loads over the tie than the crib. However, with wheel defects, the negative tie load should be random and infrequent. At Madison Street (12 ft) and Upland Avenue (15 ft), the negative tie load ratios were consistent. Therefore, negative tie load ratios at this location are attributed to wheel bouncing from broken or damaged ties near the instrumented tie. This could result in consistently greater rail bending above the tie.

The tie load ratios of each passing wheel load at NS bridges MP 352.2 (31 ft), MP 352.2 (13 ft), MP 352.8 (29 ft), and MP 352.8 (11 ft) are shown in Figure 48 through Figure 51, respectively. MP 352.2 (31 ft) in Figure 48 displays consistent tie load ratios, ranging from 40 to 50 percent, as does Upland (60 ft). This indicates good tie support. However, MP 352.2 (13 ft) in Figure 49, MP 352.8 (29 ft) in Figure 50, and MP 352.8 (11 ft) in Figure 51 display wider ranges of tie load ratio, which indicate poor tie support.

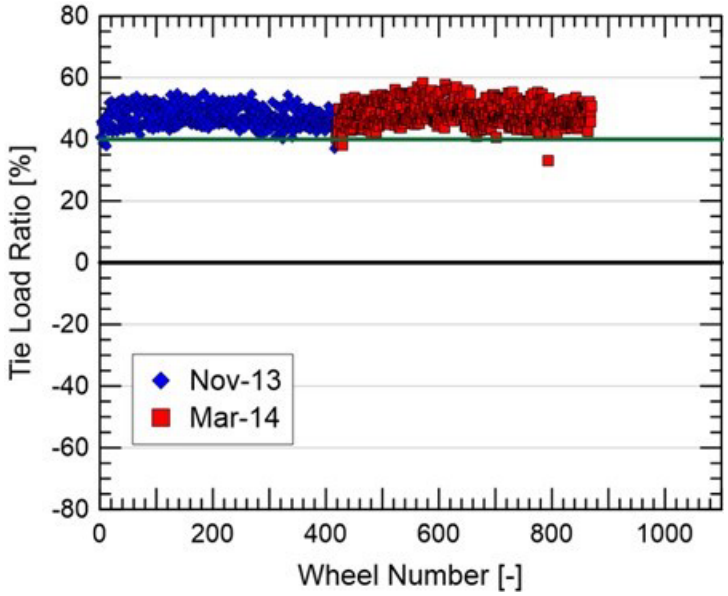

Figure 48. Tie load ratio at NS bridge MP 352.2 (31 ft) for each passing wheel

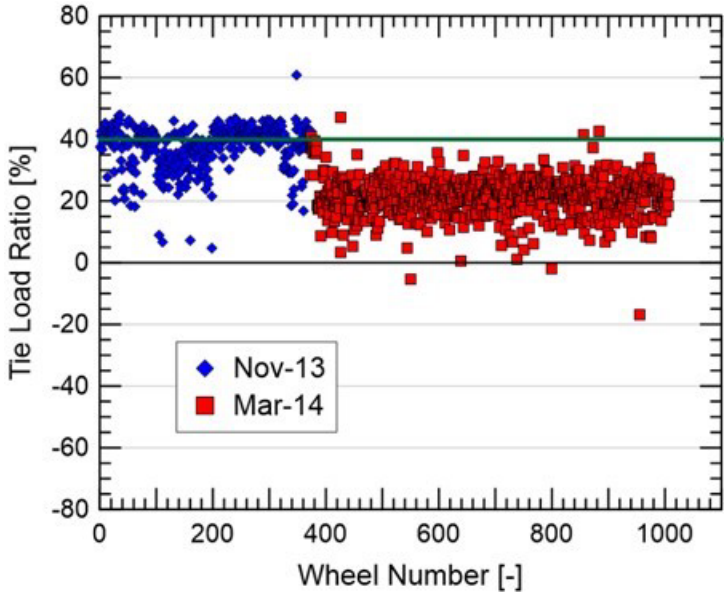

Figure 49. Tie load ratio at NS bridge MP 352.2 (13 ft) for each passing wheel

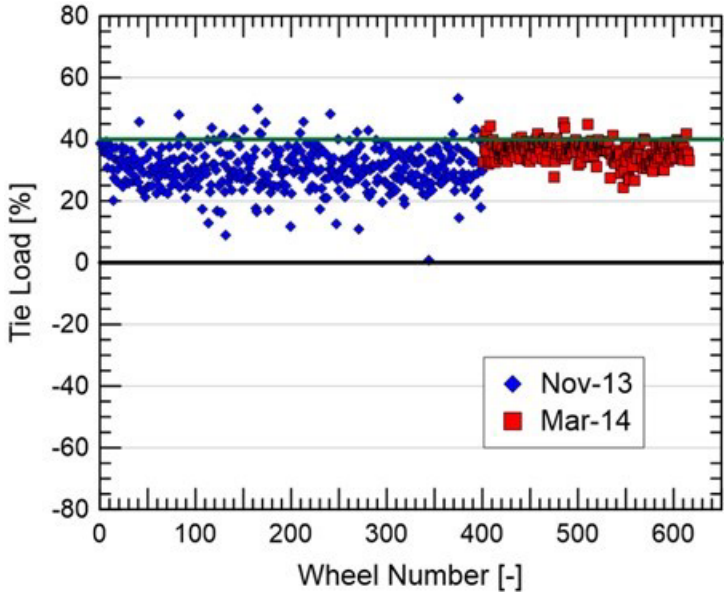

Figure 50. Tie load ratio at NS bridge MP352.8 (29 ft) for each passing wheel

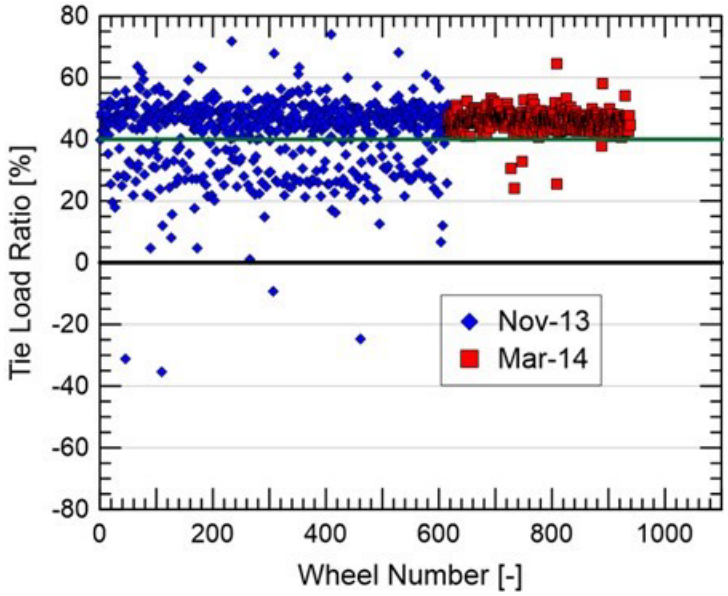

Figure 51. Tie load ratio at NS bridge MP352.8 (11 ft) for each passing wheel

Table 8. Average tie load ratio at the NS bridge instrumentation sites

MP 352.2		MP 352.8	
13 ft.	**31 ft.**	**11 ft.**	**29 ft.**
27.4%	47.9%	43.5%	32.4%

4.5 Combined Tie Load Ratio and Wheel Load

Another method to identify the quality of tie support is to plot tie load ratio as a function of wheel load. Good tie support is characterized by a constant tie load ratio with increasing wheel load. Conversely, if the tie load ratio is initially low and increases with increasing wheel load, this indicates poor tie support at low wheel loads and a closing of the tie-ballast gap as the wheel load increases. Figure 52 through Figure 57 show the comparison of tie load ratio and wheel load at all six NEC instrumented sites. The green line at a tie load ratio of 40 percent in each of these figures is indicative of a well-supported tie.

Figure 52 and Figure 53 show relatively good tie support because the tie load ratio was relatively constant with increasing wheel load. Comparing the tie load ratio with applied wheel loads shows that Madison (12 ft) and Upland (15 ft) display poor tie support behavior (i.e., have a tie-ballast gap) in Figure 54 and Figure 55, respectively. For example, Figure 54 shows initially low tie load ratios at low wheel loads and increasing tie load ratio with increasing wheel loads. The other four sites displayed constant tie loads with increasing wheel loads, implying good or consistent support behavior.

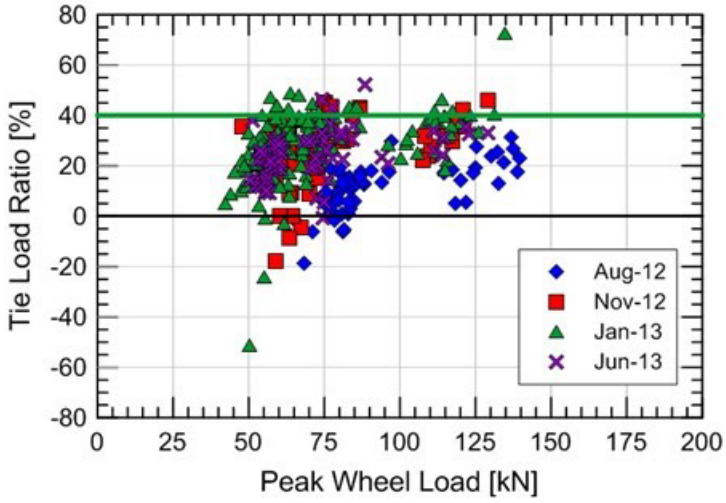

Figure 52. Comparison between tie load ratio and wheel load at Caldwell (East)

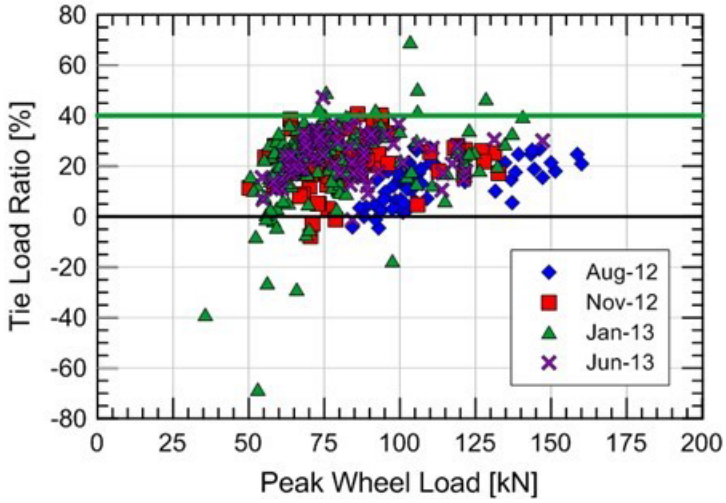

Figure 53. Comparison between tie load ratio and wheel load at Caldwell (West)

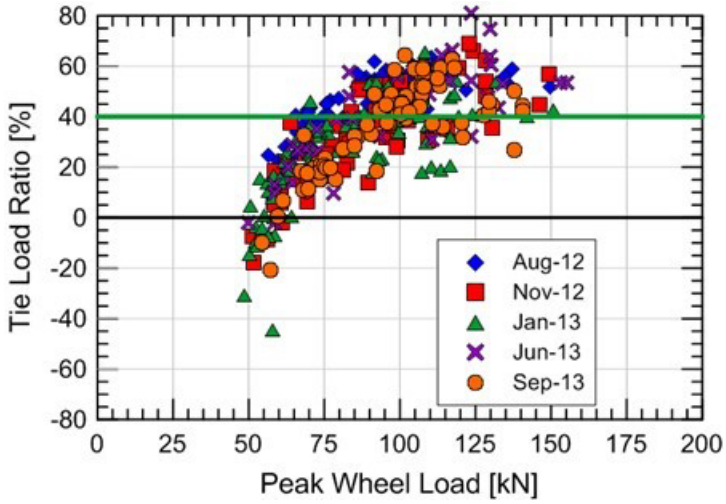

Figure 54. Comparison between tie load ratio and wheel load at Madison (12 ft)

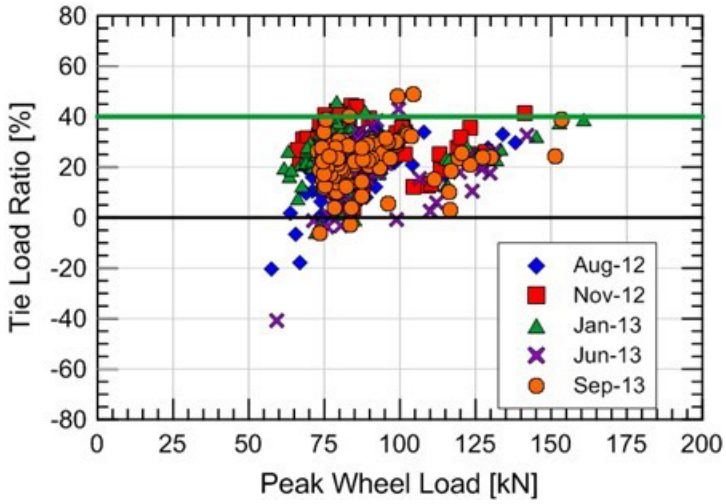

Figure 55. Comparison between tie load ratio and wheel load at Madison (60 ft)

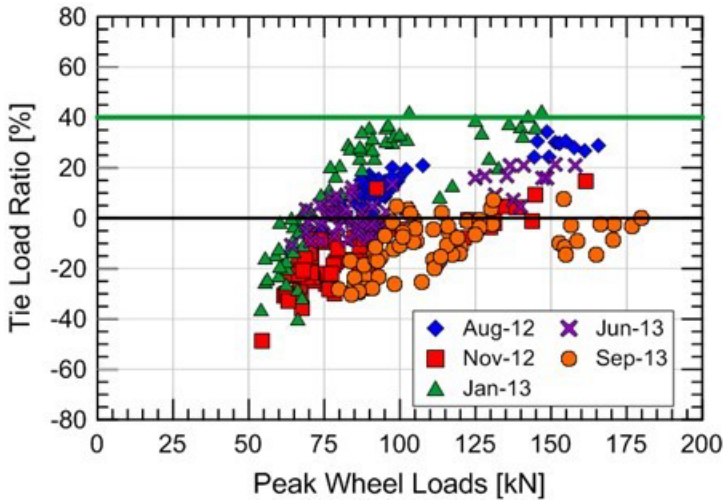

Figure 56. Comparison between tie load ratio and wheel load at Upland (15 ft)

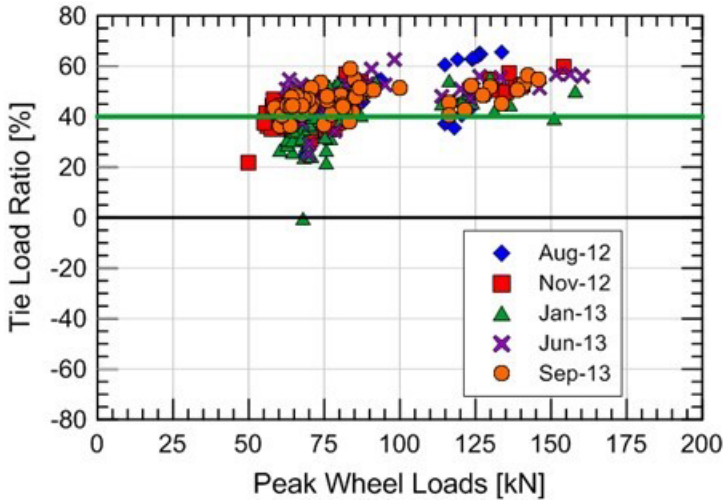

Figure 57. Comparison between tie load ratio and wheel load at Upland (60 ft)

While it was expected that Upland (15 ft) would display poor tie support at low wheel loads (see Figure 56), the team was surprised that Madison (12 ft) showed poor tie support at low wheel loads while also displaying good tie support at high wheel loads (see Figure 54). In summary, large changes in tie load ratio with increasing wheel loads can be an indicator of poor tie support.

Figure 58 through Figure 61 compare the tie load ratio for the corresponding wheel load at the NS bridge sites. At MP 352.2 (31 ft) (see Figure 58), the results showed good support, but the passing train consisted of only fully loaded freight cars so it could not be determined whether the tie was poorly supported at low wheel loads. At bridge MP 352.2 (13 ft) (see Figure 59), the tie load ratio increased with increasing wheel loads, indicating possible unsupported behavior. After a wheel load of about 11240 lbf (50 kN), the tie load ratio remained about constant with the increasing wheel load. This implies that this load level was required for the tie to establish contact with the ballast. After closing the tie-ballast gap, the load resistance of the ballast was mobilized, and the load was supported. As a result, this wheel load is referred to as a seating load, which closes the tie-ballast gap and seats the tie on the top of the ballast.

The passing train at NS bridge MP 352.8 (29 ft) and (11 ft) (see Figure 60 and Figure 61) consisted of unloaded cars, so the majority of data lie below the tie seating load of about 11240 lbf (50 kN). This explains the wide range and inconsistent tie load ratios shown in Figure 61. However, the recorded loads above 22480 lbf (100 kN) showed good tie support at both MP 352.8 bridge sites.

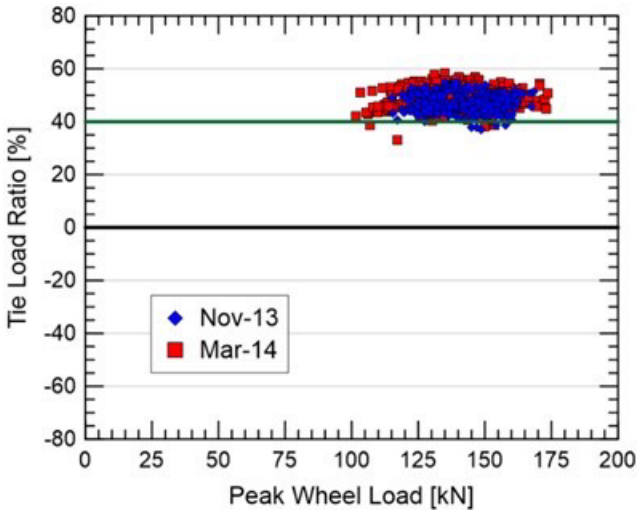

Figure 58. Comparison between tie load ratio and wheel load at NS bridge MP 352.2 (31 ft)

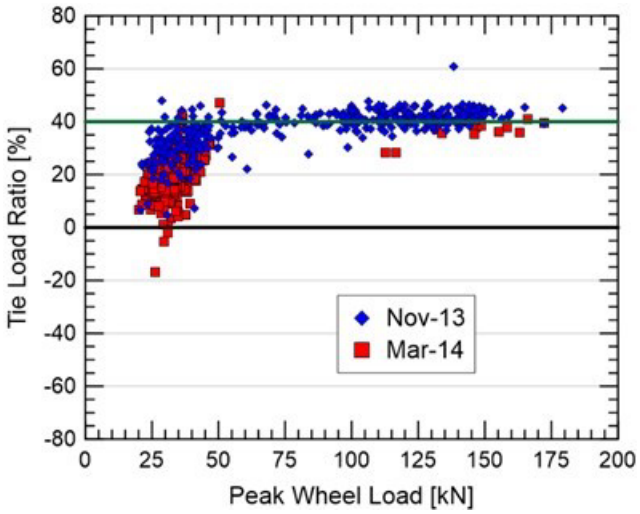

Figure 59. Comparison between tie load ratio and wheel load at NS bridge MP 352.2 (13 ft)

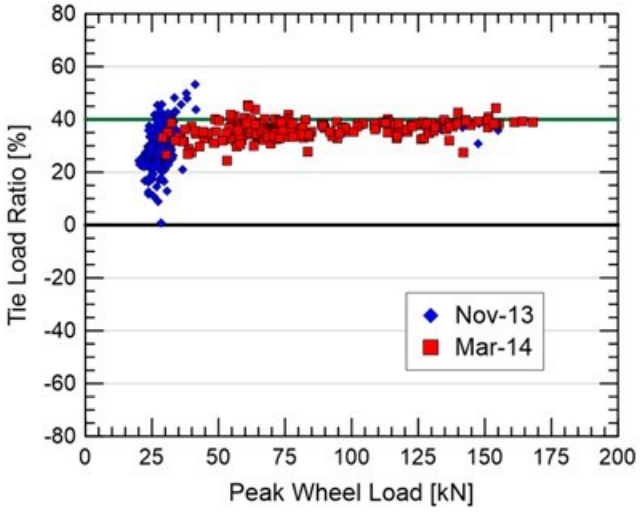

Figure 60. Comparison between tie load ratio and wheel load at NS bridge MP 352.8 (29 ft)

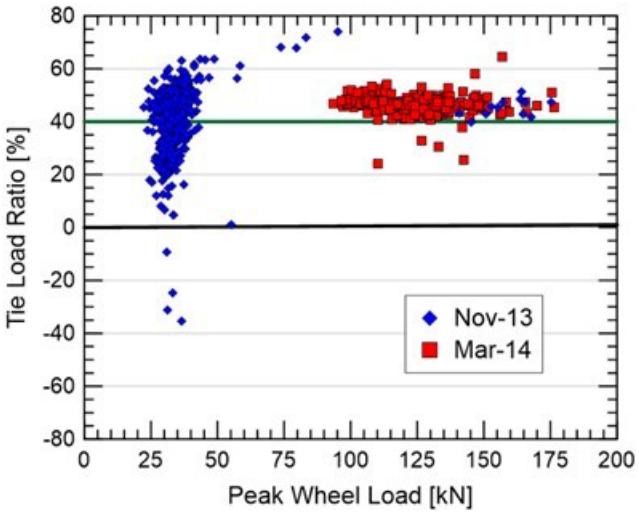

Figure 61. Comparison between tie load ratio and wheel load at NS bridge MP 352.8 (11 ft)

4.6 Summary

Tie reaction and tie load ratio can be used to estimate the quality of tie support and the load being applied to the tie. At Amtrak's NEC sites, the two instrumentation sites displaying poor tie support (i.e., Upland (15 ft) and Madison (12 ft)) also displayed the highest permanent vertical displacements. Conversely, Upland (60 ft) displayed the best tie support and experienced the lowest permanent vertical displacement. Therefore, tie support played an important role in determining and explaining the root cause of the measured permanent vertical displacements at these locations.

At the NS sites, the wide range in measured wheel loads made it difficult to compare tie support between these sites. However, the tie load ratio versus wheel load data suggested better support conditions at MP 352.8 (29 ft) and MP 352.2 (31 ft) compared to MP 352.2 (13 ft) and MP 352.8 (11 ft).

5. Subsequent Field Investigations

Researchers made two visits to Amtrak's NEC instrumentation sites to assess the condition of the track and transition zones. The main observations the team took from the visits were: (1) damaged ties, (2) standing water in the ballast layer, (3) poor ballast drainage, and (4) abutment and masonry wall leakage near the transition zone (i.e., locations of large measured permanent vertical displacements).

5.1 Tie Condition

Damaged ties are an important consideration during data analysis because they influence the load distributed to the tie and the load transferred to the ballast. If a tie is damaged (e.g., missing, broken, or hanging), a redistribution of load occurs from the damaged tie to adjacent ties. This may overload the adjacent ties, leading to more damaged ties and the further redistribution of load to adjacent ties. Impact loads and wheel bouncing are other potential consequences of damaged ties because of the transient vertical displacement required to mobilize some tie supports. Figure 62 and Figure 63 show damaged ties around the instrumentation locations of Madison (12 ft) and Upland (15 ft), respectively, which experienced the largest measured permanent vertical displacements during this study.

Figure 62. Damaged tie to the left of the MDD instrumentation location (see red arrow) at Madison (12 ft) on 4 September 2013

Figure 63. Photo of two damaged ties near the Upland (15 ft) instrumentation location (red arrows) (Damaged ties are three ties to the left and one tie to the right of the instrumented tie)

Damaged ties surrounding the Madison (12 ft) and Upland (15 ft) sites increased the load on the instrumented tie, and became a factor in the large, permanent, vertical displacements measured at these sites. The ties around the open-track sites (i.e., Upland (60 ft), Madison (60 ft), and Caldwell (80 ft)) did not show as much tie damage. Tie loads were larger at track transition locations, resulting in greater tie damage.

Videos taken of passing trains within the Madison (12 ft) transition zone showed the effect of poor tie-ballast contact by recording large vertical tie displacements and rebounding. As the train passed, the ties moved up and down, possibly hitting the ballast, and then rebounding due to the stiffness of the rail. Proper contact did not exist at the tie-ballast interface. This tie-ballast gap must be closed before the ballast can resist the applied load. In addition, the amount of transient vertical movement varied from tie to tie and within the same section of track. This suggests that tie support can vary significantly between adjacent ties and at opposite ends of the same tie.

5.2 Drainage Conditions

Poor drainage conditions can lead to a decrease in stiffness and shear strength of the ballast and increased ballast fouling, ballast erosion, and mud pumping. For example, laboratory ballast box studies by Han and Selig (1997) measured a significant increase in ballast settlement when the ballast was wet and fouled. This suggests the track displaying wet fouled ballast may settle at greater rates than track displaying clean ballast, even under identical load conditions.

Figure 64(a) shows water splashed up on the side of a tie near Madison (12 ft), and Figure 64(b) shows water ponded near the bottom of this concrete tie on 4 September 2013. Figure 65 shows mud covering the ballast and several ties near Madison (12 ft). Figure 66(a) shows seepage of water out of the abutment at the Upland bridge, and Figure 66(b) shows seepage from the north-

south trending wall north of the Upland Avenue bridge near Upland (15ft). Some seepage from the abutment wall was also observed at the bridges near the Upland (15 ft) and Madison (12 ft) instrumentation sites. Water was observed flowing from the masonry wall shortly after a precipitation event in January 2013 and splashing on ties from the ballast during train passage in January 2013.

In summary, the poor drainage and fouling observed at the transition zone locations (e.g., Upland (15 ft) and Madison (12 ft)) may be contributors to the increased permanent vertical displacements in those areas.

(a)

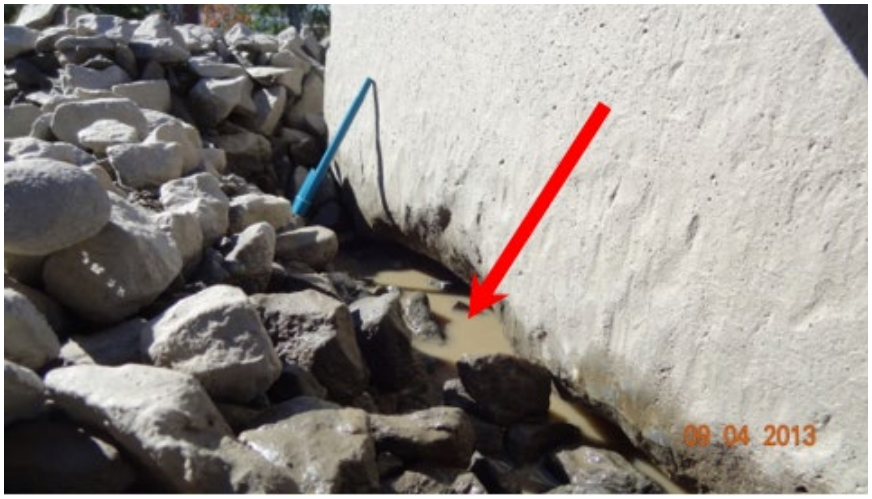

(b)

Figure 64. Water collecting (a) on and (b) below (see red arrow and blue pen for scale) concrete tie on 4 September 2013

Figure 65. Fouling material covering ballast and concrete ties on Track 1 at Madison (12 ft) on 4 September 2013

(a) **(b)**

Figure 66. Water seeping from (a) masonry abutment wall under Upland Avenue bridge and (b) north-south trending masonry wall north of Upland Avenue bridge on 8 August 2013

6. Measured Transient Vertical Displacements from LVDTs

This section presents an analysis of the transient vertical displacements measured at the Amtrak and NS sites.

6.1 Substructure Behavior to Transient Loads

Figure 67 shows a typical set of wheel loads and the corresponding measured LVDT transient vertical displacements from a passing Acela high-speed passenger train. The dataset was measured at Upland (60 ft) on 7 August 2012 at 10:17 AM EDT and showed that the transient response of the LVDTs matched the wheel loads for the entire train. As each wheel passed over the instrumented tie, the loaded tie displaced the underlying LVDTs.

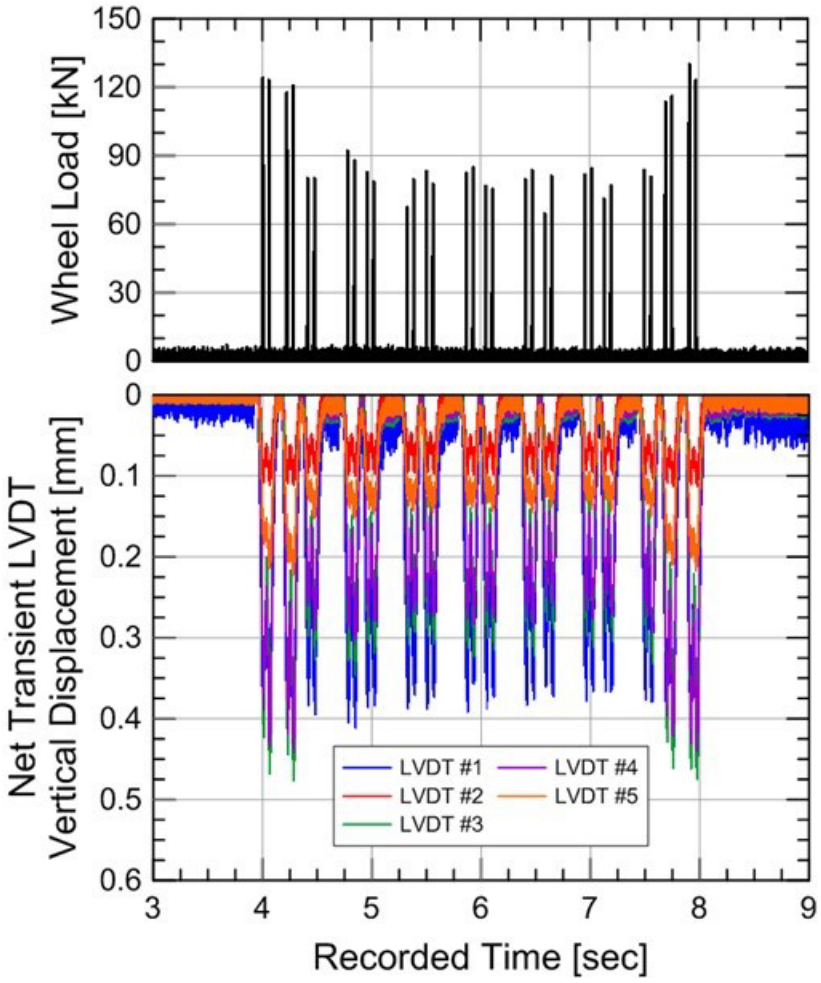

Figure 67. Measured wheel loads and corresponding net transient vertical displacements at Upland (60 ft) on 7 August 2013 at 10:17 a.m.

Figure 68 and Figure 69 focus on the transient displacement response from four wheel loads (i.e., a single car) of a passing high-speed Acela train at Upland (60 ft) and Upland (15 ft), respectively, on 7 August 2012 at 10:17 AM EDT. Figure 68 also includes the corresponding tie reaction time history for Upland (60 ft) (i.e., good tie support), which shows LVDT transient displacements occurred as the tie began experiencing load. Conversely, the tie reaction for

Upland (15 ft) in Figure 69 does not show simultaneous response because of a tie-ballast gap, (i.e., poor tie support).

Researchers chose Upland (60 ft) and Upland (15 ft) because they exhibited the smallest and largest amounts of permanent and transient vertical displacement, respectively, and large differences in transient vertical displacements. The vertical axes of Figure 68 and Figure 69 are scaled differently to emphasize the different behavior of these two sites. The transient vertical displacements measured at Madison (12 ft), Madison (60 ft), Caldwell (East), and Caldwell (West) are presented in Appendix B in Figures B.1 through B.4 for comparison purposes. Madison (12 ft) and Madison (60 ft) showed similar behavior as Upland (15 ft) and Upland (60 ft), respectively. The tie instrumented at Caldwell (East) and Caldwell (West) also showed good support because it was 80 ft from the bridge.

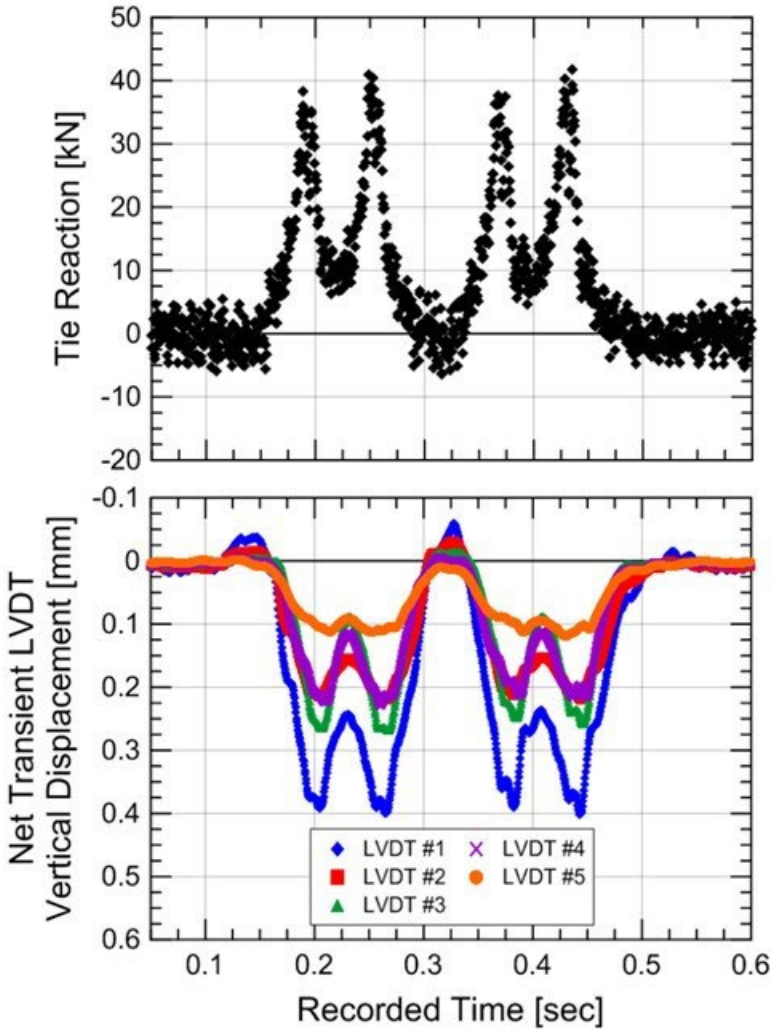

Figure 68. Tie reaction and net transient LVDT vertical displacement response at Upland (60 ft) on 7 August 2012

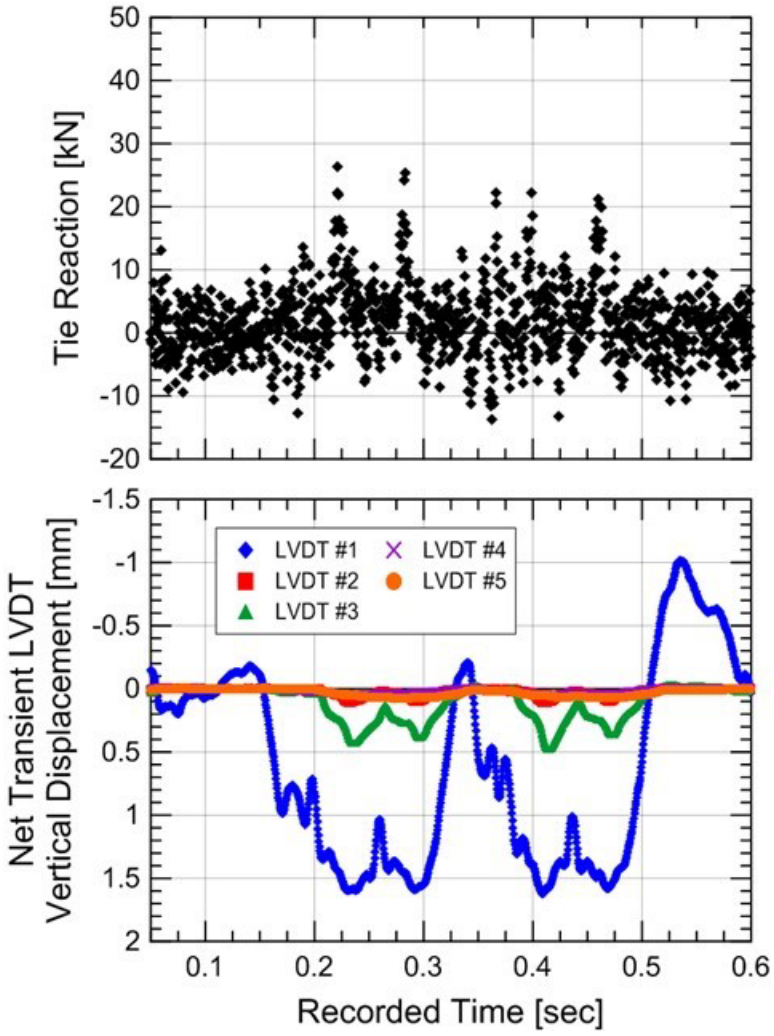

Figure 69. Tie reaction and net transient LVDT vertical displacement response at Upland (15 ft) on 7 August 2012

Figure 68 and Figure 69 show that as a passing wheels imparted load to the substructure, the underlying LVDTs displaced downwards. Eventually each LVDT reached a peak value of vertical displacement and then returned to or near its original position when unloaded. Due to the proximity of the wheels on the same truck (~ 9 ft), the substructure reloaded before reaching its original unloaded position resulting in two local peaks for each passing truck. This fundamental behavior was observed at both Upland (60 ft) (Figure 68) and Upland (15 ft) (Figure 69).

Many differences existed between the measured transient vertical displacements at the Upland (60 ft) and Upland (15 ft) sites.

1. The peak transient vertical displacement of LVDT 1 at Upland (60 ft) was much smaller than Upland (15 ft), 0.4 mm versus 1.5 mm, which is evident by comparing the different vertical axes in Figure 68 and Figure 69.
2. At Upland (60 ft), all five LVDTs displaced in unison. At Upland (15 ft) there was a delay in the load transfer from the tie to the underlying materials. The vertical

displacements for LVDTs 2 through 5 were recorded after LVDT 1 due to the tie-ballast gap at this site.

3. The vertical displacements in LVDT 1 were smooth at Upland (60 ft) and an erratic response was observed in LVDT 1 at Upland (15 ft), including a few "bumps" at a vertical displacement of 1 mm.
4. A significant amount of vertical rebound was measured at Upland (15 ft), while there appeared to be little to no rebound at Upland (60 ft) because of a smaller tie-ballast gap.

These observations indicated poor tie support at Upland (15 ft) and better tie support at Upland (60 ft). If the concrete tie was not in good contact with the underlying ballast, LVDT 1 would have experienced vertical displacement before the four underlying LVDTs responded. This delay was due to the tie having to establish contact with the underlying ballast before the deeper four LVDTs could be loaded and undergo vertical displacement. This is referred to subsequently as a seating load and resulted in larger measured transient vertical displacements in LVDT 1 than the underlying LVDTs. This implies the measured LVDT 1 transient vertical displacement may not equate to that of the ballast because LVDT 1's transient vertical displacement included the closure of a tie-ballast gap before ballast displacement could occur. Also, poor tie-ballast contact can give the tie freedom to move, explaining the erratic behavior and rebound observed at Upland (15 ft) in Figure 69.

The transient vertical displacements measured at Madison (12 ft), Madison (60 ft), Caldwell (East), and Caldwell (West) are presented in Appendix B in Figures B.1 through B.4, which show similar behavior. For example, transient vertical displacements showed good tie support for both Caldwell instrumentation sites and the Madison (60 ft) site – all of which were open track sites (i.e., not adjacent to bridge transitions). Conversely, the transient vertical displacements at Madison (12 ft) showed poor tie support and thus vertical displacements like those of Upland (15 ft) because of a tie-ballast gap.

Figure 70 and Figure 71 present transient data from NS bridges MP 352.2 (31 ft) and MP 352.2 (13 ft) sites near Bluefield, West Virginia. Figure 70 shows nine passing wheels at bridge MP 352.2 (31 ft) while Figure 71 shows eight passing wheels at bridge MP 352.2 (13 ft). As with Figure 68 and Figure 69 for Upland (60 ft) and (15 ft), respectively, the transient vertical displacement axes are scaled differently to emphasize the transient behavior. The corresponding measured wheel load time histories are also included in Figure 70 and Figure 71 for reference purposes.

Both the open track and the bridge transition measurements at NS bridge MP 352.2 displayed behavior like that of Upland (60 ft) and (15 ft). The transient vertical displacement responses for NS bridge MP 352.2 (31 ft) and (13 ft) were compared, as was those for Upland (60 ft) and (15 ft). The team noted the following differences:

1. The peak transient vertical displacement of LVDT 1 at MP 352.2 (31 ft) was much smaller than MP 352.2 (13 ft), 0.6 mm versus 3.8 mm, which is evident by comparing the different vertical axes and confirms poor tie support at MP 352.2 (13 ft).
2. At MP 352.2 (13 ft), all five LVDT transient vertical displacements began at the same time, while the vertical displacements for LVDTs 2 through 5 were delayed at MP 352.2 (31 ft), indicating the presence of a tie-ballast gap. This was another sign of poor tie support at MP 352.2 (13 ft).

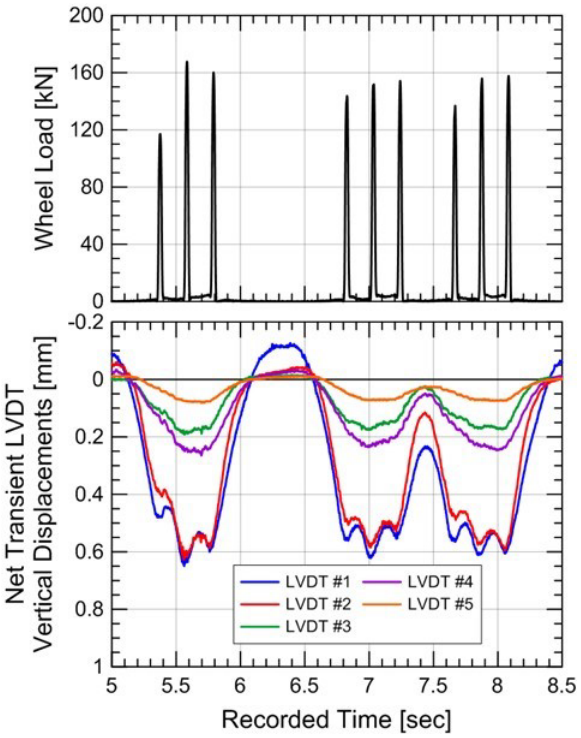

Figure 70. Net transient LVDT displacement response at NS bridge MP 352.2 (31 ft) on 2 November 2013

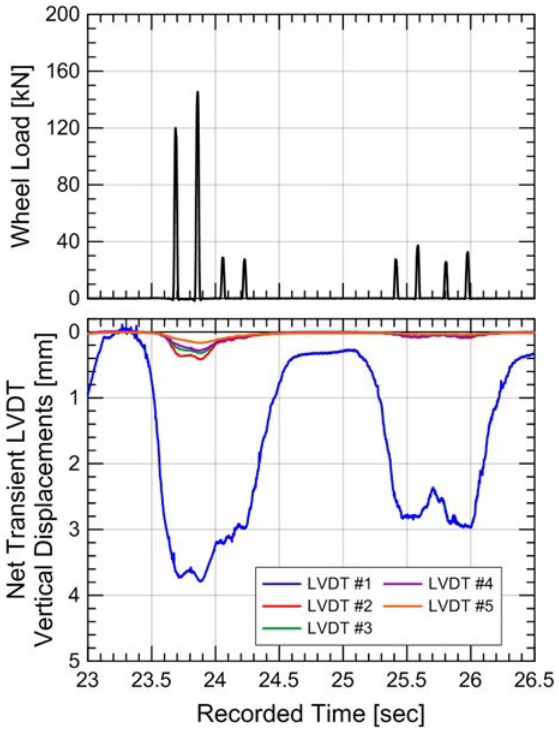

Figure 71. Net transient LVDT displacement response at NS bridge MP 352.2 (13 ft) on 2 November 2013

Researchers observed the differences in transient response between the high-speed passenger trains and slow-moving freight trains by comparing the Amtrak and NS data. These differences are summarized below:

1. The greater depth of LVDTs 3-5 at NS bridge MP 352.2 sites resulted in a single peak displacement for a group of three or four passing wheels instead of the single peak per passing wheel observed at the NEC sites. This reduced response with depth was due to stress distribution with depth.
2. Despite unsupported behavior at NS bridge MP 352.2 (13 ft), LVDT 1 did not display erratic behavior or rebound after a passing wheel set. This was likely due to the slower velocity of the passing freight wheels compared to Amtrak.

6.1.1 Summary of Substructure Behavior

Comparing the open track and bridge approach transient displacement time histories at selected Amtrak and NS instrumentation sites (e.g., Upland Avenue and NS bridge MP 352.2) showed a difference between supported and unsupported tie behavior. Unsupported ties at the bridge approach displayed much larger peak transient LVDT 1 displacement and a delay in response time between LVDT 1 and 2, as the tie-ballast gap closed with the applied load.

The team also observed a difference in unsupported tie behavior of high-speed passenger and slow-moving freight trains. The higher-velocity trains of the Amtrak NEC showed a more erratic transient LVDT 1 displacement response and rapid rebound after wheel passage than the NS freight trains. This implied that damage and unwanted movement was amplified as train velocity increased.

6.2 LVDT Transient Vertical Displacements

To gain an understanding of the depth and site locations at which the majority of the transient vertical displacement occurred, the maximum transient vertical displacement of each LVDT was recorded and compared in Figure 72 through Figure 80 for each passing wheel. The y-axes in the figures are scaled differently to emphasize which LVDTs experienced the largest transient vertical displacement at each instrumented site. In each plot, the data are separated by month recorded (e.g., August 2012, November 2012, January 2013, and June 2013). Due to calibration issues, the data for LVDT 2 during the January 2013 recording of Madison (12 ft) is not included in Figure 74.

Comparing transient vertical displacement trends in Figure 72 through Figure 80 illustrates the different responses between sites experiencing good and poor tie support. For example, Figure 72 and Figure 73 present the net transient vertical displacements for all subsurface LVDTs at Upland (15 ft) and (60 ft), respectively. Field data suggested that Upland (15 ft) displayed poor tie support while Upland (60 ft) showed good tie support, which is also reflected in the transient vertical displacements. Figure 72 (Upland 15 ft) shows only LVDT 1 undergoing significant transient vertical displacement. Conversely, Figure 73 (Upland 60 ft) shows similar transient vertical displacements in LVDTs 1, 3, and 4. This implied that large transient LVDT 1 vertical displacement indicate poor tie support.

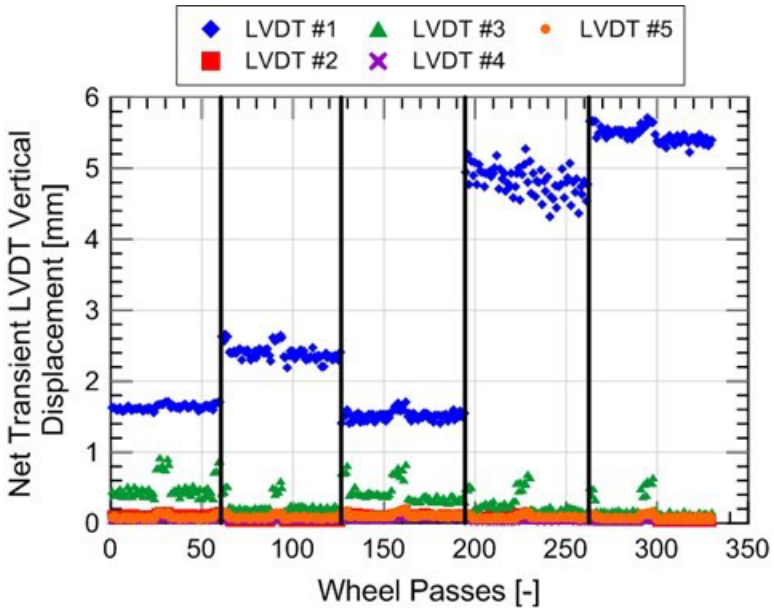

Figure 72. Comparison of net transient vertical displacements for all subsurface LVDTs at Upland (15 ft) for each passing wheel

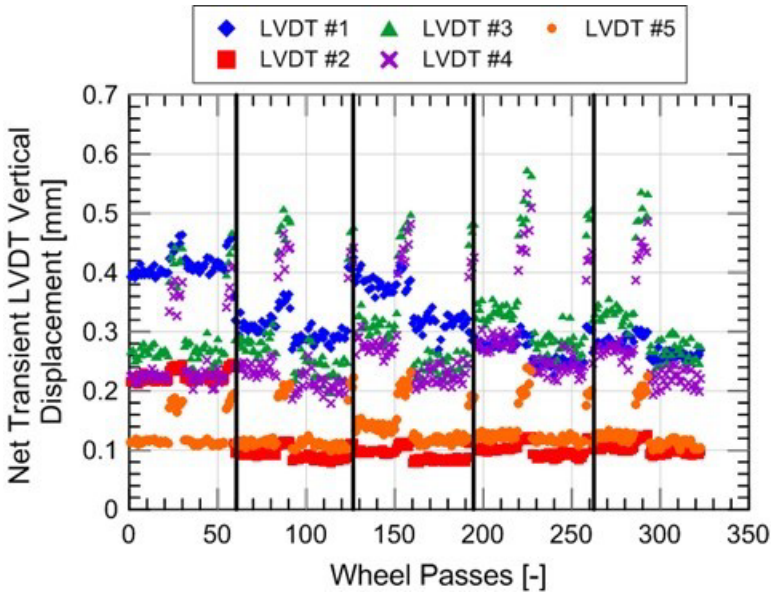

Figure 73. Comparison of net transient vertical displacements for all subsurface LVDTs at Upland (60 ft) for each passing wheel

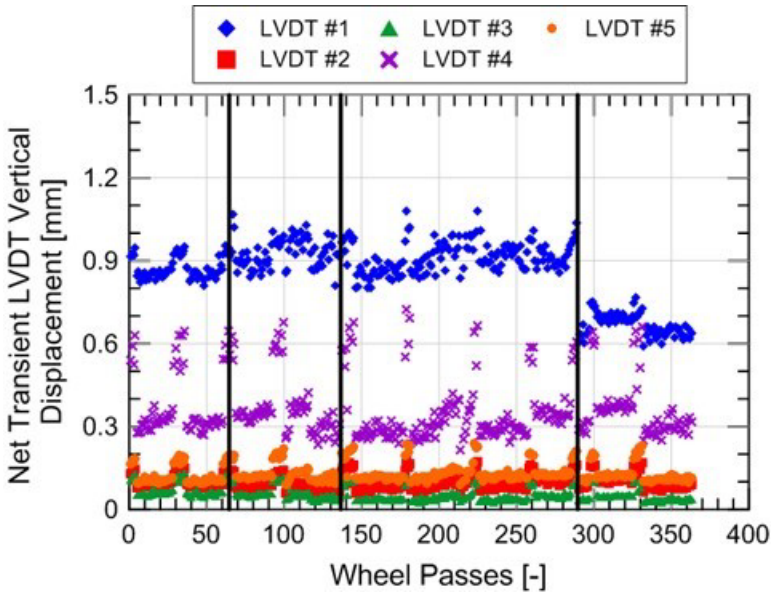

Figure 74. Comparison of net transient vertical displacements for all subsurface LVDTs at Caldwell (east) for each passing wheel

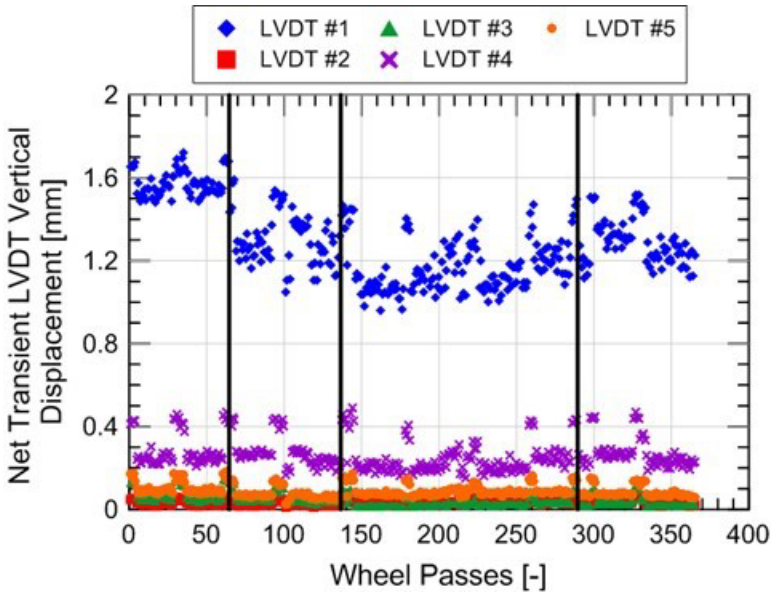

Figure 75. Comparison of net transient vertical displacements for all subsurface LVDTs at Caldwell (east) for each passing wheel

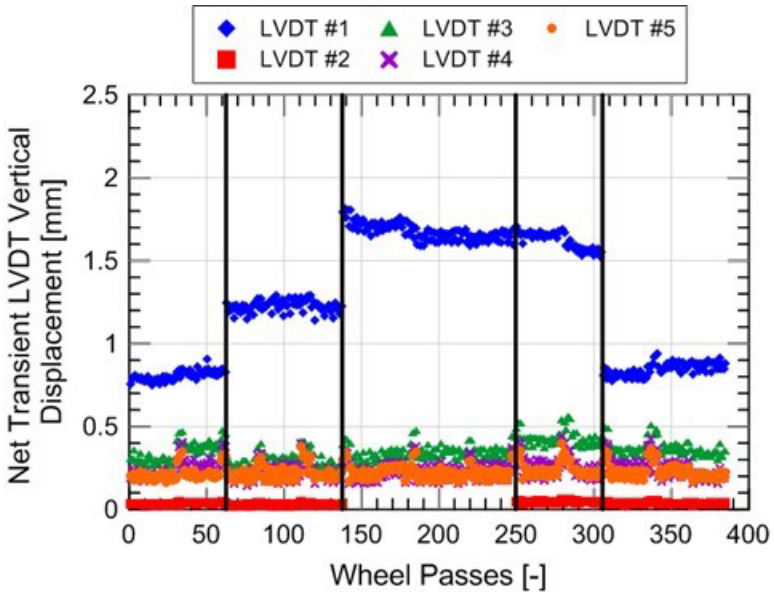

Figure 76. Comparison of net transient vertical displacements for all subsurface LVDTs at Madison (12 ft) for each passing wheel

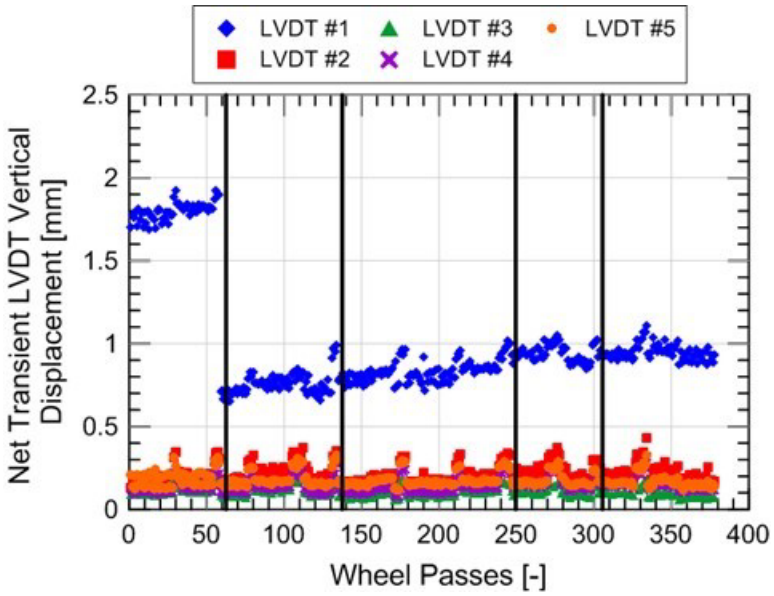

Figure 77. Comparison of net transient vertical displacements for all subsurface LVDTs at Madison (60 ft) for each passing wheel

To compare transient LVDT vertical displacements between the MDD instrumentation sites, the team calculated the average transient vertical displacement for each LVDT. Table 9 and Table 10 show the average transient vertical displacement of each LVDT, expressed as a displacement value in mm in Table 9 and as a percentage of total LVDT 1 through 5 displacements in Table 10. The transient vertical displacements in LVDTs 2 through 5 were much smaller than LVDT 1. The percentages in Table 10 show a similar trend.

Table 9. Average transient vertical displacement of each LVDT

Instrumented Site	LVDT #1 [mm]	LVDT #2 [mm]	LVDT #3 [mm]	LVDT #4 [mm]	LVDT #5 [mm]	Total [mm]
Caldwell (East)	0.859	0.097	0.055	0.362	0.129	1.502
Caldwell (West)	1.293	0.032	0.042	0.264	0.087	1.718
Madison (12 ft.)	1.377	0.035	0.347	0.237	0.224	2.220
Madison (60 ft.)	1.019	0.204	0.103	0.138	0.180	1.643
Upland (15 ft.)	2.624	0.088	0.356	0.058	0.091	3.216
Upland (60 ft.)	0.332	0.124	0.308	0.269	0.131	1.165

Table 10. Average transient vertical displacement of each LVDT as a percentage of total transient vertical displacement

Instrumented Site	LVDT #1 [%]	LVDT #2 [%]	LVDT #3 [%]	LVDT #4 [%]	LVDT #5 [%]
Caldwell (East)	57	6	4	24	9
Caldwell (West)	75	2	2	15	5
Madison (12 ft.)	62	2	16	11	10
Madison (60 ft.)	62	12	6	8	11
Upland (15 ft.)	82	3	11	2	3
Upland (60 ft.)	29	11	26	23	11

Large variations in LVDT 1 displacement were apparent between these sites. For example, despite identical ballast layer heights, the measured transient LVDT 1 displacement at Upland (60 ft) was only 0.33 mm, while 2.63 mm was observed at Upland (15 ft). Like permanent vertical displacements, the largest transient LVDT 1 displacement occurred at the bridge approach sites.

The LVDT displacements of the four NS sites are displayed in Figure 78 through Figure 81. As with the Amtrak sites, the y-axis is different at each location to emphasize variations in LVDT displacement and the black line separates the two trains recorded at each site. (Note: LVDT 1 was not working properly at MP 352.8 (11 ft), so data from LVDT 1 was omitted.)

The results showed large LVDT 1 displacements at MP 352.2 (13 ft), indicating poor tie support, while the other three sites showed LVDT 1 displacements of less than 1.0 mm, suggesting good or decent tie support. While it appeared significant variation in LVDT displacements occurred at both MP 352.8 sites, this difference was due to the response of unloaded and loaded trains. Train 1 was unloaded for both MP 352.8 sites, and therefore the displacement were lower; Train 2 was loaded, and therefore the displacements were higher. However, the Train 1 locomotive matched the response of the loaded cars of Train 2, indicating a similar response.

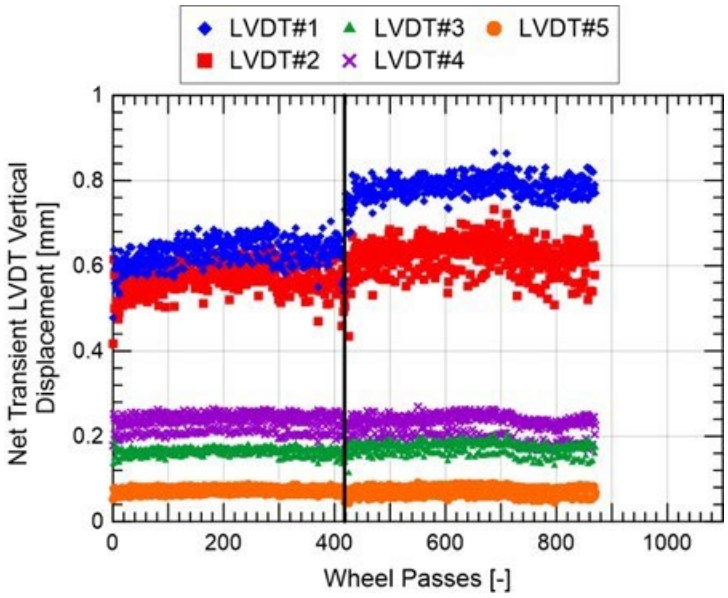

Figure 78. Comparison of net transient vertical displacements for all subsurface LVDTs at MP 352.2 (31 ft) for each passing wheel

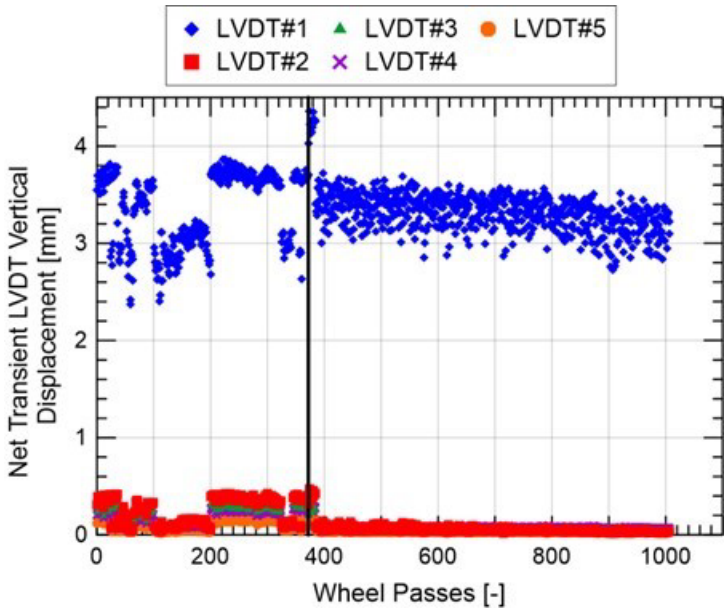

Figure 79. Comparison of net transient vertical displacements for all subsurface LVDTs at MP 352.2 (13 ft) for each passing wheel

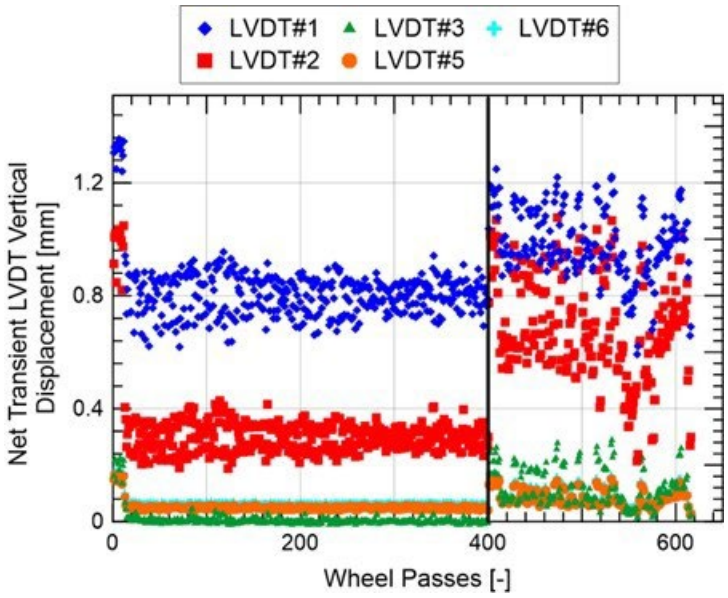

Figure 80. Comparison of net transient vertical displacements for all subsurface LVDTs at MP 352.8 (29 ft) for each passing wheel

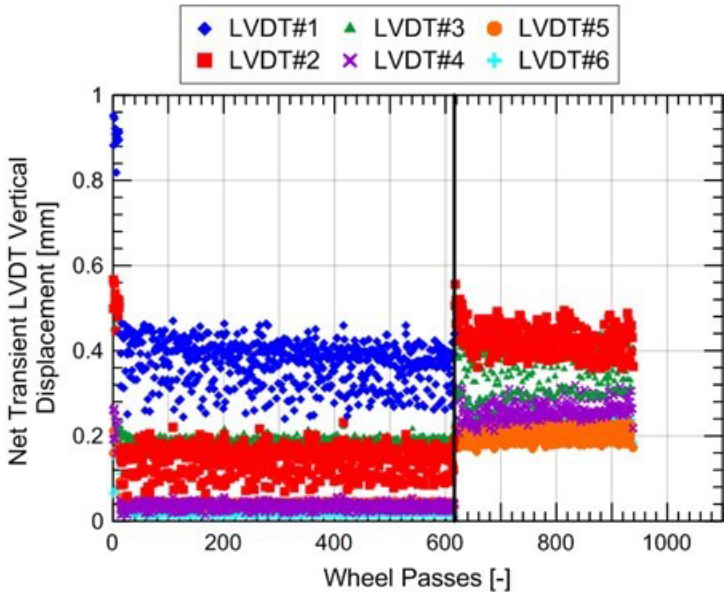

Figure 81. Comparison of net transient vertical displacements for all subsurface LVDTs at MP 352.8 (11 ft) for each passing wheel

The average transient vertical displacements of each LVDT are displayed in Table 11 and the percentage of total transient vertical displacement is displayed in Table 12. The results showed similar behavior between MP 352.2 (31 ft), MP 352.8 (11 ft), and MP 352.8 (29 ft), but significantly greater LVDT 1 displacement at MP 352.2 (13 ft). This further suggested that MP 352.2 (13 ft) was unsupported, while the other locations had some tie support. The greater transient LVDT 1 displacement at MP 352.2 (13 ft) also agreed with the large permanent LVDT 1 displacement at that location.

Table 11. Average transient vertical displacement of each LVDT

Instrumented Site	LVDT #1 [mm]	LVDT #2 [mm]	LVDT #3 [mm]	LVDT #4 [mm]	LVDT #5 [mm]	LVDT #6 [mm]	Total [mm]
MP 352.2 (31 ft.)	0.711	0.598	0.168	0.231	0.074	-	1.782
MP 352.2 (13 ft.)	3.345	0.130	0.113	0.116	0.056	-	3.760
MP 352.8 (29 ft.)	0.877	0.451	0.046	-	0.063	0.073	1.150
MP 352.8 (11 ft.)	0.384	0.153	0.189	0.040	0.043	0.035	0.844

Table 12. Average transient vertical displacement of each LVDT as a percentage of total transient vertical displacement

Instrumented Site	LVDT #1 [%]	LVDT #2 [%]	LVDT #3 [%]	LVDT #4 [%]	LVDT #5 [%]	LVDT #6 [%]
MP 352.2 (31 ft.)	40	34	9	13	4	-
MP 352.2 (13 ft.)	89	3	3	3	2	-
MP 352.8 (29 ft.)	58	30	3	-	4	5
MP 352.8 (11 ft.)	46	18	22	5	5	4

6.3 Tie-Ballast Interaction (Amtrak NEC Sites)

The previous section shows a wide variation in transient LVDT 1 displacement and a possible link between transient and permanent LVDT 1 behavior. This section investigates the causes of varying LVDT 1 displacement at the Amtrak NEC instrumentation sites. Section 6.4 focuses on the reasons of varying LVDT 1 displacement at the NS N-Line sites.

Because LVDT 1 measured the displacement from the top of the tie to the bottom of the ballast layer, LVDT 1 displacement can be divided into the following four main components:

1. Vertical deformation of the concrete tie
2. Closure of any gap between the tie bottom and ballast surface (δ_{gap})
3. Initial non-linear behavior of the ballast, referred to as "seating deformation" (δ_{seat})
4. Displacement of the ballast layer due to the applied load ($\delta_{mobilized}$)

Concrete ties are much stiffer than ballast, therefore their displacement can be considered negligible. This leaves the closure of a gap, non-linear seating displacement, and mobilized ballast vertical displacements as the three main components of LVDT 1 vertical displacement. The conceptual model for these three components is shown in Figure 82, which displays the theoretical transient displacement behavior of a tie with a gap between the tie and the ballast.

The solid line represents the theoretical tie displacement behavior. Prior to loading, a gap between the tie and ballast is assumed to exist (δ_{gap}). As the tie is loaded, the gap closes and the ballast supports the tie by mobilizing shear resistance from particle friction and interlocking. The tie displacement during the shear mobilization of the ballast is represented by δ_{seat} and the load to fully mobilize the ballast is called the tie-seating load. Any tie displacement after tie seating is due to displacement of the ballast and underlying soils ($\delta_{mobilized}$). The tie should displace linearly

with increasing applied load in accordance with the mobilized stiffness (k_{mob}) of the ballast and underlying soils.

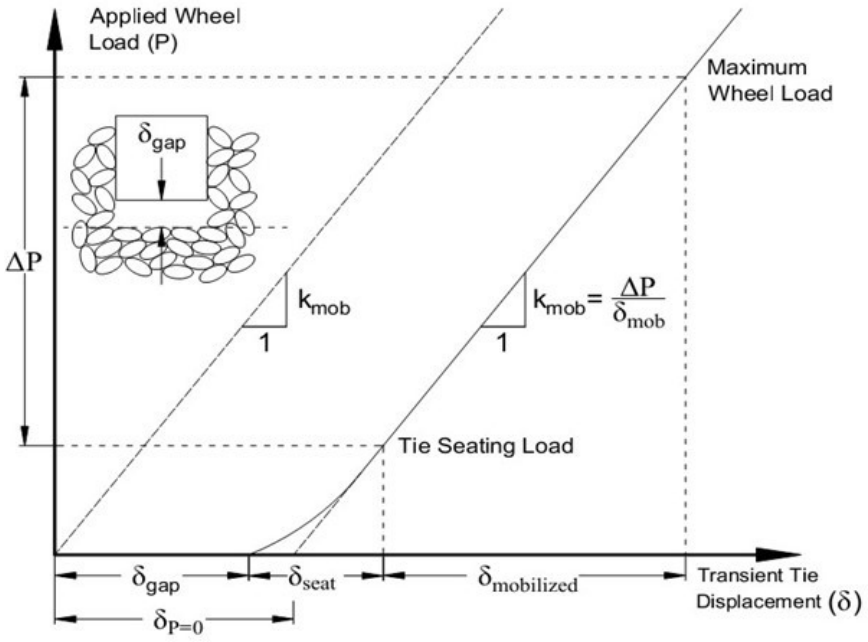

Figure 82. Theoretical displacement behavior of a tie with a gap

The gap between the bottom of the tie and ballast is the key feature of this conceptual model. While a gap may be non-existent in some cases, it is usually present after the passing of a single train due to the initial loose nature of the ballast. For example, newly laid or recently tamped track should have a loose ballast layer in intimate contact with the overlying tie (Figure 83). As a train loads the track structure, the ballast particles transiently rearrange into a more compact state (δ_{seat}) and displace under the applied load ($\delta_{mobilized}$). After the train passes, the ballast does not elastically rebound to its initial state because of plastic deformation under the initial loading and remains in a more compact form. The rail stiffness then pulls the tie back up, creating a gap between the tie and ballast (Figure 82).

For analysis of LVDT 1, it is imperative that the tie-ballast gap (δ_{gap}) be separated from the mobilized ballast displacement ($\delta_{mobilized}$) to determine which component is problematic. However, one issue that arises when separating components is determining the tie-ballast gap (δ_{gap}) and seating displacement (δ_{seat}) as measurements below the tie-seating load are rarely obtained. To overcome this, the tie-ballast gap is estimated by extrapolating k_{mob} to the unloaded condition (P=0). This estimated "gap" is represented as $\delta_{P=0}$. While this method overestimates the actual tie-ballast gap, the seating displacement (δ_{seat}) is expected to be small as the ballast will be compacted due to prior tie displacements. The transient ballast displacement can then be calculated by subtracting the estimated tie-ballast gap ($\delta_{P=0}$) from the transient LVDT 1 displacement.

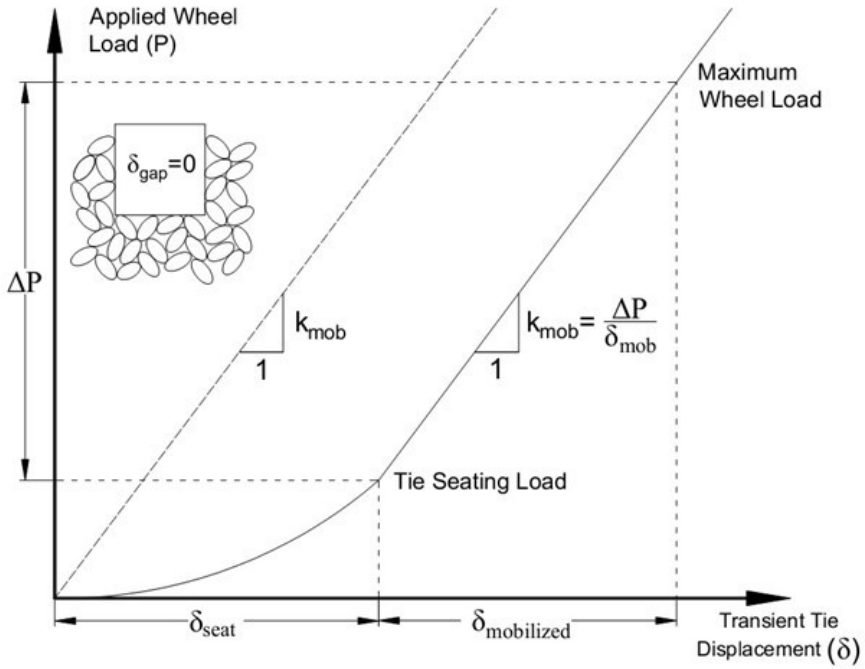

Figure 83. Theoretical tie displacement behavior of a tie with no gap

To determine the estimated tie-ballast gap ($\delta_{P=0}$) at each instrumented site, the peak wheel load and corresponding peak transient LVDT 1 vertical displacement were recorded for each passing wheel. Caldwell (East) during the 26 January 2013 measurement is used as an example in Figure 84. The following linear mathematical relationship can be fitted to the field data to represent the transient LVDT 1 vertical displacement behavior:

$$\delta_{LVDT\#1} = \delta_{P=0} + \frac{P}{k_{mob}}$$

with the inverse of the slope representing the mobilized ballast stiffness (k_{mob}).

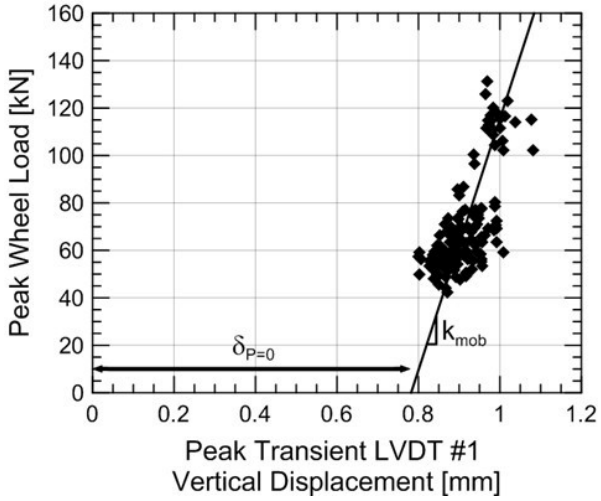

Figure 84. Transient LVDT 1 vertical displacement behavior at Caldwell (East) on 26 January 2013

It was determined that the force-displacement behavior at LVDT 1 (and LVDTs 2–5) was similar for multiple trains recorded on the same day. This was expected because the ballast and underlying soil behavior should not have changed significantly from trains passing within the same hour. To show this, Figure 85 displays the force-displacement results from five recorded trains at Caldwell (East), measured on 26 January 2013.

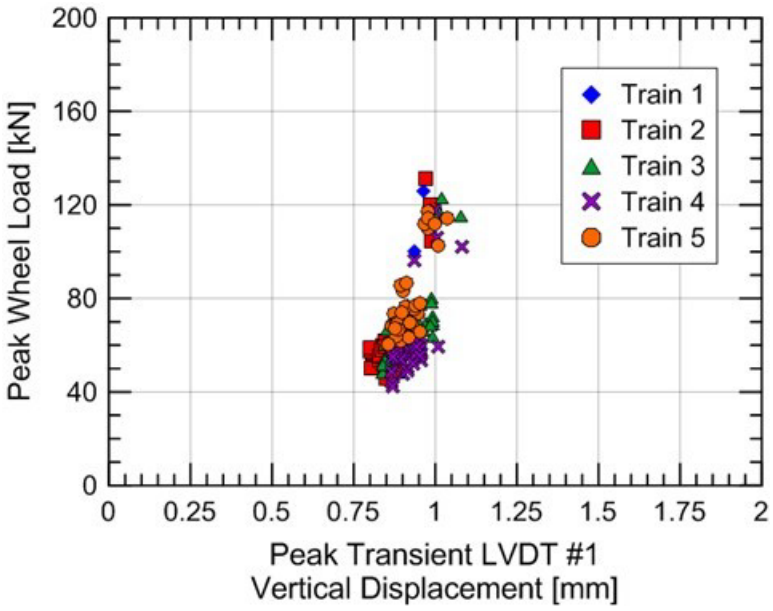

Figure 85. Transient LVDT 1 vertical displacement behavior at Caldwell (East) on 26 January 2013

Figure 86 through Figure 88 compare the force-displacement behavior at LVDT 1 for both instrumented sites at the three bridge approaches on 26 January 2013. Figure 86 compares Caldwell (East) and Caldwell (West), located on the same tie about 80 ft away from the abutment. Figure 87 compares Madison (12 ft) and Madison (60 ft), both located on the west end of the ties. Figure 86 compares Upland (15 ft) with Upland (60 ft), also both located on the west end of the ties. The numerical values of the estimated tie-ballast gap ($\delta_{P=0}$) mobilized ballast stiffness (k_{mob}), and the ballast modulus (E) estimated using FLAC3D (see Section 12) are displayed in Table 13. For comparison purposes, the values of ballast modulus measured using seismic testing range from 140 to 380 MPa. This includes clean, dry-fouled, and wet-fouled ballast. More detailed discussion of ballast modulus values is presented in Section 12.

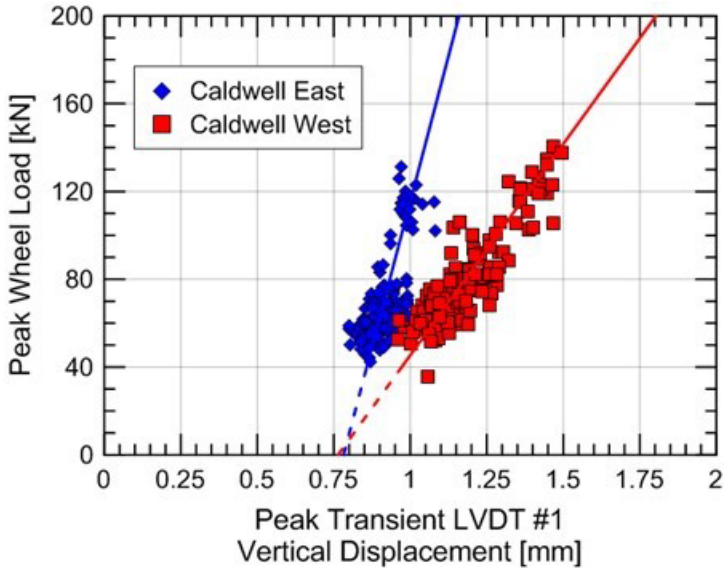

Figure 86. Comparison of transient LVDT 1 vertical displacement behavior at Caldwell (East) and Caldwell (West) on 26 January 2013

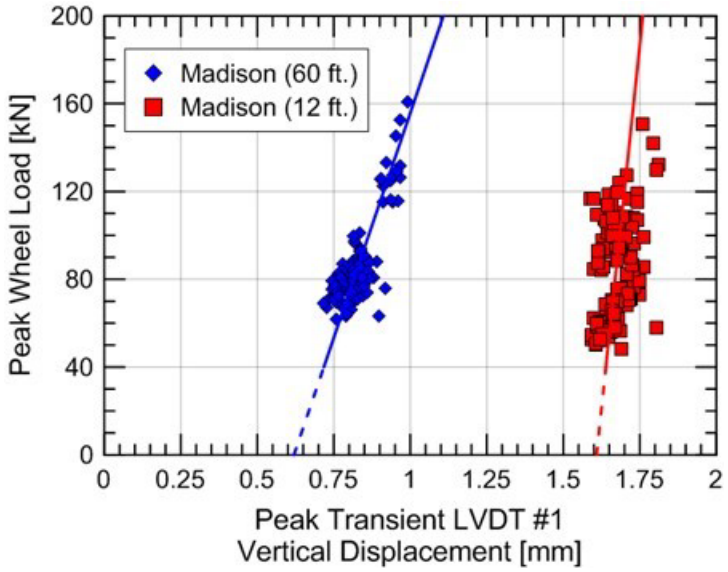

Figure 87. Comparison of transient LVDT 1 vertical displacement behavior at Madison (12 ft) and Madison (60 ft) on 26 January 2013

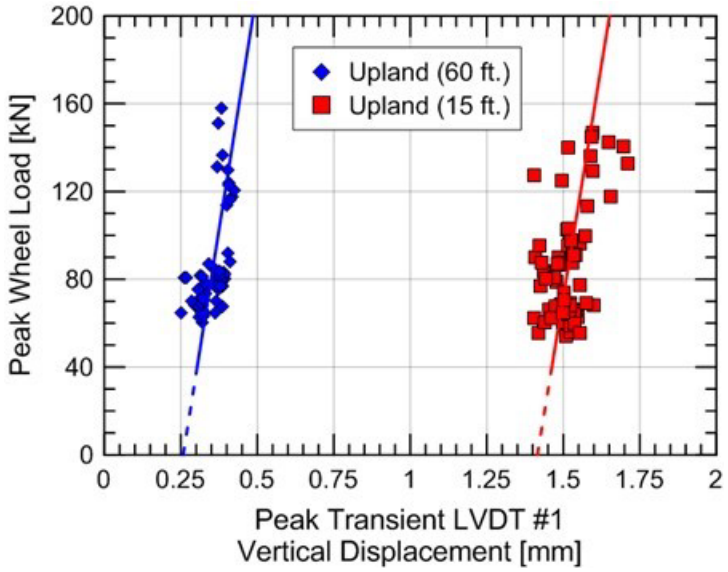

Figure 88. Comparison of transient LVDT 1 vertical displacement behavior at Upland (15 ft) and Upland (60 ft) on 26 January 2013

Table 13. Values of estimated tie-ballast gap, mobilized ballast stiffness, and Young's modulus at all six instrumented sites for 26 January 2013

Instrumented Site		Caldwell		Madison		Upland	
		East	West	12 ft.	60 ft.	15 ft.	60 ft.
$\delta_{P=0}$	[mm]	0.78	0.76	1.61	0.62	1.42	0.26
k_{mob}	[kN/mm]	530	192	1322	410	848	876
E via FLAC3D	[MPa]	132	51	271	110	200	202

The estimated tie-ballast gap ($\delta_{P=0}$) was similar at both Caldwell sites (0.78 mm and 0.76 mm); however, the stiffness at Caldwell (East) was greater than at Caldwell (West). Due to the similar tie-ballast gap at both ends of the tie, the team inferred that the gap under the tie was likely uniform. The differential stiffness at Caldwell (80 ft) could have been the result of multiple factors, including greater wheel loads on the west rail due to the west rail being 1/8 in lower than the east rail, different degrees of fouling, and differences in drainage. It was also possible the different wheel loads caused differential fouling and cross-level along the Caldwell (80 ft) tie.

At the Madison site, the estimated tie-ballast gap was much greater at Madison (12 ft) than Madison (60 ft), with gap heights of 1.61 mm and 0.62 mm, respectively. This corresponded with past observations from other indicators (e.g., tie reaction and transient vertical displacement) that Madison (12 ft) had less tie support than Madison (60 ft). A possible reason for the larger tie-ballast gap at Madison (12 ft) was two broken ties (Figure 63) near the instrumented tie and being located 12 ft from the bridge abutment. Both can result in wheel load redistribution and impact loads. The stiffness was greater at Madison (12 ft) than Madison (60 ft) and may have been due to greater compaction of the ballast near the transition zone due to wheel impact loads.

The difference in the estimated tie-ballast gap was greatest at the Upland site, with a 0.26 mm gap at Upland (60 ft) and 1.42 mm gap at Upland (15 ft). This also corresponded with past observations that Upland (60 ft) displayed good tie support, while Upland (15 ft) had poor tie support (Figure 63). Also, the stiffness at both Upland sites was similar.

By quantifying the tie-ballast gap and mobilized ballast stiffness, it was then possible to relate these two parameters to the permanent vertical displacement values calculated in Section 3. First, to establish a relationship between tie-ballast gap ($\delta_{P=0}$) and permanent LVDT 1 vertical displacement, researchers plotted the two values against each other (Figure 89). This relationship was reasonable since, as the tie-ballast gap increased, impact loads and load redistribution were expected to increase the applied load on the ballast, as observed in the data. This increase in applied load could accelerate ballast degradation, particle rearrangement, and fouling.

Figure 89 shows a strong correlation, suggesting that the tie-ballast gap may have been the root cause of the permanent vertical displacements. Remedial measures should aim to decrease the tie-ballast gap or prevent gap formation altogether.

While it may be unrealistic to eliminate the tie-ballast gap, this analysis suggests that tie-ballast gaps ($\delta_{P=0}$) greater than 1 mm can cause load redistribution and become problematic. This is also the tie-ballast gap measurement that, when surpassed, displayed indications of poorly supported behavior with tie reaction (Section 4.2) and transient vertical displacements (Section 6.1). Therefore, the team recommends tie-ballast gaps be reduced to less than 1 mm during remedial measures (e.g., stone blowing). In addition, the tie-ballast gap ($\delta_{P=0}$) plus the permanent vertical displacement should be less than about 4 mm, assuming no additional displacement between the top-of-rail (TOR) and top-of-tie.

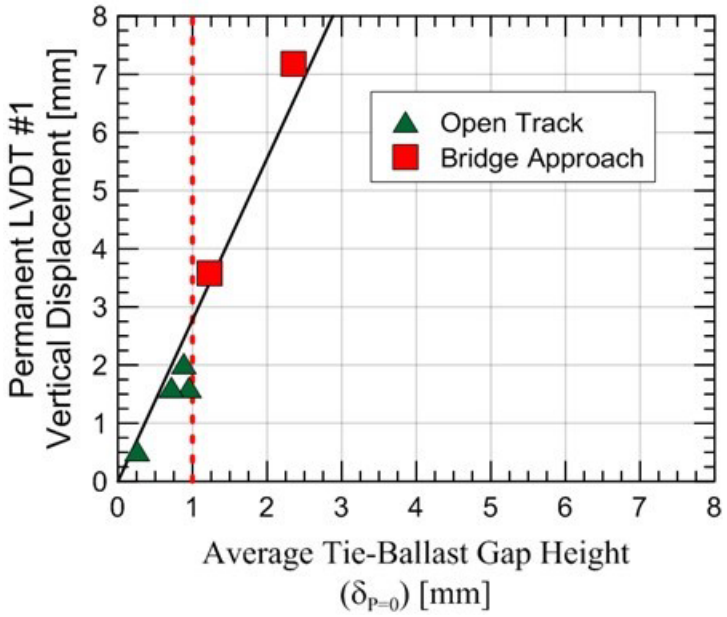

Figure 89. Correlation between average tie-ballast gap height and net permanent LVDT 1 vertical displacement

Next, team members plotted mobilized ballast stiffness (k_{mob}) against permanent LVDT 1 vertical displacement. Ballast stiffness is typically related to track quality, and larger transient vertical displacements were expected to result in permanent vertical displacements. Therefore,

researchers often attempt to obtain a high ballast modulus by ensuring it is free of fouling and/or dry. Also, many potential fixes to the excessive permanent displacements at bridge abutments have historically involved stiffening the ballast (Li and Davis, 2005).

The relationship between mobilized ballast stiffness and permanent vertical displacements is displayed in Figure 90. The figure shows that a weak correlation exists between the two factors. While the open track and bridge approach sites with the lowest permanent vertical displacement (i.e., Upland (60 ft) and Madison (12 ft)) showed the highest mobilized ballast stiffness, the difference between open track and bridge approach data implied that ballast modulus did not explain the differences in permanent vertical displacement because the ballast material should have been the same in both locations.

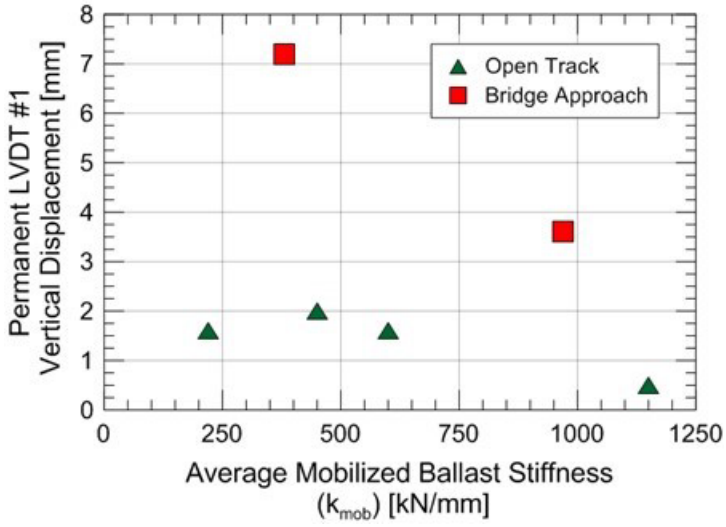

Figure 90. Correlation between average mobilized ballast stiffness and net permanent LVDT 1 vertical displacement

Another interesting observation was that a wide range of mobilized ballast stiffness was measured at the six instrumented sites. Caldwell (West) displayed the lowest, with 221 kN/mm, while Upland (60 ft) displayed the highest, with 1,147 kN/mm – over five times greater than Caldwell (West). This suggested that increases in ballast stiffness may not significantly affect the performance of the track if a gap is present.

In summary, this section presented a method for separating tie-ballast gap and ballast displacement from measured LVDT 1 displacements by extrapolating the best-fit LVDT 1 force-displacement response to a condition of zero load. The two resulting parameters, tie-ballast gap ($\delta_{P=0}$) and mobilized ballast stiffness (k_{mob}), were then correlated with permanent LVDT 1 vertical displacement. The results showed a strong correlation with tie-ballast gap and a weak correlation with mobilized ballast stiffness. This implied the tie-ballast gap was a potential root cause of the permanent vertical displacements, and remedial measures should focus on this mechanism.

6.4 Tie-Ballast Interaction (Norfolk Southern N-Line Sites)

The LVDT 1 force-displacement relationship (Figure 86 through Figure 88) for the six Amtrak NEC sites showed significant variations in tie support conditions. However, because the range in

peak wheel loads was limited for the NEC sites (i.e., primarily Acela trains accessed the instrumentation sites), only the linear portion of the proposed conceptual tie displacement model (Figure 78) was defined. This means the tie-ballast gap ($\delta_{P=0}$) could only be estimated by extrapolating the linear best-fit line to zero wheel load (P=0), which overestimated the actual tie-ballast gap (δ_{gap}). The non-linear seating displacement (δ_{seat}) was small due to ballast compaction at this location.

A benefit from instrumenting the NS N-Line was the wide range of recorded peak wheel loads because the trains often consisted of both loaded and unloaded freight cars. This means the portion of force-displacement relationship below the seating load was measured and could be quantified instead of assumed in the Amtrak case. This range of loaded and unloaded freight cars differed from the NEC sites, where the passenger cars weighed about the same and the two power cars weighed about the same, so the variation in load was limited.

To illustrate the non-linear load-vertical displacement behavior of LVDT 1, a freight train measured at MP 352.2 (13 ft) on 2 November 2013 at 8:43 AM EST is used as an example in Figure 91. The range of data in Figure 91 was sufficient to delineate the seating load, or the load that established good contact between the tie and ballast. The seating load for the freight train on 2 November 2013 was about 80 kN. Above the seating load, the response was nearly linear and thus similar to the measured response at the Amtrak NEC sites in Figure 86 through Figure 88. Below the seating load, the LVDT 1 response was also non-linear, as observed with the NEC sites.

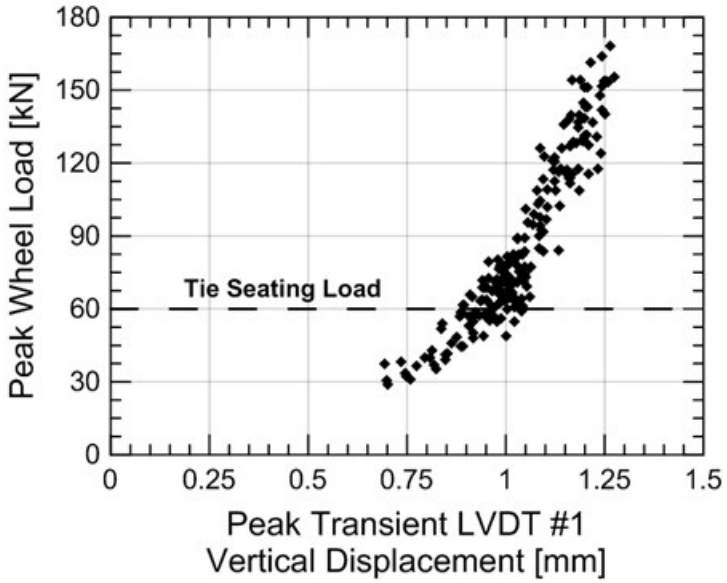

Figure 91. Non-linear transient LVDT 1 vertical displacement behavior at MP 352.2 (13 ft) on 2 November 2013

By studying the non-linear response below the seating load, the team was able to determine the following three displacement values for the conceptual model presented in Figure 82: δ_{gap}, δ_{seat}, and $\delta_{P=0}$. The lowest recorded peak wheel load was 30 kN, so the non-linear relationship still had to be extrapolated to the zero wheel load (P=0). To do this, two non-linear relationships, bi-linear and cubic, were used to approximate the data. Logarithmic, exponential, power, parabolic, and

higher-order relationships also were considered. However, none represented the data trend better than the bi-linear and cubic functions.

The equations for a bi-linear representation of the data in Figure 91 are as follows for above and below the seating load in the figure (i.e., P_{seat}):

$$\delta_{LVDT\#1} = \delta_{P=0} + \frac{P}{k_{mob}} \qquad if\ P \geq P_{seat}$$

$$\delta_{LVDT\#1} = \delta_{gap} + \frac{P}{k_{seat}} \qquad if\ P < P_{seat}$$

where the linear portion above the seating load is the same as shown for the Amtrak data where k_{mob} is the stiffness of the ballast underlying the tie. Below the seating load, δ_{gap} represents the tie-ballast gap and k_{seat} represents the stiffness of the unmobilized ballast.

The equation for a cubic representation of the data in Figure 91 is as follows:

$$\delta_{LVDT\#1} = a_1 P^3 + a_2 P^2 + a_3 P + a_4$$

where a_1, a_2, a_3, and a_4 are best fit parameters. The last best fit parameter (a_4) equals the tie-ballast gap (δ_{gap}).

The seating displacement, δ_{seat}, is calculated by subtracting the tie-ballast gap from the LVDT 1 displacement at the seating load:

$$\delta_{seat} = \delta_{LVDT\#1}(P_{seat}) - \delta_{gap}$$

The graphical representations for the bi-linear and cubic models are shown in Figure 92 with the NS field data. The parameter values for each model are displayed in Table 14. Figure 92 shows that both models fit the data reasonably well within the range of measured peak wheel loads (30 kN < P < 160 kN). However, the cubic model provided a better representation at low peak wheel loads (i.e., less than 40 kN) than the bi-linear model. The greater non-linearity of the cubic relation resulted in a smaller estimate of δ_{gap} than the bi-linear model, which was like the extrapolation used for the Amtrak data. However, when extrapolating to wheel loads larger than the measured values, the cubic model curved away from the measured data, resulting in lower tangent stiffness values at high loads. Conversely, the bi-linear model assumed the stiffness remained constant for peak wheel loads greater than 80 kN (i.e., P_{seat}).

In summary, the team will use the cubic model in future research activities to represent the transient load-displacement behavior and estimate ballast stiffness under the tie.

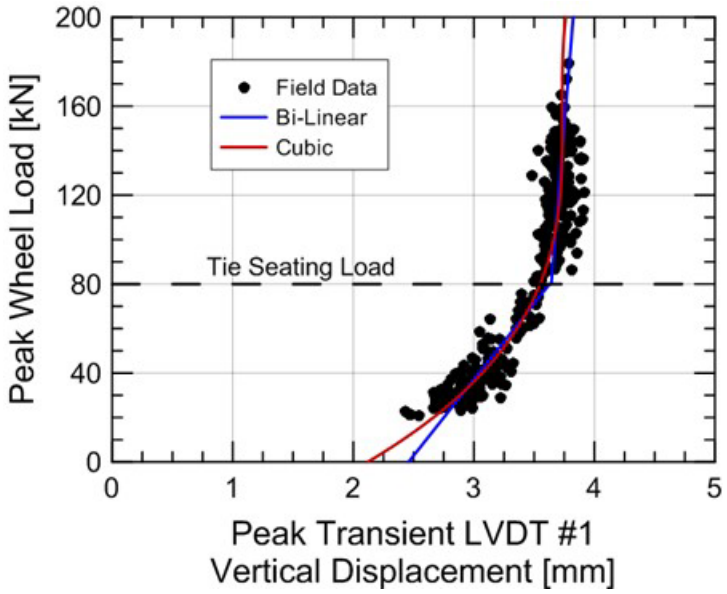

Figure 92. Mathematical representation of transient LVDT 1 vertical displacement behavior at MP 352.2 (13 ft) on 2 November 2013

Table 14. Best-fit parameters for bi-linear and cubic models for NS data

Bi-linear		Cubic	
k_{mob}	568	a_1	6.50×10^{-7}
$\delta_{P=0}$	3.46	a_2	2.59×10^{-4}
k_{seat}	65	a_3	0.0356
δ_{gap}	2.41	a_4	2.01

Table 15 displays the values of δ_{gap}, δ_{seat}, and $\delta_{P=0}$ and shows a seating displacement (i.e., δ_{seat}) of 1.2–1.5 mm was predicted by the bi-linear and cubic models. This value was significant because it meant the estimated tie-ballast gap ($\delta_{P=0}$) from the Amtrak data was overestimated by 40 to 70 percent because, in the Amtrak analysis, the reported values of $\delta_{P=0}$ assumed δ_{seat} was 0 mm.

As a note, the $\delta_{P=0}$ value was determined using the method presented in the previous section (Section 6.3) and was included for comparison purposes. This meant the value of $\delta_{P=0}$ would be constant regardless of which non-linear model was used to determine δ_{gap} and δ_{seat}.

Table 15. Values of estimated tie-ballast gap, actual tie-ballast gap, and seating displacement at MP 352.2 (13 ft) on 2 November 2013

Fitting Model	$\delta_{P=0}$ [mm]	δ_{gap} [mm]	δ_{seat} [mm]
Bi-Linear	3.46	2.41	1.19
Cubic	3.46	2.01	1.52

The strong relationship between estimated tie-ballast gap and permanent vertical displacement observed for the Amtrak NEC instrumentation sites may apply to a freight railway. Limited permanent vertical displacements measurements at the NS sites prevented correlations with tie-ballast. However, it was already possible to determine which sites displayed supported and unsupported tie behavior using transient LVDT 1 data. The force-displacement responses of LVDT 1 for MP 352.2 (13 ft) and MP 352.2 (31 ft) are compared in Figure 93. This comparison shows the MP 352.2 (13 ft) displayed unsupported tie behavior because about 2.5 mm of transient vertical displacement was required to support the peak wheel load. Conversely, MP 352.2 (31 ft) showed only about 0.5 mm of transient vertical displacement was required to support the peak wheel load, indicative of good tie support. The behavior of the (13 ft) and (31 ft) sites was similar to the results observed for Amtrak's Upland Avenue site because the open track sites exhibited good tie support, while the bridge approach sites exhibited poor tie support. As a result, NS MP 352.2 was a good site to study the effect of tie support under freight loading instead of passenger loading.

The load-displacement responses of the four sites for all train passes are displayed in Figure 93 through Figure 97. LVDT 1 was not working properly for MP 352.8 (11 ft) in March 2014. The results showed a large gap disparity between MP 352.2 (13 ft) and (31 ft), which agreed with the measured difference in permanent LVDT 1 displacement during the same period. Slightly larger gaps were observed between November 2013 and March 2014. At MP 352.8, both sites were relatively well-supported, with higher gaps at the 29 ft location than the 11 ft location. The permanent LVDT 1 displacements were not known, preventing direct comparison.

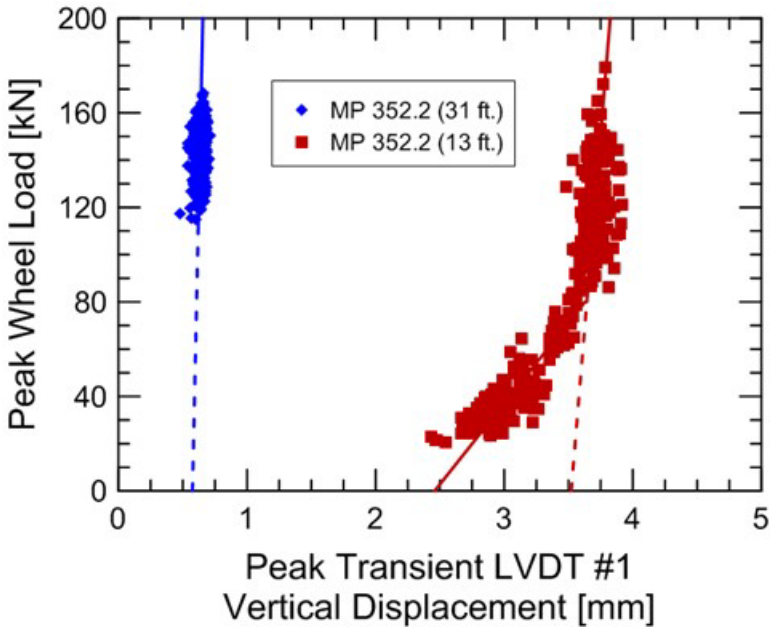

Figure 93. Comparison of transient LVDT 1 vertical displacement behavior at MP 352.2 (31 ft) and MP 352.2 (13 ft) on 2 November 2013

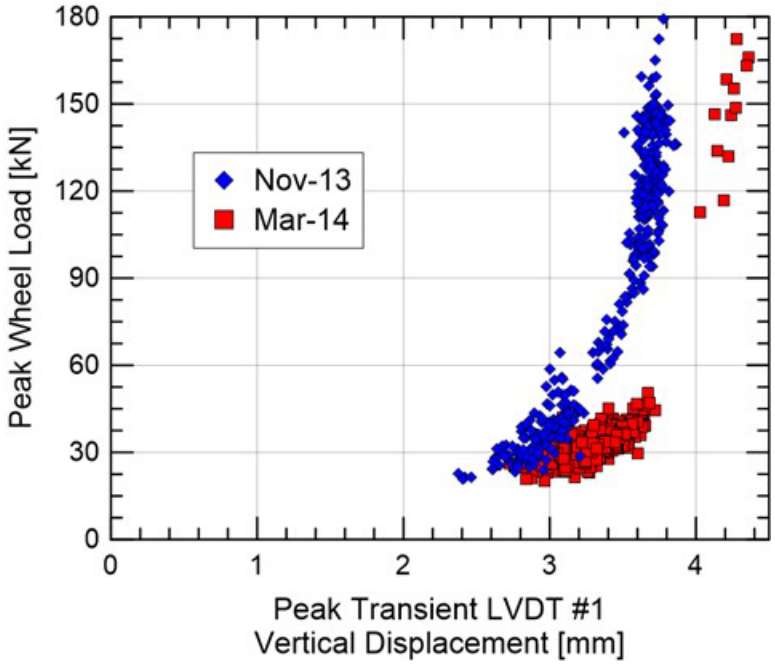

Figure 94. Transient LVDT 1 vertical displacement behavior at MP 352.2 (13 ft)

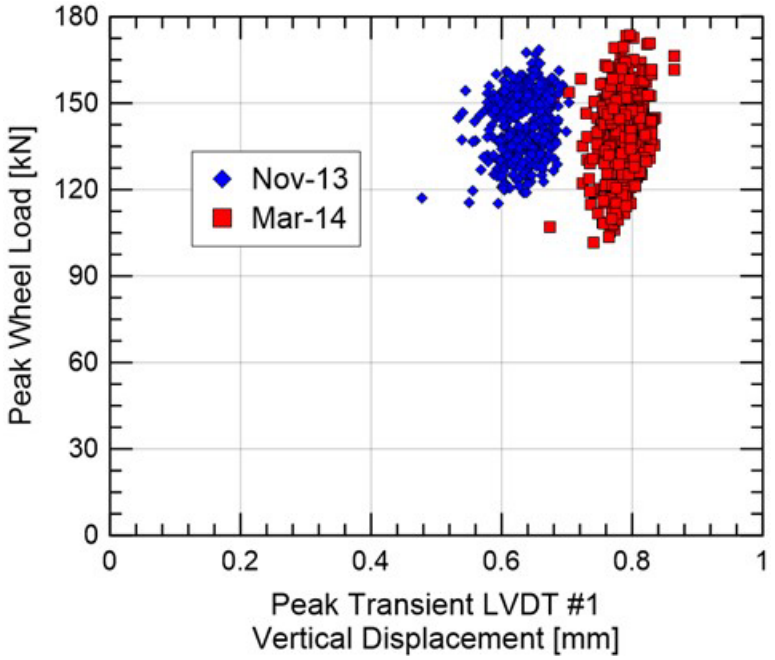

Figure 95. Transient LVDT 1 vertical displacement behavior at MP 352.2 (31 ft)

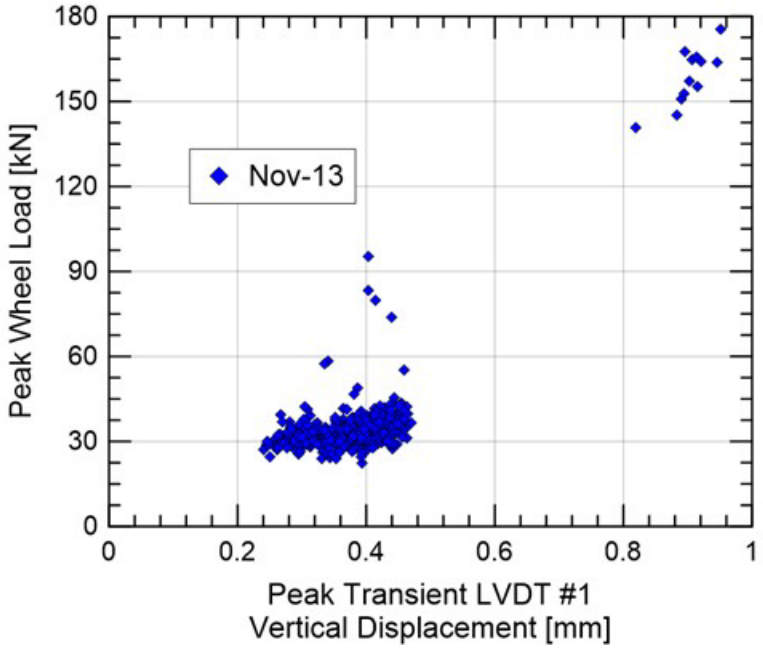

Figure 96. Transient LVDT 1 vertical displacement behavior at MP 352.8 (11 ft)

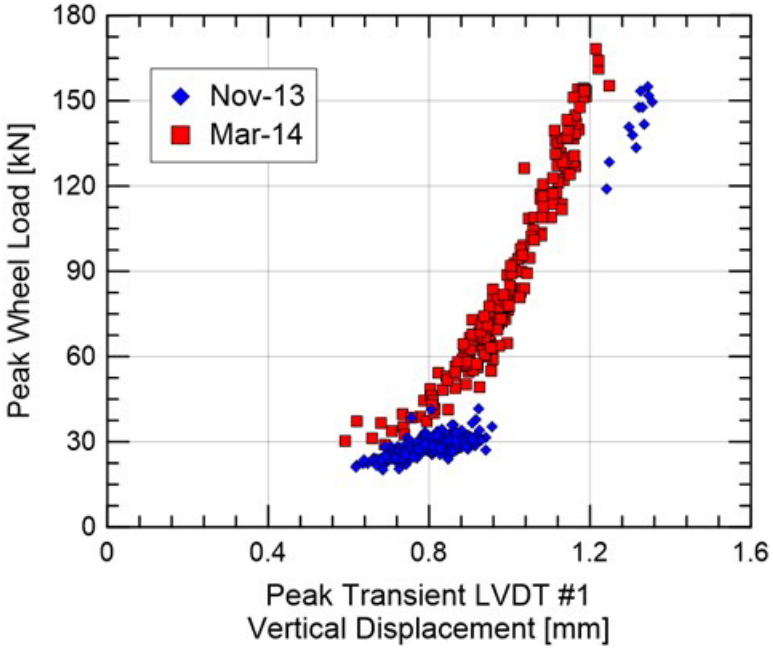

Figure 97. Transient LVDT 1 vertical displacement behavior at MP 352.2 (29 ft)

Table 16 compares the values of mobilized ballast stiffness and tie-ballast gap for the Upland Avenue and MP 352.2 locations. These values of ballast stiffness agreed with the values for Upland Ave. (15 ft) and (60 ft), also shown in Table 16. This means the ballast reached a similar stiffness after a few passes whether it involved freight or passenger loading.

Table 16. Values of estimated tie-ballast gap and mobilized ballast stiffness for the Amtrak Upland Avenue sites and NS MP 352.2 sites

Instrumented Site		Upland		MP 352.2	
		15 ft.	60 ft.	13 ft	31 ft
$\delta_{P=0}$	[mm]	1.42	0.26	3.46	0.48
k_{mob}	[kN/mm]	848	876	568	1018

6.5 LVDT 2 through 5 Force-Displacement Behavior (Amtrak)

Creating a method to quantify substructure behavior into mathematical parameters is important for determining track modulus and calibrating numerical models. The methodology to determine the behavior of LVDTs 2 through 5 was like that of LVDT 1. For each passing wheel, the peak wheel load and transient LVDT vertical displacement was recorded and plotted against each other. Two examples – LVDT 3 at Madison (12 ft) on 7 August 2012 and LVDT 4 at Upland (60 ft) on 29 January 2013 – are shown in Figure 91 and Figure 92.

Unlike LVDT 1, a gap is not present between substructure layers; however, slight non-linear behavior of the material prevented the best-fit trend line from passing through the origin. Therefore, $\delta_{P=0}$ does not represent a gap but instead non-linearity in the form of an "apparent gap" for LVDTs 2 through 5. Also, the results from Figure 98 and Figure 99 show the apparent gap ($\delta_{P=0}$) can either be positive or negative.

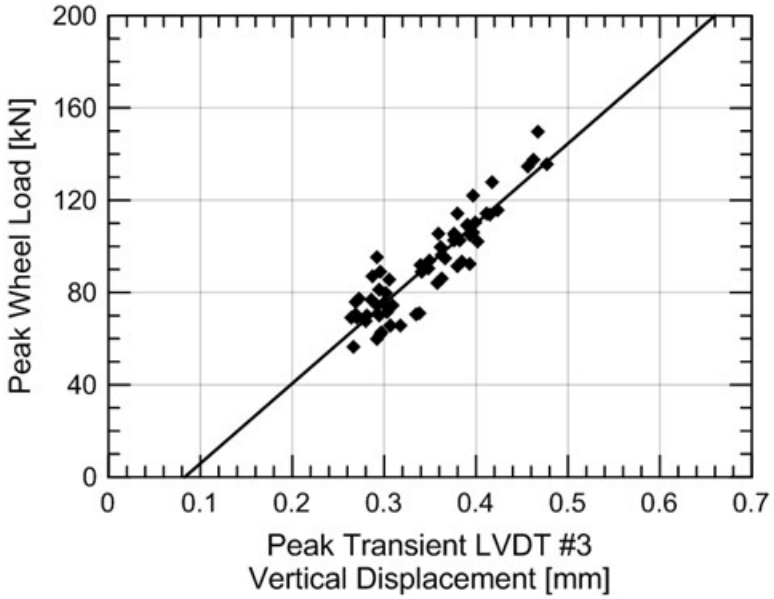

Figure 98. Transient LVDT 3 vertical displacement behavior at Madison (12 ft) on 7 August 2012

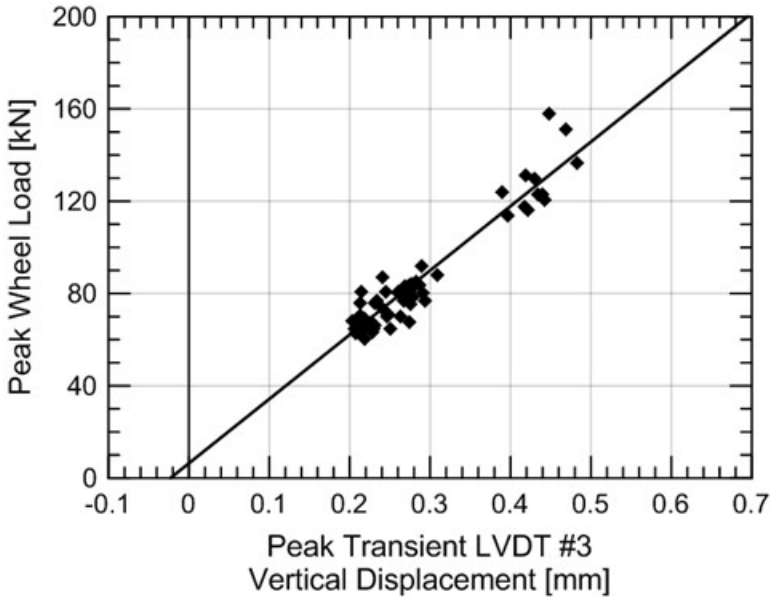

Figure 99. Transient LVDT 4 vertical displacement behavior at Upland (60 ft) on 29 January 2013

Using the same terminology as LVDT 1, the mathematical representation of LVDT 2 through 5 behavior is:

$$\delta_{LVDT\#2-5} = \delta_{P=0} + \frac{P}{k_{mob}}$$

However, $\delta_{P=0}$ does not represent a gap but takes non-linear behavior into account in the form of an apparent gap.

Using this mathematical representation, the apparent gap ($\delta_{P=0}$) and mobilized LVDT stiffness (k_{mob}) can be determined by applying a best-fit line to the data. The average values from all measured trains are displayed in Table 17 and Table 18, as well as LVDT 1 (for completeness).

Table 17. Average mobilized LVDT stiffness (k_{mob}) values for the NEC sites

Instrumented Site	LVDT #1 [kN/mm]	LVDT #2 [kN/mm]	LVDT #3 [kN/mm]	LVDT #4 [kN/mm]	LVDT #5 [kN/mm]
Caldwell (East)	609	809	825	166	566
Caldwell (West)	243	1415	737	245	645
Madison (12 ft.)	1041	3068	351	364	400
Madison (60 ft.)	464	307	548	411	404
Upland (15 ft.)	575	964	165	1875	886
Upland (60 ft.)	1211	2340	286	307	694

Table 18. Average tie-ballast gap (LVDT 1) and apparent gap (LVDTs 2–5) values for the NEC sites

Instrumented Site	LVDT #1 [mm]	LVDT #2 [mm]	LVDT #3 [mm]	LVDT #4 [mm]	LVDT #5 [mm]
Caldwell (East)	0.711	0.000	-0.039	-0.086	-0.019
Caldwell (West)	0.948	-0.032	-0.083	-0.094	-0.052
Madison (12 ft.)	1.236	0.004	0.086	-0.012	-0.003
Madison (60 ft.)	0.885	-0.099	-0.062	-0.085	-0.051
Upland (15 ft.)	2.353	0.008	-0.125	-0.008	-0.010
Upland (60 ft.)	0.262	0.091	0.013	-0.006	0.008

The substructure behavior at the six NEC sites can be compared with the parameters in Table 17 and Table 18. This was accomplished by calculating the cumulative transient displacements (e.g., total vertical movement at various depths) of the six LVDT strings. Comparing all six instrumented sites provided insight into potentially stiff or soft layers at different locations.

The cumulative transient displacements were calculated using the following method:

1) First, the net transient vertical displacement of each LVDT was determined using the formula below, assuming a load (P) of 100 kN. This load was used because it was close to the average peak wheel load of the NEC sites.

$$\delta_{LVDT\#2-5} = \delta_{P=0} + \frac{P}{k_{mob}}$$

2) Second, the cumulative transient displacement of a particular LVDT equaled the sum of the transient LVDT displacement and any transient LVDT displacement below it. For example, the cumulative transient displacement of LVDT 4 was the sum of the net transient displacement of LVDT 4 and 5. The cumulative transient displacement of LVDT 1 was the sum of all five net transient LVDT displacements. The cumulative transient displacements with depth are shown in Figure 100 and Figure 101.

3) Third, because the tie-ballast gap was a large component of transient LVDT 1 displacement and therefore cumulative transient displacement, it is included in Figure 100 and excluded in Figure 101 for comparison purposes. The calculated total cumulative transient displacement (e.g., a depth of zero) is displayed in Table 19 for situations where the tie-ballast gap was included and not included.

   If the tie-ballast gap was excluded from the analysis (Figure 101), the substructure behavior was similar for all six NEC sites. LVDT 2 and 3 appeared to be stiffer at Caldwell (West); however, the difference was small. This further suggested that for the six instrumented NEC sites, the tie-ballast gap was the root cause of the different permanent vertical displacements and not the substructure materials.

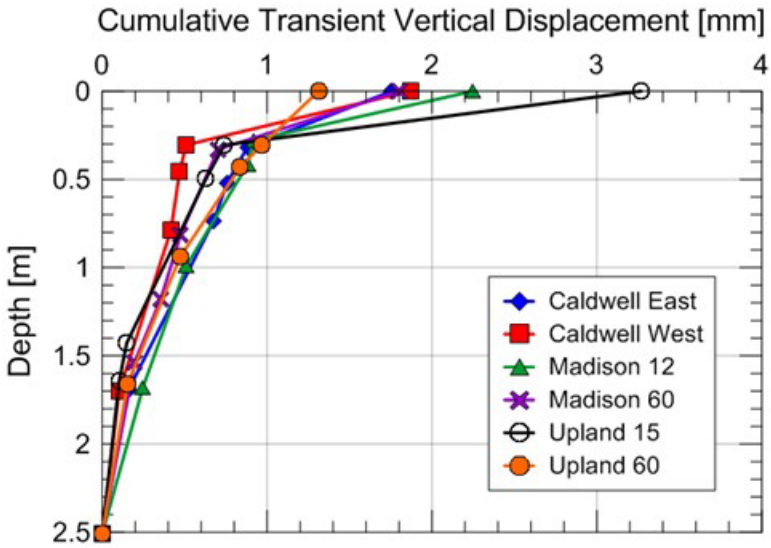

Figure 100. Comparison of cumulative transient vertical displacement at the six NEC sites (with tie-ballast gap included)

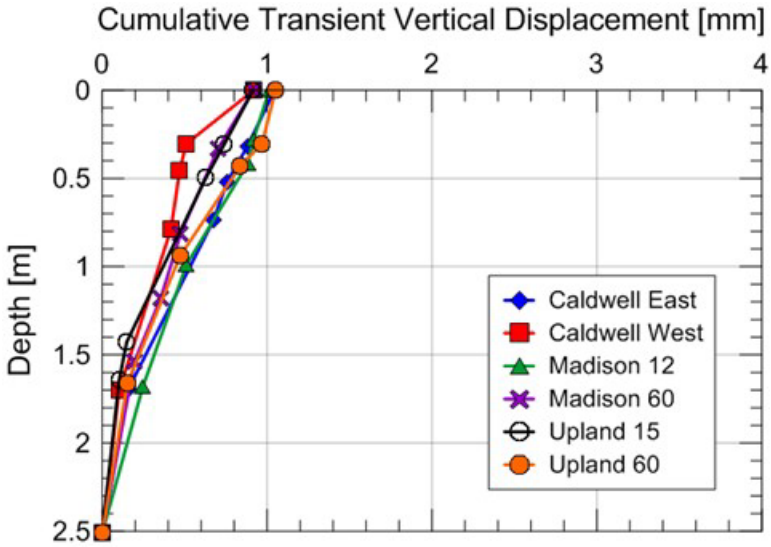

Figure 101. Comparison of cumulative transient vertical displacement at the six NEC sites (without tie-ballast gap included)

Table 19. Total cumulative transient displacement values for the six NEC sites

Instrumented Site	Caldwell		Madison		Upland	
	East [mm]	West [mm]	12 ft. [mm]	60 ft. [mm]	15 ft. [mm]	60 ft. [mm]
$\delta_{P=0}$ Included	1.76	1.87	2.25	1.80	3.27	1.31
$\delta_{P=0}$ Excluded	1.05	0.92	1.01	0.92	0.92	1.05

4) Fourth, sub-ballast and subgrade transient vertical displacements were plotted against permanent LVDT 1 vertical displacement. Correlations between sub-ballast and subgrade with permanent vertical displacements are displayed in Figure 102 and Figure 103. No

trends were observed from this data. A small range of subgrade stiffnesses was measured at the six instrumented sites so the effects of a stiff or soft subgrade could not be inferred. This data indicated that sub-ballast and subgrade was not a significant factor at the six instrumented sites in the NEC for high-speed trains. This conclusion could not be extended to sites with poor subgrades.

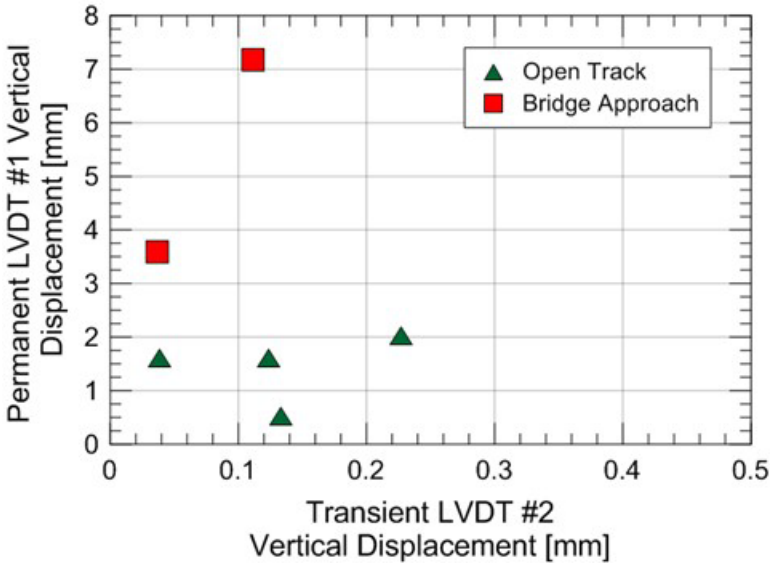

Figure 102. Relationship between average transient LVDT 2 vertical displacement and permanent LVDT 1 vertical displacement at all six instrumentation sites

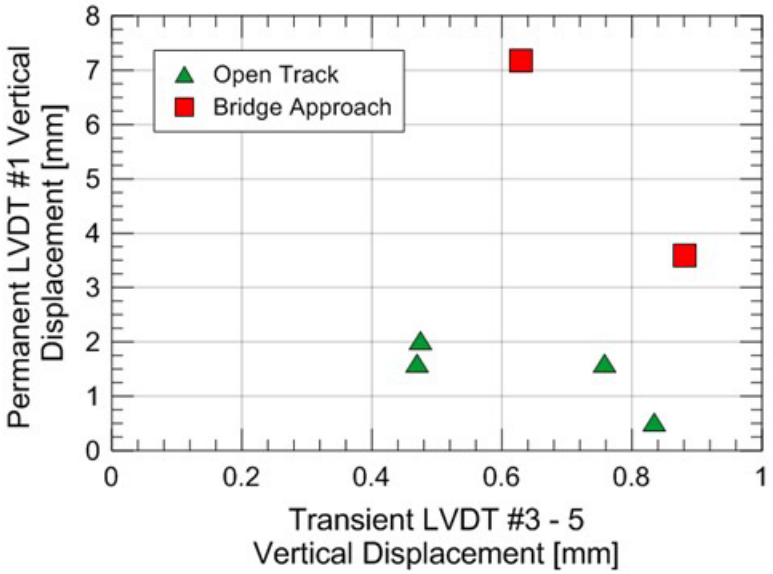

Figure 103. Relationship between average transient LVDT 3–5 vertical displacement and permanent LVDT 1 vertical displacement at all six instrumentation sites

In summary, this section introduced a process to characterize transient LVDT displacement behavior with the use of two mathematical parameters: "apparent gap" ($\delta_{P=0}$) and mobilized LVDT stiffness (k_{mob}). From the Amtrak NEC data, the team concluded that the subgrade stiffness was similar for all six instrumented sites and no relation between sub-ballast or

subgrade transient displacement and permanent LVDT 1 displacement was observed. The NS data showed similar behavior, but there was limited data for analysis.

6.6 LVDT 2 through 6 Force-Displacement Behavior (Norfolk Southern)

Table 20 displays the estimated tie-ballast gap and the mobilized LVDT stiffness from the NS data. As with the Amtrak results, the NS results showed a wide range of stiffness values with little variation between sites besides MP 352.8 (11 ft), which has a softer subgrade.

Table 20. Average mobilized LVDT stiffness (k_{mob}) values for the NS sites

Instrumented Site	$\delta_{P=0}$ [mm]	LVDT #1 [kN/mm]	LVDT #2 [kN/mm]	LVDT #3 [kN/mm]	LVDT #4 [kN/mm]	LVDT #5 [kN/mm]	LVDT #6 [kN/mm]
352.2 (31 ft.)	0.655	2500	200	741	476	1485	-
352.2 (13 ft.)	3.600	444	313	500	435	909	-
352.8 (29 ft.)	0.765	308	126	769	-	1000	870
352.8 (11 ft.)	0.320	271	274	400	526	645	645

Comparisons of the transient vertical displacement with depth between the four NS sites are displayed in Figure 104 and Figure 105. Figure 104 includes the tie-ballast gap and shows significantly greater surface displacements for MP 352.2 (13 ft), due to the large tie-ballast gap at that location. When the tie-ballast gap was excluded, the surface displacements were similar, (like the Amtrak results in Figure 35). As mentioned, MP 352.8 (11 ft) had a softer subgrade but stiffened near the surface. The total cumulative transient displacement values (i.e., surface displacements) are displayed in Figure 79.

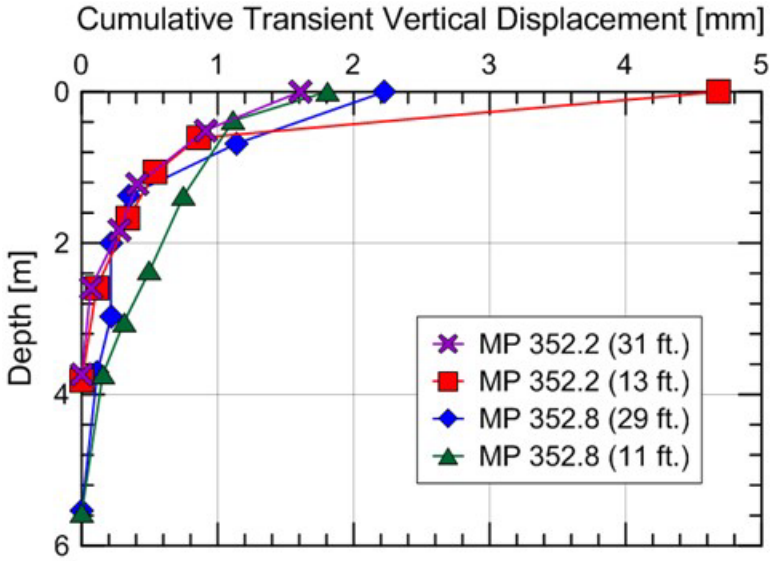

Figure 104. Comparison of cumulative transient vertical displacement at the four NS sites (with Tie-ballast gap included)

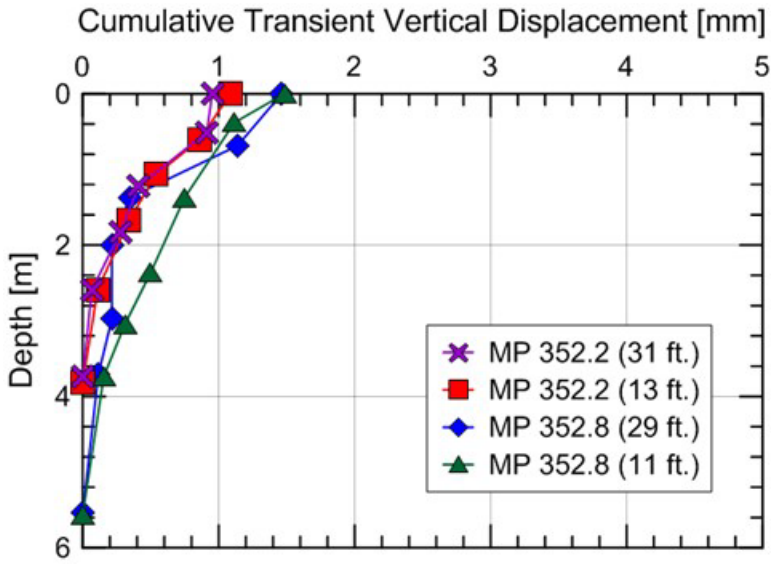

Figure 105. Comparison of cumulative transient vertical displacement at the four NS sites (without tie-ballast gap included)

Table 21. Total cumulative transient displacement values for the four NS sites

	MP 352.2		MP 352.8	
Instrumented Site	13 ft.	31 ft.	11 ft.	29 ft.
	[mm]	[mm]	[mm]	[mm]
$\delta_{P=0}$ Included	4.68	1.61	1.80	2.23
$\delta_{P=0}$ Excluded	1.08	0.95	1.48	1.46

6.7 Track Modulus

One of the most common and useful indicators of track support is track modulus because it characterizes track deflection under a railcar. Track modulus is defined as the supporting force per unit length of track per unit track deflection (Selig and Li, 1994) and is a measure of the stiffness of all the track layers.

It is suggested that the optimal track modulus should be between 14–69 N/mm/mm (Selig and Li, 1994). A low track modulus often implies a weak subgrade, while a track modulus that is too high can enhance dynamic vehicle/track interaction.

Track modulus can be calculated using the following equation (Selig and Waters, 1994):

$$u = \frac{k^{4/3}}{(64EI)^{1/3}}$$

$$k = \frac{P}{Y}$$

where u is track modulus [N/mm/mm], P is vertical wheel load, Y is deflection, E is Young's modulus of the rail, and I is the moment of inertia of the rail cross section.

Typically, the deflection (*Y*) is measured from the TOR using a track-loading vehicle (TLV). In this research, researchers made all measurements at the tie level and below. This means rail deflection and any displacement from the rail pads or fastening system was not included in the data. Therefore, the team assumed that tie displacements roughly equaled TOR displacements when comparing the calculated track modulus with typical values. For the NEC sites, the subgrade displacements were only measured to a depth of 2.5 meters (8 ft, 3 in), while a depth of 3.8 m (12 ft, 6 in) and 5.6 m (18 ft, 3 in) was recorded at the NS N-Line sites. If transient displacement occurred below this depth, those displacements were not included in the track modulus calculations for these sites. These calculated track modulus values were higher than those using traditional methods.

To determine track modulus, the total cumulative transient displacement (Table 22 and Table 23) is input as deflection (*Y*), *P* is assumed as 100 kN, and both the Young's modulus (*E*) and moment of inertia (*I*) of the rail cross-section are determined for the rail used. For 136-RE rail, (i.e., the type of rail at the NEC sites), the *E* and *I* values are 200 GPa (29 E^6 psi) and 3.9 E^7 mm^4 (93.7 in^4), respectively.

Table 22 displays the NEC track modulus for situations where the tie-ballast gap was included and not included. When including the tie-ballast gap, the results showed a soft track structure (12 to 27 N/mm/mm) slightly above the lower limit for an acceptable track modulus (14 N/mm/mm). However, when excluding the tie-ballast gap, the track modulus showed a stiff track structure (55 to 66 N/mm/mm) around the upper limit of 69 N/mm/mm. At Upland (15 ft), the site with the largest tie-ballast gap, excluding the gap raised the track modulus by a factor of 5.5.

Table 22. Track modulus values for the six NEC sites

Instrumented Site	Caldwell		Madison		Upland	
	East [N/mm²]	West [N/mm²]	12 ft. [N/mm²]	60 ft. [N/mm²]	15 ft. [N/mm²]	60 ft. [N/mm²]
$\delta_{P=0}$ Included	28	25	20	27	12	41
$\delta_{P=0}$ Excluded	55	65	57	66	66	55

Table 23 displays the NS track modulus for situations where the tie-ballast gap was included and not included. The results were like the NEC results and showed a significant tie-ballast gap difference in track modulus.

Table 23. Track modulus values for the four NS sites

Instrumented Site	MP 352.2		MP 352.8	
	13 ft. [N/mm²]	31 ft. [N/mm²]	11 ft. [N/mm²]	29 ft. [N/mm²]
$\delta_{P=0}$ Included	7	31	27	20
$\delta_{P=0}$ Excluded	53	63	35	35

7. Accelerometers to Monitor Tie Behavior

The field data at Amtrak's NEC sites suggested that unsupported ties were problematic and were part of the root cause of permanent vertical displacements. Identification and quantification of tie support currently requires strain gages and/or LVDTs. These instruments are costly, invasive, and difficult to install. In this project, the team chose alternative instrumentation techniques.

After considering a wide variety of instrumentation techniques, researchers selected accelerometers for data collection and track assessment because they provided an inexpensive, non-invasive, durable, and reusable means to evaluate tie and track behavior by measuring tie acceleration time histories. The accelerometers used were 13 mm long, weighed less than 3 g, and were connected to a concrete or timber tie with a drop of superglue. A photograph of an accelerometer attached to a concrete tie is displayed in Figure 106. This set up was quick, non-invasive, and did not interfere with train operations.

Figure 106. Accelerometer attached to concrete tie

This section presents the results of a single instrumentation trip on 1 July 2014. Accelerations were measured at Upland (15 ft) and Upland (60 ft). In addition to the acceleration, the previously mentioned wheel loads, tie reactions, and LVDT displacements at Upland (15 ft) and Upland (60 ft) were also measured.

7.1 Accelerometers

Acceleration time histories are beneficial for evaluating tie support because they provide insight into the dynamic movements of the tie. Tie accelerations can be generated from many events, including:

(1) Wheel-rail impacts

(2) Wheel-rail vibrations (e.g., braking)

(3) Rail-tie impacts

(4) Tie loading

(5) Track and tie vibrations

(6) Tie-ballast impact due to a tie-ballast gap

(7) Tie displacement from train loading (as it directly relates to track support)

Each event tends to have its own unique signature that can be identified from analyzing tie accelerations in both the time and frequency domain. Well-supported track will typically display tie accelerations from only tie loading but can also show wheel-rail impacts and wheel-rail vibrations because those tie accelerations are associated with the train vehicle. The remaining events are typically indicative of poorly supported track. However, because poor tie support is the focus of this report, factors (5), (6), and (7) are emphasized because they are typically produced in track environments experiencing transient or permanent displacements, like a bridge transition.

The transfer of load from the rail to the tie produces the most basic tie acceleration signature. The signature usually includes a gradual increase in tie acceleration until a maximum value is obtained, followed by a gradual decrease in acceleration as the wheel or wheelset exits the measurement zone. Maximum accelerations typically range from 1 to 5 g for well-supported track but can be much higher for poorly supported track (10 to over 100 g). The dominant frequencies of the tie typically range from 50 to 300 Hz but are sometimes difficult to isolate because of the presence of multiple sources of tie acceleration and the coupling of vibration modes.

Another common source of tie acceleration is tie and track vibration. All deformable materials exhibit unique bending or vibration modes, and multiple laboratory investigations have identified the first three vibration modes for concrete ties at 100-150 Hz, 330 Hz, and 630 Hz. These distinct vibration modes can be detected by monitoring the resulting tie vibration of an isolated, unsupported tie after each wheel loading. This behavior is comparable to how a bell rings after being struck. Unsupported ties will not be damped and constrained by the underlying and nearby ballast. If a group of ties are unsupported, the entire track may vibrate. The tie vibration modes become less distinct due to the coupling of track vibration modes.

Tie accelerations from an unsupported tie contacting the ballast can also amplify the force being applied to the ballast. These impacts often result in sharp peaks in tie accelerations at frequencies of approximately 50 to 300 Hz, depending on train speed and track compliance. These high-impact forces are also indicative of poorly supported track.

Tie displacement accelerations generally have low-amplitude, low-frequency signatures, typically between 0 and 15 Hz. Accelerations and displacements have a second-order polynomial relationship with respect to time (acceleration ≈ displacement/(time squared)). The time required to displace a tie large distance (~50 mm) is long enough to keep the tie accelerations low compared to the sudden and large accelerations produced from impacts and low-displacement vibrations. These signatures are difficult to analyze unless double-integration techniques of the time history are used.

External factors affecting tie acceleration signatures include train weight, speed, bouncing, wheelset dimensions, tie spacing and type, track curvature, etc. For well-supported track where load transfer from the wheel to substructure is smooth, these external factors do not seem to have a significant influence because of the low magnitudes of tie displacement. Based on several sites investigated by Wilk et al. (2015), well-supported track consistently produces tie accelerations from tie loading at or below 5 g for a variety of passenger and freight train weights, lengths, and speed.

External factors significantly influence accelerations for poorly supported track because of the larger tie movement. For example, a higher train weight or speed will either displace the tie at a quicker rate or apply greater force which results in greater tie accelerations. Different types of wheelsets also may affect how the tie is loaded and therefore its acceleration magnitudes. For this reason, accelerometers are considered suitable for qualitatively measuring tie support and can give additional insight into how these external factors affect track movement and loading.

7.2 Site Location

The Upland Street site was initially instrumented with strain gages and LVDT strings and later instrumented with eight accelerometers to evaluate tie support and to compare accelerometer data with the strain gage and LVDT equipment. The instrumentation layout for the Upland Street bridge is shown in Figure 107. This report analyzes only Accelerometers 4 and 8, installed at the two LVDT string locations and referred to here as Upland (15 ft) and Upland (60 ft), respectively.

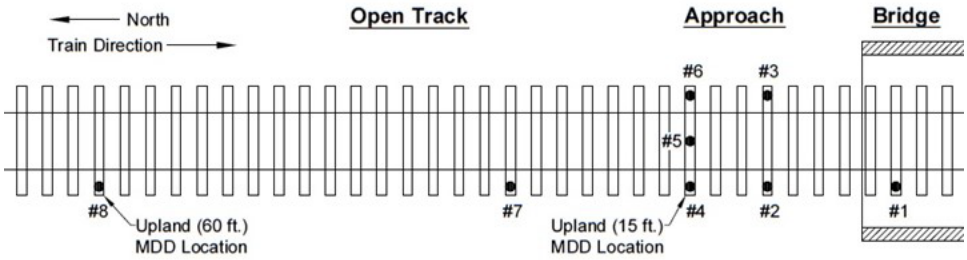

Figure 107. Instrumentation location of accelerometers and LVDTs at the Upland Street bridge approach

7.3 Tie Behavior

The following sections describe the tie response to load at the measurement sites.

7.3.1 Ballast/LVDT 1 Response

To aid comparisons between the LVDTs and accelerometers at Upland (15 ft) and Upland (60 ft), researchers analyzed the transient track response. Transient behavior is important because negative effects of each passing train can accumulate into noticeable, permanent track geometry problems. Therefore, identifying and remediating problems within the transient timescale can identify track structure and track geometry problems.

The most apparent transient behavior difference between the two Upland Street sites was the vertical displacement magnitudes within LVDT 1. LVDT 1 measured the transient vertical displacements from the top of the concrete tie to the bottom of the ballast layer (0.3 m in depth).

LVDT 1 data included both the closure of the tie-ballast gap and the displacement of the ballast underneath the tie, as stated in Section 6. For simplicity, this section will reference LVDT 1 displacement as vertical tie displacement because LVDT 1 was fixed to the tie, so the displacements measured by LVDT 1 correspond to tie movement.

Figure 108 displays the wheel load, tie transient vertical displacement, and tie acceleration time histories for Upland (15 ft) and Upland (60 ft) resulting from the same Amtrak passenger train. The Upland (60 ft) time histories were shifted so the peak wheel loads matched the Upland (15 ft) time history. Upland (15 ft) showed peak vertical tie displacements of about 7.0 mm, while Upland (60 ft) displayed peak tie displacements of only about 0.4 mm. The significantly larger peak vertical tie displacement (i.e., 17 times larger) at Upland (15 ft) suggested a tie-ballast gap was present at that location, because this difference in tie displacement magnitude cannot be explained by variation of ballast stiffness. The tie accelerations are discussed in the next section.

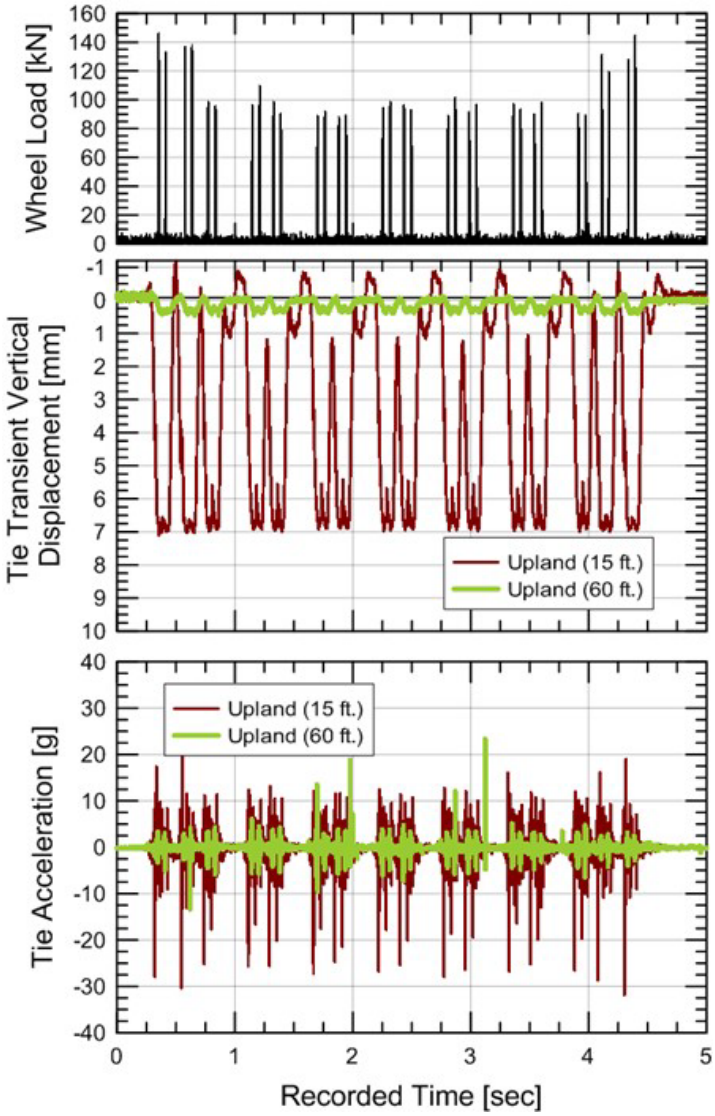

Figure 108. Recorded time histories of wheel load, tie transient vertical displacements, and tie accelerations at Upland (15 f.t) and Upland (60 ft) on 1 July 2014

Figure 109 shows a detailed view of the last three wheelsets of the passenger train after 3.75 to 4.75 seconds. At about 3.38, 4.08, and 4.30 seconds, sharp changes in tie displacement occurred, attributed to the tie contacting the ballast. Additionally, the Upland (15 ft) tie rebounded (positive vertical displacement) after the passing wheel set because the rail pulled the tie upward when it was unloaded. These measurements indicated the tie at Upland (15 ft) was poorly supported.

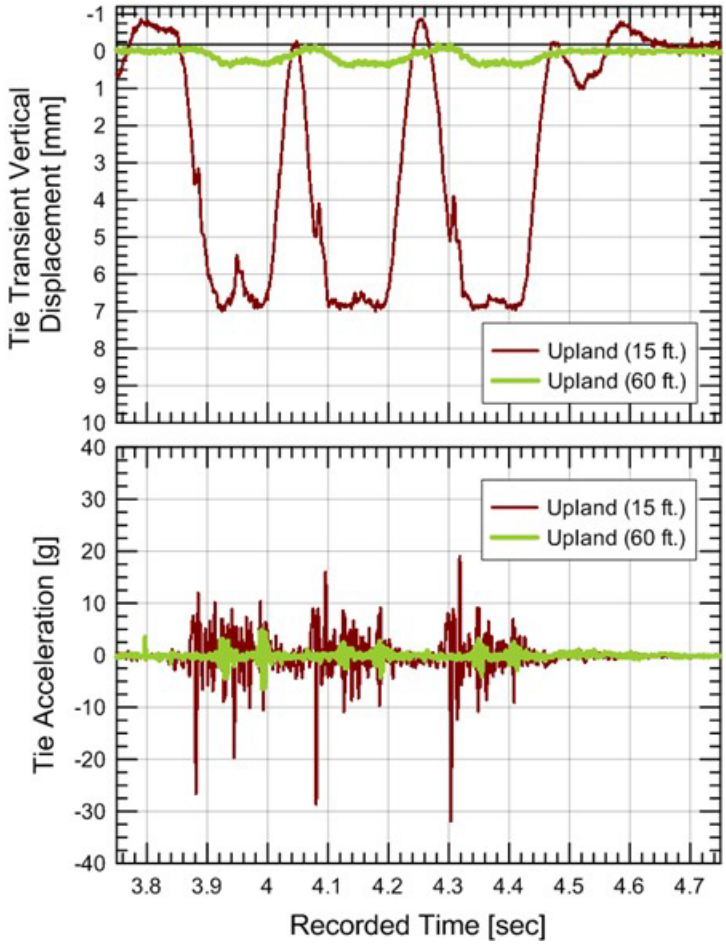

Figure 109. Tie transient vertical displacement and tie acceleration response from a passing Acela power car at Upland (15 ft) and Upland (60 ft) on 1 July 2014

Using the techniques presented in Section 6, the load-displacement measurements in Figure 110 show a significant difference in the estimated tie-ballast gap ($\delta_{P=0}$) between these locations: 0.29 mm at Upland (60 ft) and 6.74 mm at Upland (15 ft). The tie-ballast interaction displayed non-linear behavior below the seating load (i.e., the load at which the tie contacted the ballast and the ballast became fully mobilized and displayed linear behavior). Therefore, the actual tie-ballast gap (δ_{gap}) at Upland (15 ft) was expected to be smaller and about 5 mm, which was in agreement with Figure 108 and Figure 109. The ballast particles likely rearranged after each loading, so the actual tie-ballast gap (δ_{gap}) would vary after each wheel pass.

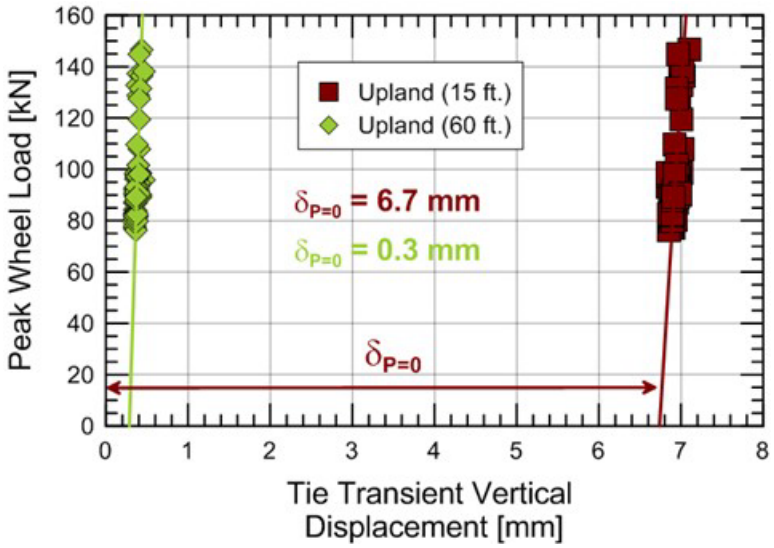

Figure 110. Tie load-displacement behavior at Upland (15 ft) and Upland (60 ft)

7.3.2 Accelerometer Response

The acceleration time histories for the same Amtrak passenger train are displayed in Figure 108 and Figure 109. To eliminate high-frequency movement, the time histories were passed through a low-band Butterworth filter at 500 Hz. As with the LVDT displacements, a significant difference in tie acceleration response was observed. Upland (15 ft) displayed much greater consistent peak accelerations of about 30 g, while Upland (60 ft) showed consistent peak accelerations of less than or equal to 5 g.

The large downward accelerations (~30 g) of Upland (15 ft) typically appeared immediately prior to a wheel pass. By comparing the tie transient vertical displacement and tie acceleration time histories in Figure 109, the tie acceleration peaks occurred at recorded times of 3.38, 3.95, 4.08, and 4.30 seconds. This corresponded to the sharp change in displacement when the tie was contacting the ballast. The only exception was the second wheel of the Acela power car wheelsets (wheel loads of about 140 kN), in which the tie remained in full mobilized contact with the ballast (see Figure 109). The team hypothesized that the large downward accelerations (~30 g) were produced from the tie establishing contact with the ballast and possibly amplifying the tie-ballast load from impact, though more evidence would need to be gathered to verify this. The remaining movement (~10 g) was likely from load transfer and vibrations of the track and tie. The tie accelerations at Upland (60 ft) showed distinct responses (~5 g) from the loading of each passing wheel. A few isolated high-frequency peaks can be observed in Figure 110, likely from wheel or data anomalies.

Figure 111(a) and (b) compare the acceleration time histories in Figure 108 in the frequency domain using fast Fourier transform (FFT) techniques. Figure 111(a) shows a range from 0 to 250 Hz, which emphasizes the larger Fourier amplitudes from train loading and track and tie vibrations at Upland (15 ft). Sites with poor tie support experienced greater tie acceleration magnitudes and offered less damping and resistance to tie and track vibration than well-supported sites, and they had larger Fourier amplitudes within that frequency range.

Figure 111(b) shows a frequency range from 0 to 20 Hz, to highlight the tie displacement, and compares LVDT 1 tie displacement response of Upland (15 ft), tie accelerometer response at Upland (15 ft), and the tie acceleration response at Upland (60 ft). Three dominant frequencies appeared from the LVDT 1 response: 1.8, 3.6, and 5.4 Hz. These frequencies were associated with unloading between the wheelsets, loading from a wheelset, and loading from an individual wheel, respectively. The Upland (15 ft) tie accelerations showed dominant frequencies at identical frequencies but are strongest at 5.4 Hz. Tie displacements could be obtained from these data. The Upland (60 ft) tie accelerations were low, which agreed with the low measured displacement values.

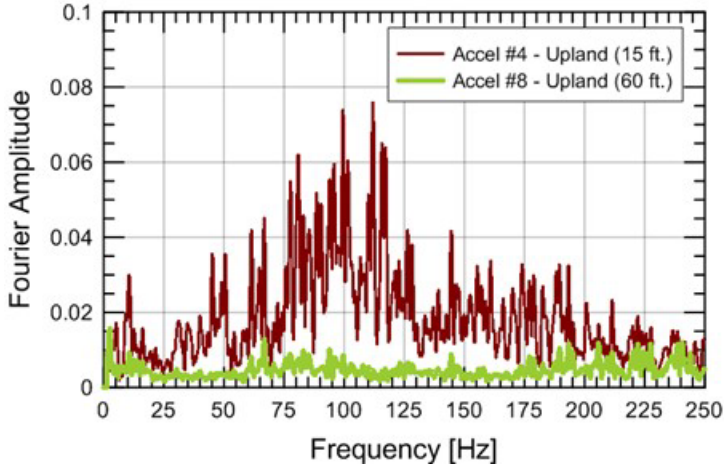

(a)

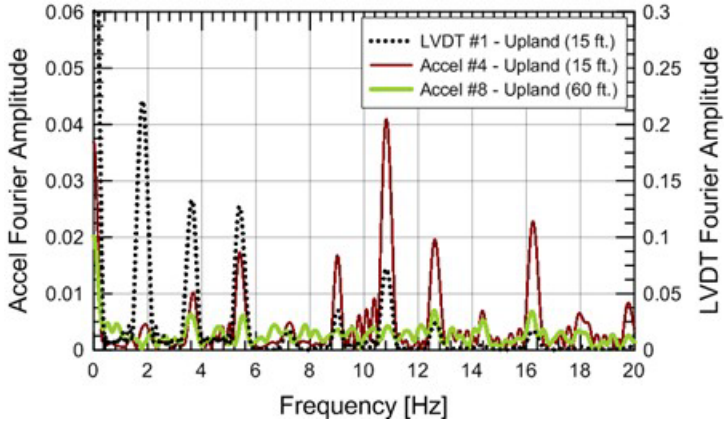

(b)

Figure 111. (a) Measured tie acceleration time histories for Upland (15 ft) and Upland (60 ft) and (b) recorded LVDT 1 and measured tie acceleration time histories for Upland (15 ft) and Upland (60 ft) in Figure 108 converted to frequency domain for a passing train on 1 July 2014

Table 24 summarizes the permanent vertical displacement rate, peak transient displacements, estimated tie-ballast gap ($\delta_{P=0}$), and peak tie acceleration values for Upland (15 ft) and Upland (60 ft). These results showed significant differences in track behavior between the transition zone and open track due to the presence of tie-ballast gaps in the transition zones. This poor tie support, identified by both LVDTs and accelerometers, can lead to additional permanent vertical

displacements from impact loading and load redistribution. The low, consistent peak accelerations (<5 g) at Upland (60 ft) indicated well-supported track with smooth load transfer and small tie-ballast gaps.

Table 24. Values of permanent vertical displacement rates, peak transient displacement, estimated tie-ballast gap values ($\delta_{P=0}$), and peak accelerations for Upland (15 ft) and Upland (60 ft)

Site Location	Rate of permanent vertical displacement [mm/yr]	Peak transient displacement [mm]	$\delta_{P=0}$ [mm]	Peak tie acceleration [g]
Upland (15 ft.)	15	7.0	6.7	30
Upland (60 ft.)	0.8	0.4	0.3	~5

7.4 Summary

Researchers installed accelerometers at the Upland Street location to assess the benefits of using a non-invasive measuring system to evaluate tie support and impacts. The main findings are summarized below:

- LVDT and accelerometer measurements could identify poorly supported ties, which experienced greater tie displacement and track and tie vibrations. The impact between the tie and ballast resulted in large tie accelerations. These movements typically occurred within a 50 to 300 Hz frequency range. Analyzing the acceleration time history in the frequency domain showed greater Fourier amplitudes within this frequency range.
- Various types of impacts and vibrations could be identified by analyzing tie acceleration signatures in the time and frequency domains. Each type of impact and vibration tended to exhibit a unique signature. These signatures can be useful for identifying poorly supported track, assessing how the track is moving under load, and identifying the forces the track components experience.

8. Highway Bridge Transition Comparison

The research team based this study for differential movement at railway transitions on a study for the Illinois Department of Transportation (IDOT) in the late 1990s conducted by Stark (Stark et al., 1995; Long et al., 1999). The main objectives of the IDOT study were:

- Identify the causes of differential settlements of highway bridge transitions
- Develop design methods to reduce post-construction differential settlements at the bridge-approach fill interface
- Develop maintenance and rehabilitation measures to mitigate problematic differential movement at the bridge-approach fill interface (Stark et al., 1995; Long et al., 1999)

The team used these objectives to develop the objectives for this project. Because the objectives are similar, one of the tasks of this study was to compare the location and causes of the observed differential movements along Amtrak's NEC with those derived from that highway bridge transitions study. This section presents the results of this comparison, which include some interesting observations and ideas for designing and remediating railway transitions.

Stark et al. (1995) and Long et al. (1999) found that 27 percent of 1,181 highway bridge approaches in Illinois exhibited significant differential movement at the approach embankment-bridge interface. The observed differential movement at these 1,181 bridge approaches was divided into the following six major causes:

- Local compression or erosion of materials at the approach embankment-bridge interface
- A broken approach slab
- Compression of foundation soils
- Compression or internal erosion of embankment soils
- Poor construction grade control and/or fill control
- Areal distortion of foundation soils caused by mine subsidence or other areal mechanisms (Stark et al., 1995; Long et al., 1999).

Some of these are applicable to the six MDD instrumentation sites in Chester, Pennsylvania (e.g., broken ties, compression or internal erosion of embankment soils or ballast, and local compression or erosion of materials at the approach embankment-bridge interface).

More importantly, Stark et al. (1995) found that significant rider discomfort occurred with a differential settlement of greater than or equal to 2 to 3 in (50 to 75 mm) or an approach gradient of 1/125 for existing bridges. The approach gradient is defined as the differential settlement divided by the length over which the settlement or vertical displacement occurs. Long et al. (1999) recommend an approach gradient of less than 1/200 for design of a new approach. This is important because the criterion for high-speed rail should be even more stringent because of rider sensitivity and safety at higher speeds.

The difficulty of achieving an approach gradient of less than 1/125 for high-speed rail can be put in perspective by comparing the axle loads applied to the transition zone by an Acela engine and a fully loaded tractor-trailer truck on an interstate highway. On highways, the federally regulated

maximum highway load of a commercial vehicle is 80,000 lb, and for a single axle is 20,000 lb. The weight of an Acela Express power car is 204,000 lb. Each power car has four axles or eight wheels, resulting in axle loads of 51,000 lb. If a single tie experiences 40 percent of the axle load, this produces tie loads of 20,400 lb for an Acela Express power car. This quick calculation indicates that the Acela power car may be applying more than twice the axle load of a highway truck – a load being distributed to the ballast only by narrow ties instead of a continuous approach slab or pavement.

While there are many key differences between highway bridges and railroad bridges (e.g., load distributions, lack of asphalt overlayment, and larger ballast particles), a few highway bridge design techniques could be applicable to railroad bridges. These include the following:

- Allowing more bridge movement
- Confinement of approach materials
- Higher quality fill material

The design recommendations for railroad bridge transitions are presented in Section 10 of this report.

9. Field Evaluation Summary

This section presents the data, analyses, and interpretations of the field measurements of the monitored railway transitions along the Amtrak NEC near Chester, Pennsylvania, and the NS N-Line bridges in southern West Virginia. This section identifies the depth and location of the permanent vertical displacements and proposes three root causes of the measured permanent and transient vertical displacements. Summaries of the three main points of this report are presented below.

9.1 Depth and Location of Permanent Vertical Displacements

The team measured the permanent vertical displacements of interest within the Madison and Upland Avenue bridge transition zones. Most of the measured permanent vertical displacement occurred in LVDT 1 (i.e., the ballast layer). The Upland (15 ft) site exhibited the largest permanent LVDT 1 vertical displacement at 7.17 mm, followed by Madison (12 ft) at 3.58 mm. Both locations are within the transition zone for the nearby bridge. Madison (60 ft) and both Caldwell Avenue bridge (80 ft) sites experienced similar permanent vertical displacements of 1.61 to 2.02 mm, with the least amount of permanent vertical displacement occurring at Upland (60 ft), at 0.52 mm. To determine possible root causes of the measured permanent vertical displacements, the team focused analysis on the permanent vertical displacements at Upland (15 ft) and Upland (60 ft) because they represented the largest and smallest measured permanent vertical displacements.

9.2 Tie-Ballast Gaps

From analysis of the Amtrak NEC field data and field investigations, researchers established a strong correlation between the permanent vertical displacements of LVDT 1 (i.e., ballast and tie-ballast gap) and tie or track support. The team determined five potential indicators of poor tie support:

- Visual observation of large tie vertical displacements and rebounding
- Measured transient vertical displacements
- Accelerometer data for selected ties
- Measured tie reactions
- Permanent vertical displacements

The field data suggested that tie-ballast gaps ($\delta_{P=0}$) above 1.0 mm can cause an increase in the applied loads on the ballast at the instrumented tie and can lead to larger permanent vertical displacements (see Section 7). In addition, the tie-ballast gap ($\delta_{P=0}$) plus the permanent vertical displacement should be less than about 4.0 mm, assuming there is no additional displacement between the TOR and top of tie.

Two possible mechanisms exist for the correlation between tie-ballast gaps and permanent vertical displacements:

1. The development of tie-ballast gaps is a natural result of differential permanent displacement between the transition zone track and bridge abutment. As the ballast in the transition zone naturally settles, the rail in the transition zone will still be supported by

the ties on the bridge abutment. This will produce tie-ballast gaps in the transition zone, as illustrated in Figure 112.

2. The presence of tie-ballast gaps increases the measured permanent vertical ballast displacements by either (1) increasing the applied loads to the ballast or (2) increasing ballast degradation because of the additional movement and impact between the tie and ballast. Field evidence of the impact between the tie and ballast is presented in Section 7. Laboratory evidence of increased ballast degradation from tie-ballast gaps is presented in Appendix D. Figure 112 also shows that the presence of tie-ballast gaps can cause the rear wheels of a passing truck to impact the abutment because the front wheel is at a higher elevation to enter the bridge deck.

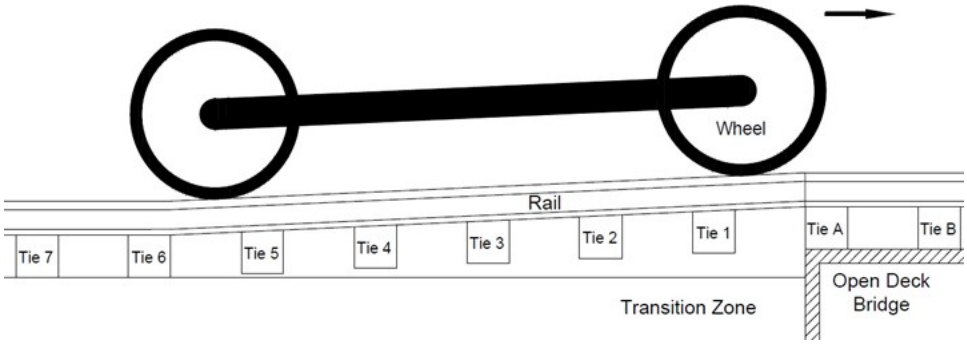

Figure 112. Development of tie-ballast gaps from uneven settlement in the transition zone

Both mechanisms were expected to contribute to the increased permanent vertical displacements in the transition zone ballast layer. Tie-ballast gaps initially develop because of the differential settlement between the transition zone and bridge deck. Consequentially, tie ballast gaps increase the applied loads and ballast degradation, resulting in further permanent vertical displacements in the transition zone ballast layer.

9.3 Wet, Fouled Ballast

From multiple visits to the Amtrak instrumented site, researchers observed that wet, fouled ballast was present in the transition zone regions (i.e., Upland (15 ft)) and were greater than observed in the open track regions (i.e., Upland (60 ft)). This was expected to also contribute to the greater permanent vertical displacements at the transition zone site, addressed in more detail in Appendix B. Potential reasons for the increased fouling in the transition zone region are increased ballast degradation due to increased loading, tie damage due to the presence of tie-ballast gaps, and fines shaken from the passing cars when the wheels hit the bridge abutment, as illustrated in Figure 112. The presence of the bridge abutment was also expected to slow or impede drainage of the ballast.

10. Root Cause of Permanent Vertical Displacements

One of the main objectives of this study was to identify the root or initiating cause(s) of the measured permanent vertical displacements at the NEC MDD instrumentation sites. Importantly, this can be used to locate the place in the causal chain where an intervention could reasonably be implemented to change the observed performance or prevent an undesirable outcome. This section identifies the root cause(s) and potential remedial measures that can change the negative observed performance at the Amtrak NEC sites.

The team identified the undesirable outcome as permanent vertical displacements of the ballast under train loading. Field data at the Amtrak NEC sites showed most of the permanent vertical displacement occurring in the ballast layer (i.e., LVDT 1) and within the two bridge approach sites, Upland (15 ft) and Madison (12 ft). The four open track sites showed lower permanent vertical displacements, with the Upland (60 ft) site experiencing the lowest.

10.1 Root Causes

An analysis of the transient train data, field investigations, numerical simulations, and a literature review identified three primary root causes of the observed permanent vertical displacements in the ballast layer include:

1) Track stiffness variation between the bridge structure and the adjacent track
2) Increased dynamic loads in the transition zone
3) Undesirable ballast conditions in the transition zone

The earthen open track approach sections are less stiff than the rigid bridge that is built on deep foundations. This difference in stiffness causes differential settlement of the open track sections relative to the stiff bridge in response to dynamic train loads. As the approach track settles, a change in rail elevation between the approach track and bridge deck develops, resulting in tie-ballast gaps.

The second root cause, increased applied loads in the transition zone, can be produced from multiple factors:

- Rapid change in axle elevation
- Impact loads from tie-ballast gaps
- Load concentrations and redistributions
- Broken track components

The rapid change of axle elevation is produced when the front axle of a train must accelerate upwards to move from the lower elevated approach to higher elevated bridge deck. This upward acceleration causes a coupling between the front and back axles which increases the dynamic load of the back wheels. This location of increased dynamic load is typically 6 to 12 ft off the bridge end, in the approach track. This mechanism can be produced from both differential stiffness (transient vertical displacements) and differential settlement (permanent vertical displacements) between the approach track and bridge deck. However, numerical results show that the increased dynamic loads produced from differential settlement are significantly greater

(>100 percent increase in tie load) than the increased dynamic loads produced from differential stiffness (<20 percent increase in tie load).

Impact loads from tie-ballast gaps have been observed from measuring the accelerations of ties displaying tie-ballast gaps. The data shows a peak in tie acceleration at the moment of impact, suggesting an increased dynamic load because of Newton's Second Law, which states force (F) equals mass (m) times acceleration (a). However, the exact force is difficult to quantify without directly measuring the force at the tie-ballast interface.

Load concentrations and redistributions from tie-ballast gaps have been shown numerically in both open track and bridge approach simulations (see Section 15). Simulations showed that the wheel load shed away from poorly supported ties and concentrated on more well supported ties. This can potentially result in increased dynamic tie loads of greater than 100 percent in the transition zone.

Track irregularities observed over the course of the monitoring period can also contribute to the increased dynamic loads. Track irregularities include broken ties, broken fastening systems, and rail height differences and can increase dynamic loads from the redistribution of loads and impacts. The effects of track irregularities was not a major focus of the research but are still expected to contribute to increasing dynamic loads in the transition zone.

The third root cause, undesirable ballast conditions in the transition zone region, refers to degraded, wet, fouled ballast. Multiple laboratory tests showed that this type of fouled ballast can result in significantly greater ballast settlement than clean, dry ballast.

10.2 Chain of Events

After identifying the root causes of the observed permanent vertical displacements identified, researchers sought to explain the chain of events leading to the observed permanent vertical displacements in transition zones. Because the exact chain of events can differ for a given transition zone, the proposed chain of events below should be viewed conceptually and open for modification or change based on site location.

The various mechanisms leading to the observed permanent vertical displacements are expected to occur simultaneously, so multiple mechanisms will be explained in each stage. These mechanisms may appear contradictory at times, e.g., impact loads increasing the applied load of unsupported ties while load redistribution reduces the applied load of unsupported ties, suggesting that dominant mechanism may vary depending on the situation. However, all mentioned mechanisms are expected to play a role in the chain of events leading to the observed permanent vertical displacements and for assessing the behavior of other track systems:

1. Ideally, the initial state of track has a constant rail elevation between the open track, transition zone, and bridge. This represents the state immediately after track placement or tamping. This is illustrated in Figure 113 as Stage 1.

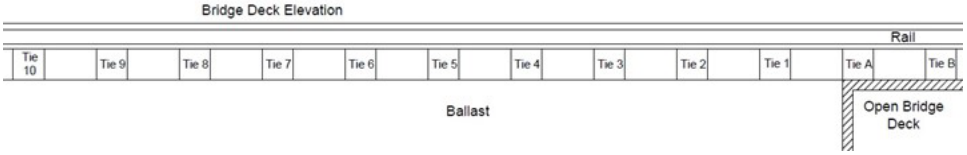

Figure 113. Schematic of anticipated rail and ballast profiles during Stage 1

2. As the first train axle loads the ballast, the ballast in the open track and bridge approach settles. The magnitude and rate of settlement will primarily be dependent on the level of ballast compaction because the ballast particles are primarily expected to re-arrange into a denser, more compact state, as illustrated in Figure 80 and Figure 81 at distances of 29 and 11 ft from the bridge. Both figures show large vertical transient displacements (0.8 to 1.3 mm in LVDT 1) for five to ten trains and then a significant decrease to 0.4 to 0.8 mm because some ballast compaction occurred due to the first trains. Wet, fouled ballast is anticipated to result in greater ballast settlement magnitudes and rates. Tie-ballast gaps may develop at the ties closest to the bridge abutment depending on the magnitude of settlement.

   Additionally, the differential stiffness between the approach and bridge is also expected to increase the dynamic tie loads at about ten ft from the bridge abutment. This will result in slightly greater ballast settlements underneath those ties. The anticipated rail and ballast profile in Stage 2 is displayed in Figure 114.

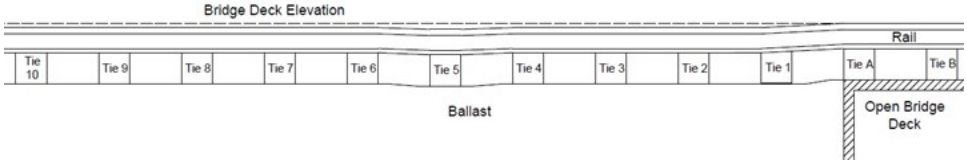

Figure 114. Schematic of anticipated rail and ballast profiles during Stage 2

3. As trains continue to load the ballast, the differential settlement between the approach track and bridge deck will further increase the dynamic loads experienced in this transition zone. Additionally, tie-ballast gaps may develop near the bridge abutment. This is illustrated in Figure 115.

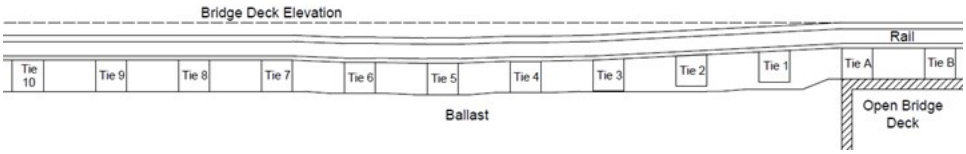

Figure 115. Schematic of anticipated rail and ballast profiles during Stage 3

4. The tie-ballast gaps should begin to concentrate and redistribute the wheel load to the well-supported ties in the approach. This process will expand the transition zone as more ties become unsupported.

   The ballast settlement under unsupported ties can also increase due to impacts between the tie and ballast. This can increase dynamic loads and degrade the ballast.

   Further differential settlement between the approach and bridge will also increase the dynamic loads at about 10 ft from the bridge deck. Therefore, the ballast settlement is expected to be greatest in this region.

   The ballast in the transition zone and approach may also begin degrading from load repetitions. This can lead to degradation and fouling of the ballast matrix, producing increased rates of permanent vertical ballast displacement.

   The anticipated rail and ballast profile in Stage 4 is displayed in Figure 116.

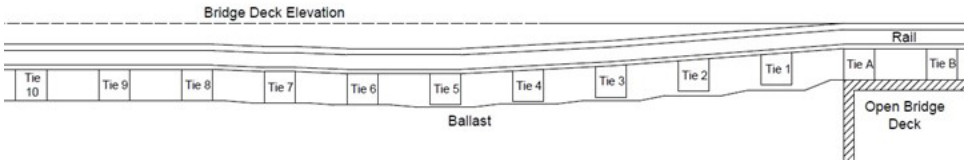

Figure 116. Schematic of anticipated rail and ballast profiles during Stage 4

5. The mechanisms mentioned in Stage 4 are expected to continue and amplify. This results in a self-perpetuating system of incrementally increasing applied loads and levels of ballast fouling, which increases the rate of permanent vertical displacements of the ballast layer. This results in significantly greater permanent vertical ballast displacements in the transition zone than open track, which agrees with field observations in Section 3. An example is shown in Figure 117.

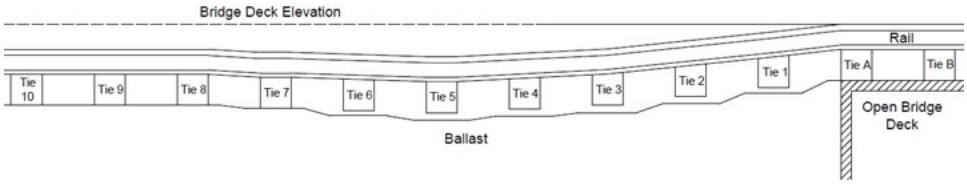

Figure 117. Schematic of anticipated rail and ballast profiles during Stage 5

10.3 Design and Remediation Recommendations

Based on the chain of events proposed in the previous section, preventing the final self-perpetuating state from occurring is primarily dependent on reducing ballast settlement in the approach. Once the ballast settles, tie-ballast gaps are expected to develop, consequentially increasing the dynamic loads and rate of ballast degradation. At this point, it is unlikely that the transition zone degradation process can be stopped, and recurrent resurfacing will be required.

To help prevent transition zone degradation, researchers propose the following design recommendations:

1. Decrease the stiffness of the bridge by installing a ballasted bridge deck and a combination of other stiffness-reducing elements, including rail pads, tie pads, and ballast mats. This should reduce the increased dynamic loads from rapid changes in wheel elevation.
2. Place the track with compacted ballast, and install adequate drainage systems. If the ballast is not compacted after placement or tamping, the first wheel pass will re-arrange the ballast particles in a more compact state (see Figure 80 and Figure 81). This compaction process produces differential rail elevations between the approach and bridge deck and tie-ballast gaps will develop, both of which will increase the dynamic loading of future trains. Strong ballast material is recommended to reduce the eventual ballast breakdown and subsequent fouling. Installing and maintaining a system that adequately drains the ballast is also important to maintain desirable ballast conditions.
3. Reduce ballast and subgrade settlement by confining the approach areas. Increasing approach confinement produces a stronger ballast and subgrade soil matrix and lowers both transient and permanent vertical displacements. Confinement stiffens the ballast and

subgrade and reduces settlement. This can be accomplished by installing concrete wing walls, hot-mixed asphalt (HMA) underlayment, geotextiles, or other similar systems.

4. Reduce ballast settlement by increasing the tie-ballast contact area with under-tie pads (UTPs). The combination of stiff concrete ties and large, angular ballast particles produces a small contact area between the bottom of the tie and underlying ballast particles. This small contact area will increase the contact stress on the ballast particles and can increase ballast degradation. By installing a compliant pad at the tie-ballast interface, the contact area will increase and reduce both tie and ballast degradation.

While researchers do not propose that all four design recommendations be required to prevent transition zone degradation, they recommend a combination of two or three of the proposed remedies. Bridge approaches with only a single design recommendation tend to continue to experience transition zone degradation. Most successful designs involve two or three of the above recommendations.

If the transition requires frequent resurfacing to maintain track geometry, the team proposes the following remedial recommendations:

1. Use specialty tampers that produce a dense, compact ballast state during the tamping process. By compacting the ballast, the initial ballast settlement can be reduced, which can slow down the transition zone degradation process. Additionally, tamping procedures that reduce ballast breakdown during tamping would also be desirable.
2. Leave the ballast in its dense, compacted state during resurfacing and “extend” ties by installing a shim underneath the tie during resurfacing. If the operation can be proven practical, this technique can reduce initial settlement after resurfacing and increase tie and ballast life if the shim is resistant, as it will act like a UTP.
3. Replace damage and/or broken track components.
4. Clean the ballast.

11. Numeric Modeling – Introduction

The section presents the numerical modeling performed to simulate monitored railway transitions to better understand the factor(s) contributing to the measured transient and permanent vertical displacements as well as to predict future performance with and without remedial measures. Researchers used two software packages to complete the numerical analysis portion of this study: FLAC3D and LS-DYNA. These models could allow the impact of train loading and speed, ballast, sub-ballast, approach fill, and subgrade to be investigated and allow understanding of the observed transient and permanent differential movement and the effect of different rehabilitation techniques on the transition performance to be quantified.

The four main tasks of the numerical modeling effort are summarized below:

- Develop numerical models and material properties of monitored railway transitions
- Use field vertical displacement measurements to calibrate the models and use calibrated models to predict future transition performance with and without remedial measures
- Use calibrated numerical models to predict performance of rehabilitation techniques proposed for field implementation, such as approach confinement, asphalt underlayment, decreased tie spacing, UTPs, and stone blowing
- Use calibrated numerical models to predict the performance of promising design techniques to prevent/minimize differential movement at railway transitions

Models were calibrated using the measured vertical displacements and wheel loads at the single instrumented ties on the Amtrak NEC in Chester, Pennsylvania, and the NS in West Virginia. However, to predict the behavior of the entire approach, future studies should monitor several ties in the approach to provide insight to the many factors that contribute to the transient and permanent vertical displacements in a bridge approach. For example, accelerometers and/or video cameras could be used to non-invasively monitor several ties leading to the Upland Avenue bridge in Chester. Developing a calibrated model with predictive capabilities requires knowledge of the ballast settlement under most, if not all, of the ties in the transition zone to develop settlement model that represents the range of ballast conditions, tie-ballast gaps, and tie condition in the transition zone.

From the analysis of field data, researchers discovered a strong correlation between the presence of tie-ballast gaps ($\delta_{P=0}$) and permanent vertical displacements. The existence of a tie-ballast gap was also supported by measured tie reaction, observed large tie vertical displacement and rebounding, transient vertical displacements, acceleration time histories, and permanent vertical displacements. Field investigations of the Amtrak NEC sites further showed that damaged ties and other defects around the instrumented tie also experienced large permanent vertical displacements.

However, the physical mechanism linking the tie-ballast gap and permanent vertical displacements was only hypothesized based on field measurements. One goal of this study was to use numerical methods to show how tie-ballast gaps and differential settlement between the bridge and transition zone can increase the applied loads on the ballast and provide a comprehensive understanding of the linkage between tie-ballast gaps and permanent vertical displacements. This linkage included tie-ballast gaps causing load redistribution between

adjacent ties and dynamic impact loads, which further contribute to increased permanent vertical displacements.

11.1 Software Introduction

Analyzing railroad track involves studying the interaction between train wheels, rail, fastening systems, ties, ballast, and subgrade. Historically, modeling the track system usually involved either the superstructure (e.g., rail, fastening systems, and ties) or substructure (e.g., ballast and subgrade). To add further complexity, ballast consists of discrete particles of rock that interact in a manner that cannot be directly replicated by commonly used continuum models. Discrete element techniques can be used with continuum models, such as PFC with FLAC3D, to model the ballast behavior and was investigated as part of this project.

At the time of this report, no numerical modeling software package can simulate the full track interaction with discrete ballast particles. To account for this, the team used two numerical modeling philosophies: (1) the wheel-rail-tie-ballast-subgrade interaction modeling the ballast as a continuum (i.e., "macro") and (2) the tie-ballast interaction modeling the ballast as a discrete material (i.e., "micro"). The macro analysis is primarily used in this research because discrete element modeling is still in its infancy and does not replicate all mechanisms of ballast degradation and the computational requirements to perform couple discrete element method (DEM) ballast modeling with continuum track components under dynamic loads (e.g., PFC with FLAC3D) are substantial. A third simplified analysis, using FLAC2D, is also included to estimate the modulus values of the ballast, sub-ballast, and subgrade layers using measured wheel loads and vertical displacements at the Amtrak and NS instrumentation sites.

The following three sections briefly introduce the three software packages used herein, i.e., FLAC2D, FLAC3D, and LS-DYNA. Each section briefly explains the capabilities of the software package and the reasons for its selection.

11.1.1 FLAC2D and FLAC3D

Fast Lagrangian Analysis of Continuum (FLAC)3D v5.0 (Itasca, 2012) is a three-dimensional finite difference method (FDM) software package that specializes in geotechnical continuum problems. It is distributed by the Itasca Consulting Group in Minneapolis, Minnesota. FLAC also can be used in two-dimensions (i.e., FLAC2D). This package is capable of simulating static, dynamic, and hydro-mechanical behavior. The FLAC-ISH (FISH) coding language component of FLAC3D allows the user to control almost all aspects of the analysis, including user-defined material models and complex geometries. Other researchers have used FLAC3D to investigate the effect of high-speed trains on transition zones, e.g., Smith et al. (2006; 2007) and Lobo-Guerrero and Vallejo (2006). One limitation of FLAC3D is the difficulty of modeling the superstructure (i.e., rails and ties) because of the increase in execution time when these components are included. Therefore, another program, LS-DYNA, described in Section 11.1.2, was used to model the complex track system and rolling stock and used a larger time step than FLAC3D because it uses the finite element method (FEM) instead of FDM.

Researchers used FLAC3D for inverse analysis to estimate material stiffness or modulus values of the five substructure layers using field-measured vertical displacements and wheel loads. FLAC3D was selected for this analysis because the FISH coding language allows for complete automation of the inverse analysis of material stiffness and calibration of the model. This

automation is not possible with other track software packages, such as LS-DYNA, GeoTrack, PLAXIS, etc., because the user cannot introduce code to these packages to automate the inverse analysis, which necessitates time-consuming manual iteration.

11.1.2 LS-DYNA

LS-DYNA is a three-dimensional FEM program distributed by Livermore Software Technology Corporation that specializes in non-linear transient dynamic finite element analysis. LS-DYNA stands for the Livermore Software DYNA program, which originated from the three-dimensional finite element program DYNA3D developed by Dr. John O. Hallquist at Lawrence Livermore National Laboratory in 1976. LS-DYNA can model the entire track behavior along with the inclusion of train cars and wheel systems. Other researchers have used LS-DYNA to investigate the effect of freight trains on track systems, e.g., Nicks (2009) and Lundqvist and Dahlberg (2005).

The team used LS-DYNA to perform the macro analysis, which modeled the entire track structure (i.e., railcar truck or cart, rail, tie, ballast, and subgrade) and the coupled interaction. Because LS-DYNA is widely used in mechanical engineering applications (e.g., car crash simulations and metal stamping), it is well suited for complex geometries, moving vehicles, and dynamic contact forces.

12. Static Inverse Analysis of Field Modulus (FLAC3D)

The team used FLAC3D to perform the static inverse analysis that estimated the modulus values of ballast, sub-ballast, and subgrade from the measured field vertical displacements at the Amtrak and NS instrumentation sites. The objective of the analysis was to create a flexible model that could quickly and easily estimate modulus values from the measured wheel loads and transient vertical displacements. This was beneficial, as the moduli of many sites needed to be estimated from an inverse analysis.

FLAC3D was selected to back-calculate the layer moduli of the monitored railway transitions because the built-in FISH coding language allows complete automation of the static inverse analysis. This automation process is not possible within LS-DYNA or other track software (e.g., GeoTrack, PLAXIS, etc.) and the determination of material properties using other software requires time-consuming manual iteration.

The team also selected FLAC3D for its flexibility in inverse analysis. An example of this flexibility is the ability to manually input the load distribution between ties based on the measured tie-ballast gap instead of solving for it directly within the model. The existence of a tie-ballast gap changes the load distribution, and this must be accounted for in the analysis. For example, if all ties are in intimate contact with the ballast (Figure 118), the load distribution to surrounding ties is about 35 percent, 22.5 percent, and 10 percent (i.e., Tie 1 experiences 35 percent of the wheel load, Tie 2 experiences 22.5 percent, and Tie 3 experiences 10 percent).

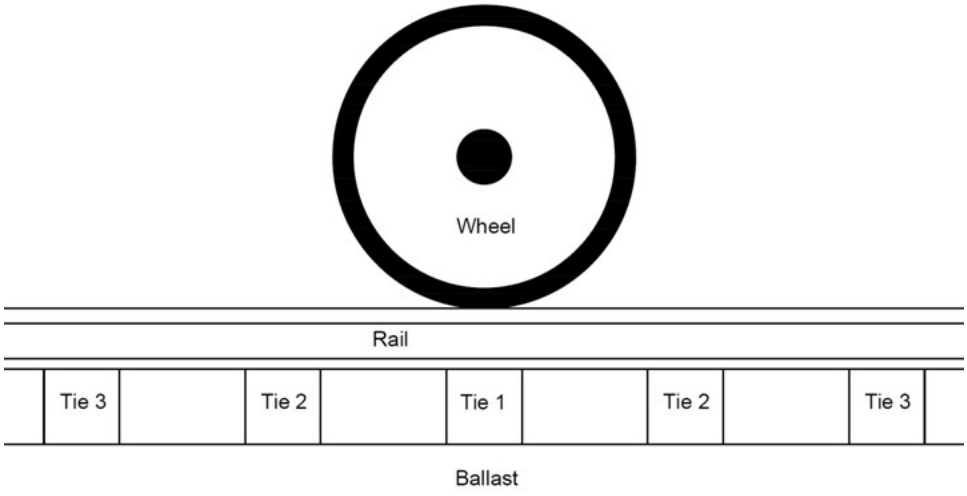

Figure 118. Wheel-rail-tie-ballast model showing ties in intimate contact with ballast

If a gap exists between the tie and ballast (Figure 119), extra bending in the rail causes load redistribution from the initial 35/22.5/10 percent distribution to some other percentage (e.g., 2/27/22 percent). To numerically simulate the load redistribution, a gap must be physically present in the numerical model. Most track substructure-specific software (e.g., GeoTrack, KENTRACK, ILLTRACK) cannot represent this gap and load redistribution because they assume intimate tie-ballast contact within the software. On the other hand, analyses using general finite element packages that can physically represent the gap with a contact model (e.g., LS-DYNA) are computationally detailed and time-consuming.

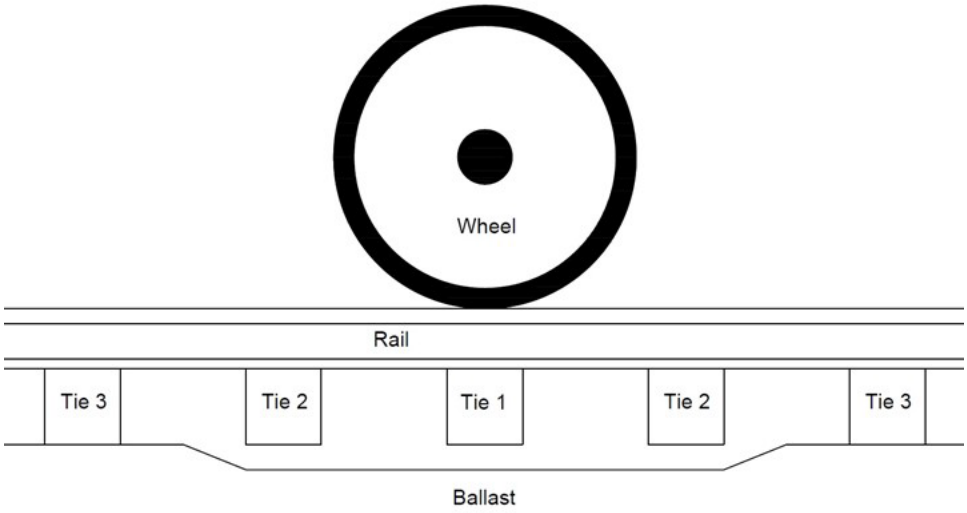

Figure 119. Wheel-rail-tie-ballast model showing a tie-ballast gap under Ties 1 and 2

One objective of the numerical modeling was to use LS-DYNA to investigate the effects of load redistribution from the existence of tie-ballast gaps. For example, if a 0.5 mm gap exists at Tie 1 and 0.25 mm gap exists at Tie 2, the load redistributes to 25/22.5/16 percent. Using field measured tie-ballast gaps, the resulting load distribution can be manually input into the FLAC3D analysis to estimate the modulus values of the substructure layers. Therefore, manually inputting the load distribution with FLAC3D allows for computationally manageable analyses while also incorporating the actual load redistribution from measured tie-ballast gaps estimated using LS-DYNA.

The tie-ballast gaps for ties surrounding the instrumented tie were not known, so the load redistribution was not known. Therefore, all analyses involving FLAC3D assumed an initial load distribution of 35/22.5/10 percent.

12.1 Methodology

This section presents the methodology of the static inverse analysis using FLAC3D. This model is simpler than the LS-DYNA model used in subsequent analyses, but it provided a good estimate of modulus for substructure layers that were advantageous when analyzing multiple sites. Therefore, assumptions such as static loads, symmetry about the rail and instrumented tie centerline, linearly elastic material models, and initial load distributions (e.g., 35/22.5/10 percent) were considered sufficient.

The static inverse analysis with FLAC3D involves a completely automated iterative scheme consisting of the following steps:

1. Create a five-layer model representing the track and subsurface geometry
2. Input measured wheel loads from measured data
3. Input initial estimate of modulus for all five layers
4. Execute the model and compare outputted transient vertical displacements with measured transient vertical displacements

5. Select new modulus values for all five layers to develop better agreement between calculated and measured transient vertical displacements
6. Iterate until numerical and measured transient vertical displacements compare within an acceptable tolerance (i.e., 0.01 mm)

One beneficial feature of the Amtrak NEC sites was the similar subsurface geometry for all six sites. Each site consists of a five-layer system with no vertical or horizontal curves in the track. Therefore, researchers assumed symmetry along the rail and instrumented tie centerline. Because of these similarities, only layer heights and element densities (i.e., number of elements per linear foot) were required as geometric inputs for the FISH code. The geometry and finite difference mesh for Upland (60 ft) is shown in Figure 120 as an example, but similar models were created for all other instrumented sites.

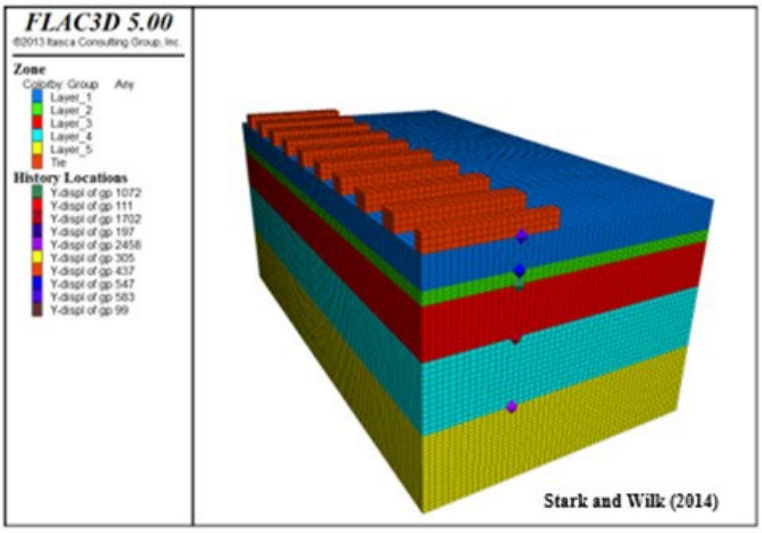

Figure 120. FLAC3D mesh for Upland (60 ft) with LVDT locations shown with small diamonds

The methodology for selecting input parameters of peak wheel load and measured transient displacement (Steps 2 and 4) are described in Section 6.5. From the field data, the team developed a mathematical relationship between wheel load and transient LVDT vertical displacement to represent the behavior of each substructure layer as a function of applied load. This method was chosen because the scatter of data and non-linear behavior of the soils could have caused maximum values to be unrepresentative of the overall layer behavior.

Due to the linear elastic mathematical representation of the substructure behavior at the Amtrak NEC sites, the team assumed an arbitrary peak wheel load to facilitate comparison of the various analyses. As described in Section 6.5, 100 kN was selected because it was close to the average peak wheel load and was an easy value to work with and compare. To determine the transient displacements, the following equations were used:

$$\delta_{LVDT\,\#1} = \frac{P}{k_{mob}}$$

$$\delta_{LVDT\#2-5} = \delta_{P=0} + \frac{P}{k_{mob}}$$

where P is the wheel load (100 kN), k_{mob} is the mobilized LVDT stiffness of the layer, and $\delta_{P=0}$ is the "apparent gap" of LVDTs 2–5.

The displacement created from closing the tie-ballast gap was omitted from LVDT 1 because it did not actually represent the displacement of the ballast. Figure 121 shows how this process eliminated the influence of the tie-ballast gap from the analysis to estimate k_{mob}.

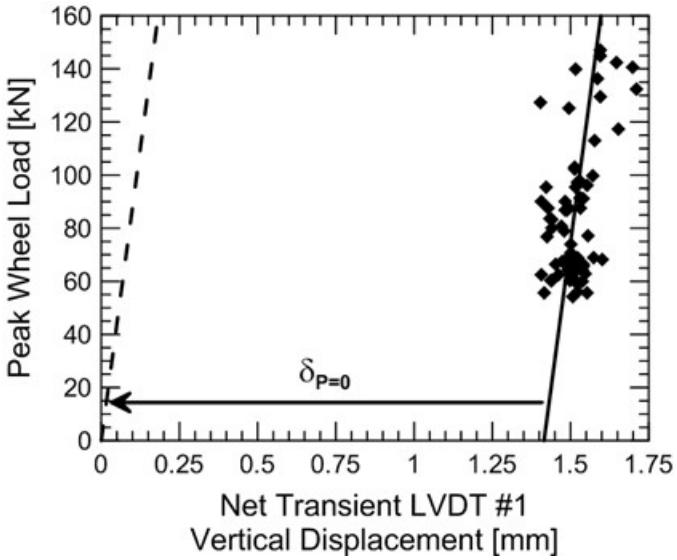

Figure 121. LVDT 1 force-displacement behavior of Upland (15 ft) showing best fit line with and without tie-ballast gap included

Researchers input the initial modulus values into the FISH code and the model was executed until equilibrium was reached. The FISH code returned the relative displacement between each LVDT, which the team compared to the measured vertical displacements. The difference between the numerical and field displacements of each LVDT was calculated and checked to determine if they were below a specified tolerance (i.e., 0.01 mm). If they were not, researchers calculated new modulus values for all five layers and the process repeated until the difference between the numerical and field transient displacements for all five layers were below the specified tolerance.

The team used the following equation to estimate the new modulus values:

$$E_{new} = E_{old} * \left(\frac{\delta_{num} - \delta_{field}}{\delta_{field}}\right)$$

where E_{new} is the new or updated modulus value, E_{old} is the previous modulus value, δ_{num} is the numerical displacement measured by FLAC3D, and δ_{field} is the field displacement calculated using the methodology in Section 6.5. Each inverse analysis required about 20 minutes to perform due to the automated nature of the analysis in FLAC3D.

12.2 Comparison with Other Software and Testing Methods

To ensure reliable results, the team compared the FLAC3D static inverse analysis modulus values with results from other software and testing techniques. Using the same process as described above, the modulus values were back-calculated using the track software packages GeoTrack and LS-DYNA. Also, surface wave testing of similar railways provided a range of modulus values for ballast and subgrade materials (Stark et al., 2016) and were used for comparison with the inverse analyses to ensure reasonable values were derived.

The inverse analysis used to estimate values of track modulus for the field instrumentation sites consisted of the data recorded from Upland (60 ft) on 29 January 2013. The team chose Upland (60 ft) because it displayed the best tie support and track behavior. This means the assumed initial load distribution of 35/22.5/10 percent likely applied, and the influence of the gap was smaller, compared to the other NEC sites. The subsurface profile is shown in Figure 122. Table 25 presents the layer heights and net transient vertical displacements and cumulative transient vertical displacements for each layer.

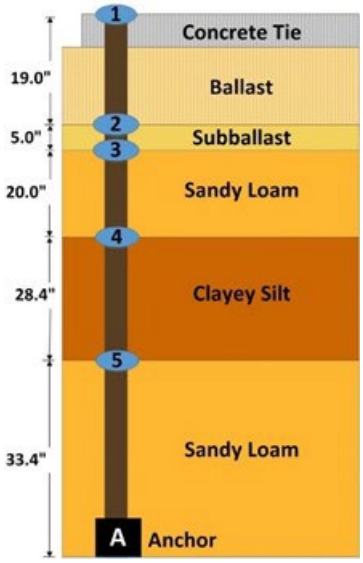

Figure 122. Subsurface profile for MDD location 60 ft north of the Upland Street bridge (Upland (60 ft)

Table 25. Substructure values for Upland (60 ft) on 29 January 2013

Layer Number	MDD Depth [m]	Layer Thickness [m]	Net Layer Transient Vertical Displacement [mm]	Cumulative Layer Transient Vertical Displacement [mm]
1 – Ballast	0.305	0.305	0.114	1.078
2 – Sub-ballast	0.432	0.127	0.099	0.964
3 – Sandy Loam	0.940	0.508	0.366	0.865
4 – Clayey Silt	1.661	0.721	0.336	0.499
5 – Sandy Loam	2.510	0.849	0.163	0.163

A plan view of the GeoTrack model and the LS-DYNA mesh used for this analysis are shown in Figure 122 and Figure 123, respectively. The FLAC3D mesh is shown in Figure 120. In GeoTrack and LS-DYNA, a standard track gauge of 4 ft, 8.5 in, and a 136 RE rail were used.

The actual depth and location of the LVDTs in the MDD string were used in the model because GeoTrack, FLAC3D, and LS-DYNA are all 3D software packages. The LVDT depths are shown in Table 26, and the MDD was about 3 ft (0.919 m) from the center of the tie or 1 ft, 4 in (0.381 m) from the edge of the tie. This location corresponds to the region under Segment 2 in a GeoTrack analysis (see Figure 123). The closest elements and nodes to this location were used to obtain results from FLAC3D and LS-DYNA for comparison with the GeoTrack results. For example, the Upland (60 ft) locations of the LVDTs in the MDD string in the FLAC3D mesh are shown in Figure 120. In all three software models, symmetry was assumed along both the track and Tie 1 centerline to reduce computational complexity.

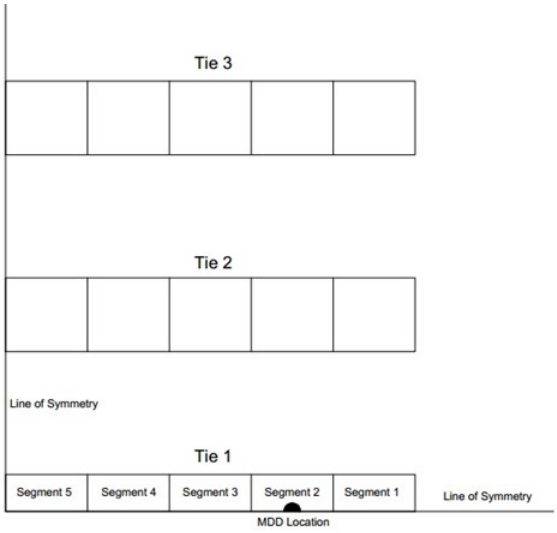

Figure 123. Plan view of track model used in GeoTrack simulation

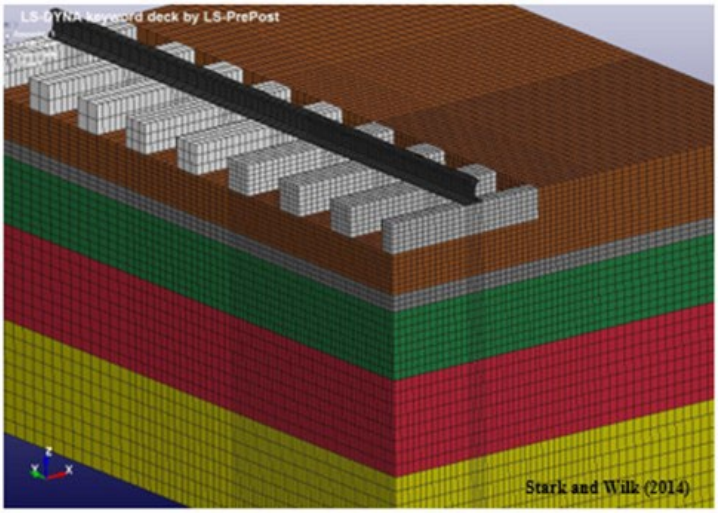

Figure 124. LS-DYNA Model for Upland (60 ft) showing rail and portion of concrete tie

The final modulus values for all five layers at Upland (60 ft) on 29 January 2013 are shown in Table 27. While there was some variation, the values were relatively close to each other. Differences were likely due to small variations in how the load was distributed between the ties.

Table 26. Comparison of inverse analysis modulus values for Upland (60 ft) on 29 January 2013 at 10:21 a.m.

Layer Number	GeoTrack [MPa]	FLAC3D [MPa]	LS-DYNA [MPa]
1 – Ballast	171	202	201
2 – Sub-ballast	238	210	278
3 – Sandy Loam	30	30	22
4 – Clayey Silt	32	34	27
5 – Sandy Loam	60	56	47

The team used a second technique to verify the static inverse analysis modulus results, comparing the values in Table 27 against other methods for estimating modulus, such as seismic surface wave testing. The ballast modulus from seismic surface wave testing is displayed in Table 27 and ranged from 138 to 380 MPa, depending on the condition of the ballast. Therefore, the ballast modulus value of 202 MPa from FLAC3D agreed with seismic testing results for ballast that is fouled to clean and slightly wet.

Table 27. Range of ballast modulus values obtained from seismic surface wave testing

		Clean ballast	Dry fouled ballast	Wet fouled ballast
Modulus	[MPa]	220 – 260	345 – 380	138 - 172

12.3 Results

This section presents the results of the static inverse analysis for all six instrumented sites along the Amtrak NEC in Chester, Pennsylvania. Researchers obtained data for this analysis during four site visits.

The soil profiles used for these analyses are shown in Section 2.4 (Figure 6 – Figure 11), and the transient LVDT vertical displacements were calculated using the methodology and results presented in Section 6.5. The modulus values for each layer from the static inverse analyses are shown in Table 28 through Table 33. The results showed a wide range of ballast modulus values from LVDTs 1 and 2, while moduli were similar for LVDTs 3 through 5.

Table 28. Inverse analysis of modulus with time at Caldwell (East) using FLAC3D

LVDT	August 2012 [MPa]	November 2012 [MPa]	January 2013 [MPa]	June 2013 [MPa]
1	164	70	132	141
2	64	59	47	47
3	85	82	91	104
4	41	31	31	25
5	65	49	44	64

Table 29. Inverse analysis of modulus with time at Caldwell (West) using FLAC3D

LVDT	August 2012 [MPa]	November 2012 [MPa]	January 2013 [MPa]	June 2013 [MPa]
1	103	52	51	51
2	246	187	123	130
3	239	185	257	243
4	62	45	45	44
5	100	91	74	80

Table 30. Inverse analysis of modulus with time at Madison (12 ft) using FLAC3D

LVDT	August 2012 [MPa]	November 2012 [MPa]	January 2013 [MPa]	June 2013 [MPa]
1	104	126	110	150
2	66	55	67	52
3	66	66	83	73
4	34	34	43	29
5	49	53	71	55

Table 31. Inverse analysis of modulus with time at Madison (60 ft) using FLAC3D

LVDT	August 2012 [MPa]	November 2012 [MPa]	January 2013 [MPa]	June 2013 [MPa]
1	224	242	271	142
2	249	268	297	198
3	33	40	29	29
4	42	44	41	45
5	35	32	32	34

Table 32. Inverse analysis of modulus with time at Upland (15 ft) using FLAC3D

LVDT	August 2012 [MPa]	November 2012 [MPa]	January 2013 [MPa]	June 2013 [MPa]
1	237	67	200	59
2	54	45	98	89
3	40	45	25	77
4	51	83	117	66
5	123	91	72	113

Table 33. Inverse analysis of modulus with time at Upland (60 ft) using FLAC3D

LVDT	August 2012 [MPa]	November 2012 [MPa]	January 2013 [MPa]	June 2013 [MPa]
1	255	279	202	379
2	102	172	210	141
3	34	30	30	26
4	41	35	34	32
5	64	59	56	58

Researchers compared the modulus values for each layer to investigate the variation in modulus across the six instrumentation test sites. For example, all the modulus values for LVDT 1 were compared for the six sites because LVDT 1 was representative of the ballast layer at each of the

six sites. LVDT 2 was representative of the sub-ballast layer while LVDTs 3 through 5 yielded the modulus of the subgrade layers.

Figure 125 compares the modulus values of LVDT 1 (ballast) for all six instrumentation sites for the four months data was collected. The red lines show the range in ballast moduli calculated from seismic surface wave testing (140 to 380 MPa) from a previous FRA project. The numerical values are also displayed in Table 34.

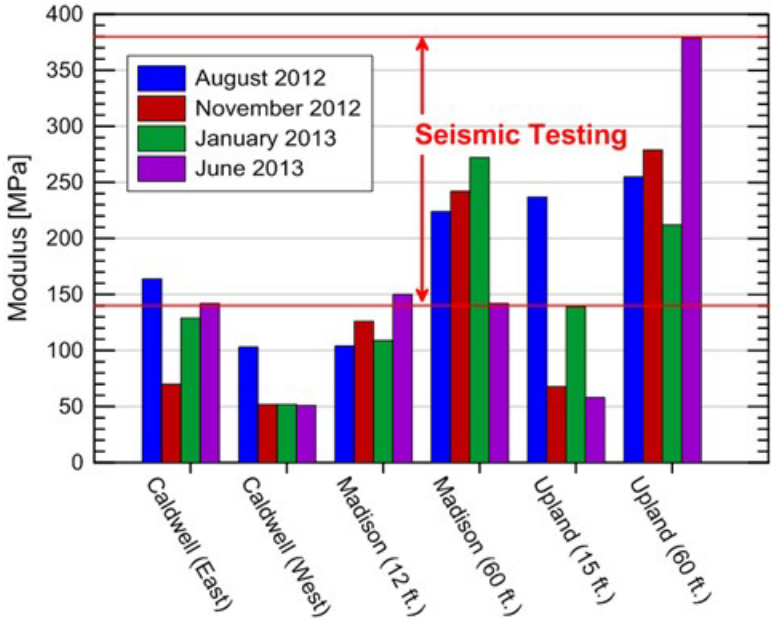

Figure 125. LVDT 1 (ballast) modulus values from static inverse analysis with FLAC3D compared against seismic testing results

Table 34. Comparison of ballast moduli from static inverse analysis using FLAC3D for all MDD instrumented sites

	Caldwell Avenue		Madison Avenue		Upland Avenue	
	East	West	12 ft.	60 ft.	15 ft.	60 ft.
	[MPa]	[MPa]	[MPa]	[MPa]	[MPa]	[MPa]
August 2012	164	103	104	224	237	255
November 2012	70	52	126	242	67	279
January 2013	132	51	110	271	200	202
June 2013	141	51	150	142	59	379

Madison (60 ft) and Upland (60 ft) reported ballast modulus values in the best agreement with the seismic testing results. These sites likely contained clean or slightly fouled ballast because they were outside the transition zone. Caldwell (East) and Madison (12 ft) yielded ballast modulus values along the lower bound of wet, highly fouled ballast moduli from the seismic testing. Therefore, it was likely that these two sites were highly fouled and wetted, which was confirmed by field observations. The lower modulus values calculated at Caldwell (East) and Upland (15 ft) also may have been due to very high levels of fouling or load distributions differing from the assumed 35/22.5/10 percent distribution.

The results also showed ballast modulus values could vary significantly by month, with Upland (15 ft) showing the largest variation. Because Upland (15 ft) displayed the most unsupported behavior, it was likely the load distribution changed from month to month as the tie reaction did in a similar pattern for Upland (15 ft).

Figure 126 compares calculated modulus values for the sub-ballast (i.e., LVDT 2) for all six instrumented sites for the four months of collected data. The numerical values are presented in Table C.1 in Appendix C and discussed below. The sub-ballast layer (i.e., LVDT 2) also exhibited a large variation in modulus, with values ranging from 45 to 297 MPa. However, the large variability was between different sites, not at the same site. This may have reflected the importance of different material type in the sub-ballast layer on the measured transient vertical displacements and thus the modulus values calculated using the FLAC3D inverse analysis. While there were exceptions, the sub-ballast modulus values were relatively consistent with time for a particular site, which may have indicated those sites were experiencing better drainage than sites that showed variability with time. Some of the instrumentation sites (e.g., Upland (15 ft)) may not have been quickly draining precipitation from the sub-ballast and/or underlying layers, as evidenced by water seeping through the masonry retaining walls well after a precipitation event. Otherwise, a particular site should be expected to yield consistent modulus values because the approach fill material has been in-place for a significant amount of time at the NEC instrumentation sites.

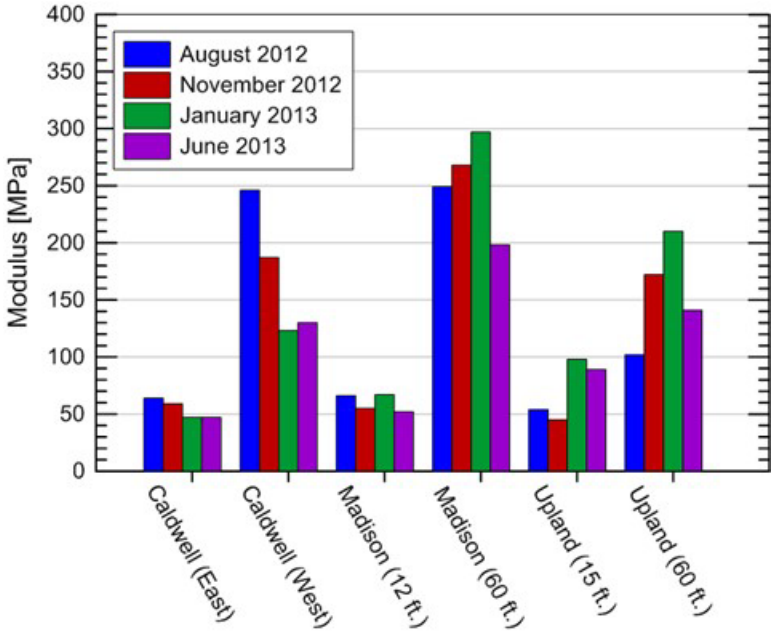

Figure 126. LVDT 2 (sub-ballast) modulus values from static inverse analysis with FLAC3D

Figure 127 through Figure 129 show the calculated modulus values of the subgrade layers (LVDTs 3, 4, and 5) for all six instrumented sites for the four months of collected data. The red lines show the range in subgrade moduli calculated from seismic surface wave testing (20 to 100 MPa). The numerical values can be found in Tables C.2 through C.4 in Appendix C.

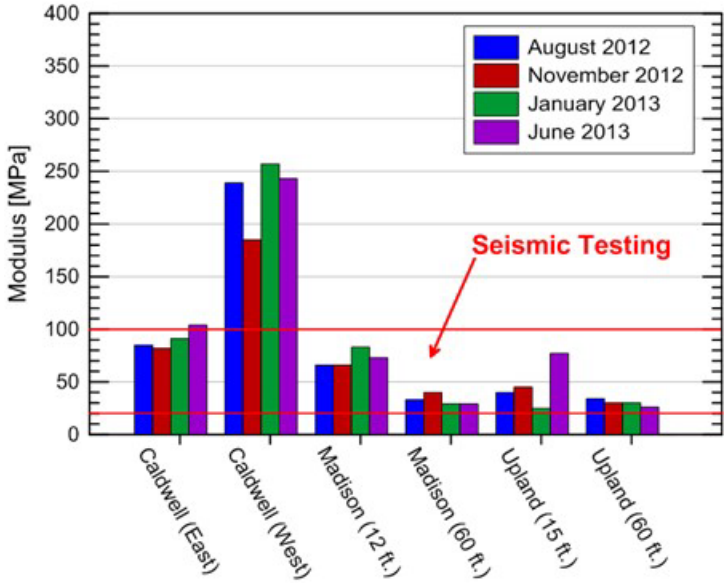

Figure 127. LVDT 3 (subgrade) modulus values from static inverse analysis with FLAC3D compared against seismic testing results

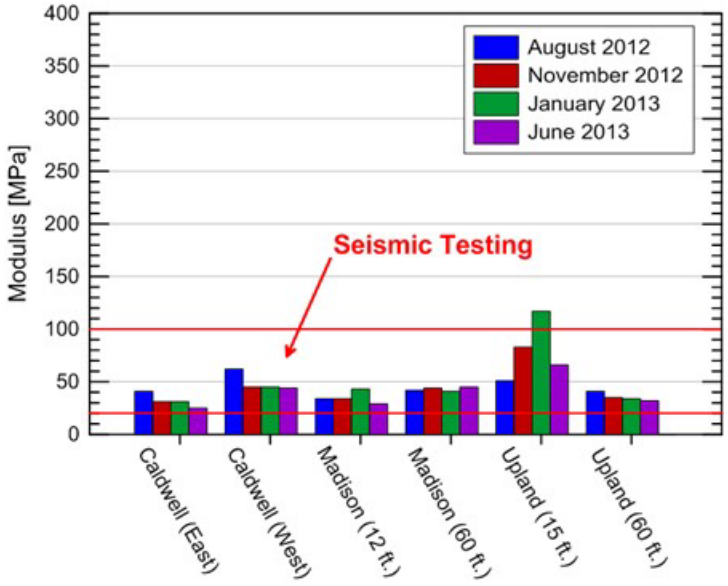

Figure 128. LVDT 4 (subgrade) modulus values from static inverse analysis with FLAC3D compared against seismic testing results

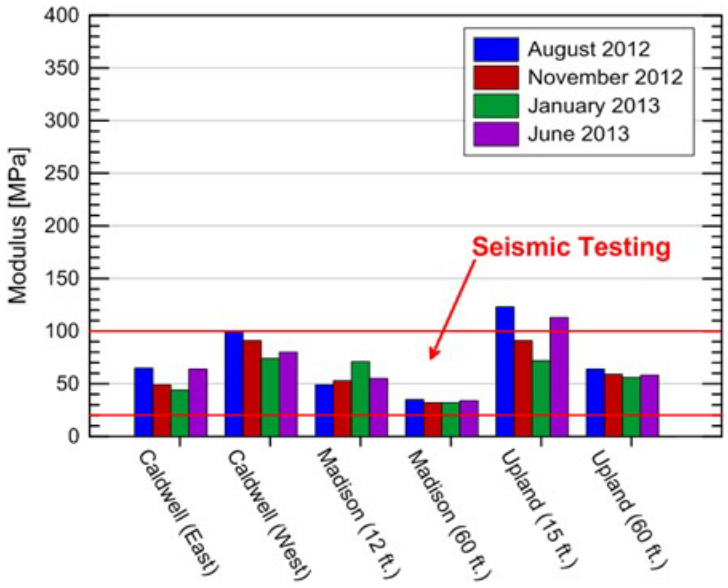

Figure 129. LVDT 5 (subgrade) modulus values from static inverse analysis with FLAC3D compared against seismic testing results

Except for Caldwell (West), all subgrade layers fell within the expected range of 20 to 100 MPa from the seismic surface wave testing of subgrade soils and are shown in Table C.2, C.3, and C.4 in Appendix C. The Caldwell (West) site may have been different because of the material makeup of the soil.

12.4 Factors Affecting Static Inverse Analysis

The inverse analysis performed to estimate modulus values for the various substructure layers using FLAC3D and the measured transient vertical displacements and wheel loads was dependent on several factors, including (1) physical ballast properties, (2) representative values of applied load and transient vertical displacement, and (3) an accurate numerical simulation of field behavior. Some of the physical ballast properties that affected the estimated modulus values included level of fouling, rock type and angularity, presence of water, density, and type of fouling material. Representative values of applied wheel load and transient vertical displacement were the most important input parameters to the inverse analysis, and they were measured by the strain gages on the rail and LVDTs in the MDD strings, respectively. However, the field instruments were focused on the applied wheel load and tie reaction on the rail and not the applied stress at the tie-ballast interface. The interface behavior was important because the transient vertical displacement was being measured from the top of the tie to the bottom of the ballast and not just the ballast itself.

Errors in any of these factors could have led to unrepresentative values of ballast modulus. For example, if a lack of intimate contact exists between the tie and ballast, the measured input loads do not account for load redistribution, or any additional load created from the momentum of the moving tie contacting the underlying ballast to close the tie-ballast gap.

Some of the conditions that could have affected the physical ballast properties over time at the MDD sites were ballast degradation, fouling, and tamping. Degradation and fouling were expected to cause a decrease in modulus with time, although the results to date did not indicate

this trend consistently for all MDD sites. This is likely due to the short duration of the measurements.

Tamping was expected to cause a decrease in modulus because the ballast was loosened or "fluffed" by vibrating forks squeezing together. The loosened ballast particles would undergo compression under the subsequent applied loads, causing an increase in modulus after the train loading re-compacted the ballast. However, this general trend was not clearly discernible from the field measurements and corresponding inverse analyses. It was anticipated that subsequent train loading quickly re-compacted the newly tamped ballast, so the decrease in modulus due to tamping was removed before the next instrumentation reading occurred. Thus, this increase in modulus with applied loading was not captured at any of the six NEC instrumentation sites. Typically, instrumentation readings were obtained 1 or 2 months after tamping at the NEC sites. In addition, there was heavy rainfall in January 2013, which may have impacted the modulus values, but such a general trend also was not discernible.

The fourth factor which could have impacted the inverse analysis using FLAC3D was ensuring the numerical model accurately replicated the field system behavior with emphasis on tie-ballast interaction. Some of the factors considered in replicating the field conditions in the numerical model were linear or non-linear elastic stress-stain assumptions for the ballast, representative stress-distribution with depth, continuum versus discrete particle assumptions (i.e., using FLAC3D versus a DEM code to model the ballast, such as PFC), and soil constitutive models for the continuum layers in FLAC3D. In future studies and coupled analyses, it is anticipated that all four of these factors will impact the ballast moduli values estimated from an inverse analysis.

12.5 Summary of Inverse Modulus Analysis

In summary, the research team used FLAC3D to estimate the in-situ modulus of the five substructure layers at each instrumentation site. Table 35 summarizes the modulus values and compares them to values obtained from seismic surface wave testing. The values in the table were used to develop input modulus values for the LS-DYNA analyses discussed below.

Table 35. Recommended modulus values for all six NEC instrumentation sites

Layer Number	Upland (15 ft) [MPa]	Upland (60 ft) [MPa]	Caldwell (East) [MPa]	Caldwell (West) [MPa]	Madison (12 ft) [MPa]	Madison (60 ft) [MPa]
1	200 – 250	200 – 380	130 - 165	50	100 – 150	220 – 270
2	45 – 100	100 – 210	45 - 65	120 - 250	50 - 70	200 - 300
3	25 - 75	25 – 35	80 - 105	185 – 260	65 – 85	30 – 40
4	50 – 120	30 – 40	25 - 40	45 – 65	30 – 45	40 – 45
5	70 - 120	55 - 65	45 - 65	75 -100	50 – 70	30 - 35

13. Wheel-Rail-Tie-Ballast Interaction (LS-DYNA)

LS-DYNA performs a “macro” analysis of the track system because it can simulate complex geometries, moving vehicles, and contact surfaces. The goal of the analysis is to calibrate a model that replicates the field-measured transient load and displacements while incorporating all required mechanisms from the wheel-rail-tie-ballast interaction.

13.1 Mechanisms that Increase Applied Loads on Ballast

One of the main objectives of the macro analysis was to understand how the wheel, rail, tie, and ballast interacted when a gap was present below the tie. This not only facilitates understanding of track system behavior but is also a primary factor causing the measured permanent vertical displacements near bridge approaches. Section 6 presents a strong link between unsupported ties (e.g., tie-ballast gap) and permanent vertical displacement. However, the effect of impact loads and load redistribution on the applied loads and permanent vertical displacements was not quantifiable from the field measurements. Therefore, the team performed numerical analyses of the interaction to understand and quantify the mechanisms that increased the applied loads on the ballast, such as impact loads, load redistribution by the rail, and rail stiffness (see Figure 130).

The consideration of a gap between the tie and ballast is an important feature because it significantly changes the loading of the ballast from a passing train to surrounding ties. Typically, track design does not account for this gap but, as explained in Section 6, a single train pass can result in gap formation between the tie and ballast. A diagram of a single tie-ballast gap is shown in Figure 130.

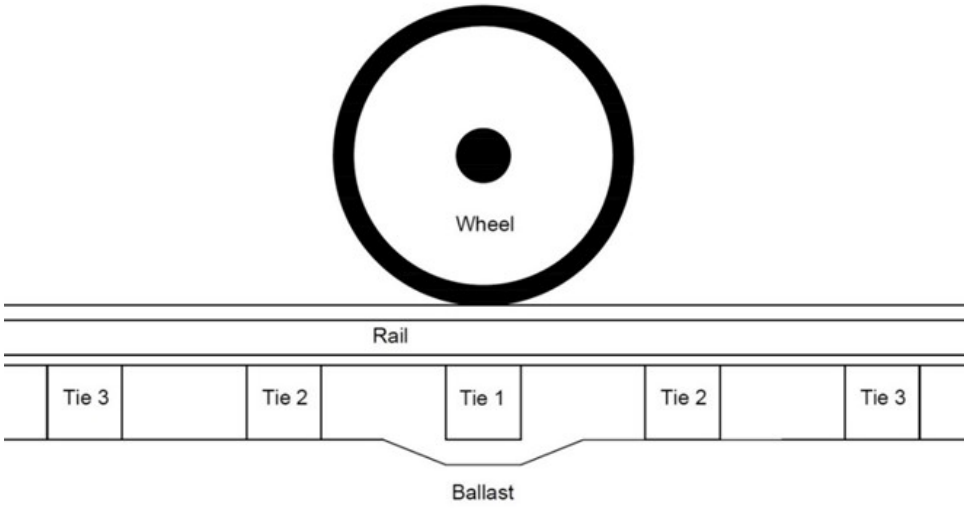

Figure 130. Wheel-rail-tie-ballast model showing tie-ballast gap at Tie 1

The presence of a gap results in the coupled interaction of three mechanisms:

- Impact load
- Load redistribution
- Rail bending/stiffness

Impact loads result from momentum of the tie when it contacts the ballast. Increasing the gap may result in a larger downward velocity of the tie, creating a larger force during impact.

Load redistribution addresses changes in how the wheel load is spread to the ties due to the presence of a gap. If all ties are in intimate contact and the track modulus under each tie is identical, the load distribution between Ties 1, 2, and 3 (see Figure 130) should be around 35/22.5/10 percent, where Tie 1 experiences 35 percent of the wheel load, Tie 2 experiences 22.5 percent, and Tie 3 experiences 10 percent. This load distribution is dependent on rail bending/stiffness. If the rail is completely rigid (e.g., infinite bending stiffness), the wheel load evenly distributes over all supporting ties. As the rail is not completely rigid, the rail bends and the tie under the wheel receives most of the wheel load. In other words, the more flexible the rail, the more load the underlying tie experiences.

However, if a gap is present, the rail must also bend to create contact between the tie and ballast. This mobilizes the rail stiffness which redistributes the load to surrounding ties. This causes the load distribution to differ from the typical 35/22.5/10 percent.

Rail stiffness does not directly affect applied loads, but it does affect load distribution and the velocity of the tie because rail stiffness is directly proportional to rail bending. Rail bending is important because it determines how the wheel load is distributed to ties, and it is rail bending that the strain gages are measuring. Also, when the rail bends to establish contact between the tie and ballast, the rail acts like a spring that resists the downward displacement of the tie. This reduces the impact load on the ballast and pulls the tie back up after the wheel passes.

In the analysis, a gap was physically simulated between the tie and ballast with LS-DYNA, as shown in Figure 131. The tie-ballast contact force was calculated using contact surfaces along the bottom of the tie. When the nodes of the "dominant" surface (i.e., tie) penetrated the nodes of the "underlying" surface ballast, a resisting force was simulated to bring the nodes on the master surface to the slave surface. This resisting force was the contact force in the following results.

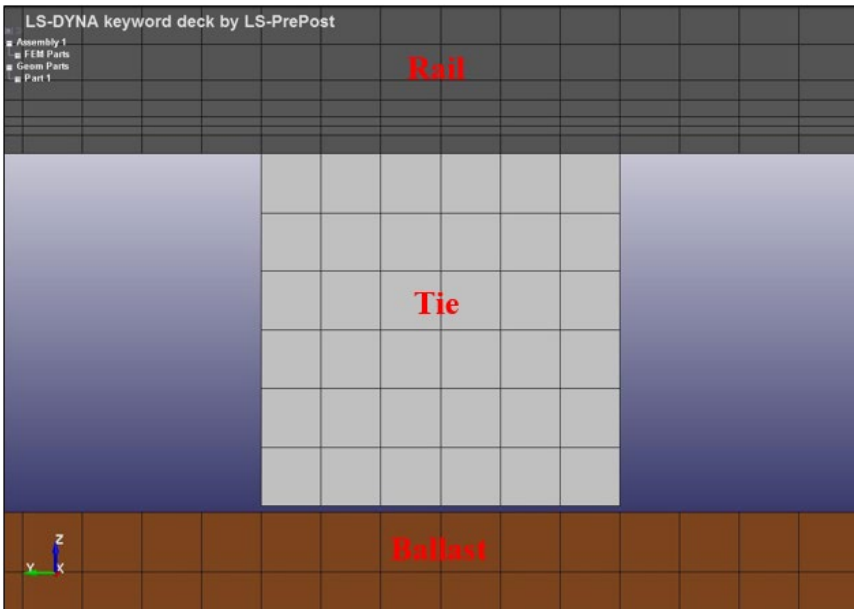

Figure 131. Tie-ballast gap in LS-DYNA

The LS-DYNA models used the data recorded at Upland (60 ft) on 29 January 2013 to perform an inverse analysis of a well-supported tie. The inverse analysis was used to estimate material properties that were used in subsequent LS-DYNA analyses. The calibration process is presented following this section because an understanding of the load redistribution mechanism for a moving wheel is required to understand the inverse analysis.

13.2 Impact Loads – Without Rail

The first analysis simulated the simplest situation for incorporating a tie-ballast gap by only including the tie, ballast, and subgrade. The objectives of this analysis were first to show that LS-DYNA can model the impact between the tie and ballast and that impact forces amplified as the change in momentum from tie movement increased. This mechanism is essentially Newton's Second Law: $F = ma$. As the moving tie impacted the ballast and the tie stops moving (deceleration), the resulting change in momentum of the tie mass amplified the force on the ballast, as shown below:

$$F = m * a = m * \frac{dv}{dt}$$

where F is force, m is the mass of the tie, a is tie acceleration, and dv/dt is the change in momentum of the tie after impacting the ballast.

To isolate the mechanism of impact load amplification, the rail was omitted from the analysis, which resulted in an upper bound of the impact load amplification. Inclusion of the rail reduced the impact because the rail slowed the downward movement of the tie. This simulation only required a single tie gap due to the lack of interaction between ties because the rail was omitted. The tie was loaded using a tie reaction history of a passing wheel with a tie gap. A schematic diagram of the gap and loading is shown in Figure 132.

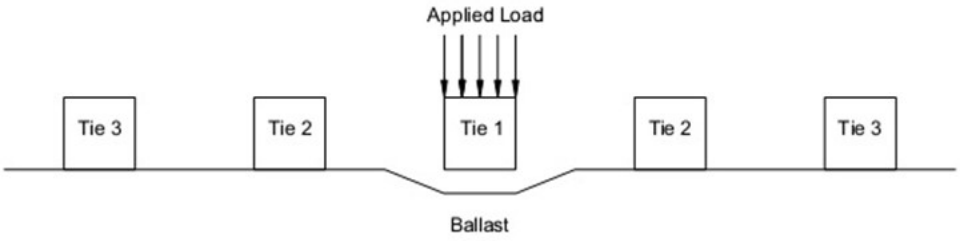

Figure 132. Tie-ballast model showing tie-ballast gap at Tie 1

By omitting the rail, a direct relation between tie-ballast gap height and tie velocity at impact could be created. Increasing the gap height increased the tie velocity at impact and thus produced a greater force on the ballast. Since the rail was omitted, this simplified analysis only provided an upper-bound solution because the rail would distribute load away from unsupported ties, which decreased the velocity of the moving tie.

To determine how the gap height influenced the contact force between the tie and ballast, various gap heights from 0 to 10 mm were simulated in the mesh, shown in Figure 131. As the tie was loaded, the contact force between the tie and ballast (i.e., tie-ballast contact force) was recorded and output at regular time intervals during the LS-DYNA analysis. The tie-ballast contact force was then normalized by the maximum value of the applied load. This normalized value was defined as normalized tie load. If the calculated tie-ballast contact force equals the maximum

applied load (gap = 0.0 mm), the normalized tie load equals 100 percent. If the output tie-ballast contact force is two times greater than the maximum applied load, the normalized tie load equals 200 percent, as shown below.

$$Normalized\ Tie\ Load = \frac{Tie - Ballast\ Contact\ Force}{Maximum\ Applied\ Load}$$

The term "maximum applied load" was used because the load was manually input using a time history function. Subsequent analyses used the term "static wheel load" because the rail system was loaded directly by a wheel in the LS-DYNA model.

Two normalized tie load time histories calculated using the equation above are shown in Figure 133 as examples. The two analyses involved a tie-ballast gap of 1.0 and 6.0 mm to illustrate the increase in applied load. The 1.0 mm tie-ballast gap analysis (blue line) showed impact occurring slightly before 0.1 second, with a maximum normalized tie load from impact of around 80 percent of the applied load. As the tie continued to be loaded, the maximum applied load reached the maximum normalized tie load of 100 percent but did not exceed 100 percent.

The 6.0 mm tie-ballast gap analysis (red line in Figure 133) showed impact occurring around 0.15 second – later than the 1.0 mm gap. This was expected because closing a 6.0 mm gap takes longer to close than a 1.0 mm gap. Due to the larger tie velocity at impact, the maximum normalized tie load from impact reached 240 percent. After impact, the tie followed an identical load history to the 1.0 mm gap simulation. Therefore, the maximum normalized tie load of the entire analysis was 240 percent, which means the impact more than doubled the applied load.

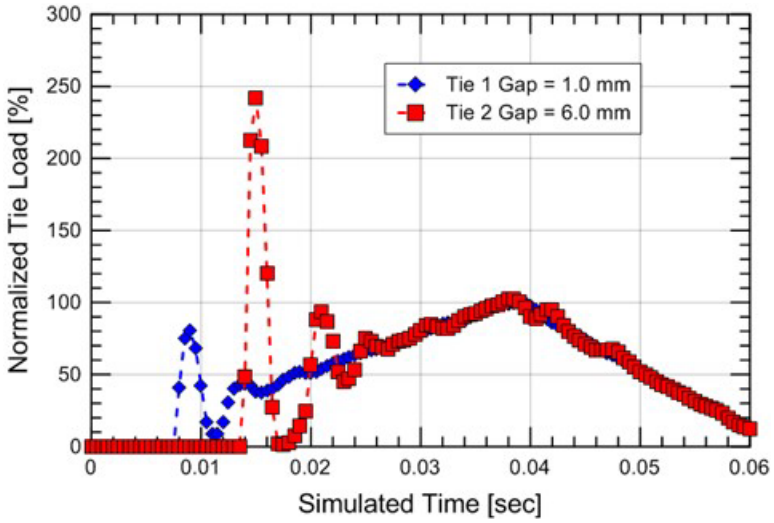

Figure 133. Normalized tie load (tie-ballast contact force/applied load) time history for gaps of 1.0 and 6.0 mm

The maximum normalized tie load for the various tie-ballast gaps analyzed between 0 and 10 mm are displayed in Figure 134. In addition, the maximum normalized tie load from impact is shown for comparison with the maximum normalized tie load. If the tie gap equals 1.0 mm (see Figure 133), the maximum normalized tie load of the entire analysis equals 100 percent, while the maximum normalized tie load from impact is only 80 percent.

Figure 134 shows the maximum normalized tie load equaled 100 percent for tie-ballast gap heights at or below 1.5 mm. This was caused by the tie-ballast contact force from impact being

less than the maximum applied load. Once a tie-ballast gap height of 1.5 mm was surpassed, the tie-ballast contact force amplified from impact and became greater than the maximum applied load. At 10.0 mm, the maximum normalized tie load reached over 300 percent.

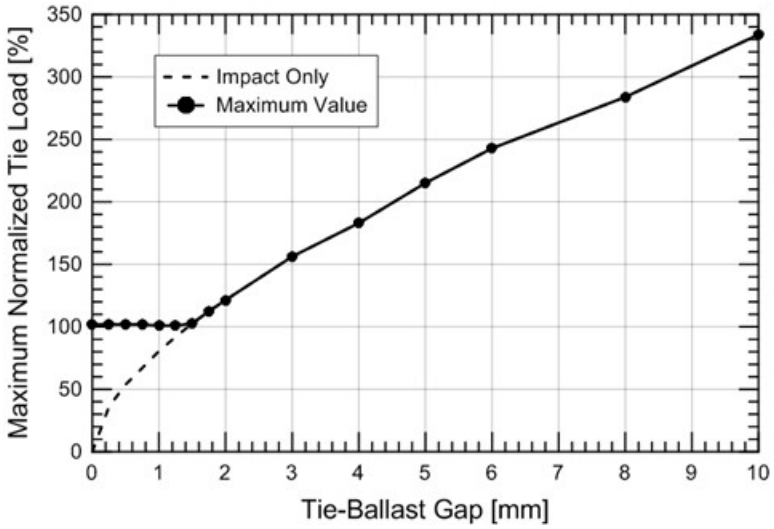

Figure 134. Maximum normalized tie load (tie-ballast contact force / applied load) with tie-ballast gap height

To illustrate how the tie-ballast gap was related to tie velocity at impact, the two variables are plotted in Figure 135. The trend was similar to the maximum normalized tie load, which confirmed that tie-velocity at impact directly resulted in load amplification.

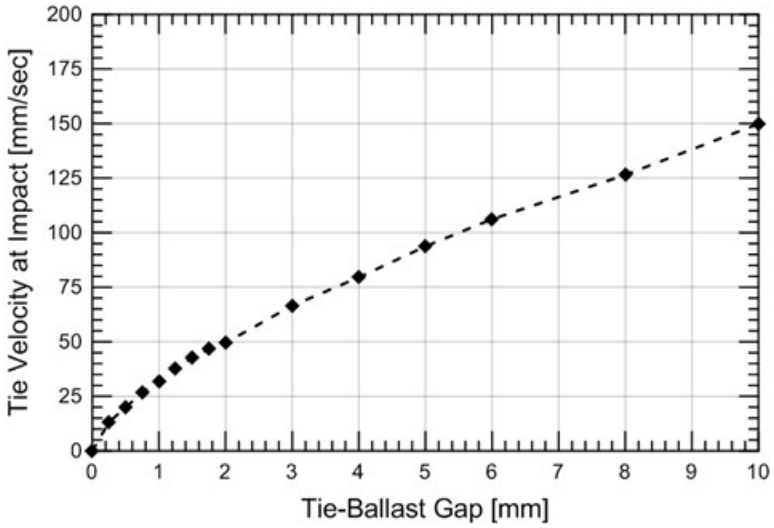

Figure 135. Tie velocity at impact with increasing tie-ballast gap height

The data shown in Figure 133 through Figure 135 are upper-bound solutions because the rail was not included in the analyses. These results demonstrated the impact load mechanism and how changes in momentum from a tie hitting the ballast could increase the applied loads. Once a rail was included in the analysis, the rail would distribute the wheel load to multiple ties and resist bending, which significantly changed tie velocity at impact. Therefore, this analysis should only be viewed as upper bound. However, this section is important because it shows the mechanism

of impact load influenced the analysis, along with confirming a direct link between tie velocity at impact and load amplification.

13.3 Load Redistribution

The next level of complexity in the analysis is including the rail in the tie, ballast, and subgrade finite element mesh (see Figure 136). Among other purposes, the rail distributes the wheel load to the underlying and surrounding ties. If all ties are in intimate contact with the ballast, the distribution should be around 35/22.5/10 percent. However, when a tie-ballast gap exists, the rail redistributes the load in a manner that favors the supported ties.

For this analysis, symmetry was assumed to be along the centerline of both the track and Tie 1. Therefore, only a single rail was required. The tie reaction load history was applied on the nodes on top of the rail along the symmetric boundary. To account for the symmetric boundary condition, the load magnitude was divided by a factor of two. The resulting LS-DYNA model is shown in Figure 136.

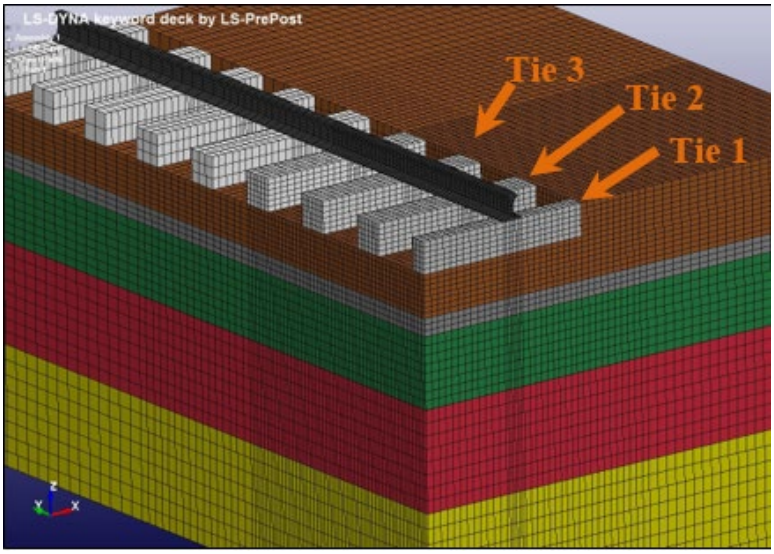

Figure 136. LS-DYNA model for Upland (60 ft) showing rail and portion of concrete tie

For verification purposes, an initial analysis was conducted where all ties were in intimate contact with the ballast. The results showed a distribution of 38/20/10 percent – in good agreement with the 35/22.5/10 percent distribution. This demonstrated that the load was being distributed as expected, and the inverse analyses using FLAC3D to estimate modulus were reasonable.

To illustrate the mechanism of load redistribution, researchers conducted three parametric analyses. All tie-ballast gap heights were below 1.0 mm to avoid force amplification, so the mechanism of load redistribution could be isolated. The three parametric analyses were as follows:

- Varying Tie 1 gap only (0–1 mm)
- Varying Tie 2 gap only (0–1 mm)
- Varying Tie 1 = Tie 2 gap (0–1 mm)

The first analysis assumed a gap only at Tie 1 (see Figure 137). The maximum normalized tie loads experienced by Ties 1, 2, and 3 are displayed in Figure 138. With the presence of a gap at Tie 1, the additional rail bending required for Tie 1 to contact the underlying ballast mobilized the rail stiffness and shed load away from Tie 1 to Tie 2. At a gap height of 1.0 mm, Tie 1 ceased to contact the ballast during loading (i.e., maximum normalized tie load = 0.0 percent), and the maximum normalized tie load of Tie 2 increased from about 20 percent to 40 percent. Tie 3 was not significantly affected because Tie 2 was fully supported; it increased from 8.5 percent to 9 percent, or still about 10 percent, as shown above.

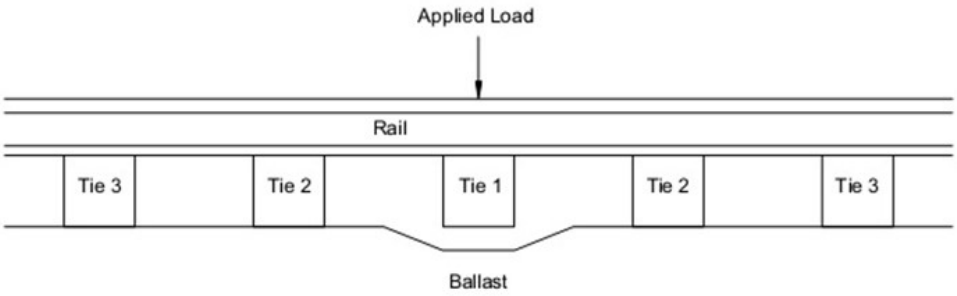

Figure 137. Wheel-rail-tie-ballast model showing tie-ballast gap at Tie 1

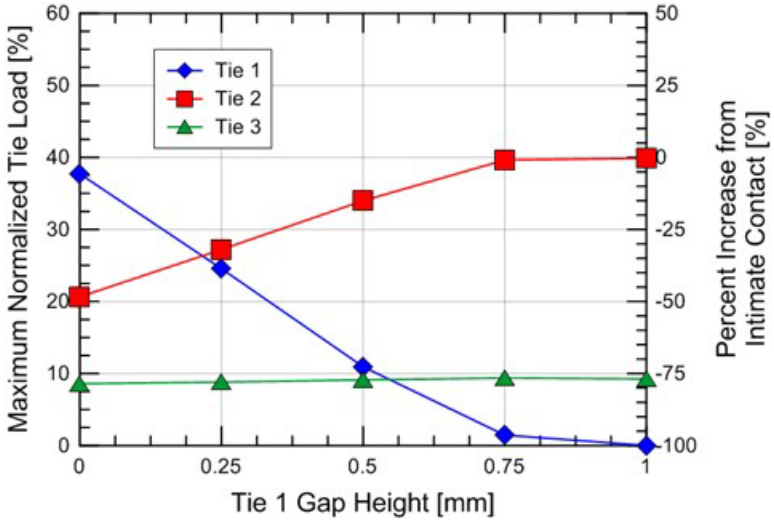

Figure 138. Maximum normalized tie load (maximum tie-ballast contact force/wheel load) for Tie 1, 2, and 3 with varying Tie 1 gap heights

The second analysis assumed a gap only at Tie 2 (see Figure 139). Due to symmetry this assumes the gap was present on both sides of Tie 1. The maximum normalized tie load experienced by Ties 1, 2, and 3 are displayed in Figure 140. Because gaps existed at both Tie 2 locations in Figure 139, the load redistributed in favor of the supported ties, e.g. Ties 1 and 3. At a Tie 2 gap of 0.75 mm, Tie 2 ceased contact with the ballast and the entire wheel load distributed to Ties 1 and 3. The maximum normalized tie load between Tie 1 and the underlying ballast increased from 35 percent to around 58 percent, while Tie 3 increased from 8.5 percent to 20 percent.

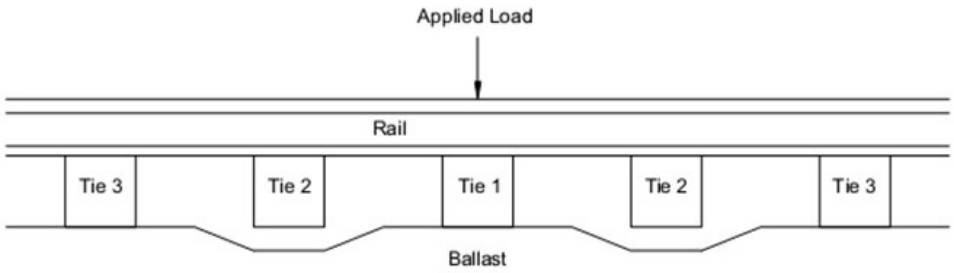

Figure 139. Wheel-rail-tie-ballast model showing tie-ballast gap at only Tie 2

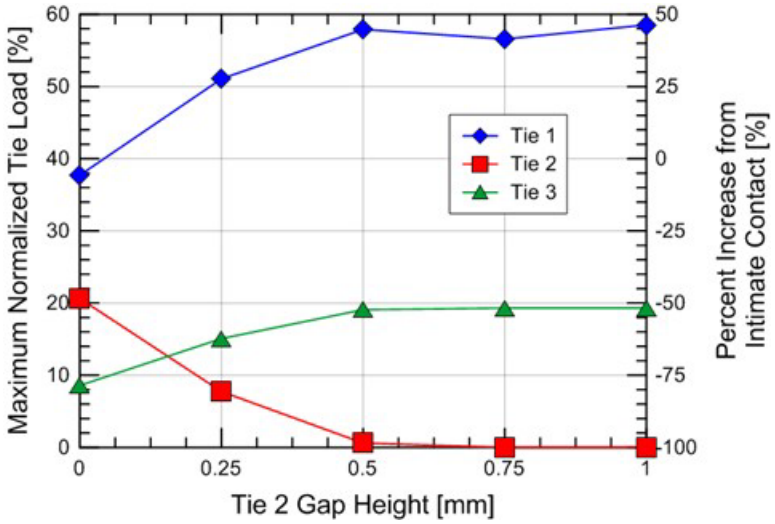

Figure 140. Maximum normalized tie load (maximum tie-ballast contact force / wheel load) for Ties 1, 2, and 3 with varying Tie 2 gap heights

The third analysis assumed equal gap heights at Ties 1 and 2 and full support under Tie 3 (see Figure 141). The maximum normalized tie load experienced by Ties 1, 2, and 3 are shown in Figure 142 and show a significant shift of wheel load away from Tie 2 (20.5 percent to 0 percent) and onto Tie 3 (8.5 percent to 32.5 percent). The maximum normalized tie load at Tie 1 stayed relatively about the same, at around 35 percent.

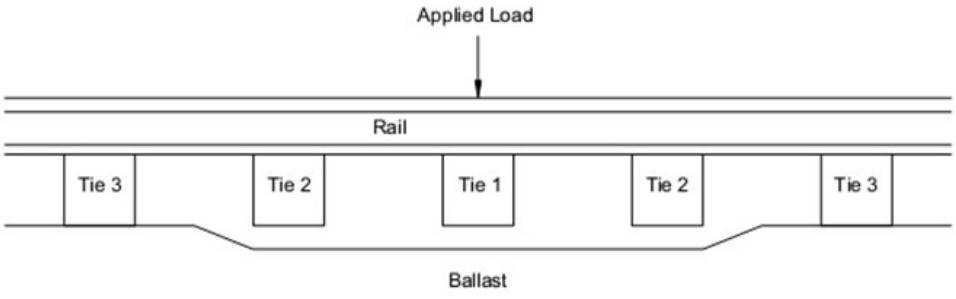

Figure 141. Wheel-rail-tie-ballast model showing tie-ballast gaps at Ties 1 and 2

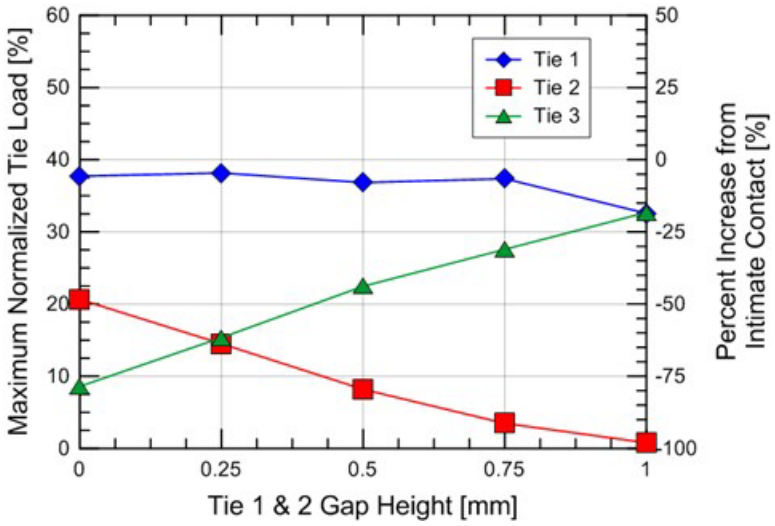

Figure 142. Maximum normalized tie load (maximum tie-ballast contact force/wheel load) for Tie 1, 2, and 3 with varying Tie 1 and 2 gap heights

The objective of these simulations was to illustrate the mechanism of load redistribution and how, by including the rail in the analysis, it redistributed wheel load away from unsupported ties to supported ties. This was a separate mechanism from impact load and acted in an opposite manner. Only a few select analyses are presented and only tie-ballast gaps up to 1.0 mm are shown in the figures. More in-depths parametric analyses are presented in later sections of this report.

13.4 Single Wheel

The next level of complexity involved adding a moving wheel to the LS-DYNA model. This section demonstrates how a moving load could change and amplify the load redistribution to the ties.

With the addition of a moving wheel to the model, the assumption of symmetry along the Tie 1 centerline was no longer valid, so the entire track system had to be modeled. Therefore, a new model was used with a moving wheel, 136-RE rail, 34 concrete ties, and a substructure consisting of five layers that mimicked the Upland (60 ft) instrumented site in Figure 143. All elements were modeled as linear-elastic, and a line of symmetry was assumed at the track centerline to limit model size and reduce execution time. Of the 34 ties incorporated in the model, only Ties 15 through 23 were of interest in the analysis, and the instrumented tie at Upland (60 ft) was located at Tie 19 for calibration purposes.

The wheels were modeled as a semi-thin-walled cylinder (Figure 144) that moved along the rail at 177 kph (110 mph), the operating speed of Amtrak high-speed trains at the Upland Street bridge. The density of the wheel was such that it applied a static wheel load of 124 kN, and the two wheels were spaced 2.8 m (9.33 ft) apart to replicate the measured wheel load of the first axle of a single Amtrak power car. The rail geometry was modeled after continuous 136-RE rail with the density, Young's modulus, and Poisson's ratio representing the steel in a 136-RE rail, which are 7.85 g/cm3, 200 GPa, and 0.28, respectively. The concrete ties had a spacing of 0.6 m (2 ft), a width of 0.23 m (0.75 ft), and density, Young's Modulus, and Poisson's Ratio matching the values of concrete, which are 2.97 g/cm3, 21 GPa, and 0.15, respectively. Besides the

symmetric boundary condition at the track centerline, the remaining boundaries were pinned and had non-reflective boundary conditions. The non-reflective boundary conditions absorbed pressure and shear waves, preventing the pressure waves from reflecting into the model. The distances to the boundaries were sufficient to prevent boundary effects from influencing the model.

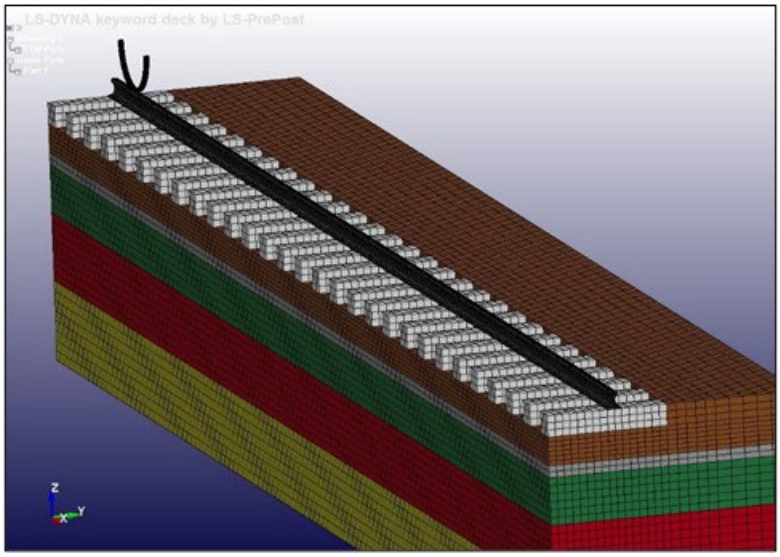

Figure 143. LS-DYNA model showing the open track with a sliding wheel

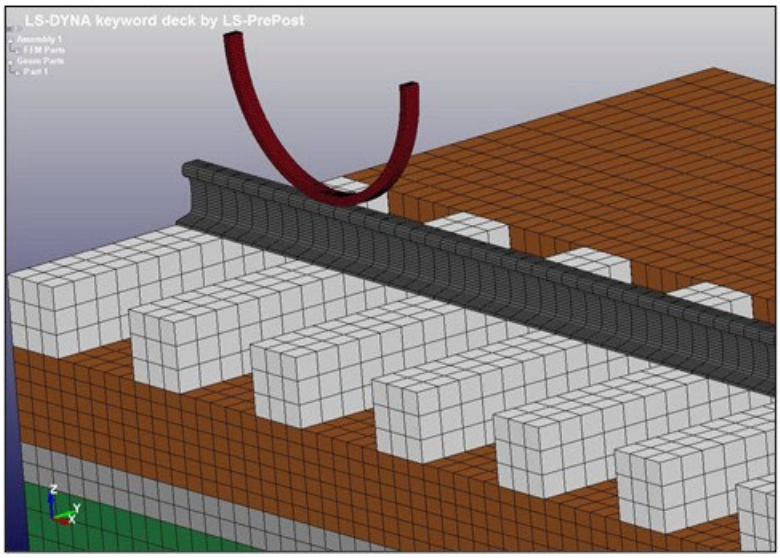

Figure 144. LS-DYNA model of wheel

For verification purposes, the model first simulated no tie-ballast gaps. The contact force between the wheel and rail should have remained close to the static wheel load throughout the analysis and the maximum tie-ballast contact forces of Ties 16 to 24 should have roughly equaled 35-40 percent. Because gravity was then included in the analysis with the wheel, the weight of the rail and tie was then incorporated into the tie-ballast contact force and represented about 3 percent of the wheel load. This additional force was not excluded because it was

experienced in the field. The time histories of the wheel-rail contact force and calculated normalized tie loads are shown in Figure 145 and Figure 146.

During the first 0.2 seconds of the analysis, the wheel-rail contact force of the stationary wheel matched the static wheel load (100 kN), confirming the application of gravity. As the wheel started moving at 0.2 seconds, high-frequency loads were produced. These frequencies also existed physically, and the model naturally dampened them as the physical rail and tie did in the field. Therefore, the wheel-rail contact force history was filtered using a 20 Hz filter, eliminating frequencies above 20 Hz. The results of the unfiltered, filtered, and static wheel-rail contact force are displayed in Figure 145. Once filtered, the wheel-rail contact force remained close to the static wheel load throughout the analysis.

With the additional weight of the rail and tie, the tie-ballast contact forces showed maximum values of around 40 kN, or 40 percent of the wheel load. This indicated that good load distribution was occurring within the model because all ties were in intimate contact. Small differences in maximum tie-ballast contact force did exist, and these were attributed to small oscillations in the wheel-rail contact force, shown in Figure 145.

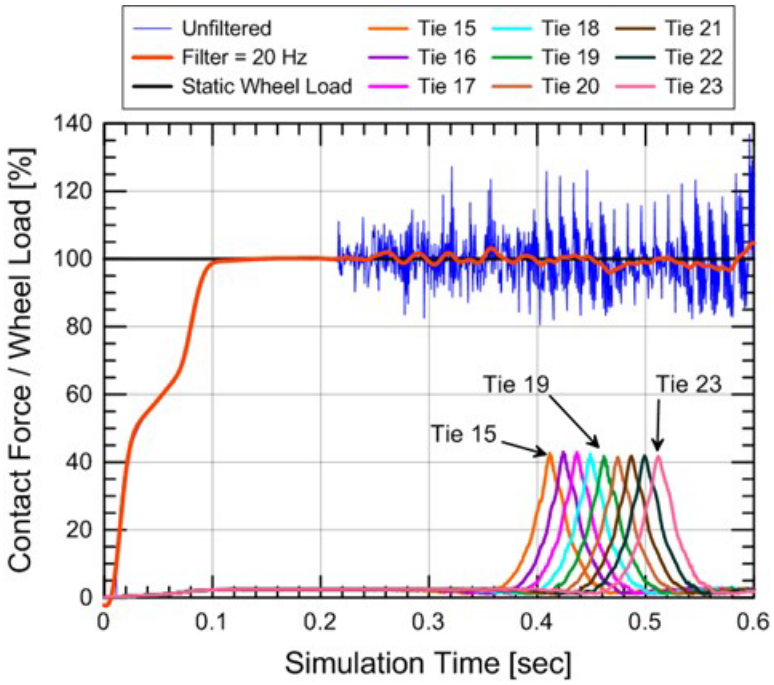

Figure 145. Wheel-rail and tie contact force time history; unfiltered, 20 Hz filtered, and static load are shown

Figure 146 shows the distribution of wheel load between the surrounding four ties at the exact timeframe when the wheel was directly over Tie 19 (0.461 seconds). The results showed about 40 percent of the wheel load being applied to Tie 19, 22.5 percent of the wheel load being applied to Ties 18 and 20, and about 10 percent of the wheel load being applied to Ties 17 and 21. The remaining 5 percent was taken by ties further away from Tie 19. This led to the general load distribution of about 40 percent, 20 percent, and 10 percent between adjacent ties.

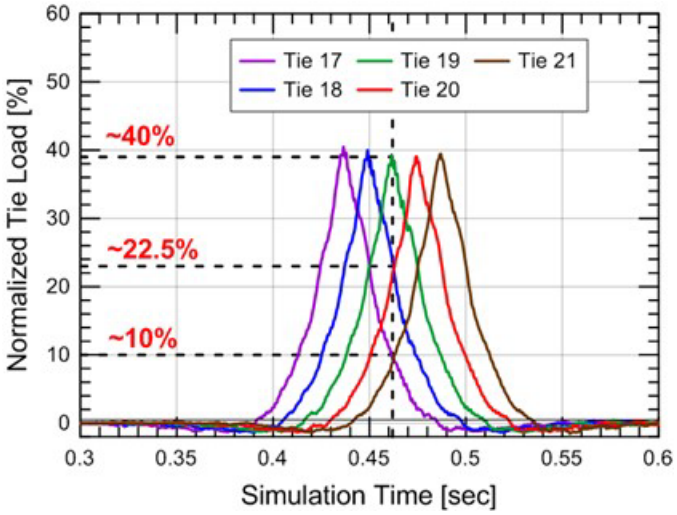

Figure 146. Load distribution at a single timeframe

With the model validated using fully supported ties, various parametric analyses were conducted to investigate track behavior. These include the following situations:

- Tie-ballast gap at Tie 19 only (0–1 mm)
- Tie-ballast gaps at Ties 18 and 20 (0–1 mm)
- Equal tie-ballast gaps at Ties 18 to 20 (0–4 mm)
- Unequal tie-ballast gaps at Ties 18 to 20 (0–1 mm)

The first three analyses were repeated to emphasize the effect of a moving wheel and presence of a rail. The third analysis demonstrated how the interaction of various tie-ballast gap combinations affected load redistribution among adjacent ties.

The first parametric analysis simulated the effect of an isolated, poorly supported tie and assumed a gap only under the instrumented tie (i.e., Tie 19), while all the other ties remained in intimate contact with the ballast (Figure 147). The gap at Tie 19 varied from 0.0 to 1.0 mm in 0.25 mm intervals.

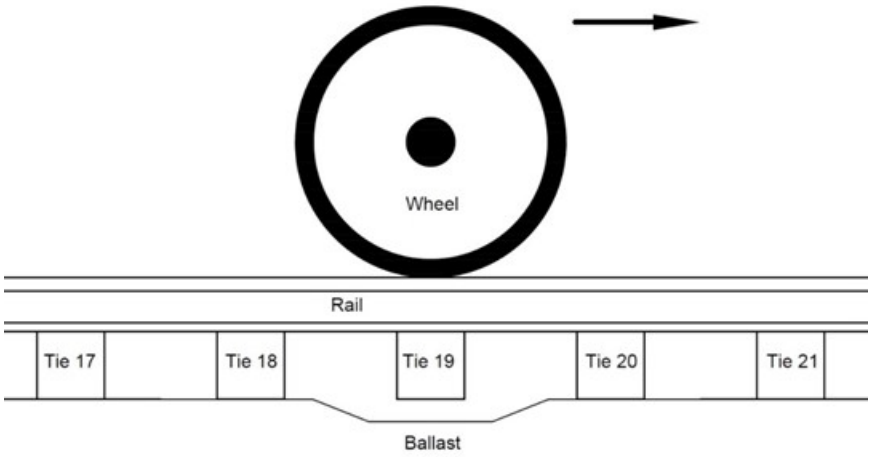

Figure 147. Wheel-rail-tie-ballast model showing a tie-ballast gap at Tie 19

Figure 148 through Figure 150 compare the tie-ballast contact force time histories as normalized tie loads for Ties 19, 18, and 20, respectively, for tie-ballast gap heights of 0.0, 0.25, 0.5, 0.75, and 1.00 mm. While only the maximum normalized tie loads are shown in later analyses, the full time histories are shown in these figures to emphasize changes in behavior due to a moving wheel. Understanding these behaviors was helpful when attempting to calibrate the LS-DYNA model in Section 14 of this report.

Figure 148 shows increasing the tie-ballast gap significantly decreased the maximum normalized tie load for Tie 19. The gap produced more bending in the rail, redistributing the load away from unsupported Tie 19 to Ties 18 and 20, which increased the load on those ties.

Figure 149 shows an increase in maximum normalized tie load and change in behavior of Tie 18 with increasing gap height at Tie 20. The maximum normalized tie load increased because when the wheel was above Tie 18, Tie 19 did not receive any load, and the load remained on Tie 18. As the wheel moved to Tie 19, the load continued to remain on Tie 18, increasing the duration of load on that tie. The response of Tie 20 (see Figure 150) was similar to Tie 18 (see Figure 149), but with greater normalized tie loads and an increase in force prior to maximum loading instead of after the wheel.

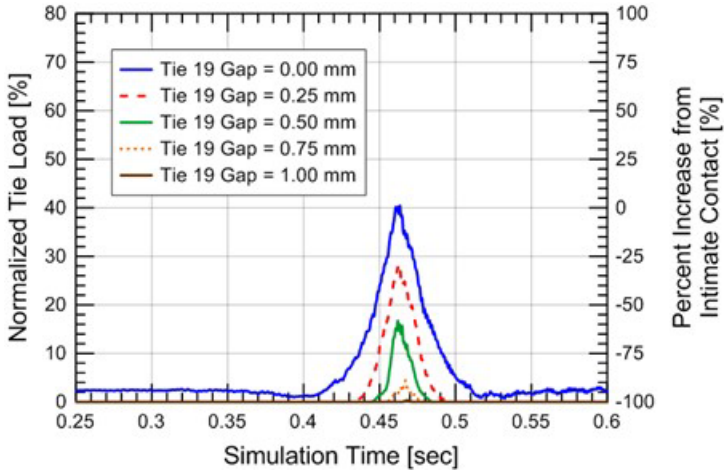

Figure 148. Normalized tie load time histories for Tie 19 with various Tie 19 gap heights

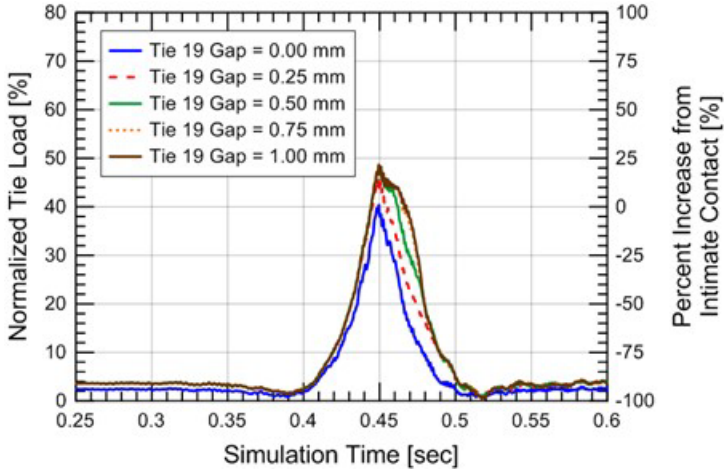

Figure 149. Normalized tie load time histories for Tie 18 with various Tie 19 gap heights

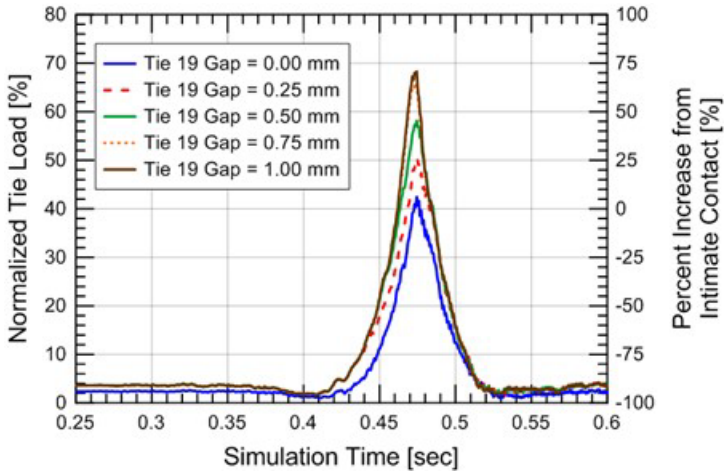

Figure 150. Normalized tie load time histories for Tie 20 with various Tie 19 gap heights

The maximum normalized tie load experienced by Ties 18, 19, and 20 along with their percent increase from intimate contact (normalized tie load = 40 percent) are shown in Figure 151. The maximum normalized tie load is the worst-case situation and therefore was used instead at a particular timeframe because the maximum tie load was of primary interest. Referencing Figure 145 where the tie-ballast gap at Tie 19 was 0.0 mm, the maximum normalized tie load experienced by Ties 18, 19, and 20 were all about 40 percent, as expected. However as the tie-ballast gap at Tie 19 increased, the additional rail bending required for Tie 19 to establish contact with underlying ballast caused the rail to shed some of the load away from Tie 19 to better support Ties 18 and 20. At a gap height of 1.0 mm, Tie 19 ceased to contact the ballast during loading (maximum normalized tie load = 0.0 percent), and Ties 18 and 20 reached their maximum normalized tie loads of 49 percent and 68 percent, respectively. This was an increase of 23 percent and 70 percent from the assumed 40 percent at intimate contact. Tie 20 experienced a greater increase than Tie 18 because Tie 20 was located after the unsupported tie (Tie 19) and would have amplified effects from the moving wheel being forced to accelerate upwards after the greater vertical rail displacement above Tie 19. This was the primary difference between the results of this analysis and the previous analysis. The effect on Ties 17 and 21 were minimal (<2 percent difference) and therefore not displayed.

Varying the stiffness of any track component will change the results but the general trend will remain. A stiffer track will have higher tie loads assuming intimate contact (>40 percent) but will fully distribute the load at lower tie-ballast gap heights (<1.0 mm), while a softer track will have lower tie loads assuming intimate contact (<40 percent) but will fully distribute the load at higher tie-ballast gaps (>1.0 mm). This suggests that softer track is preferable when focusing on the load redistribution mechanism.

If the 1.0 mm gap under Tie 19 had occurred due to local ballast fouling or poor compaction under the tie, the ballast under Ties 18 and 20 would settle to a greater extent than Ties 17, 19, and 21 because of the increased load. This would eventually decrease load redistribution as the tie loading becomes more evenly distributed among the ties and potentially result in the "stabilization" of the region. This is illustrated in Figure 151 by decreasing the "relative" gap height of Tie 19.

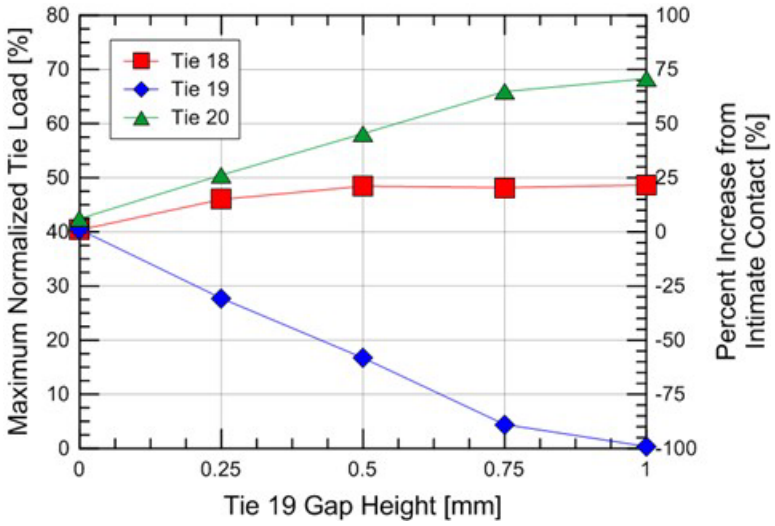

Figure 151. Maximum normalized tie load (maximum tie-ballast contact force/wheel load) for Ties 18, 19, and 20 with varying Tie 19 gap heights

The second parametric analysis differs from the first analysis because the tie-ballast gap at the adjacent ties (i.e., Ties 18 and 20) were increased with train passage, while the instrumented tie (i.e., Tie 19) remained in intimate contact (Figure 152). The gaps at Ties 18 and 20 varied from 0.0 to 1.0 mm at 0.25 mm intervals. This resulted in the opposite situation as the first parametric analysis in which load was shed away from Tie 19. In this analysis, the load shed away from the adjacent unsupported ties (i.e., Ties 18 and 20) and to Tie 19, which increased the load on Tie 19. Because two ties were unsupported instead of one, the maximum normalized tie load at Tie 19 increased from 40 percent to 74 percent, an increase of 85 percent (Figure 153).

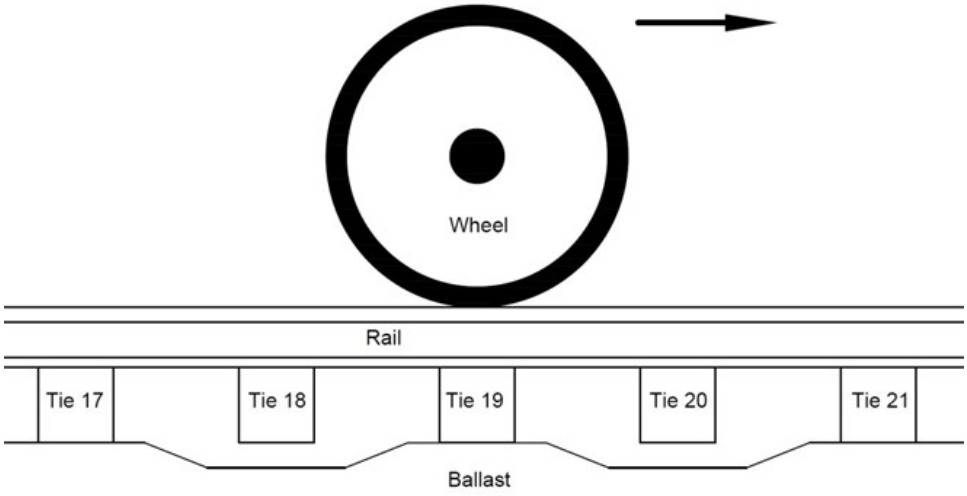

Figure 152. Wheel-rail-tie-ballast model showing equal tie-ballast gaps at Ties 18 and 20

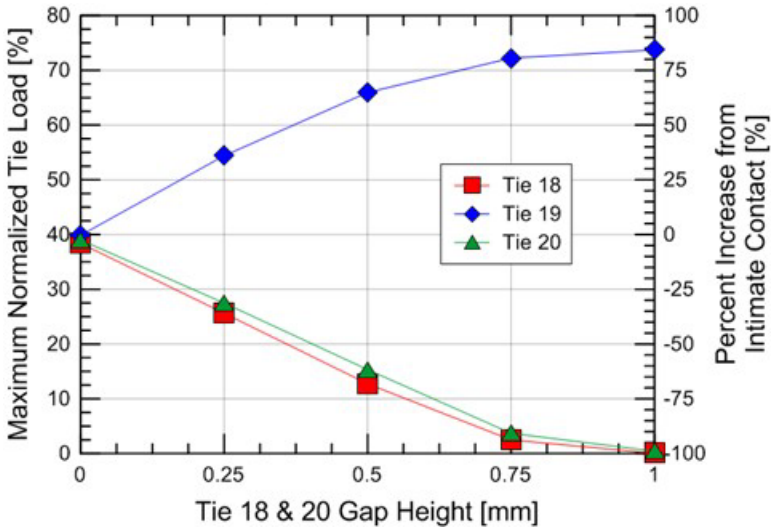

Figure 153. Maximum normalized tie load (maximum tie-ballast contact force/wheel load) for Ties 18, 19, 20, and 21 with varying gap heights but Tie 18 = 19 = 20 gap heights

The third parametric analysis extended the previous two with different tie-ballast gaps by investigating the load applied to supported ties. This parametric analysis investigated the applied loads on supported ties following a group of unsupported ties. Unsupported tie behavior was often observed over a group of ties instead of a single tie. This was representative of a site with localized fouling and the resulting tie-ballast gaps. For this analysis, equal tie-ballast gaps existed at the instrumented tie (i.e., Tie 19) and adjacent ties (i.e., Ties 18 and 20), and the gap varied from 0.0 to 4.0 mm because that was the gap height at which Tie 19 ceased contact with the ballast during loading to model the full range of gap situations (Figure 154).

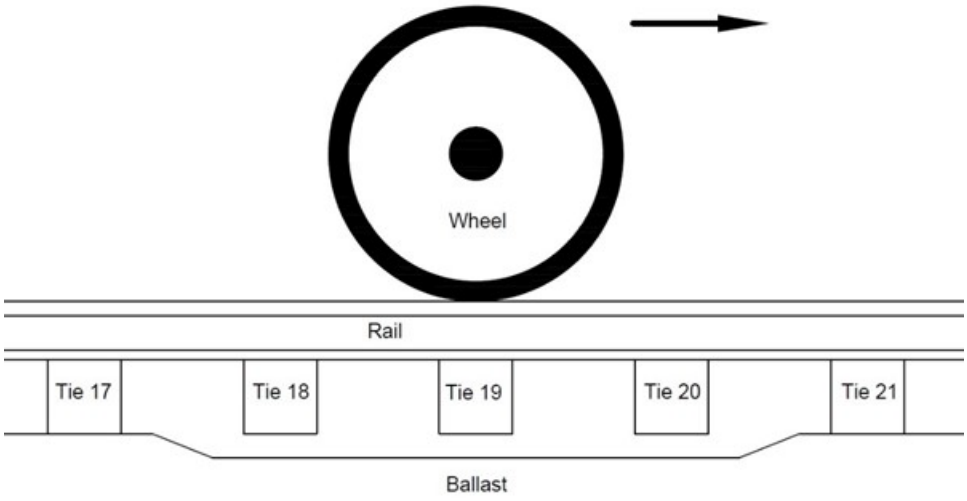

Figure 154. Wheel-rail-tie-ballast model showing equal tie-ballast gaps at Ties 18, 19, and 20

The changes in maximum tie-ballast contact force for Ties 18, 19, 20, and 21, along with their percent increase from intimate contact, are illustrated in Figure 155. The figure shows decreasing maximum normalized tie loads at Ties 18, 19, and 20, while significantly increasing at Tie 21

(~160 percent at 4.0 mm). The maximum normalized tie load at Tie 19 increased slightly for gap heights of 1.0 to 1.5 mm and then transitioned to a completely unsupported condition at a gap of 4.0 mm. Tie 19 experienced larger maximum normalized tie loads than Ties 18 and 20 because it was located between the surrounding supported ties (i.e., Ties 17 and 21), so more rail displacement occurred at that location. This allowed Tie 19 to establish ballast contact earlier than the adjacent ties (i.e., Tie 18 and 20).

The large, normalized tie loads experienced by Tie 21 (~160 percent at 4.0 mm) indicated load redistribution from a group of poorly supported ties could result in large increases in applied load to the next supported tie. This increased load may have damaged the tie or produced a tie-ballast gap at Tie 21 because of increased settlement. If this occurs, it would be expected that the load would shift to Tie 22, and that tie may develop a tie-ballast gap and be damaged. This "progressive loss of tie support and subsequent failure" mechanism can spread the damage of a single or small group of poorly supported ties to a larger track section. This field condition would likely be a group of unsupported ties with a gradual increase in tie support until a completely supported tie is reached. For example, if Ties 18 through 20 have a gap of 2.0 mm, Tie 21 may have a gap of 1.5 mm, Tie 22 of 1.0 mm, Tie 23 of 0.5 mm, and Tie 24 being completely supported. This configuration would result in a temporarily stable situation, impeding the spread of damage until additional substructure settlement occurs. However, track geometry maintenance may still be required. This also suggests that failure of track superstructure components like rail, fastening systems, and ties may be due to substructure settlement.

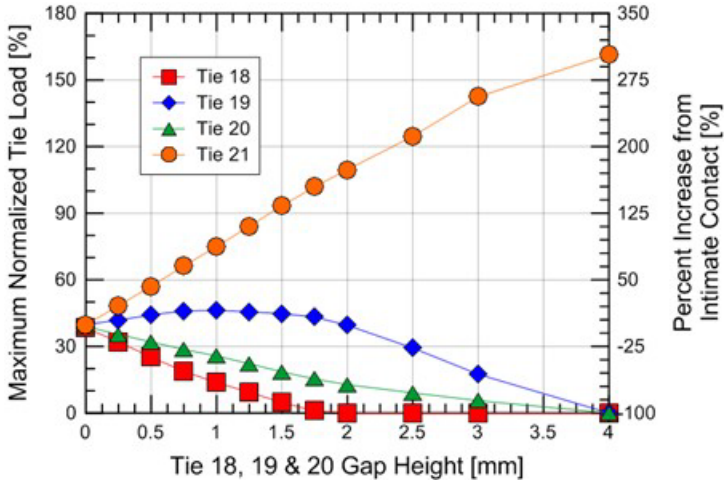

Figure 155. Maximum normalized tie load (maximum tie-ballast contact force/wheel load) for Ties 18, 19, 20, and 21 with varying gap heights but Tie 18 = 19 = 20 gap heights

The final parametric analysis for a single wheel emphasized how varying tie-ballast gap heights could significantly alter load redistribution. This is of great importance because tie-ballast gap heights vary in field conditions (Lundqvist and Dahlberg, 2005; Varandas et al., 2011) and measuring the tie-ballast gap height at only a single tie does not provide sufficient information to determine the magnitude of load redistribution. For the calibration of a single tie in open track, the results suggested that five adjacent ties should be instrumented to assess tie support and load distribution.

For this analysis, tie-ballast gaps at Ties 18, 19, and 20 are varied with equal gaps under Ties 18 and 20. This situation is displayed in Figure 156. The difference in gap heights from Tie 19 and Ties 18 and 20 illustrates the sensitivity of gaps under adjacent ties to the load redistribution.

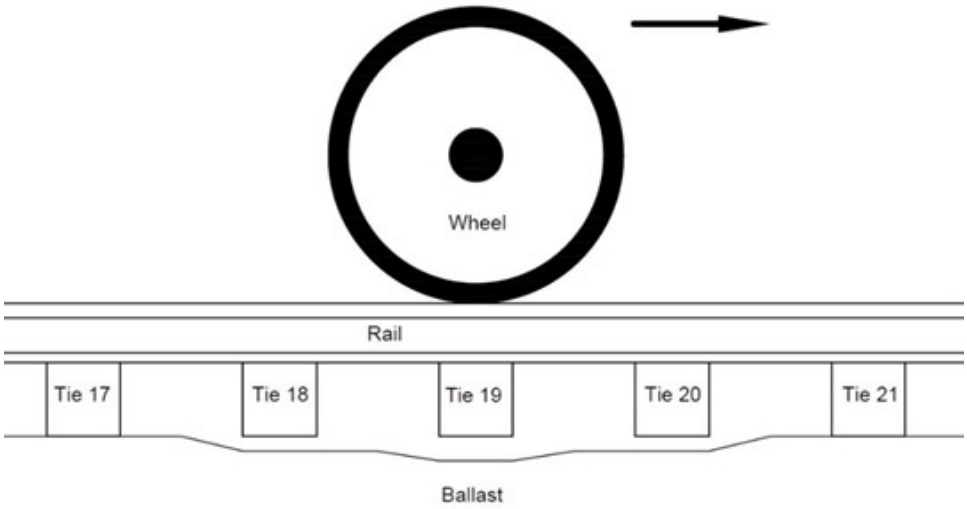

Figure 156. Wheel-rail-tie-ballast model showing unequal tie-ballast gaps at Ties 18, 19, and 20

Figure 157 shows the maximum normalized tie load and percent increase from intimate contact results only for the instrumented tie (i.e., Tie 19). Researchers observed a wide variation of normalized tie loads (0 percent to 75 percent), depending on the gap heights of the instrumented (i.e., Tie 19) and adjacent ties (i.e., Ties 18 and 20). As expected, the maximum normalized tie loads decreased with increasing tie-ballast gap magnitudes at Tie 19 because the load was shifting toward better-supported ties. However, the maximum normalized tie load at Tie 19 increased with increasing tie-ballast gaps at Ties 18 and 20 because those ties were carrying less load due to reduced tie support. To demonstrate the sensitivity of load redistribution from tie-ballast gaps of adjacent ties, a 0.75 mm tie-ballast gap at Tie 19 is presented as an example. Depending on the tie-ballast gaps of adjacent ties (i.e., Ties 18 and 20), the maximum normalized tie load experienced by Tie 19 ranged from 3 to 55 percent. This represented a 93 percent decrease to a 38 percent increase in tie load from the assumption of 40 percent when all ties were in intimate contact. These two possibilities would significantly change the back-calculated modulus values obtained using FLAC3D.

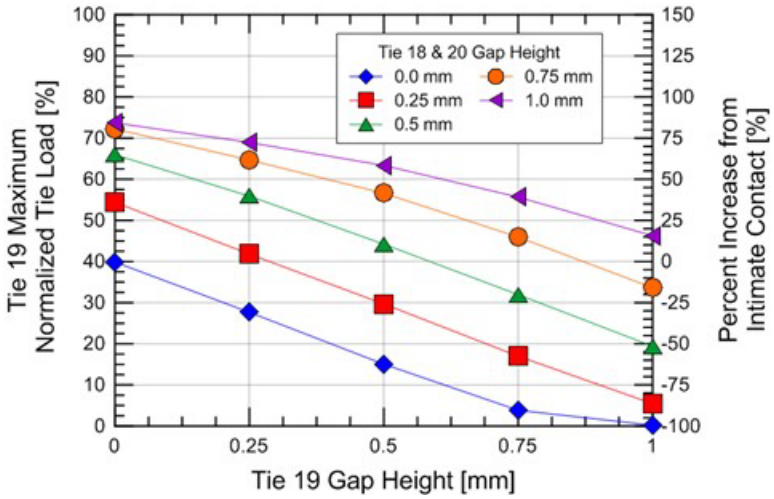

Figure 157. Maximum normalized tie load (maximum tie-ballast contact force/wheel load) for Tie 19 with varying gap heights for Ties 18, 19, and 20

13.5 Multiple Wheels

The simulation of a single moving wheel across the rail in the prior section incorporated all components required for modeling wheel-rail-tie-ballast interaction except the presence of multiple wheels. Simulating multiple wheels is important not only to accurately calculate the loading applied by a passing train but also to accurately calibrate the model because the field measurements used in the calibration reflected the presence of multiple wheels. This section applies a full railcar truck (i.e., two wheelsets) to illustrate the influence of two wheels on the model response. A single axle of an Acela power car was modeled in this analysis.

Figure 158 presents the dimensions of an Acela power car, including wheel spacing on each truck. The center-to-center wheel spacing for a single axle is 9 ft, 4 in, and these wheel distances will be simulated in the LS-DYNA analysis (Figure 159).

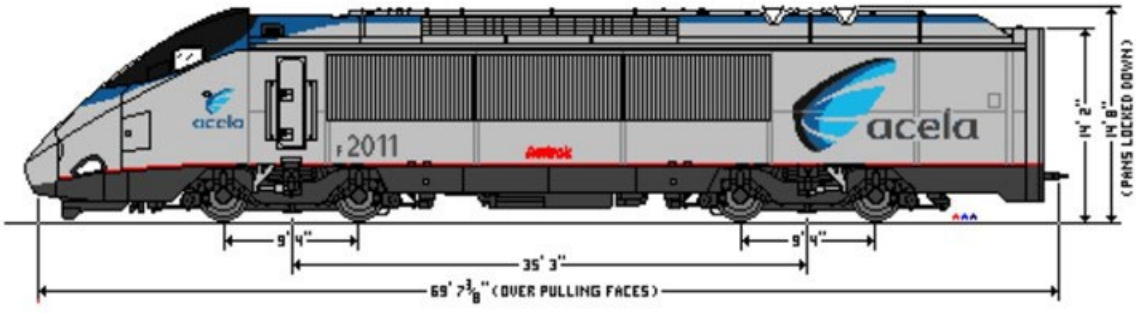

Figure 158. Diagram and dimensions of Amtrak power car (National Railroad Passenger Corporation, 2005)

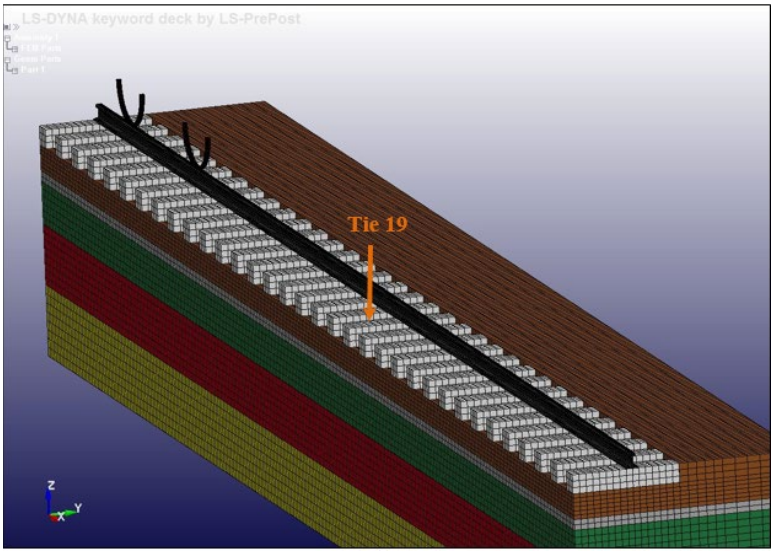

Figure 159. LS-DYNA model of Upland (60 ft) with two wheels

To verify the model, the initial situation assumed all ties were in intimate contact with the ballast. The two wheel-rail contact forces should remain around the static wheel load throughout the analysis and the peak tie-ballast contact forces should be approximately equal for both wheels because of intimate tie contact. For the two-wheel analysis, both filtered (20 Hz) wheel-rail contact force time histories are shown in Figure 160 and the normalized tie load time history for Ties 15 through 23 are shown in Figure 161.

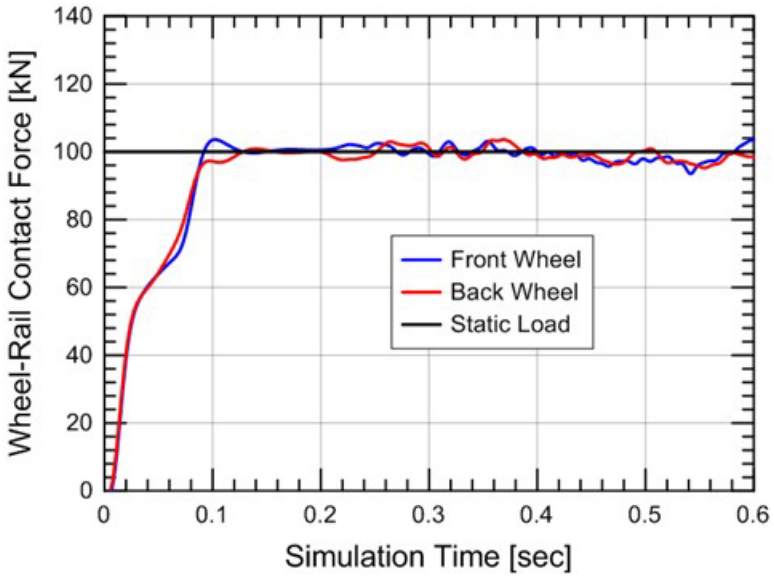

Figure 160. Filtered (20 Hz) wheel-rail contact force time history for wheels 1 and 2

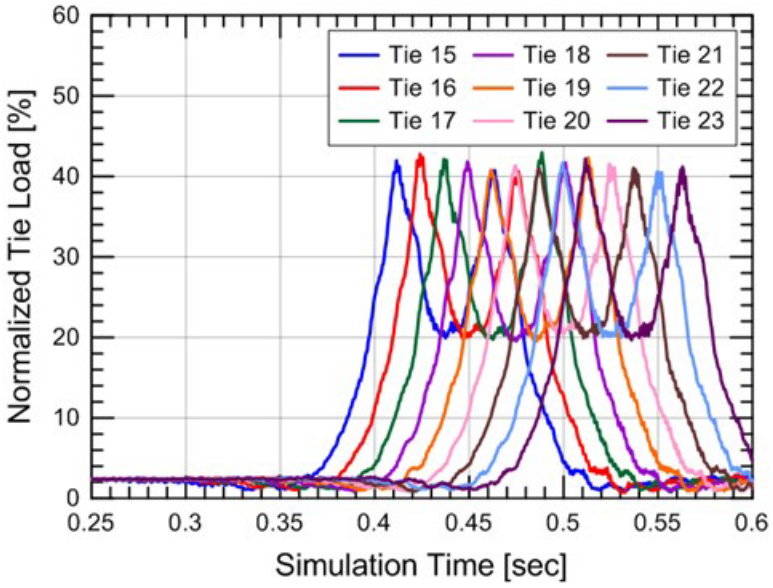

Figure 161. Normalized tie load time history for Ties 11 through 19 assuming two wheels

After verification with intimate tie contact, gaps were inserted below single and multiple ties to investigate the impact of multiple wheels on wheel-rail-tie-ballast interaction. When including a gap in the analysis, the results were similar to the single-wheel analyses presented above with respect to tie-ballast contact force. The data are presented in Section 15.2.4.

13.6 Summary and Future Work

The main findings and conclusions from these numerical analyses of track support and gaps were:

- Tie-ballast gaps can increase the applied loads on the ballast by the following two mechanisms: (1) load redistribution and (2) dynamic impact loads.
- The amplification of applied due to impact is dependent upon the velocity of the tie before it contacts the ballast. Greater tie velocities result in greater change of tie momentum when the tie impacts the ballast, which causes greater load amplifications.
- The existence of tie-ballast gaps causes the applied wheel loads to redistribute to adjacent ties with good tie support. Increasing gap heights require greater rail bending to establish contact between the tie and ballast, which sheds the load through the rail to adjacent supported ties.
- A moving wheel causes the load redistribution to favor ties in the direction of movement. The temporary increase in total vertical displacement of the rail from the tie-ballast gap causes an amplification of load at the next supported tie as the wheel moves displacement upwards due to supported conditions of that tie. This increase in applied load to the next supported tie promotes ballast compaction and progressive tie failure by overloading the adjacent or nearby supported tie(s) due to an unsupported or poorly supported tie.
- The tie-ballast gaps of adjacent ties significantly affect load redistribution. This emphasizes the importance of instrumenting a group of ties (at least 5 is recommended) instead of a single tie in future studies to model the different tie-ballast gaps along a

section of track. Without knowing the tie-ballast gaps for a group of ties, the actual load redistribution cannot be determined, which is needed to accurately predict future performance of this track with and without remedial measures.

- Including multiple wheels in the analysis does not significantly affect the calculated tie-ballast contact force or transient vertical displacement.

14. Field Calibrated Model at Upland (60 ft)

An inverse analysis to estimate layer modulus values for the Amtrak NEC instrumentation sites with FLAC3D is presented in Section 12. FLAC3D is useful compared to LS-DYNA when the moduli of multiple layers must be estimated quickly because the analysis can be automated by programming the process using the FISH coding option in FLAC3D. However, the static inverse analysis does not replicate all mechanisms affecting track behavior, so it cannot be considered a fully calibrated model. As a result, this section also presents a calibrated LS-DYNA model that replicates the transient track behavior by incorporating wheel-rail-tie-ballast interactions in the inverse modulus analysis. The team also performed this LS-DYNA analysis to determine if there was a significant difference in the modulus values obtained using FLAC3D (static analysis) and LS-DYNA (dynamic analysis).

14.1 Static Inverse Analysis (FLAC3D) versus Field Calibrated Dynamic Model (LS-DYNA)

This sub-section summarizes and explains the differences between the static inverse analysis performed with FLAC3D and the field calibrated dynamic analysis performed with LS-DYNA.

1. Computational Time: The FLAC3D static inverse analysis takes about 20 minutes for each site to estimate modulus values for the ballast, sub-ballast, and the various subgrade layers. The LS-DYNA field calibrated dynamic model, with manual iterations of modulus, requires 3 to 6 days for each site.
2. Scope and Outputs: Both analyses yield layer modulus values; however, the FLAC3D static inverse analysis only replicates peak transient displacement values, while the LS-DYNA field calibrated dynamic model replicates the entire vertical displacement time histories of the tie reaction and measured LVDT displacements.
3. Load Distribution: The FLAC3D static inverse analysis does not directly calculate the distribution of the wheel load to underlying and surrounding ties; it requires an initial assumption. LS-DYNA calculates the actual load distribution, including the influence of tie-ballast gaps and wheel-rail-tie-ballast interactions and the effects on the modulus values.
4. Non-linear Subgrade Response: The FLAC3D and LS-DYNA analyses use different methods to account for the measured non-linear LVDT behavior in the sub-ballast and subgrade layers. The peak wheel load versus peak transient LVDT 2 vertical displacement response at Upland (60 ft) is shown as an example in Figure 162. The significant non-linear behavior the team observed and the assumed mathematical models used to estimate the field behavior for FLAC3D and LS-DYNA are shown in this figure.

For the FLAC3D static inverse analysis, only peak transient displacements are required. Therefore, an “apparent gap” can be used to account for the non-linear force-displacement response. For example, if a peak wheel load of 100 kN is assumed, the field data in Figure 162 shows about 0.1 mm of transient LVDT 2 vertical displacement with an apparent gap of about 0.06 mm. Therefore, the numerical FLAC3D analysis varies Young’s modulus of Layer 2 until 0.04 mm of vertical displacement is obtained (0.1 to 0.06 mm). Because both the material model in FLAC3D and the field response are assumed to be linear, the advantage of this method is the FLAC3D model can replicate peak LVDT displacements throughout the entire measured range

(60 to 160 kN). This better replicates the mobilized state of the sub-ballast and subgrade under train loading and implies the estimated FLAC3D modulus is a "tangent modulus."

Conversely, LS-DYNA models the entire force-displacement relationship and not just peak transient vertical displacement, so an apparent gap cannot be used. This means the force-displacement response passes through the origin (apparent gap = 0.0 mm) because the time history includes an unloaded condition (wheel load and displacement = 0), loaded condition (peak wheel load and peak displacement), and the load-displacement response in between. This implies the estimated LS-DYNA modulus is a "secant modulus" and is required to calibrate an entire time history displacement relationship.

In summary, while the calibrated LS-DYNA and FLAC3D models both predicted 0.1 mm in LVDT 2 for an assumed wheel load of 100 kN, the estimated modulus values would be different because of the different analyses. While the non-linear behavior in the Figure 162 example was significant, almost all field measured LVDT responses displayed small non-linear responses (apparent gap ≈ 0.0 mm), so the estimated tangent modulus from FLAC3D and secant modulus from LS-DYNA were similar. Only LVDT 2 at Upland (60 ft) experienced significant non-linear behavior, so the fully non-linear elastic material models in LS-DYNA were required at this time and FLAC3D could be used to estimate moduli.

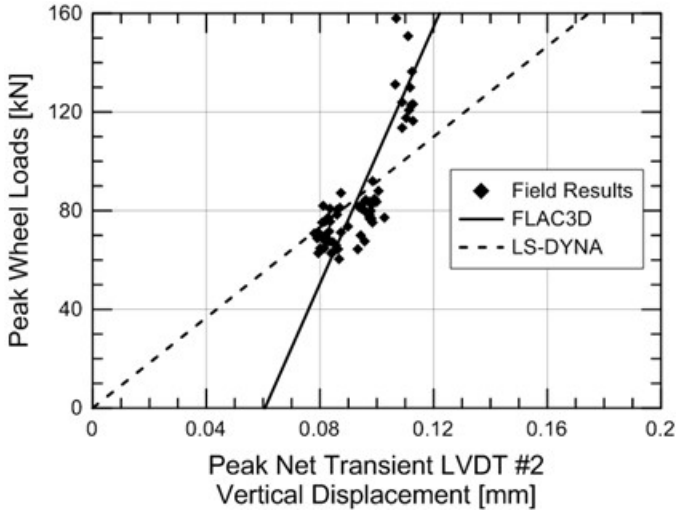

Figure 162. Different interpretations of LVDT 2 behavior at Upland (60 ft) recorded on 29 January 2013 at 10:21 a.m. from FLAC3D and LS-DYNA

14.2 Field Measurements at Upland (60 ft)

As with previous analyses, the data recorded at Upland (60 ft) on 29 January 2012 was used for LS-DYNA calibration. The model replicated the first axle of a single Amtrak power car as two sliding wheels at the wheel spacing shown in Figure 158.

To be considered a calibrated model, the LS-DYNA model should be able to replicate the following measured field behavior:

- Tie reaction time histories
- Transient LVDT vertical displacements

The field measured tie reaction time history was compared against the numerical tie-ballast contact force time history at Tie 19 (i.e., the instrumented tie). While the two parameters were two different measurements, the comparison was informative for ties with good support. Tie reaction measures the magnitude of rail bending above the tie and relates the amount of rail bending to load experienced by the tie. This was considered representative of the tie-ballast contact force for supported ties. This was reasonable for Upland (60 ft) because this site was experiencing good tie support. Unsupported ties can still transfer load while experiencing significant bending, so the two different measurements were not comparable in unsupported situations.

The field measured transient LVDT vertical displacements were compared to relative vertical displacement time histories of nodes closest to the LVDT locations in the model. LS-DYNA output the total transient vertical displacement of each node. The net transient vertical displacement of each layer could be calculated by subtracting the total displacements between two nodes representing the two LVDTs.

The field measured time histories used to verify the LS-DYNA results involved the first axle of the Amtrak power car passing Upland (60 ft) on 29 January 2013. The corresponding wheel load, tie reaction, and transient LVDT displacement time histories are displayed in Figure 163.

The wheel load time history in Figure 163(a) was used to determine the static wheel loads of the passing wheels. The two peak wheel loads were 124 and 123 kN, yielding an average peak wheel load of 124 kN. The velocity of the moving wheels was set at 110 mph to simulate an Acela train. This train velocity could be verified by dividing the known distance between train wheels by the measured time in between peak wheel loads.

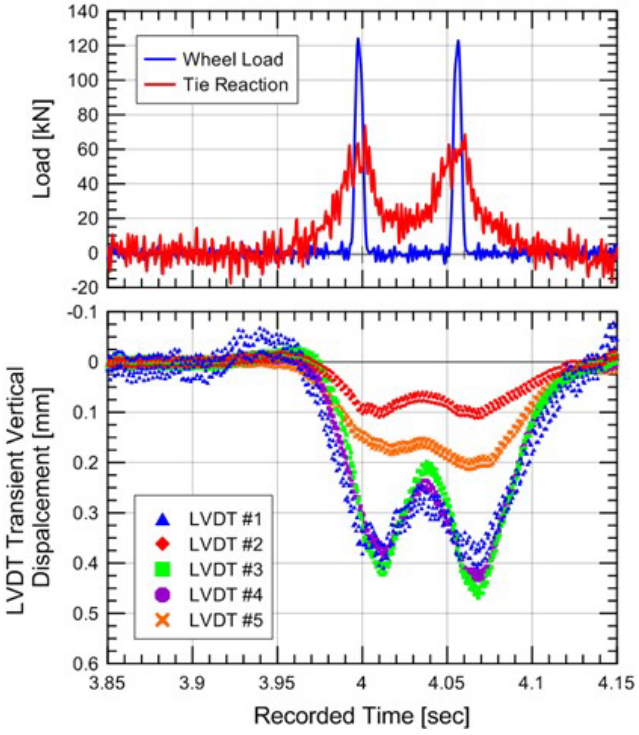

Figure 163. Measured wheel load, tie reaction, and transient LVDT displacements at Upland (60 ft) recorded on 29 January 2013 at 10:21 a.m.

14.3 Upland (60 ft) – Equal Tie-Ballast Gaps

For the LS-DYNA model, the largest unknown was the tie-ballast gap heights of the surrounding ties because the gap was only known at the instrumented tie. Knowing these values was important because they controlled the load redistribution between ties (see Section 13.3).

With the available data, only the tie-ballast gap of the instrumented tie could be calculated and compared to field measurements. Interpretation of field results suggested the tie-ballast gap at the instrumented tie was 0.25 mm. Therefore, the gaps of the surrounding ties must be assumed. In the first LS-DYNA analysis, it was assumed the tie-ballast gap measured at the instrumented tie was equal to the gaps of the two surrounding ties. As a result, Figure 164 shows the gaps under Ties 18, 19, and 20 were the same.

With these assumed tie-ballast gaps, the layer moduli were estimated using an inverse analysis and are presented in Table 36.

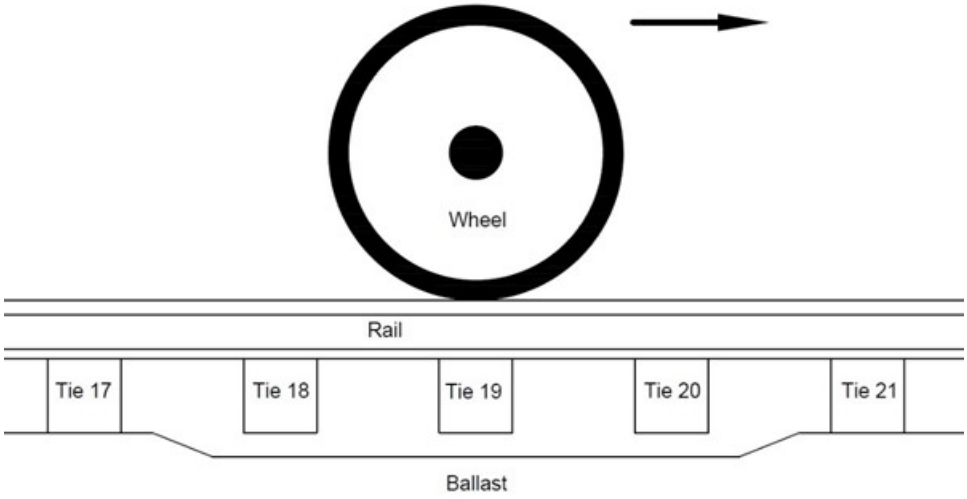

Figure 164. Wheel-rail-tie-ballast model showing equal tie-ballast gaps at Ties 18, 19, and 20

Table 36. LS-DYNA estimate modulus values at Upland (60 ft) for January 2013 assuming equal tie ballast gaps for Ties 14, 15, and 16

Layer 1	Layer 2	Layer 3	Layer 4	Layer 5
264	28	28	39	60

The results of the tie loading are displayed in Figure 165. The blue line represents the numerical tie-ballast contact force for Tie 19, while the thinner red line represents the field measured tie reaction. The figure shows good agreement between the measured and calculated tie-ballast contact force. The measured tie reactions reached about 60 kN, while the numerical results showed a peak at about 40 kN. It was possible that the surrounding ties had tie-ballast gaps greater than 0.25 mm at Upland (60 ft), so more load was redistributed to the instrumented tie than with equal tie-ballast gaps. In this LS-DYNA model, Ties 18, 19, and 20 had the same tie-ballast gap of 0.25 mm, so the load was distributed evenly. The effect of tie-ballast gaps of different heights are discussed in greater detail in Section 14.4.

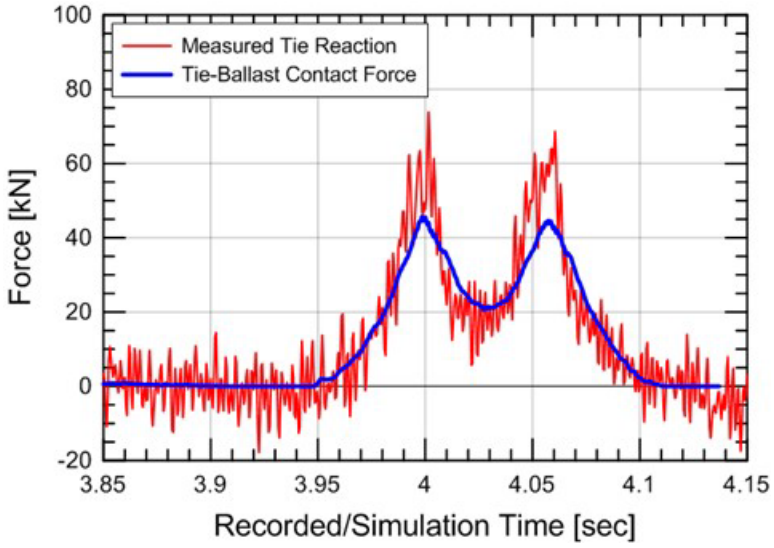

Figure 165. Comparison between measured tie reaction and tie-ballast contact force at Upland (60 ft) for data recorded on 29 January 2013 at 10:21 AM EST, assuming equal tie-ballast gaps

The calculated responses for LVDTs 1 through 5 are compared with the field measurements in Figure 166 through Figure 170.

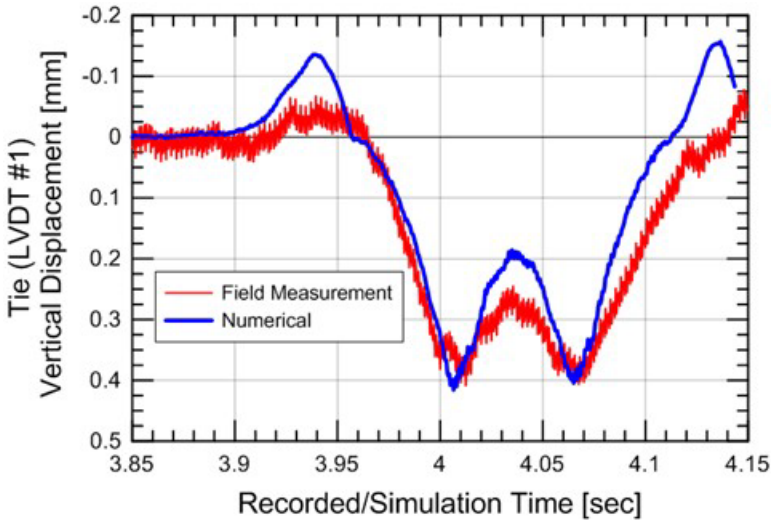

Figure 166. Comparison between field measured and numerical LVDT 1 transient displacements at Upland (60 ft) for data recorded on 29 January 2013, assuming equal tie-ballast gaps

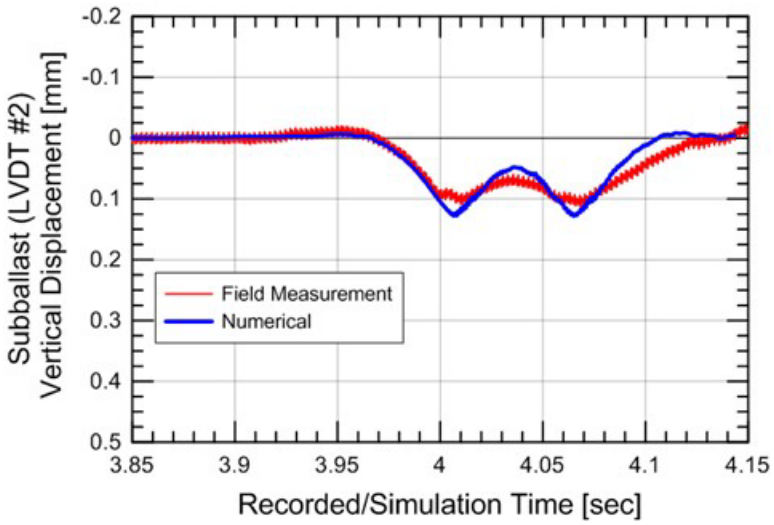

Figure 167. Comparison between field measured and numerical LVDT 2 transient displacements at Upland (60 ft) for data recorded on 29 January 2013, assuming equal tie-ballast gaps

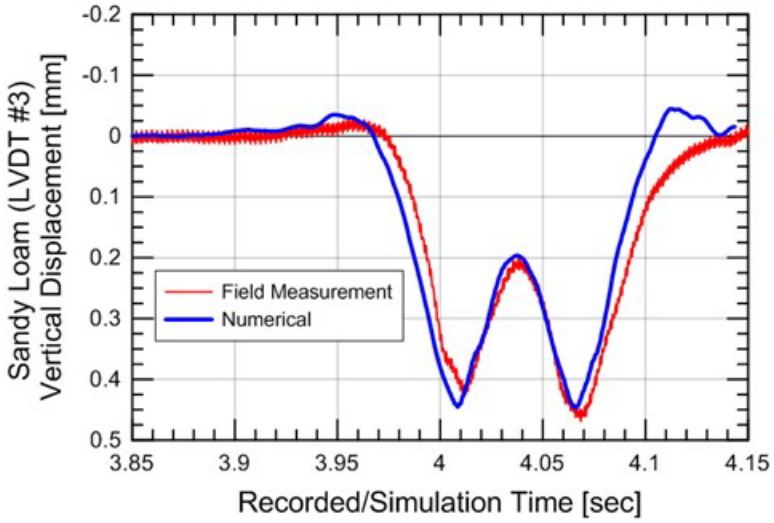

Figure 168. Comparison between field measured and numerical LVDT 3 transient displacements at Upland (60 ft) for data recorded on 29 January 2013, assuming equal tie-ballast gaps

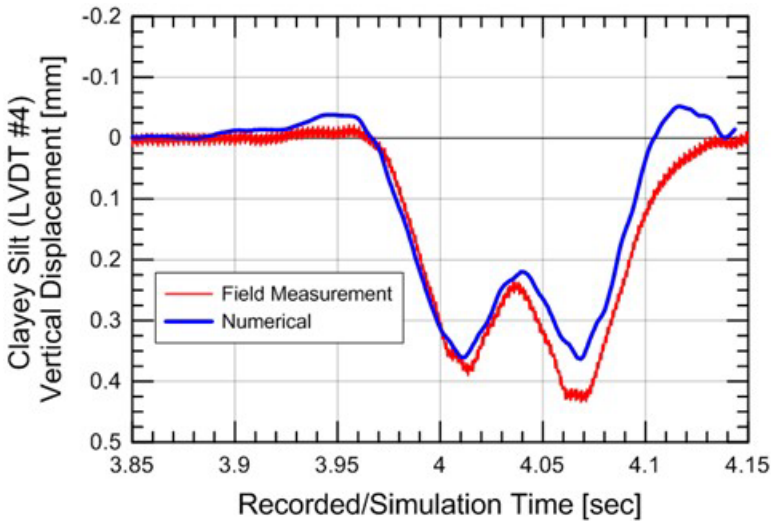

Figure 169. Comparison between field measured and numerical LVDT 4 transient displacements at Upland (60 ft) for data recorded on 29 January 2013, assuming equal tie-ballast gaps

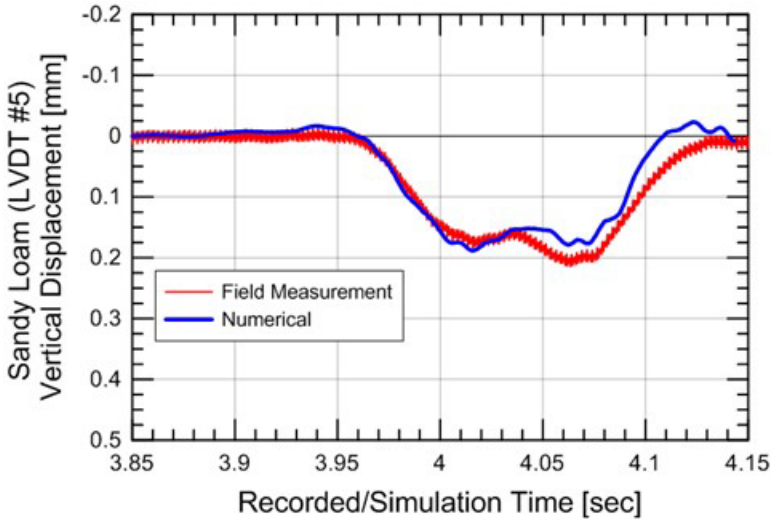

Figure 170. Comparison between field measured and numerical LVDT 5 transient displacements at Upland (60 ft) for data recorded on 29 January 2013, assuming equal tie-ballast gaps

From Figure 166 through Figure 170, the team made the following observations:

- The calculated and measured peak vertical displacements at each LVDT were in good agreement. This implied the modulus values and initial assumptions of load distribution were representative of field conditions.
- The timing and magnitude of the calculated vertical displacements matched field behavior. This suggested that the wheel spacing and velocity were representative of the passing Acela train.
- The LS-DYNA results indicated the rail unloaded at a quicker rate than field measurements. The slower unloading from the field measurements was likely due to the

influence of the next train axle, which was simulated in subsequent analyses with multiple wheels.

- The numerically replicated uplift of LVDT 1 was greater than the measured values. This was likely due to a lack of side friction along the tie resisting movement from ballast in the crib and shoulders.

14.4 Upland (60 ft) – Unequal Tie-Ballast Gaps

One of the main deviations between the calibrated model in Section 14.3 and field measurements was that the measured tie reactions showed higher peak wheel loads than the LS-DYNA tie-ballast contact forces. This was probably due to unequal tie-ballast gap heights between adjacent ties. Therefore, this next LS-DYNA analysis is an inverse analysis that estimated the tie-ballast gaps of the surrounding Ties 18 and 20 (see Figure 171) by implementing the mechanisms of load redistribution in Section 13.4.

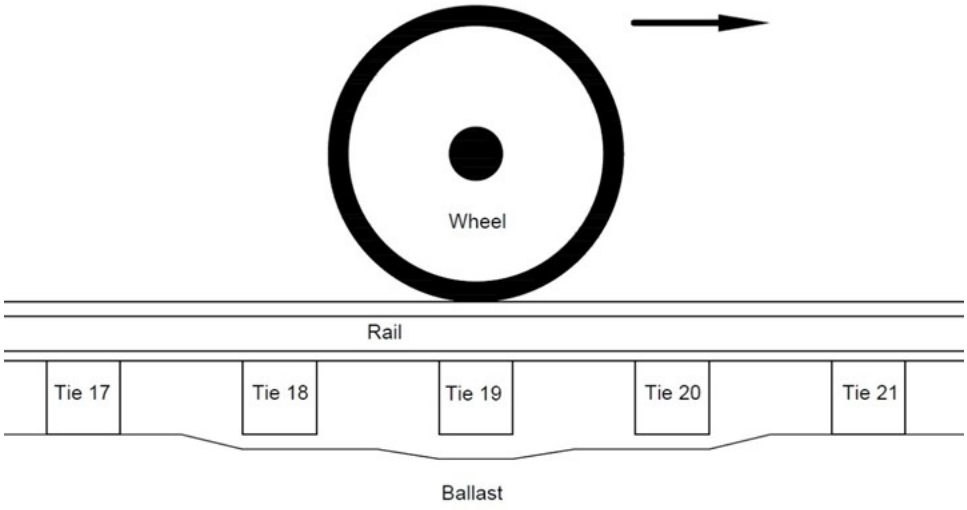

Figure 171. Wheel-rail-tie-ballast model showing unequal tie-ballast gaps at Ties 18, 19, and 20

The calculated tie load ratio (tie reaction/wheel load) of the Amtrak power car was 53 percent. To replicate this value, Figure 155 was used to determine which tie-ballast gap situations resulted in a maximum normalized tie load of 53 percent. Interpretations of the field measurements suggested the instrumented tie had a gap of 0.25 mm, so the graph states 0.45 mm gaps were required for Ties 18 and 20 to yield a maximum normalized tie load of 53 percent at Tie 19. Due to the sensitivity of load distribution to different modulus values, a tie-ballast gap height of 0.55 mm was used for Ties 18 and 20, while a gap of 0.25 mm was used for Tie 19 because of field measurements.

The updated tie-ballast gap heights affected the load distribution and the transient displacements under the tie. Therefore, new layer modulus values were estimated using an LS-DYNA inverse dynamic analysis and are shown in Table 37. These modulus values were compared to the estimated modulus values from the FLAC3D static inverse analysis in Section 12 and LS-DYNA analysis in the previous section, assuming equal gap heights. The results in Table 37 show the estimated modulus values could be significantly different for the three different analyses.

Table 37. Comparison of back-calculated modulus values from FLAC3D (Section 12), LS-DYNA assuming equal tie-ballast gaps (Section 14.3), and LS-DYNA assuming unequal tie-ballast gaps at Upland (60 ft) for January 2013 (all values in MPa)

Analysis	Layer 1	Layer 2	Layer 3	Layer 4	Layer 5
FLAC3D	201	278	22	27	47
LS-DYNA – Equal Gaps	131	37	29	36	62
LS-DYNA – Unequal Gaps	207	67	33	32	59

For Layer 1 ballast, the difference in modulus values (201, 131, and 207 MPa) were attributed to the various load distributions of each analysis. If the assumed tie-ballast gaps redistributed the load in a manner that caused the instrumented tie to experience less load (<35 percent), the stress of the underlying ballast decreased and a stiffer modulus was required to replicate the field measured peak LVDT 1 displacement. For the LS-DYNA analysis with equal tie-ballast gap heights, the load was shed away from the instrumented tie (<35 percent) resulting in a softer estimated modulus. For the LS-DYNA analysis with unequal gap heights, the load redistributed toward the instrumented tie (>35 percent), resulting in a stiffer estimated modulus.

For Layer 2 sub-ballast, the team observed the largest moduli difference between the three analyses. The main reason for this difference was how the FLAC3D and LS-DYNA analyses interpreted non-linear force-displacement behavior (Figure 162). FLAC3D included an apparent gap which resulted in the estimation of a stiffer sub-ballast tangent modulus. LS-DYNA did not include an apparent gap so the estimated secant modulus would be lower. Also, load distribution could influence the estimated sub-ballast modulus, as observed by comparing Layer 2 for both LS-DYNA analyses.

For Layers 3 through 5, only small differences were observed between the estimated modulus values. This was caused by the field measured force-displacement behavior being nearly linear for LVDTs 3 through 5 (apparent gap ≈ 0.0 mm) and the influence of load redistribution decreasing as the layer depth increased. For example, if the load redistributes away from the instrumented tie, LVDT 5 will be more likely to experience the load than LVDT 1 because vertical stress spreads horizontally with depth (2:1 ratio).

Figure 172 through Figure 177 compare the LS-DYNA model with field measurements.

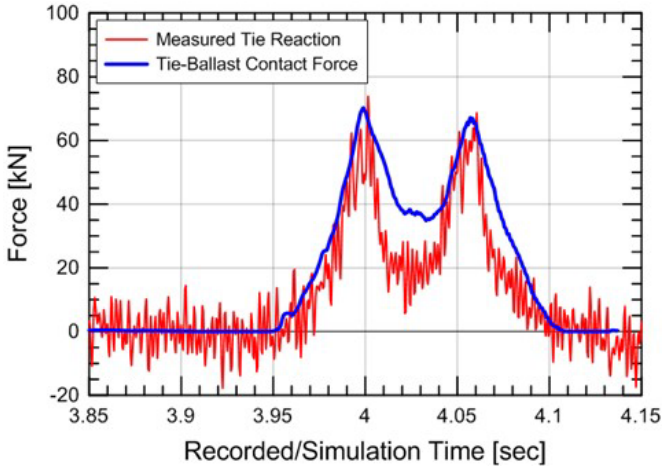

Figure 172. Comparison between measured tie reaction and tie-ballast contact force at Upland (60 ft) for data recorded on 29 January 2013, assuming unequal tie-ballast gaps

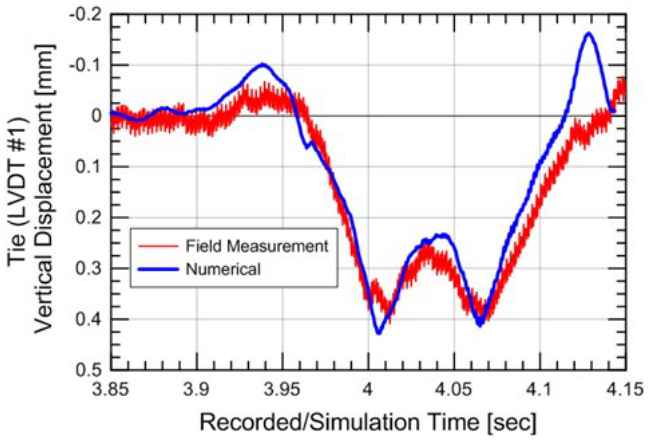

Figure 173. Comparison between field measured and numerical LVDT 1 transient displacements at Upland (60 ft) for data recorded on 29 January 2013, assuming unequal tie-ballast gaps

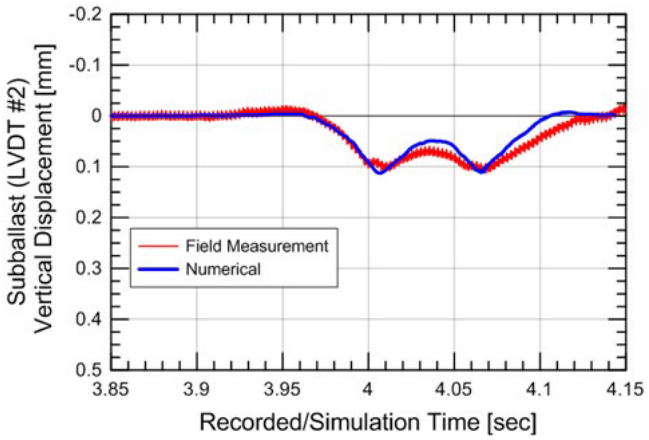

Figure 174. Comparison between field measured and numerical LVDT 2 transient displacements at Upland (60 ft) for data recorded on 29 January 201, assuming unequal tie-ballast gaps

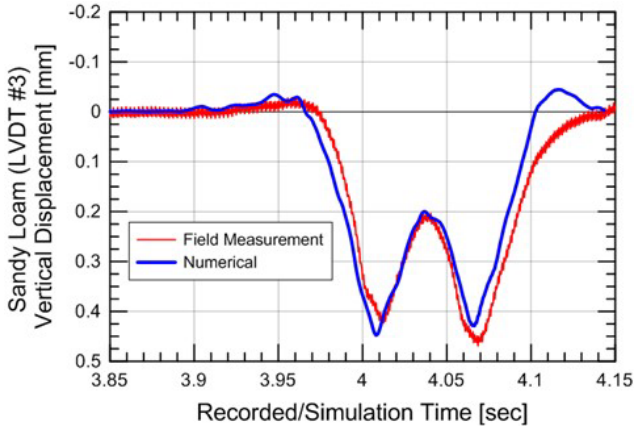

Figure 175. Comparison between field measured and numerical LVDT 3 transient displacements at Upland (60 ft) for data recorded on 29 January 2013, assuming unequal tie-ballast gaps

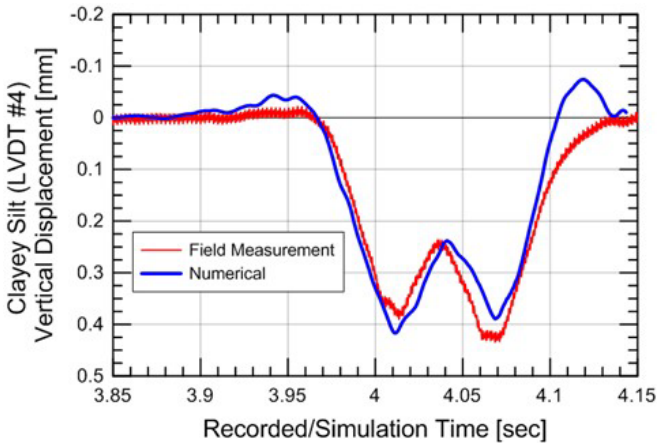

Figure 176. Comparison between field measured and numerical LVDT 4 transient displacements at Upland (60 ft) for data recorded on 29 January 2013, assuming unequal tie-ballast gaps

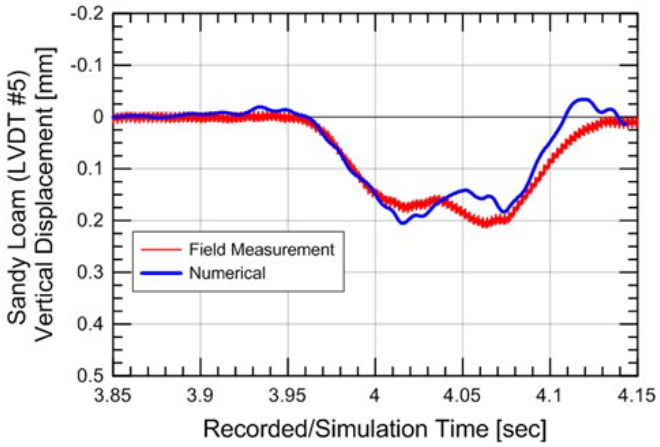

Figure 177. Comparison between field measured and numerical LVDT 5 transient displacements at Upland (60 ft) for data recorded on 29 January 2013, assuming unequal tie-ballast gaps

The team made the following observations from these analyses:

- The peak tie-ballast contact force equaled the peak tie reaction, but the measured tie reaction time history showed quicker rebound or unloading than the LS-DYNA results.
- The LS-DYNA layer displacements were in good agreement with the field LVDT displacements. The main differences were similar to those in Section 14.3, i.e., numerical unloading was quicker and the rebound in Layer 1 was greater than the field results.

This calibrated model was used as the basis of the wheel sliding models in Section 13 and the bridge approach models used in Section 15. A calibrated numerical model was not developed for the bridge approach, Upland (15 ft), because information was insufficient to accurately replicate the track geometry. For example, the settlement and tie-ballast gap heights of every tie in the transition zone were not known and were required to model the load redistribution around the instrumented tie. Various tie-ballast gap heights were assumed in the analyses presented in Section 14 to investigate the range of transition behavior.

15. LS-DYNA Mesh and Modeling

Analyses in Section 13 and Section 14 were limited to the wheel-rail-tie-ballast interaction to illustrate how load redistribution and impact loads can increase applied loads to the ballast and to calibrate the LS-DYNA model to field measurements at Upland (60 ft). This section expands on that work by investigating the effects of how a full railcar truck or rolling cart passing over the bridge abutment at the Upland Avenue site interacted and/or amplified the applied loads to the ballast when tie-ballast gaps were present.

15.1 Numerical Model

This analysis involved a bridge transition zone instead of open track to gain insight into increased dynamic loads in transition zones (see Figure 178). The bridge structure was modeled after the Upland Street bridge in Chester, Pennsylvania, and included a masonry wall, an open deck bridge with timber ties on the bridge, and W-beams underneath the bridge. The stiffness of the bridge was greater than the approach track and researchers expected this to produce impact loads when the front wheels of the cart passed onto the bridge abutment.

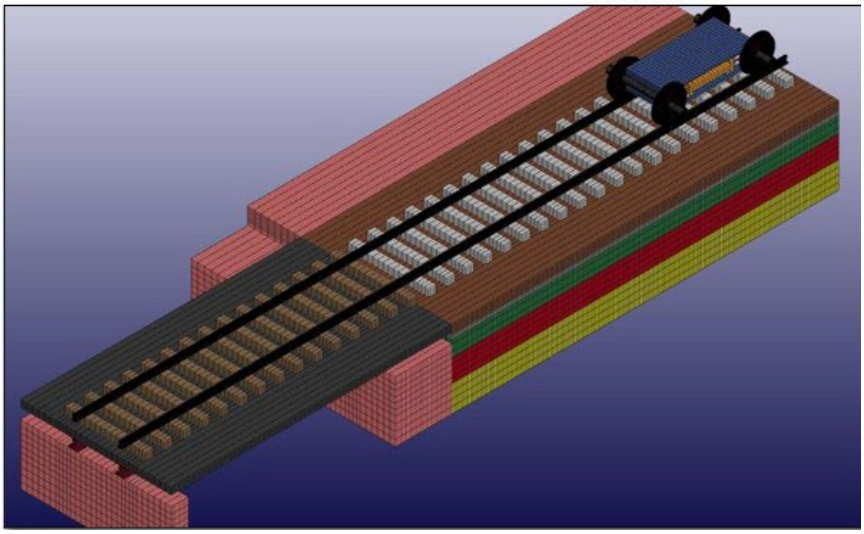

Figure 178. LS-DYNA finite element mesh showing Upland Street bridge approach track site with a rolling cart

Researchers used photos of the site to assist in modeling the Upland Avenue bridge. At Upland (15 ft), the instrumentation site was located seven ties north of the bridge on Track 3 in the southbound direction. The photograph in Figure 179 faces north and shows the large masonry wall constructed to elevate the railway at Upland Avenue. The Upland (15 ft) instrumentation site was located just above the white truck on Track 3, which was one track in from the north-south trending masonry wall. The photograph in Figure 180 faces south and illustrates the single-span bridge over Upland Avenue, modeled in the 3-dimensional LS-DYNA FEM. Amtrak provided the dimensions of the 1902 masonry abutment wall at the Upland Avenue bridge, which assumed the same geometry for the north-south trending masonry wall (Figure 181). The abutment wall is 15 ft, 10 in high with an exposed height of 13 ft, 6 in. The top and base widths of this wall are 5 ft, 8 in and 8 ft, 9 in, respectively.

Figure 179. Masonry walls at Upland Avenue below the Upland (15 ft) instrumentation location, looking north with truck adjacent to wall with MDD location on Track 3 above the truck

Figure 180. Masonry walls at Upland Avenue below the Upland (15 ft) instrumentation location, looking south, showing single-span bridge over Upland Avenue

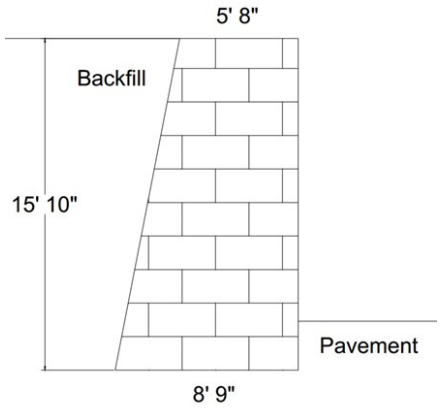

Figure 181. Diagram of masonry walls at Upland Avenue below the Upland (15 ft) instrumentation location (Diagram courtesy of Amtrak)

Figure 182 is a view of the four tracks from the top of the elevated railway, with Track 4 at the bottom of the photograph and Track 1 at the top. The Upland (15 ft) instrumentation location was on Track 3 where the Amtrak personnel are working. The figure shows this instrumentation location was seven concrete ties north (to the left) of the Upland Avenue bridge (see red arrow).

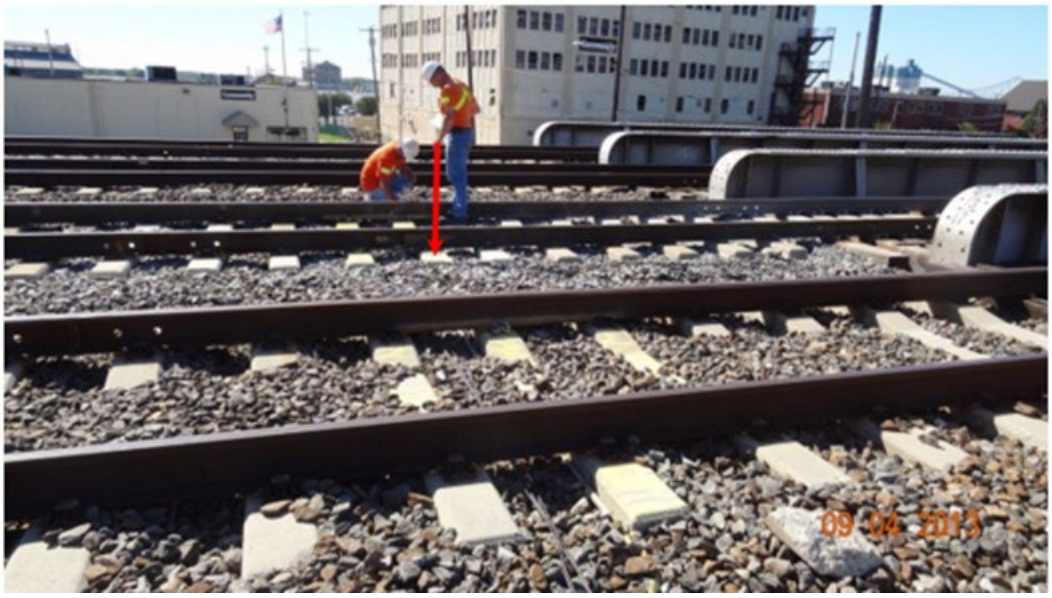

Figure 182. View of Tracks 1 through 4 at top of elevated railway with Track 4 at the bottom of the photograph and Track 1 at the top of the photograph

Instead of sliding wheels, this model used a cart to simulate the secondary suspension system of a high-speed passenger train. The cart consisted of four wheels with the axles spaced 2.8 m (9.33 ft) apart to replicate the first truck of an Amtrak Acela power car. The cart mass was located at the cart center with a density such that each wheel applied a static wheel load of 100 kN. The axles and cart mass were connected with four sets of vertical and horizontal springs and vertical dampers. The values of the vertical and horizontal springs were 7.3 x 10^5 N/m and 2.2 x 10^9 N/m, and damper values set to 7.3 x10^6 N*s/m. The velocity of the cart was 177 kph (110 mph) to replicate the operating speed of Amtrak's high-speed trains along the NEC.

The substructure layer thicknesses and moduli at the bridge approach site were the same as the open track site. While the same instrumentation as Upland (60 ft) was also installed 4.5 m (15 ft) from the Upland Street bridge abutment, the available data was not extensive enough to calibrate the bridge approach model because the tie reaction data was not considered representative of the tie loading, ballast settlements, and tie-ballast gaps of the entire transition zone (i.e., the first 7 to 10 ties). In other words, only one tie was instrumented and the highly variable conditions in the transition zone could not be extrapolated from only one tie. Therefore, the substructure layers and moduli calibrated from Upland (60 ft) were used in the Upland (15 ft) model because they were separated by only 13.7 m (45 ft).

15.2 Parametric Analyses

The simulation of a bridge approach was more complicated than open track because transition zone loading is affected not only by tie-ballast gaps within the entire approach but also increased dynamic wheel loads resulting from the abrupt change in axle elevation/track stiffness as the

front axle contacts the bridge abutment (Nicks, 2009). In the bridge approach model, the ties of interest were the seven closest ties to the bridge abutment within the transition zone. These were labeled as Ties 1 through 7 and are shown in Figure 183. The ties on the bridge were labeled as Tie A, B, etc., to prevent confusion.

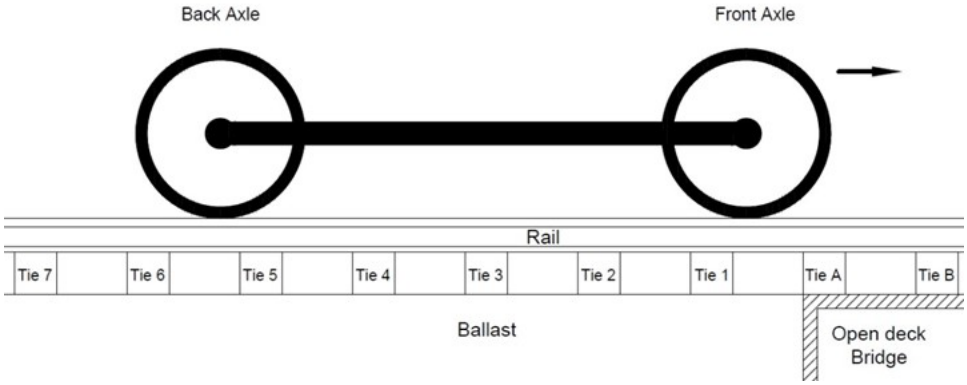

Figure 183. Wheel-rail-tie-ballast model showing no tie-ballast gaps

The primary topics to be addressed in this section are: (1) the increased loading from differential stiffness and settlement between the bridge deck and transition zone and (2) the increased loading from differential settlement within the transition zone. To investigate these two topics, this section presents five different bridge approach analyses to illustrate how varying ballast settlement in the transition zone affected the dynamic loading environment. The analyses are as follows:

- Intimate Contact (No tie-ballast gap)
- Even Ballast Settlement (0–16 mm)
- Gradual Increase in Ballast Settlement (0–2 mm)
- Uneven Ballast Settlement (0–2 mm)
- Field Measurements (Varandas et al. (2011))

15.2.1 Analysis 1: Intimate Contact

The first analysis of the cart passing over the bridge approach assumed no tie-ballast gaps present (Figure 183). This isolated the increased dynamic load from a sudden change of axle elevation and was imperative for understanding more complicated situations when tie-ballast gaps were included in the analysis (Nicks, 2009). This situation represented newly laid track immediately after tamping and prior to any ballast settlement in the approach track.

Figure 184(a) and (b) display the four wheel-rail contact forces with time and distance, respectively, in which the front wheel passed the bridge abutment at a simulation time of about 0.68 seconds and the back wheels passing the bridge abutment at a simulation time of about 0.74 seconds. Figure 184(a) shows the front wheels experienced increased dynamic loads at about 0.68 seconds, the time when the front wheels passed the bridge approach, with the back wheels experiencing an increase in wheel-rail contact force immediately afterwards. The increase in front wheel load was due to the reaction force required to accelerate the wheels and axle upward as the cart travelled from the softer approach track (i.e., lower wheel elevation) to the stiffer

bridge track (i.e., higher wheel elevation). The increase in back wheel load was a coupling reaction from the upward acceleration of the front axle, causing the cart to tilt and consequentially increase the wheel-rail force of the back axle. In this analysis, the back wheels then experienced a load increase of about 20 percent in the transition zone, similar to previous analyses by Nicks (2009). Because of the 2.8 m (9.33 ft) distance between the front and back cart axles, the increased dynamic wheel load occurred about 3 m (10 ft) or 5 ties away from the bridge abutment, as shown in Figure 184(b).

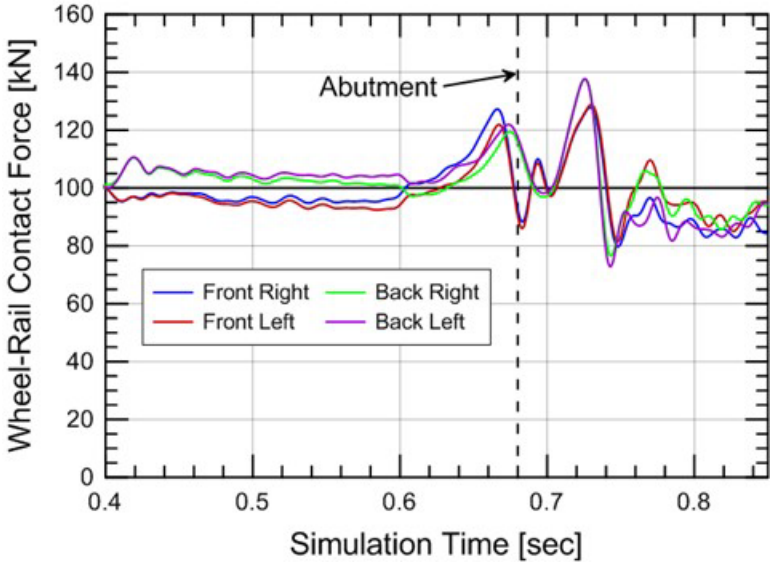

(a)

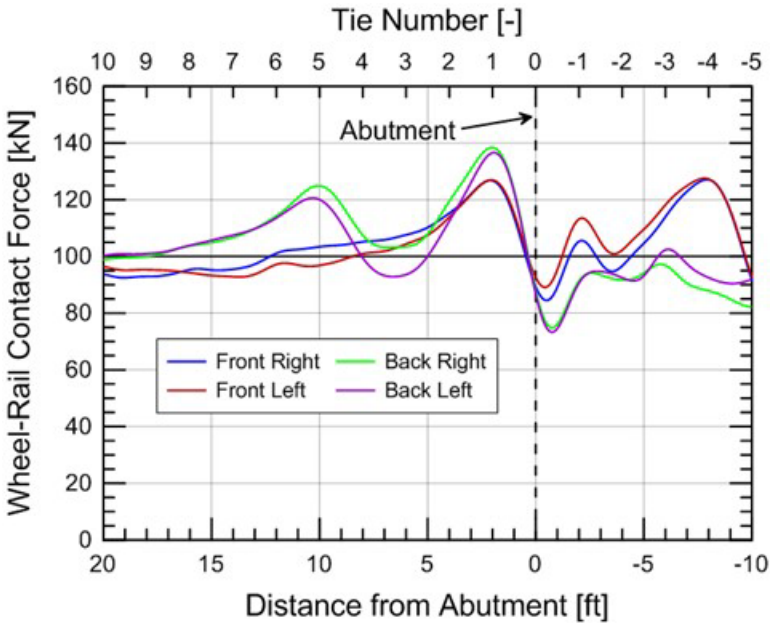

(b)

Figure 184. Wheel-rail contact forces with (a) time and (b) distance

Figure 185 shows the normalized tie loads and percent increase in tie load solely from the cart passing the abutment. Prior to the front wheels passing the bridge abutment, the tie-ballast contact force measured was about 80 kN, which equates to a normalized tie load of about 40 percent, as expected and discussed in prior sections. Because the increased dynamic load of the back wheel occurred about 3 m (10 ft) or 5 ties from the bridge abutment when the front wheel hit the abutment, Ties 5 and 6 experienced load increases of 20 percent and 7.5 percent, respectively (tie-ballast contact force of 97 and 87 kN).

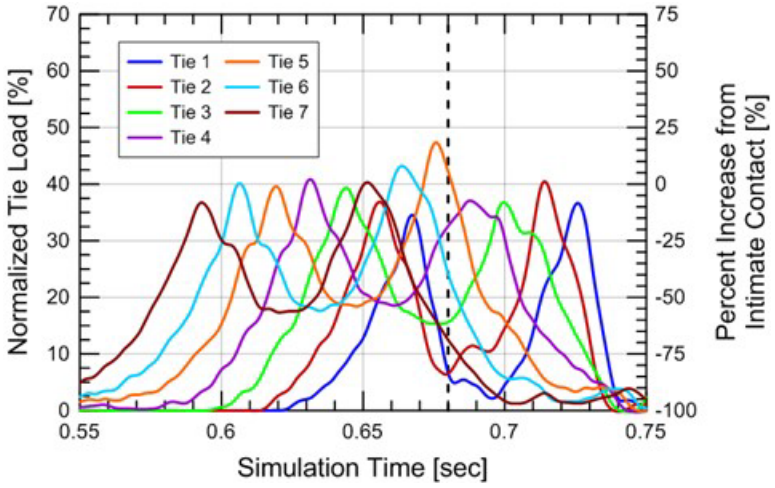

Figure 185. Time histories for Ties 1 through 7 in terms of normalized tie loads

The increase in dynamic wheel and tie load was expected to be dependent on the stiffness and damping of the secondary suspension system along with the differential stiffness between the approach and bridge. If the approach had been stiffened or the bridge had allowed more movement by adding a ballasted bridge deck, rubber pads, and/or ballast mats, this dynamic load would have decreased due to a smaller amount of differential settlement. As a result, stiffening the approach or softening the bridge deck are possible remedial measures for reducing the level of dynamic wheel load.

15.2.2 Analysis 2: Even Ballast Settlement

Repeated train loadings will eventually cause the ballast to settle over time (Selig and Waters, 1994). The second analysis assumed homogeneous substructure settlement in the transition zone to illustrate the increased dynamic load from differential settlement between the bridge deck and transition zone. A schematic is displayed in Figure 186 and shows the rail hanging from the bridge deck with the ties closest to the bridge abutment developing tie-ballast gaps.

Settlement magnitudes up to 16 mm were simulated and Figure 187 shows the normalized tie load time histories, assuming substructure settlements of 8.0 mm. The results showed significantly greater tie loads at Ties 5 and 6, with maximum, normalized, tie load values of 78 percent and 60 percent. As in previous analysis, these maximum values occurred as the front wheel passed the bridge abutment.

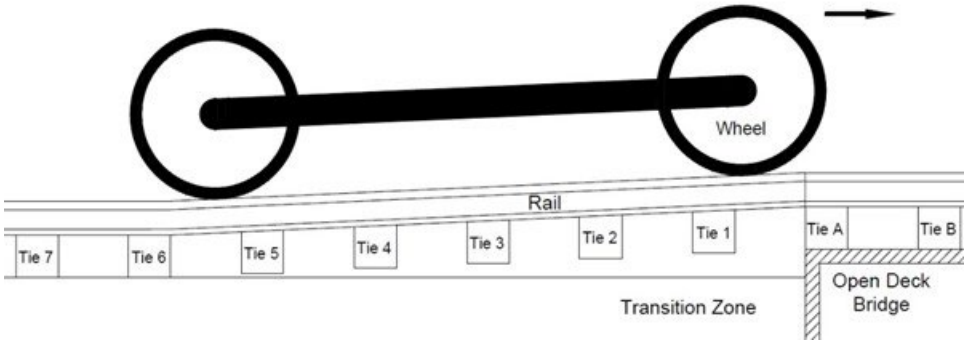

Figure 186. Wheel-rail-tie-ballast model showing even substructure settlement and unsupported ties

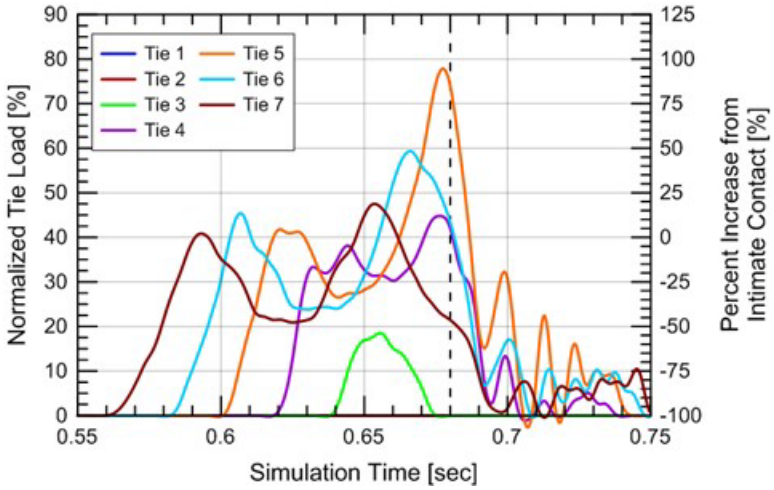

Figure 187. Normalized tie loads of Ties 1 through 7, assuming substructure settlements of 8.0 mm

To illustrate how the maximum normalized tie loads increased with increasing substructure settlement, the maximum normalized tie load values of the seven ties closest to the bridge abutment are displayed in Figure 188. At ballast settlement values of 0.0 and 8.0 mm, the maximum normalized tie loads could be verified with the time histories shown in Figure 185 and Figure 187. Figure 188 illustrates that homogenous substructure settlements resulted in load amplifications primarily at Ties 5 and 6, with maximum normalized tie loads of about 100 percent at Tie 5 (10 ft). This was nearly a 120 percent increase in load if the tie and underlying ballast were designed for 40 percent of the static wheel load. If the cutoff for problematic tie loads is a 50 percent increase (Plotkin and Davis, 2008), i.e., a normalized tie load of 60 percent, the models predicted this would occur at ballast settlements of 4.0 mm.

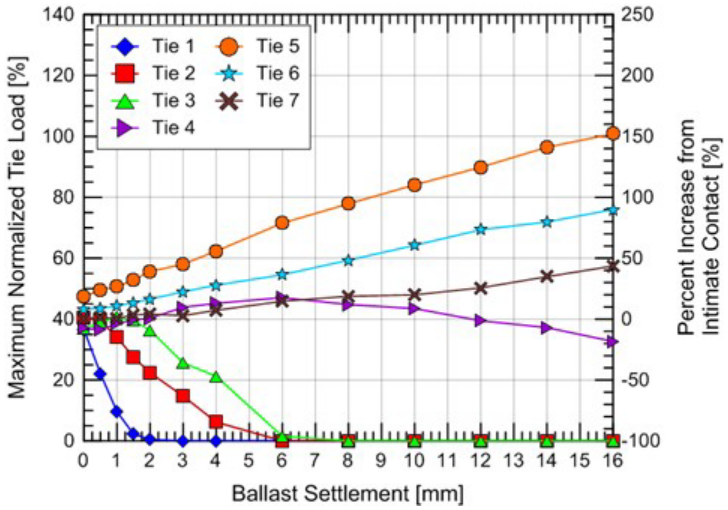

Figure 188. Normalized tie loads of back wheel for substructure settlement ranging from 0.0 to 16.0 mm

The results above agree with past analyses (Nicks, 2009; Wang et al., 2015; Paixão et al., 2014) that show differential settlement is a larger contributor to increased dynamic loads than differential stiffness because of the greater change in wheel elevation. This suggests that transition zone design should focus on arresting the substructure settlement in the transition zone before attempting to smooth the transient stiffness between the open track, transition zone, and bridge. This strategy of reducing substructure settlement is more difficult to implement because the ballast will inevitably settle but can be helped by increasing ballast confinement using wing walls, increasing ballast density after tamping, improving load distribution under a single tie with under-tie pads, and improving ballast gradation and drainage.

15.2.3 Analysis 3: Gradual Increase in Ballast Settlement

The third bridge approach analysis involved a situation in which the ballast settlement, and therefore tie-ballast gaps, incrementally increased as the bridge abutment was reached. This is illustrated in Figure 189, with the ballast settlement under Ties 1 and 2 set to a value of 4*x*, the ballast settlement under Ties 3 and 4 set to a value of 2*x*, and the ballast settlement under Ties 5 and 6 set to a value of *x*. The settlement magnitude *x* varied from 0 to 2 mm. This means the gap height of Tie 1 equaled 8 mm when Tie 5 was set to 2 mm.

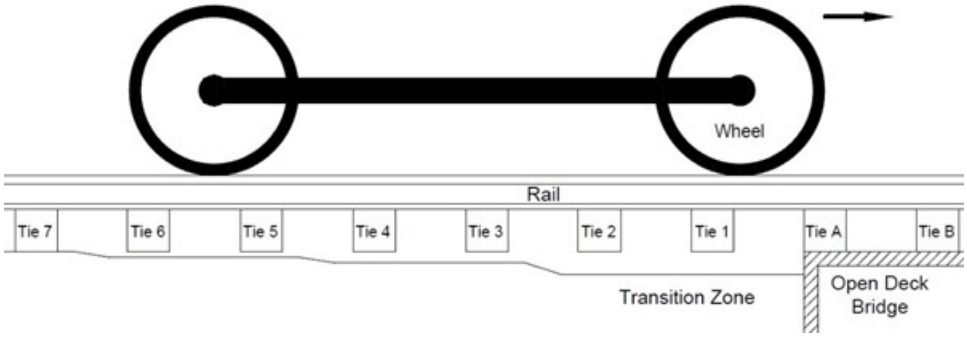

Figure 189. Wheel-rail-tie-ballast model showing a gradual increase in substructure settlement toward the bridge deck

Figure 190 displays the change in maximum normalized tie loads from the back wheels due to variation of ballast settlement *x*. For ballast settlement *x* of zero, all ties experienced maximum wheel loads of about 30 to 50 percent. As the ballast settlement increased, the maximum normalized tie load experienced by Ties 5 and 7 also increased. At a ballast settlement *x* value of 2.0 mm, the maximum normalized tie load of Tie 5 approached 120 percent, an increase of 146 percent from intimate contact, assuming a normalized tie load of 40 percent.

All other ties experienced a decrease in maximum normalized tie load with increasing ballast settlement as the load was being distributed away from these ties. This behavior agreed with the open track behavior in Section 13.4 because the load was still being redistributed from poorly supported ties to better-supported ties. For example, the good tie support at Tie 7 caused the rail to act like a simply-supported beam between Tie A and Tie 7 with pinned connections at the bridge deck (i.e., Tie A) and Tie 7. When loaded, the rail displacement would be greater at Tie 5 than Tie 6. Therefore, Tie 5 would experience a greater load. This same concept explains why Tie 3 experienced greater load than Tie 4.

Additionally, the combination of the increased dynamic load from the coupling of the front and back axles as the front axles passed the bridge abutment and Tie 5 impacted the ballast further amplified the tie-ballast contact force at Tie 5. The increase in load at Ties 5 and 7 explains how the presence of tie-ballast gaps initially located in the first 3 or so meters (10 ft) of the transition zone region could result in tie-ballast gaps spreading outward from subsequent train passes.

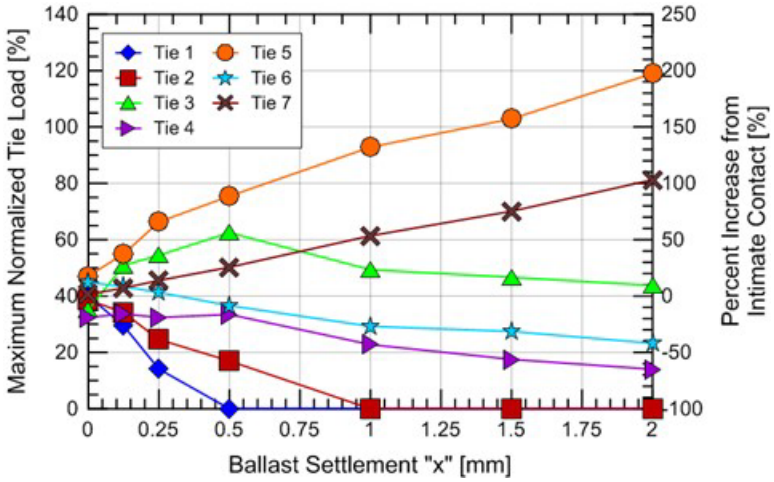

Figure 190. Normalized tie loads of back wheel for Ties 1 through 7 for a situation in which the substructure settlement gradually increases

15.2.4 Analysis 4: Uneven Ballast Settlement

The fourth bridge approach analysis involved a situation in which a single tie (Tie 3) was in intimate contact with the ballast while the ballast under the remaining ties had settled at value *x* (see Figure 191). The team observed that this situation appeared because the substructure settlement in the bridge approach would not be homogenous, meaning the substructure would settle more in certain locations than others. This may have been due to increased loads, uneven ballast compaction, rail joints, fouling, or drainage concerns.

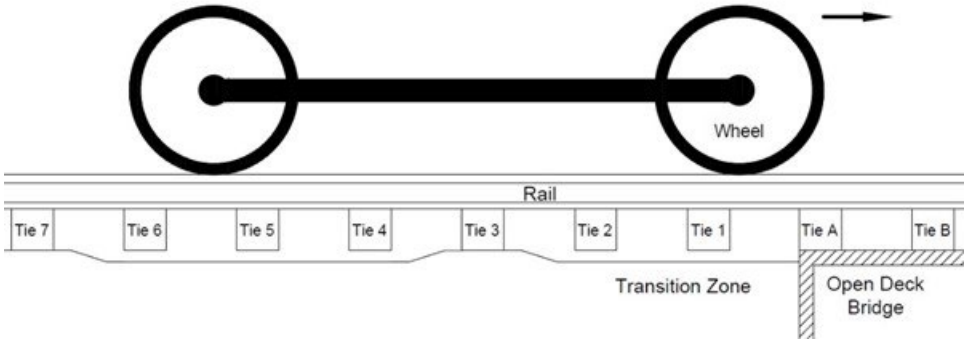

Figure 191. Wheel-rail-tie-ballast model showing an uneven substructure settlement

Figure 192 displays the change in maximum normalized tie load due to the variation of ballast settlement *x*. As the ballast settlement increased, the maximum normalized tie load experienced by Tie 3 significantly increased. At a ballast settlement value *x* of 2.0 mm, the maximum normalized tie load of Tie 3 surpassed 122 percent. This represented an increase in tie-ballast load of about 205 percent from intimate contact in which the normalized tie load was assumed to be 40 percent. Additionally, Tie 7 showed a slight increase in tie load, while Ties 1, 2, 4, 5, and 6 showed decreases in tie load. This was due to the redistribution of wheel load away from poorly supported ties to the supported ties.

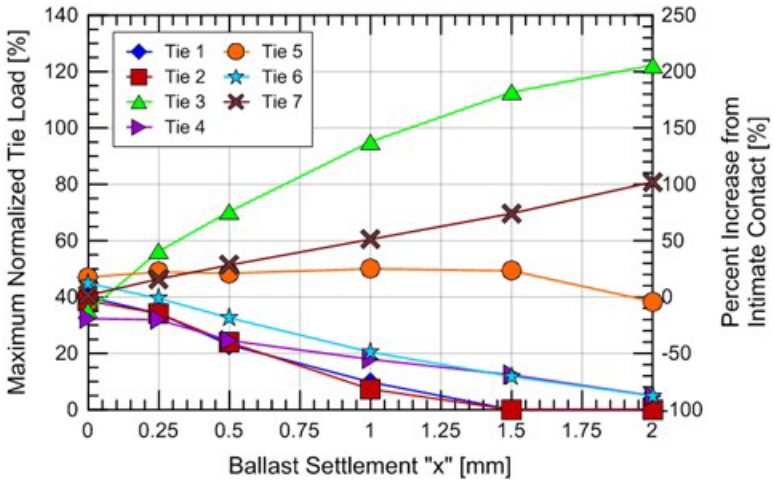

Figure 192. Normalized tie loads of back wheel for Ties 1 through 7 for an uneven substructure settlement situation

15.2.5 Analysis 5: Field Measurements

Ballast in transition zones will likely settle at different rates at different locations because of variations in loading, ballast density, and ballast gradation due to particle breakdown and fouling. This produces spatially varying ballast surface profiles and therefore varying tie-ballast gap heights. It is commonly observed that transition zones have a “dip” in the rail – typically 1.8 to 3.6 m (6 to 12 ft) away from the bridge abutment. This dip suggests the greatest ballast settlement also occurs at this distance. Multiple field investigations (Coelho et al., 2011; Varandas et al., 2011) showed this trend and dip 1.8 to 3.6 m (6 to 12 ft) away from the bridge

abutment. To investigate how the ballast surface profile affected wheel load distribution, multiple simulations were conducted with varying ballast surface profiles.

Analysis 5 compares the results of Analysis 1 (no ballast settlement or tie-ballast gaps), with two simulations roughly based on transition zone measurements in the Netherlands by Varandas et al. (2011). This field data was used because it mapped the tie-ballast gaps over the entire transition zone and better represented field behavior than the three previous analyses described above.

A visual illustration of the transition zone and the ballast settlements under each tie are presented in Figure 193, and the maximum normalized tie load values are displayed in a bar chart in Figure 194. Figure 193 shows the greatest ballast settlement occurring under Ties 2 and 3, with a gradual decrease in ballast settlement outward from the bridge structure. This condition still produces a dip in the rail at about Tie 4 or 5 because of rail bending.

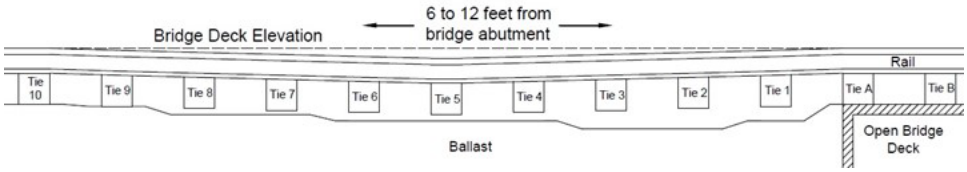

Figure 193. Wheel-rail-tie-ballast model showing a ballast surface profile based of field measurements from Varandas et al. (2011)

Three simulations are compared in Figure 194. Simulation 1was the control simulation in which no ballast settlement was assumed in the bridge approach. Simulation 2 included ballast settlement and was based on the results from Varandas et al. (2011). This case assumed ballast settlement occurred in the transition zone, but no ballast settlement occurred in the open track. Simulation 3 was like Simulation 2, but with 4 mm of ballast settlement under all ties. The objective of including Simulation 3 was to investigate the combined effects of differential settlement within the transition zone (Analysis 5, Simulation 2) and differential settlement between the bridge deck and transition zone (Analysis 2). The ballast settlement values can be referenced in Figure 194.

The maximum normalized tie load results in Figure 194 show that spatially varying but relatively smooth ballast profiles could still produce significant load redistribution and concentrated tie loads with maximum normalized tie loads ranging from 60 to 90 percent. Additionally, uniformly increasing ballast settlement in the transition zone resulted in further increased tie loads and was evident by comparing Simulation 2 and Simulation 3. This agreed with the results of Analysis 2 that differential settlement between the transition zone and bridge deck increased dynamic loads in the transition zone.

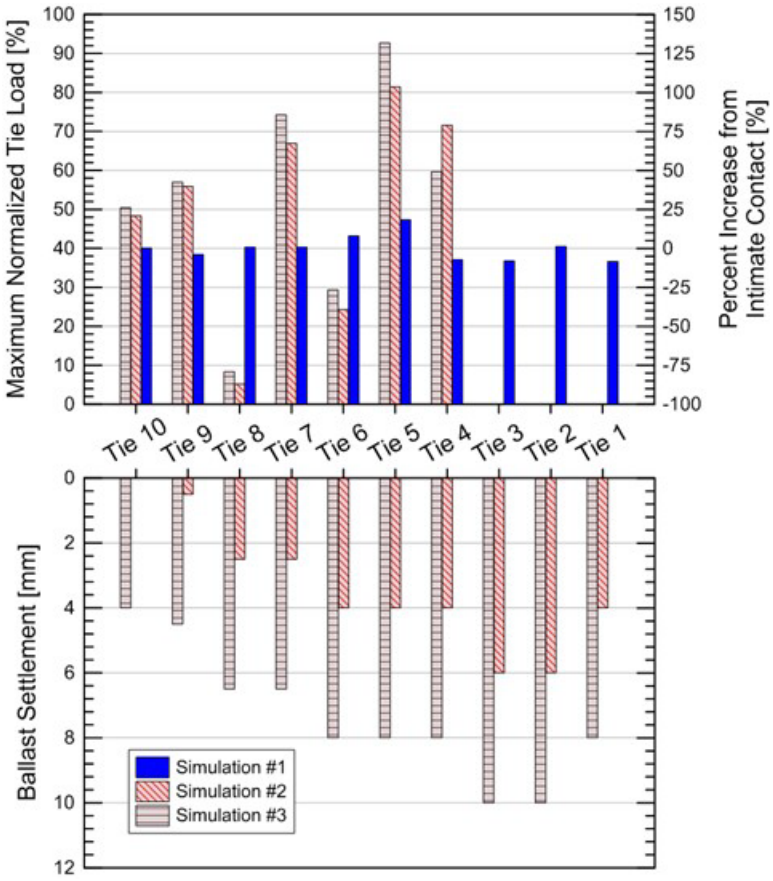

Figure 194. Maximum normalized tie load resulting from the respective ballast settlement under Ties 1 through 10 for three different simulations

In physical track, it would be expected that the ballast under ties that experienced increased tie loads would also experience significantly greater degradation and settlement. Both the ballast surface profile and loading environment would then be expected to shift and concentrate on other ties in the transition zone. It was unclear whether the transition zone would "stabilize" because of little or no settlement at the bridge deck; this is a question that should be investigated in the future. This also reinforces the idea that transition zone behavior is difficult to calibrate or accurately predict without extensive and precise instrumentation over several ties because slight changes in tie support can result in significant redistribution of loads.

15.3 Summary of LS-DYNA Bridge Approach Analyses

Researchers developed a numerical model for LS-DYNA analyses that simulated a railcar truck entering an open deck bridge and was based on the track geometry at Amtrak's Upland Street bridge in Chester, Pennsylvania. The objective of the model was to investigate how differential settlement between the bridge deck and transition zone and tie-ballast gaps increased and concentrated dynamic tie loads in the transition zone. The main findings are summarized below.

- Differential stiffness between the bridge deck and transition zone resulted in about a 20 percent increase in the dynamic back wheel load. This increased wheel load was distributed to the ties 10 and 12 ft from the bridge deck (Ties 5 and 6), resulting in 20 percent and 7.5 percent increases in tie load, respectively, at these ties.

- Evenly increasing the ballast settlement in the transition zone produced tie-ballast gaps and increased tie loads by over 100 percent. This implied the effect of differential settlement between the bridge deck and transition zone had a much greater effect than differential stiffness between the bridge deck and transition zone. This is an important finding because historically, the primary root cause associated with transition differential movement was only stiffness difference.
- Unevenly increasing the ballast settlement in the transition zone also produced tie-ballast gaps and concentrated the wheel load on the most well supported ties. Increases in tie load of over 100 percent were observed for the most well-supported ties. This suggested that differential settlement within the transition zone could be just as detrimental as differential settlement between the bridge deck and transition zone.
- The ballast settlement under each tie as reported by Varandas et al. (2011) was simulated to attempt to analyze the tie loads in physical track. The results of this analysis showed increased tie loads of about 50 to over 100 percent. This suggested that some ties in transition zones may have been experiencing double the tie load than originally anticipated.

To expand the current analyses, the team recommends that future analyses use an iterative procedure to simulate the progressive settlement observed in the instrumented transition zones. This would involve using an empirical settlement law that relates tie load to ballast settlement. If performed in an iterative fashion, this analysis will measure tie loading and ballast settlement over the lifetime of the transition zone, instead of using the assumed geometries in this research. This could give more insight into changing loading environments and how to better arrest transition zone settlement with time and optimal remedial measures.

16. Conclusions – Numeric Analysis

The research team used two software packages, FLAC3D and LS-DYNA, to model monitored railway transitions and investigate the factor(s) contributing to measured displacements and to predict future performance.

Section 2 through Section 10 discuss a strong correlation between measured permanent and transient vertical displacements and tie-ballast gap heights. The team anticipated the tie-ballast gaps to increase the applied loads to the ballast and accelerate transition zone degradation. More specifically, unsupported and/or damaged ties can result in load redistribution and impact loads which increase the applied load to the ballast. A main objective of this research was to numerically replicate the conditions that increase applied loads at the tie-ballast interface and load redistribution to adjacent ties. To accomplish this, the team calibrated the numerical model using field measurements and then performed parametric analyses on the tie-ballast interface to determine the factors that significantly impact applied loads.

Researchers also developed a bridge approach model to investigate how differential stiffness between the bridge deck and transition zone and differential settlement within the transition zone increases dynamic loads.

16.1 Modulus Estimation and Field Calibration

Prior to analyzing the tie-ballast interface, the team determined representative values of substructure stiffness using inverse analyses. This was important because the substructure stiffness not only affected load distribution and stresses within the superstructure, but it also was required to replicate the measured transient displacement time histories in the field.

The team used two methods to estimate modulus values within the substructure. For the first method, researchers used the software package FLAC3D and performed a static inverse analysis. The analysis involved many simplifications, but it included the necessary mechanisms to quickly estimate representative modulus values. First, the team manually input the initial load distribution (35/22.5/10 percent) into the FLAC3D analysis, saving computational time and allowing for the simulation of conditions outside the assumption of intimate tie-ballast contact (e.g., load distributions different than 35/22.5/10 percent). Second, researchers addressed the non-linear behavior of the tie-ballast interface and underlying geomaterials by omitting the displacement required to close the tie-ballast gap from LVDT 1 displacement and the use of an "apparent gap" for non-linear sub-ballast and subgrade behavior. If the displacement required to close the tie-ballast gap is not omitted from the analysis, the predicted ballast modulus is underestimated to a degree that makes it unreasonably low, even for sites experiencing poor tie support. The use of an "apparent gap" implied the estimated modulus would be a "tangent modulus" for the sub-ballast and subgrade.

In a second method, the team used the LS-DYNA software package to estimate substructure modulus values and performed a dynamic inverse analysis. This analysis incorporated the entire train and track system, including the wheel, rail, ties, ballast, sub-ballast, and subgrade, and determined the influence of the tie-ballast gap by directly modeling the gap below the tie in the analysis. This analysis was more computationally intensive but could be calibrated by comparing the calculated time histories with field-measured time histories. The LS-DYNA analyses simulated the tie-ballast gap directly by modeling a void between the tie and ballast instead of

including an apparent gap in the FLAC3D analyses. This resulted in a “secant modulus” for the sub-ballast and subgrade.

The results of the two analyses showed the estimated modulus values were similar for both methods and agreed with modulus values obtained from seismic surface wave testing of ballast and subgrade. A significant difference in estimated modulus values from LS-DYNA and FLAC3D was obtained at Upland (60 ft) for Layer 2 (sub-ballast). This layer displayed highly non-linear behavior, and the difference in modulus was explained by FLAC3D estimating a tangent modulus, while LS-DYNA estimated a secant modulus. Otherwise, the LS-DYNA and FLAC3D modulus values agreed for the other sites and sublayers.

The main benefit of using FLAC3D is that it is an automated analysis and modulus values can be estimated in about 20 minutes per site without manual iterations. This is beneficial when the team needed to analyze modulus values of multiple sites in a short period of time while still receiving reasonable values. LS-DYNA is beneficial when a field-calibrated model is required that can replicate current and predict future track system behavior. The LS-DYNA inverse modulus analysis is time-consuming, with estimates of modulus values for all the sublayers taking four to six days to complete.

16.2 Tie-Ballast Interface

A second objective of this study was to numerically simulate the influence of the tie-ballast interface. Ideally, the underlying ties were in intimate contact with the ballast producing a typical load distribution of 35/22.5/10 percent. Previous field measurements suggested a gap existed between the tie and ballast, resulting in increased ballast loads. The team investigated this interaction between the tie and ballast using LS-DYNA.

Load distribution between ties plays a significant role in determining how loads are applied to the ballast. When a tie-ballast gap exists, extra bending in the rail is required to establish contact between the tie and underlying ballast, which redistributes the wheel load to adjacent, supported ties. Also, the movement of the wheel causes the load redistribution to favor ties in the direction of movement. These two factors imply that load distribution not only affects the unsupported ties but also the surrounding group of ties. Overloading nearby supported ties can result in loss of support (i.e., gaps) and tie damage.

A second factor that increases applied loads on the ballast is the force amplification that can occur when the downward-moving tie contacts the ballast. The amount of load amplification is related to tie velocity at impact and with greater force amplification occurring with higher velocity.

16.3 Differential Settlement

Two factors that can increase dynamic tie loads in the transition zone region are (1) differential settlement between the bridge deck and transition zone and (2) differential settlement within the transition zone. Simulations of both scenarios suggested that, under certain track geometry situations, tie loads could double from the design or anticipated levels. This suggested that preventing differential settlement of the ballast was important for reducing and preventing significant increases in tie load in the transition zone.

Secondly, researchers determined that differential settlement increased the dynamic tie load in the transition zone to a much greater degree than differential stiffness. This suggested that reducing ballast settlement should be prioritized over smoothing the stiffness in transition zone designs.

17. References

American Railway Engineering and Maintenance-of-Way Association (2013). *AREMA Manual for Railway Engineering*. Landover, Maryland.

Bilow, D., & Li, D. (2005). Concrete Slab Track Test on the High Tonnage Loop at the Transportation Technology Center. *Proceedings of the 2005 AREMA Annual Conference*. Chicago, IL.

Chang, C.S., Adegoke, C.W., & Selig, E.T. (1980). GeoTrack Model for Railroad Track Performance. *Journal of the Geotechnical Engineering Division, 106*(11), 1201–1218.

Coehlo, B, Hölscher, P, Priest, J, Powrie, W, & Barends, F. (2011). An assessment of transition zone performance. *Proceedings of the Institution of Mechanical Engineers, Part F: Journal of Rail and Rapid Transit, 225,* 129–139

Davis, D.D., & Chrismer, S.M. (2007). Track Differential Settlement Model. *Proceedings, 2007 ASME/IEEE Joint Rail Conference and Internal Combustion Engine Spring Technical Conference.* Pueblo, CO.

Davis, D.D., Anaya, R., Chrismer, S.M. and Smith, L. (2007). Development of a Differential Settlement Model for Design and Maintenance of Track Transitions. *Technology Digest TD-07-002*, Transportation Technology Center, Inc.

DeBeer, M., Horak, E., & Visser, A. (1989). *The Multidepth Deflectometer (MDD) System for Determining the Effective Elastic Moduli of Pavement Layers* (Report No. STP19800S**).** American Society for Testing and Materials, 70–89.

Ebrahimi, A., Tinjum, J.M., & Edil, T.B. (2011). Large-Scale, Cyclic Traiaxial Testing of Railway Ballast. *American Railway Engineering and Maintenance-of-Way Association Annual Conference*. Orlando, FL.

Han, X. & Selig, E.T. (1997). Effects of Fouling on Ballast Settlement. *Proceedings of 6th International Heavy Haul Railway Conference.* Cape Town, South Africa.

Hyslip, J., Li, D., & McDaniel, C. (2009). Railway bridge Transition Case Study. *Proceedings, 8th International Conference on Bearing Capacity of Roads, Railways and Airfields*. Champaign, IL.

Itasca (2013). FLAC2D Manuals, V. 7.0.

Itasca (2012). FLAC3D Manuals, V.5.0

Li, D., & Davis, D. (2005). Transition of Railway Bridge Approaches. *Journal of Geotechnical and Geoenviornmental Engineering*, *131*(11), 1392–1398.

Lobo-Guerrero, S., & Vallejo, L.E. (2006), Discrete Element Method Analysis of Railtrack Ballast Degradation during Cyclic Loading. *Granular Matter*, *8*, 195–204.

Long, J.H., Olson, S.M., Stark, T.D., & Samara, E.A. (1999), Differential Movement at Embankment/bridge Structure Interface. *Transportation Research Record, 1633*(1), 53–60.

Lundqvist, A., & Dahlberg, T. (2005). Load Impact on Railway Track due to Unsupported Sleepers. *Proceedings of the Institution of Mechanical Engineers, Part F: Journal of Rail and Rapid Transit*, *219*(2), 67–77.

Nicks, J. (2009). *The Bump at the End of the Railway Bridge* (Doctoral dissertation). Texas A&M University.

Paixão, A., Fortunato, E., & Calçada, R. (2014). Transition Zones to Railway Bridges: Track Measurements and Numerical Modeling. *Engineering Structures, 80*, 435–443.

Plotkin, D., and Davis, D. (2008). Bridge Approaches and Track Stiffness (Report No. DOT/FRA/ORD-08-01). Federal Railroad Administration.

Qian, Y., Tutumluer, E., Hashash, Y.M.A., & Ghaboussi, J. (2014). Effects of Ballast Degradation on Permanent Deformation Behavior from Large-Scale Triaxial Tests. *Proceedings of the 2014 Joint Rail Conference*. Colorado Springs, CO.

Sasaoka, C., & Davis, D. (2005). Implementing Track Transition Solutions for Heavy Axle Load Service. *Proceedings, AREMA 2005 Annual Conference*. Chicago, IL.

Smith, M.E., Bengtsson, P.E., & Holm, G. (2006). Three-dimensional analyses of transition zones at railway bridges. *Sixth European Conference on Numerical Methods in Geotechnical Engineering.* Graz, Austria.

Smith, M.E., Bengtsoon, P.E., & Holm, G. (2007). Three-dimensional numerical analyses of a full-scale instrumented railway embankment. *Geotechnical Engineering in Urban Enviornments. Proceedings of 14th European Conference on Soil Mechanics and Geotechnical Engineering*. Madrid, Spain.

Stark, T.D., Olson, S.M., & Long, J.H. (1995). Differential Movement at Embankment/Structure Interface (*Technical Report).* Illinois Department of Transportation.

Stark, T.D., Ho, C.L., Nazarian, S., & Wilk, S.T. (2016). Seismic Testing for Track Substructure Assessment (DOT/FRA/ORD-18/30). Federal Railroad Administration.

Sussmann, T., & Selig, E., (1998). Evaluation of Increased Axle Loading on Northeast Corridor Track Substructure. Test Report for Amtrak (National Railroad Passenger Corporation). Hadley, MA: Ernest T. Selig Inc.

Sussmann, T., & Selig, E. (2000). Resilient Modulus Backcalculation Techniques for Track. *Performance Confirmation of Constructed Geotechnical Facilities,* 401–411.

Thakur, P.K., Indaratna, B., & Vinod, J.S. (2009). DEM Simulation of Effect of Confining Pressure on Ballast Behaviour. *17th International Conference on Soil Mechanics and Geotechnical Engineering.* Amsterdam, Netherlands, 602–605.

Tutumluer, E., Stark, T.D., Mishra, D., Hyslip, J., Tomas, M., & Chrismer, S. (2012). Investigation and Mitigation of Differential Movement at Railway Transitions for US High Speed Passenger Rail and Joint Passenger/Freight Corridors. *Proceedings of the ASME 2012 Joint Rail Conference*. Philadelphia, PA.

Varandas, J.N, Hölscher, P., & Silva, M.A.C. (2011). Dynamic Behaviour of Railway Tracks on Transition Zones. *Computers and Structures*, *89*(13-14), 1468–1479.

Wang, H, Markine, V.L., Shevtsov, I.Y., & Dollevoet, R. (2015). Analysis of the Dynamic Behavior of a Railway Track in Transition Zones with Differential Settlement. *Proceedings of the 2015 Joint Rail Conference*. San Jose, CA.

Wilk, S.T., Stark, T.D., & Rose, J.G. (2015). Evaluating tie support at railway bridge transitions. *Proceedings of the Institute of Mechanical Engineers, Part F: Journal of Rail and Rapid Transit*, *230*(4), 1–15.

18. Uncited References

Briaud, J., James, R., & Hoffman, S. (1997). Settlement of Bridge Approaches (The Bump at the End of the Bridge). NCHRP Synthesis of Highway Practice 234. Washington, DC: Transportation Research Board.

Briaud, J., Nicks, N., & Smith, B. (2006). The Bump at the End of the Railway Bridge. (Research Report). Texas A&M University.

Chrismer, S. (1990). Track Surfacing with Conventional Tamping and Stone Injection (Research Report No. R-719). AAR Technical Center, Chicago, IL.

Dunnicliff, J. (1993). Geotechnical Instrumentation for Monitoring Field Performance. Wiley-Interscience Publications.

ERRI. (1999). State of the Art Report-Bridge Ends Embankment Structure Interaction. ERRI Project No. D230.1. Utrecht, Netherlands.

Koch, K. (2007). Measurement of Coal Hopper Dynamic Load Environment 286,000-Pound Gross Rail Load Unit Train Service-August 2004 to May 2006 (Research Report R-984). Transportation Technology Center Inc., Association of American Railroads.

Kerr, A., & Moroney, B. (1993). Track Transition Problems and Remedies. *Proceedings, ARENA, 94,* 267–298.

Kerr, A., & Bathurst, L. (2001). Upgrading Track Transitions for High-Speed Service (Report No. DOT/FRA/RDV-02/05). Federal Railroad Administration.

McMichael, P., & McNaughton, A. (2003). The Stoneblower – Delivering the Promise: Development, Testing, and Operation of a New Track Maintenance System. *TRB 2003 Annual Meeting*.

Read, D., & Li, D. (2006). Design of Track Transitions. *Transit Cooperative Research Program: Research Results Digest 79*. Federal Transit Administration.

Rose, J., & Anderson, J. (2006). Long-Term Performance of Asphalt Underlayment Trackbeds for Special Trackbed Applications. *Proceedings, American Railway Engineering and Maintenance-of-Way Association (AREMA) Annual Conference and Exposition.*

Sasaoka, C., Davis, D., Koch, K., Reiff, R., & GeMeiner, W. (2005). Implementing track transition solutions. *Technology Digest TD-05-001*. Transportation Technology Center Inc., Pueblo, CO.

Scullion, T., Briggs, R., & Lytton, R. (1989). Using the Multidepth Deflectometer to Verify Modulus Backcalculation Procedures. *Nondestructive Testing of Pavements and Backcalculation of Moduli*, ASTM STP 1026, A. J. Bush, III and G. Baladi, eds., American Society for Testing and Materials, Philadelphia, PA, 90–101.

Selig, E., & Li, D. (1994). Track Modulus: Its Meaning and Factors Influencing It. *Transportation Research Record: Journal of the Transportation Research Board*, 47–54.

White, D., Sritharan, S., Suleiman, M., Mekkawy, M., & Chetlur, S. (2005). Identification of the Best Practices for Design, Construction, and Repair of Bridge Approaches. (Iowa DOT

Project Report No. TR-481). Center for Transportation Research and Education, Iowa State University.

Zaman, M., Gopalasingam, A., & Laguros, J. (1991). Consolidation Settlement of Bridge Approach Foundation. *Journal of Geotechnical Engineering, 117*(2), 219–240.

Appendix A: Tie Reaction Plots

Tie Reaction Plots for Madison Avenue bridge in August 2012 – Amtrak NEC

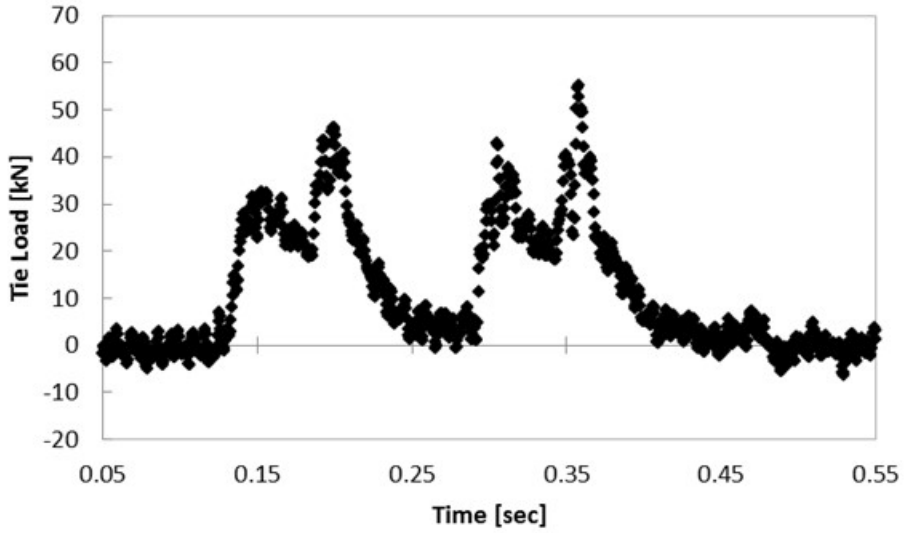

Figure A.1: Tie Loading at Madison (60 ft) on 7 August 2012

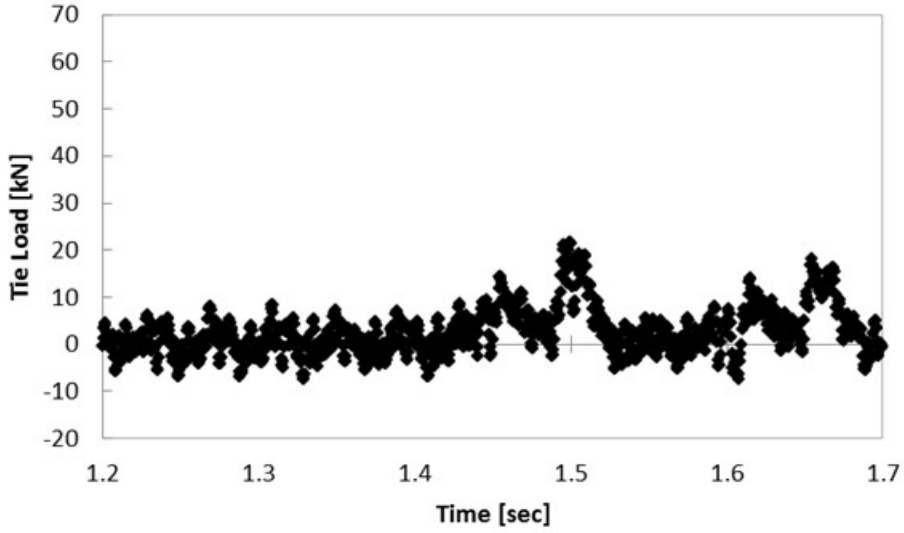

Figure A.2: Tie Loading at Madison (12 ft) on 7 August 2012

Appendix B: Transient Vertical Displacement Plots

Transient Vertical Displacements in August 2012 at Madison and Caldwell Avenue Bridges – Amtrak NEC

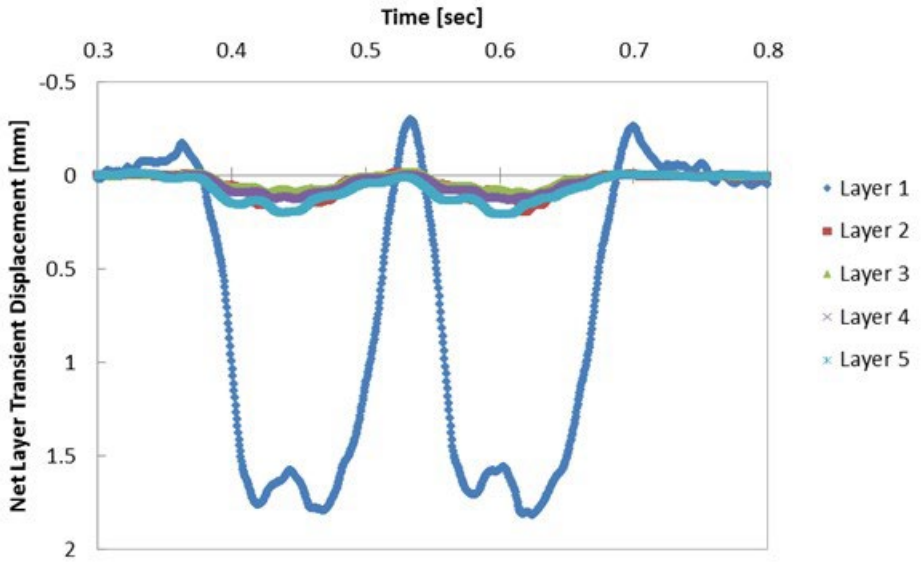

Figure B.1: Transient Response at Madison (60 ft) on 7 August 2012

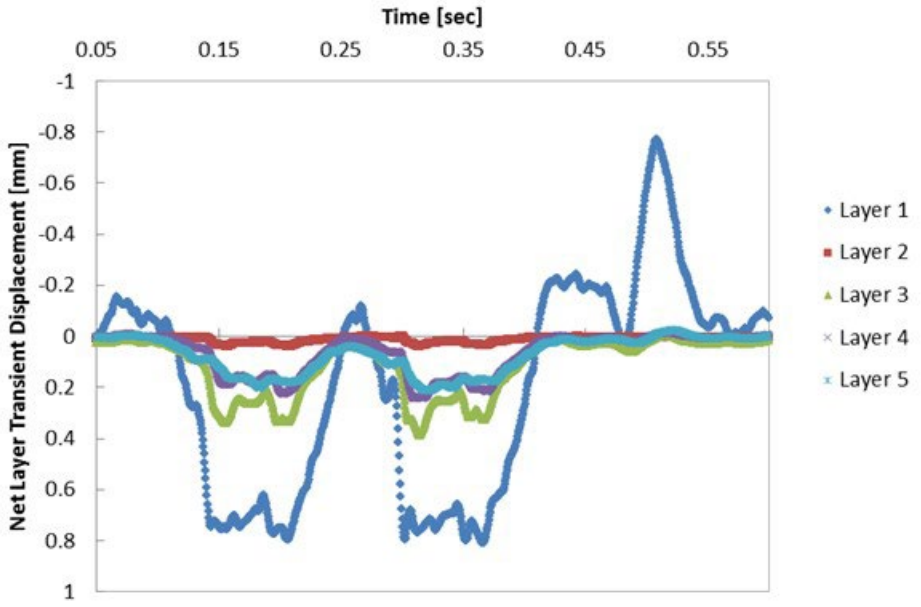

Figure B.2: Transient Response at Madison (12 ft) on 7 August 2012

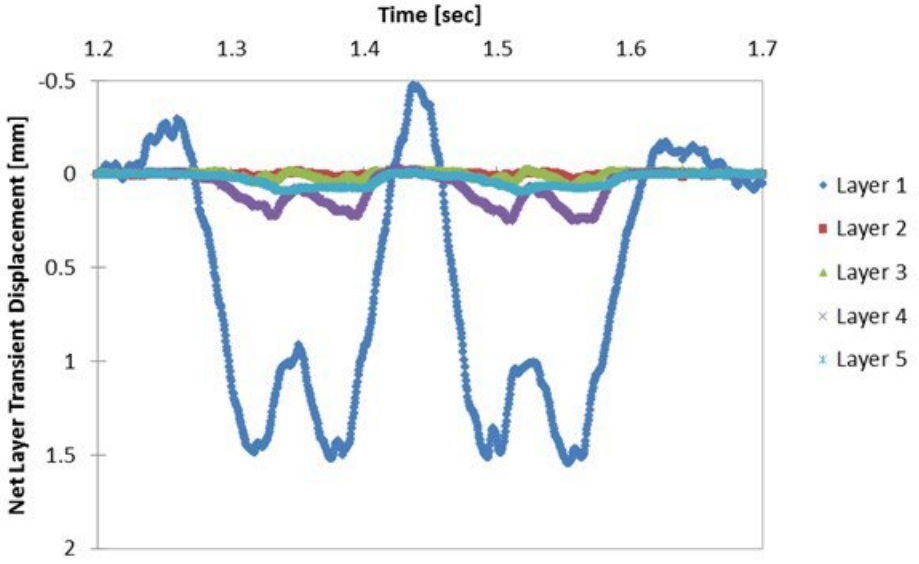

Figure B.3: Transient Response at Caldwell (West) on 6 August 2012

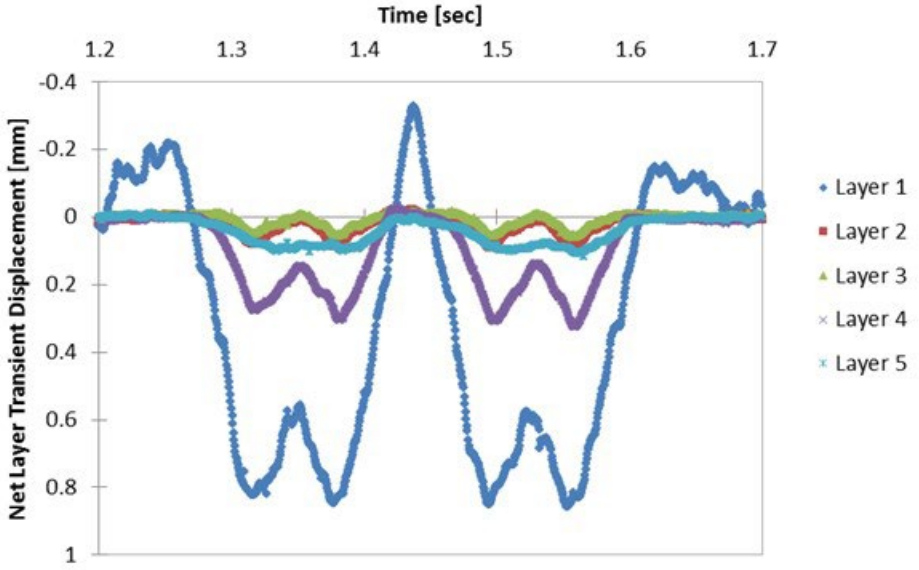

Figure B.4: Transient Response at Caldwell (East) on 6 August 2012

Appendix C: FLAC3D Results

Results of FLAC3D Static Inverse Analysis to Estimate Substructure Modulus Values – Amtrak NEC

Table C.1: Comparison of sub-ballast moduli from static inverse analysis using FLAC3D for all MDD instrumented sites

	Caldwell Avenue		Madison Avenue		Upland Avenue	
	East [MPa]	West [MPa]	12 ft. [MPa]	60 ft. [MPa]	15 ft. [MPa]	60 ft. [MPa]
August 2012	64	246	66	249	54	102
November 2012	59	187	55	268	45	172
January 2013	47	123	67	297	98	210
June 2013	47	130	52	198	89	141

Table C.2: Comparison of Layer 3 moduli from static inverse analysis using FLAC3D for all MDD instrumented sites

	Caldwell Avenue		Madison Avenue		Upland Avenue	
	East [MPa]	West [MPa]	12 ft. [MPa]	60 ft. [MPa]	15 ft. [MPa]	60 ft. [MPa]
August 2012	85	239	66	33	40	34
November 2012	82	185	66	40	45	30
January 2013	91	257	83	29	25	30
June 2013	104	243	73	29	77	26

Table C.3: Comparison of Layer 4 moduli from static inverse analysis using FLAC3D for all MDD instrumented sites

	Caldwell Avenue		Madison Avenue		Upland Avenue	
	East [MPa]	West [MPa]	12 ft. [MPa]	60 ft. [MPa]	15 ft. [MPa]	60 ft. [MPa]
August 2012	41	62	34	42	51	41
November 2012	31	45	34	44	83	35
January 2013	31	45	43	41	117	34
June 2013	25	44	29	45	66	32

Table C.4: Comparison of Layer 5 moduli from static inverse analysis using FLAC3D for all MDD instrumented sites

	Caldwell Avenue		Madison Avenue		Upland Avenue	
	East [MPa]	West [MPa]	12 ft. [MPa]	60 ft. [MPa]	15 ft. [MPa]	60 ft. [MPa]
August 2012	65	100	49	35	123	64
November 2012	49	91	53	32	91	59
January 2013	44	74	71	32	72	56
June 2013	64	80	55	34	113	58

Appendix D: Ballast Settlement Information from Literature Review

The data in this study focused on measured permanent and transient movement at the instrumented transition and open track locations. This has provided insight into track behavior after permanent vertical displacements within the ballast layer (i.e., LVDT 1) had already occurred, but the specific mechanisms producing and affecting the permanent vertical ballast displacement had not been investigated.

Laboratory ballast testing was not within the scope of this study; however, previous laboratory testing has shown a relation between increased ballast degradation, increased levels of fouling, and increased moisture content with increased permanent vertical ballast displacements. This was considered relevant to the study because of observations of ballast degradation, ballast fouling, and inadequate drainage at the transition zone site locations.

Fouled Ballast

Ballast in the U.S. typically consists of 0.75 to 3 in rock particles. This range of particle size is desirable for railroad track because it offers high strength and stiffness due to the high frictional resistance between ballast rock particles. In addition, the large voids between the ballast particles allow the drainage of water from the ballast.

Over time, the ballast particles degrade and become infiltrated by fine particles from the surface, sub-ballast, and subgrade. In the U.S., if the infiltrating particles pass a No. 4 sieve (4.75 mm), they are defined as fouling particles (Selig and Waters, 1994). The ballast is considered fouled when the fouling material fills the voids or coats the surface of the ballast particles.

A photograph of fouled material coating the ties is displayed in Figure D.1. This suggests that wet fouling material is present underneath the top layer of ballast.

D.1. Fouling material covering ballast and concrete ties on Track 1 at Madison (12 ft) on 4 September 2013

Laboratory Fouled Ballast Testing

When fouling material accumulates on the ballast particles and/or within the ballast voids, the strong frictional contact between the ballast particles is reduced and replaced by a weaker frictional contact between the ballast and/or fouling particles. This produces a weaker ballast matrix, making the ballast more susceptible to elastic (transient) and non-elastic (permanent) displacements.

The effects of fouled ballast on permanent vertical ballast displacements have been investigated using ballast box tests by Han and Selig (1997), which show a strong relationship between ballast fouling and settlement under repeated loadings. Figure D.2 (from Han and Selig, 1997) illustrates this relationship by comparing ballast settlement under repeated loading at various fouling levels, with the fouling material being a moist silt. For example, the vertical settlement values after 10,000 load cycles at 0, 10, 20, 30, and 40 percent fouling are about 0.75, 1.75, 2.75, 3.75, and 4.75 in, respectively, and represent an almost linear increase between percent fouling and fouled ballast settlement. This trend was also observed by Han and Selig (1997) for sand- and clay-sized fouling material, while increases in permanent strain during large-scale triaxial compression testing of increasingly fouled specimens was also observed by Ebrahami et al. (2011) and Qian et al. (2014). These laboratory tests suggest greater ballast and track settlement will occur as more fouling material infiltrates the ballast voids.

Han and Selig (1997) also investigated the effect of fouling moisture content on fouled ballast settlement by comparing identical clay-sized fouled ballast specimens in dry, moist, and wet conditions. Figure D.3 shows significantly greater ballast settlement occurs with increasing moisture content of the clay-sized fouling material (Han and Selig, 1997). For example, only slightly greater ballast settlement was observed in the dry clay-sized fouled ballast versus clean ballast (35 vs. 25 mm, respectively) after 100,000 load cycles, even at a percent fouling of 40 percent by weight, because the clayey fouling material was dry. When the clay-sized fouling material was wetted, the fouled ballast became unstable and displayed greater than 200 mm of settlements at a percent fouling by weight of only 30 percent clayey material, i.e., 10 percent less. This indicated that increased moisture has a larger impact than increased percent fouling. This has important implications because track may be stable in dry conditions but can become unstable after wetting.

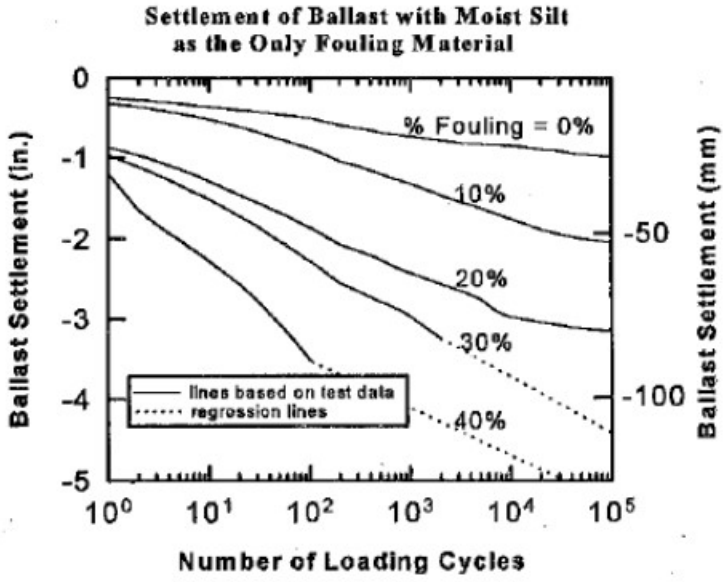

D.2. Ballast settlement of moist silt as the only fouling material (from Han and Selig 1997)

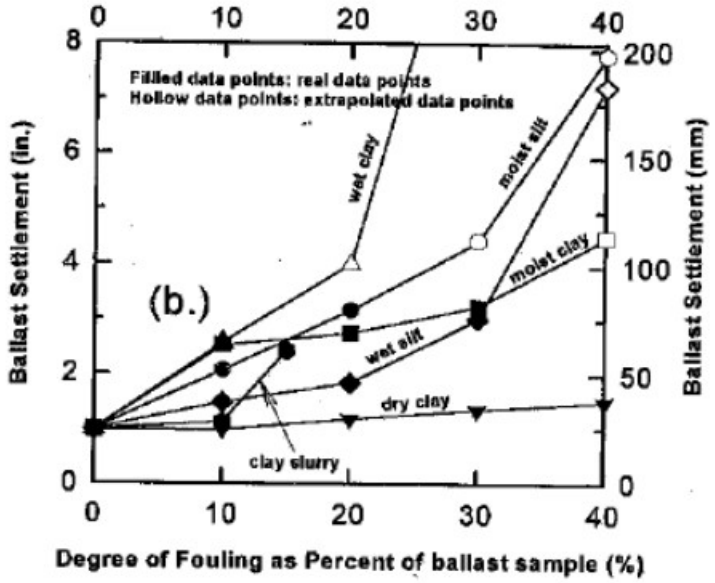

D.3. Ballast settlement from various moisture contents of silt and clay-sized fouling particles (from Han and Selig 1997)

Tie-Ballast Gaps

Section 6 presents a strong correlation between permanent vertical displacement and tie-ballast gap height. While Section 13 and Section 15 numerically investigate the effects of tie-ballast gaps on the loading applied to the ballast, previous laboratory ballast box testing by Selig and Waters (1994) has shown increased permanent vertical ballast displacements when a tie-ballast gap of 1 to 4 mm is present (Figure D.4). In clean ballast, the ballast settlement with a tie-ballast

gap appears to be about three times greater than the ballast settlement with no tie-ballast gap. If fouling is introduced, the amount of ballast settlement with a tie-ballast gap further increases.

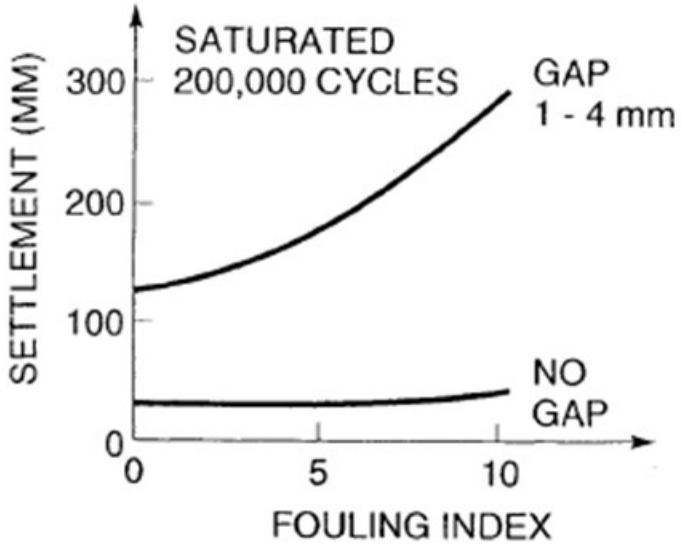

D.4. Ballast settlement from a 1 to 4 mm tie-ballast gap (from Selig and Waters, 1994)

An explanation for these increased ballast settlements is that the additional movement between the tie and ballast accelerated ballast degradation from particle breakage and wear.

The primary takeaway from this brief literature review is that the presence of degraded, fouled, and inadequately drained ballast and tie-ballast gaps can significantly increase permanent vertical ballast displacements. Because the research team observed both factors at the monitored transition zone locations (e.g., Upland (15 ft)), it was not surprising to observe a significant difference in permanent ballast displacements between the transition zone with poorly drained ballast and tie-ballast gaps (i.e., Upland (15 ft)) and open track (i.e., Upland (60 ft)) locations.

Abbreviations and Acronyms

ACRONYM	DEFINITION
DEM	Discrete Element Method
FDM	Finite Difference Method
FEM	Finite Element Method
FEM	Finite Element Method
FISH	FLAC-ISH
FLAC	Fast Lagrangian Analysis of Continuum
FRA	Federal Railroad Administration
HMA	Hot-Mixed Asphalt
IDOT	Illinois Department of Transportation
LVDT	Linear Variable Differential Transformer
MDD	Multi-Depth Deflectometer
MGT	Million Gross Tons
MP	Milepost
NEC	Northeast Corridor
NS	Norfolk Southern
TLV	Track-Loading Vehicle
TOR	Top-Of-Rail
UIUC	University of Illinois at Urbana-Champaign
UTP	Under-Tie Pad